THEORETICAL THERMOCHEMISTRY OF TUNGSTEN INCLUDING σ AND π BOND COMPONENTS

Catherine A. Moulder, B.S. Chemistry, B.S. Mathematics

Dissertation Prepared for the Degree of

DOCTOR OF PHILOSOPHY

UNIVERSITY OF NORTH TEXAS

August 2021

APPROVED:

Thomas R. Cundari, Major Professor
G. Andrés Cisneros, Committee Member
William E. Acree, Jr., Committee Member
LeGrande M. Slaughter, Committee Member and Chair of the Department of Chemistry
Pamela Padilla, Dean of the College of Science
Victor Prybutok, Dean of the Toulouse Graduate School

Moulder, Catherine A. *Theoretical Thermochemistry of Tungsten including σ and π Bond Components*. Doctor of Philosophy (Chemistry), August 2021, 250 pp., 13 tables, 33 figures, 4 appendices, comprehensive reference list, 494 titles.

Computational chemistry examination of the bond dissociation enthalpies of tungsten and main group elements. Includes quantification and calibration of theoretical methods to address the question of bond strengths including component σ and π molecular bonds.

ACKNOWLEDGEMENTS

"Cooperate and graduate!"

Mary A. Flavin-Brandel USAF Maj. Ret., MSEE, BSEE, BA

Yes, yes, we did.

Dedicated with love to my family, friends, and mentors;

and most especially to my husband of twenty years, Thomas Wesley Moulder.

TABLE OF CONTENTS

Page

LIST OF TABLES

Page

LIST OF FIGURES

Page

CHAPTER 1

INTRODUCTION

1.1 What is Thermochemistry?

Chemistry is the study of matter. Physics is the study of natural processes and phenomena, typically the application of mathematical logic to such. Chemistry and physics are intrinsically linked just as matter and energy are. This dissertation research regards the energy released when a bond is formed or broken between two elements, *i.e.*, thermochemistry. The more stable the molecular structure, the more energy is needed to break the molecular bonds between the atoms. Thermochemistry studies the thermodynamics of chemical reactions, *viz* the energy changes in the reaction.

The inherent stability or instability of the chemical bonds between two atoms determines whether or not a bond is breakable and if so, how easily. Hypothetically, all bonds between atoms can be broken under the right conditions, but some of these conditions are so impractical as to be unlikely to ever occur.

1.2 What is the Difference between Thermodynamics and Kinetics?

Introductory level students are taught the fundamentals of how a bomb calorimeter can be used to measure the enthalpies of formation for simple molecules, typically uncomplicated hydrocarbons, as part of their lessons on thermodynamics. From these lessons, a framework is built up to understand how chemical reactions occur.

Stability of a structure says nothing about how fast it may be built or wrecked. This is true for both molecules and houses to set up an analogy. Just as a well-built and maintained house will still be standing after many years, a highly stable molecule will persist until it encounters a big enough change in condition to alter it. For houses, a tornado could make it disappear instantly,

whereas an earthquake might destabilize it to the point where it collapses after a longer period of time. Both the tornado and earthquake induce major changes to the stability of the structure, yet the change in stability does not actually say much about the speed at which it falls down.

In molecules, this is the difference between thermodynamic and kinetic stability. Kinetics is about how fast things occur, *i.e.,* rates of change and often the causes. The tornado has a lot of energy and works as a fast-kinetic reaction that changes the thermodynamic stability of the house in one fell swoop. The earthquake can be a slower destabilization of the structure that changes the thermodynamic stability so that less energy is needed to push it over into a heap. The earthquake destabilized structure might still be up for some time before any major change is visible. Once it falls, it may fall very quickly but nothing in the stability of the damaged structure is directly informative about how quickly that will be. This is the difference in practical terms between stability and kinetics and why stability does not directly imply speed of reaction, kinetics.

1.3 How to Use These Theoretical Models to Inform Catalytic Design

A catalyst is a molecule that is used to speed up reactions by providing an alternate lower energy path for the reaction to take (Fig. 1.1). Catalysts are not consumed by the reactions they facilitate. In order for the catalyst to participate in the reaction without being consumed it needs to be regenerated.[1] This indicates that there has to be a balance between the energy released when the catalyst engages with the reactants and when the catalyst is reformed (Fig. 1.2). This means that the catalyst should not require much energy to reach the transition state, to release the products, nor to return to the original state. Thus, a near flat free energy diagram with stationary points close to thermoneutrality as possible is desired.

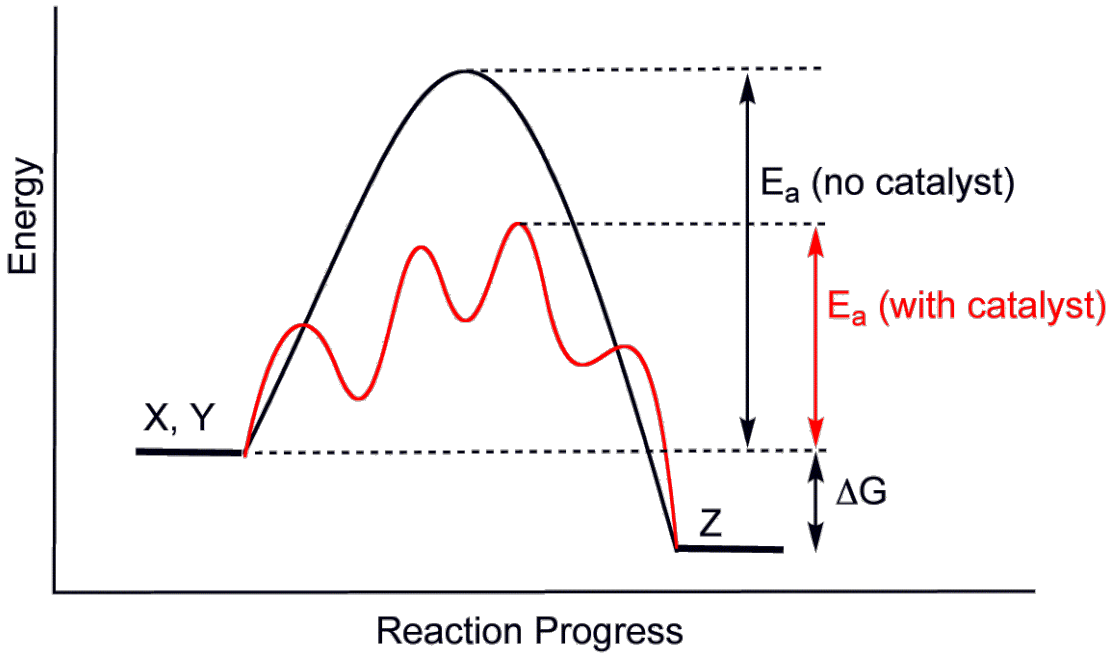

Figure 1.1*:* A generic free energy diagram for a reaction with a catalyst in red and without in black. The red path is overall lower in energy, but may have more elementary steps. The red path with the catalyst uses much less energy and thus is typically quicker to form products.[2]

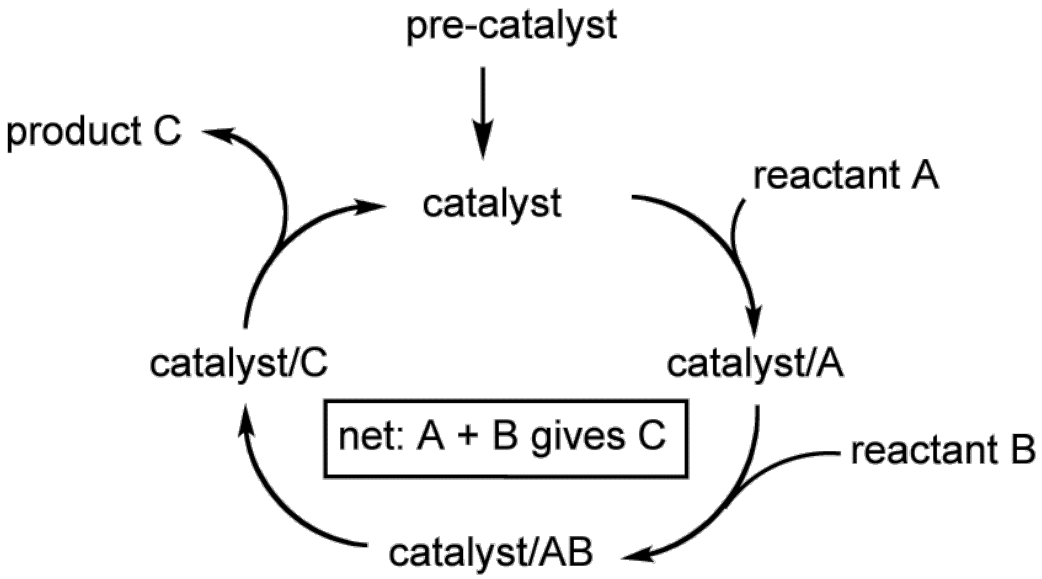

Figure 1.2: Generic general diagram of a catalytic cycle.[6]

Transition metal catalysts are particularly useful for making polymers, metal organic frameworks, and biologically active species for drug development, among other things. Early transition metal catalysts are frequently used to catalyze the formation of polymers like:

polyethylene, polypropylene, polystyrene, polyvinyl chloride, synthetic rubber, Bakelite (formaldehyde resin), neoprene, nylon, polyacrylonitrile, silicone, *etcetera*.[3-5] Myriad uses for these polymer products, all with their own specifications, has resulted from and led to a great deal of industrial research and development. There are also enzymes that have early transition metals as coenzymes that perform such functions as nitrogen fixation, carbon dioxide fixation, and the reduction of purines.[3-5] Early transition metals also happen to be more economically and ecologically "green" than many later transition metals due to their abundance in the Earth's crust and general availability (Fig. 1.3).

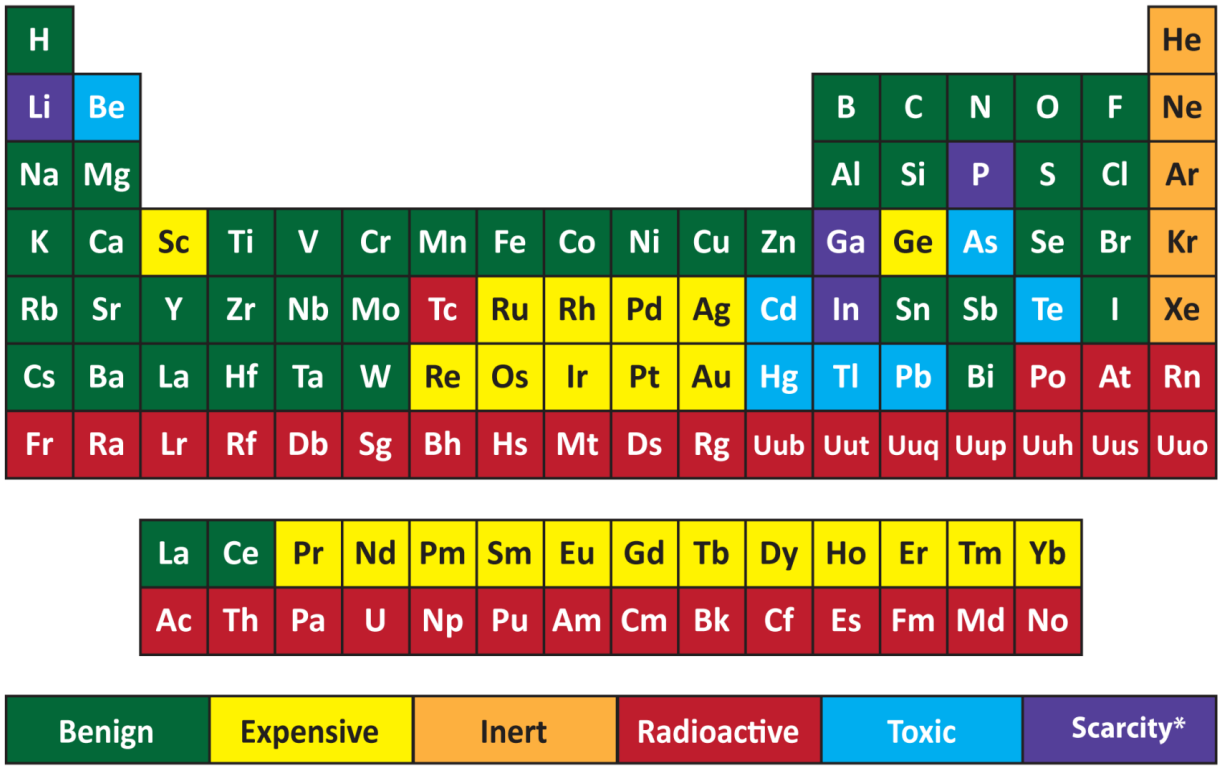

Figure 1.3: Potential scarcity of elements relative to worldwide demand.[7]

Investigations into the thermochemistry of transition metal bonds allows for better informed catalyst design. The difficulty is that there are often experimental steps missing that would be required to actually experimentally quantify precisely what the bond enthalpies are. This is where theoretical chemistry can assist and provide a bridge until those gaps in the science can

be filled by future scientists. Using computational thermochemistry, it is possible to model a molecular system with the bonds of interest and compute what the bond dissociation energy is for a metal-element bond. Furthermore, this can be expanded, for example, to model what the component σ- and π-bond enthalpies are for a metal-element multiple bond. Knowledge of π-bond enthalpies is particularly useful as many catalysts use the higher bond order of multiple bonds to create a pathway for the substrate to react with the transition metal – ligand active site of a catalyst or catalytic intermediate.

With computational modeling, it is possible to generalize the bond enthalpies of each metal-element bond to determine which bonds are most likely to be active and which will be spectators in a reaction. Some ligands are hemi-labile and can indirectly participate in the reaction by dissociating from the metal center, thus freeing a coordination site to facilitate binding of the substrate. Ancillary ligands can also be used to fine-tune reactivity at a metal center through electrostatic, covalent, dispersion, etc. interactions. Such interactions between the supporting ligands orbitals and the metal center of the catalyst can change the overall reactivity of the transition metal and are an exploitable, if often unquantified, facet of catalyst design. Indeed, such chemical interactions present both opportunities to design excellent catalysts and notable potential difficulties when the experimental design fails to account for it. It also can convolute the problem of what the bond enthalpy of a particular component is due to the tug of war for the valance electrons among the components of a catalysts, thereby strengthening or weakening the bond or bonds of interest.

1.4 How Computer Modeling Helps

Theory can provide a framework with which to design and understand why chemical reactions occur the way they do. The rise of extreme computing power through the use of

supercomputers and more powerful algorithms has allowed chemical theory to be developed into computer codes and software packages. At its core, all computer software code is a mathematical model based on a level of understanding of real physical phenomena. Theorists may fine tune and use these models to investigate the chemical world around them.[8,9]

A sound model is fit to the data, not the other way around. Theoretical models for computational chemistry work are generally validated with empirical experimental data. These modeling algorithms are checked and rechecked to ensure that the quality of the data they produce is sufficient for the work being done. When the model is validated, predictions can then be made for experimentalists to test. This is effectively how considerable research is done for drug candidate screening among other things.

Different levels of theory are best for different applications. Large scale simulations such as enzymes and proteins often benefit from broader assumptions. Small scale simulations, such as those on diatomic molecules are more likely to be modeled with extremely powerful *ab initio* methods that model every electron in the molecule as a many body problem. Note, many body problems are often beyond the current state of the art for true analytical mathematical solutions and thus numerical approximations are as close as is possible to get.[10]

Heavy elements are often not as facile for *ab initio* methods versus approximate computational models. This body of work focuses on small molecule models with transition metals which incorporate heavy elements. Heavy elements have more protons and electrons to model. This translates into more calculations performed per atom in the molecule as there is more to model. Tungsten is a heavy 5d metal and the focus of this work. Small tungsten molecules can be significantly more computationally expensive to model than relatively simple, fewer than 100 atoms, organic molecules. To manage the computational expense of these quantum calculations

approximate methods that do not model every one of the 74 electrons of the tungsten atom are often preferred.

Each atomic orbital is represented as a wave function in a "basis set," which is a representation of the quantum mechanical wavefunction that turns a set of partial differential equations into a set of algebraic equations that can be efficiently calculated by a computer. This is possible in part due to the mathematical concept of linearity, a function $X \rightarrow Y$ such that there is a commutative (addition) and distributive (multiplication) property. In 'math' this is: $\forall f: \mathbb{R}^n \rightarrow \mathbb{R}^n$ and $a \in \mathbb{R}$, $a(f+g)(x) = a(f(x) + g(x)) = af(x) + ag(x) = f(ax) + g(ax)$. The linearity of the atomic orbital wave functions allows them to be combined to form the linear combination of atomic orbital approach or LCAO for forming a set of basis functions to mathematically model molecular orbitals. The atomic orbital are one-electron wave functions for the atomic orbitals that form a finite set of basis functions represented as vectors with components that correspond to the coefficients in the linear expansion.

Every analytic function can be used to define a matrix function that maps square matrices to square matrices of the same size. The partial differential equations that are then linearly combined through the LCAO approach can then be calculated by the supercomputer as matrices. For ground state, *i.e.* lowest energy state, optimizations the expansion coefficients of the molecular orbital are generally optimized by use of the variational principle to find the local minima. In essence, the supercomputer is performing matrix math on a scale that would be impractical to perform by hand. However, even the supercomputer often needs to be provided with means to decrease the scale of calculations in the instructions. There are a few ways to do these truncations that (hopefully!) do not introduce major errors into the final results.

For most of the modeling on tungsten-element bonds, the first truncation is from the

assumption that the inner core electrons of the metal are unlikely to have significant impact on the bonding. This assumption is based on the observation that only the outermost or valence electrons in an atom generally participate in chemical bonding. The inner core electrons are thus not modeled, and can be replaced by pseudopotentials.

Another highly popular simplification for modeling molecules with heavy metal atoms is to use density functional theory (DFT in the common jargon). Density in this case refers to the electron density of an atom or molecule, specifically functionals of the spatially dependent electron density. There are many different DFT functionals, but all of them work by reducing the problem to one where the electron density is the basic variable in three dimensional space that is subject to a an external potential. The external potential represents the Coulomb potential from the nuclei on the electrons as well as any other external electromagnetic field. The Hohemberg-Kohn theorems prove an injective correspondence between the subset of external potentials and a subset of viable densities, thus allowing the energy to be expressed as a function of density rather than external potential. This transformation is a Legendre transformation; thus, the problem of finding the ground state energy is greatly reduced from the number of electrons in the wave functions to a less complex function of the electron density.

There are hundreds of different density functional theory approximations. Each one is optimized, often to serve a different chemical or physical purpose. These purposes include modeling the free energies of chemical reactions to better understand the mechanisms of reactions, estimating band gaps for semiconductors, studying the behavior of ferroelectrics, and predicting mechanical properties in solid state calculations. Which DFT functional and which valence basis set is likely to provide the best model is something that needs to be carefully and individually considered when designing a computational experimental set up. A large aspect of the present

studies on tungsten-element bonding is determining just what the optimal combinations of functional and pseudopotentials are for studying the thermochemistry. Thus, roughly half of the work in this dissertation is evaluating how best to computationally model the bond enthalpies, and what the expected accuracy and precision may be from introducing these approximations.

The DFT functionals and valence basis sets used in the first two chapters were specifically chosen not because they are the 'best' available, but because they are popular in the literature. Note that popular is not the same thing as accurate, many older less accurate DFT functionals and valence basis sets are popular as long-established methods. The popularity of those functionals and pseudopotential/valence basis sets is such that the present research is hoped to be widely useful to those interested in using DFT to model heavy element thermochemistry. The bond enthalpies calculated are compared to much more expensive higher level theory *ab initio* calculations as well as real world physical experimental data to assess quality.

Bond enthalpy calculations themselves are useful to aid in the understanding of why some complexes are more stable than others, as described earlier. With good quality theoretical work, in principle these bond enthalpy calculations can assist with the inductive and deductive reasoning used to fathom the nature of new chemical reactions, catalysts, and principles.

1.5 References

1. Atkins, P.; dePaula, J. *Atkins' Physical Chemistry*, 9th ed.; Oxford University Press, Oxford, UK, **2010**.

2. CatalysisScheme.png. Wikimedia Commons. https://commons.wikimedia.org/wiki/File:CatalysisScheme.png

3. Hartwig, J. F. *Organotransition Metal Chemistry: from Bonding to Catalysis*; University Science Books: Mill Valley, CA, **2010**.

4. Crabtree, R. H. *The Organometallic Chemistry of the Transition Metals*, 5th ed.; Wiley: Hoboken, NJ, **2009**.

5. Miessler, G. L.; Fischer, P.J.; Tarr, D. A.; *Inorganic Chemistry* 5th ed.; Pearson: New York, NY, **2014**.

6. Catcycle.png. Wikimedia Commons. https://commons.wikimedia.org/w/index.php?curid=2792355

7. Potential scarcity relative to world demand. Courtesy of the Center for Sustainable Materials Chemistry Oregon State University and the University of Oregon

8. Cramer, C. J. *Essentials of Computational Chemistry; Theories and Models,* 2nd ed.; Wiley: Hoboken, NJ, **2004**.

9. Jensen, F. *Introduction to Computational Chemistry*, 3rd ed.; Wiley: Hoboken, NJ, **2017**.

10. Levine, I. N. *Quantum Chemistry,* 7th ed. Pearson: New York, NY, **2014**.

CHAPTER 2

TUNGSTEN-LIGAND BOND STRENGTHS FOR 2P ELEMENTS INCLUDING σ- AND π-BOND STRENGTH COMPONENTS, A DFT AND AB INITIO STUDY*

2.1 Abstract

Three W^{VI} crystal structures with multifarious metal-ligand bond types are used to theoretically predict homolytic metal-element bond enthalpies with 11 popular DFT functionals, MP2 wavefunction methods, and 4 common valence basis set/pseudopotentials in order to evaluate the accuracy and precision of the resultant bond enthalpy data. To our knowledge, for the first time, estimates of component metal-ligand σ and π bond strengths are computed. The WE (E = C, N, O) bond enthalpies have the consistent trend: $\sigma > 2^{nd}\ \pi > 1^{st}\ \pi$. In contrast, the element-element BDE trend for the 2p homologs is: $2^{nd}\ \pi > 1^{st}\ \pi > \sigma$ for nitrogen and oxygen, and $\sigma > 1^{st}\ \pi > 2^{nd}\ \pi$ for carbon. These differences may underpin the differences in stability trends and thus reactivity behavior for metal-element multiple bonds as compared to the element-element multiple bonds, and metal-element triple bonds versus their corresponding double bonded counterparts. For example, Odom *et al.* show that MeI nucleophilically attacks at the imide (M=N) rather than the nitride (M≡N) ligand; the relative π-bond strengths derived herein provide a thermodynamic rationalization for this site preference. In this study, it is deduced from the calculated thermodynamics that the W-oxo ligand is more congruous with a triple bond than a double bond, consistent with the bonding model set forth in the seminal 1961 Ballhausen-Gray paper.

* This chapter is reproduced from Moulder, C. A.; Kafle, K.; Cundari, T. R., Tungsten-Ligand Bond Strengths for 2p Elements Including σ- and π-Bond Strength Components, A Density Functional Theory and ab initio Study, *J Phys Chem A* 2019, 123 (37), 7940-7949. DOI: 10.1021/acs.jpca.9b03272, with permission from the American Chemical Society.

2.2 Introduction

Thermodynamic stability or the lack thereof of a metal-ligand bond – or the σ and π components of a multiple-bond – is key to many practical applications in inorganic and organometallic chemistry, especially in the area of transition metal catalysis. To wit, Simões and Beauchamp, in their classic review, refer to metal-carbon and metal-hydrogen bond energies as "the keys to catalysis."[1] It is well-known that steric and electronic effects of supporting ligands can impact the stability and the reactivity of known organometallic catalysts and even to predict the hypothetical synthesis of new complexes.[2,3] For example, in a previous study of methane activation by nine metal-imide (L_nM=NR) complexes incorporating metals from Groups 8 - 10, it was deduced that the strength of a metal-imide π bond was a key property in determining the preferred activation mechanism.[4]

Unfortunately, experimental thermodynamic data for metal-ligand bonds are often very sparse – and essentially non-existent for bond energy components like σ and π bond strengths – especially for large, catalytically relevant transition metal complexes.[5] This gap in the literature exists because accurate experimental measurements are generally difficult to obtain for the thermochemistry of metal-containing complexes.[1] Thus, the questions arise: How can theory help bridge this gap? How sensitive are the computed metal-element bond energies and bond energy components to the level of theory? This question is particularly salient given the widespread use of density functional theory (DFT) in modeling studies of transition metal catalysis.

The present research seeks to begin to build a thermodynamic database of homolytic metal-element bond energies, particularly their σ and π components. Such data are useful to guide research in inorganic/organometallic catalyst design.[6] Using multiple levels of theory, DFT and wavefunction, benchmarks are evaluated for 3rd row transition metals that are also Earth-abundant

and hence of interest in the context of "green" catalysis. Much of the research effort in catalysis using Earth-abundant metals has focused on 3d metals; however, not all heavy transition metals are precious. Those of the early 4d and 5d series are "green" in both an economic and ecological sense (Fig. 2.1).[7-17] Additionally, in the activation of light alkanes, the generally stronger metal–C and metal–H bond strengths for 4d and 5d metal complexes versus their 3d congeners can mitigate the thermodynamic – and hence kinetic – impediments to non-radical methane activation that often arise due to weak M_{3d}–C/H bonds.[18]

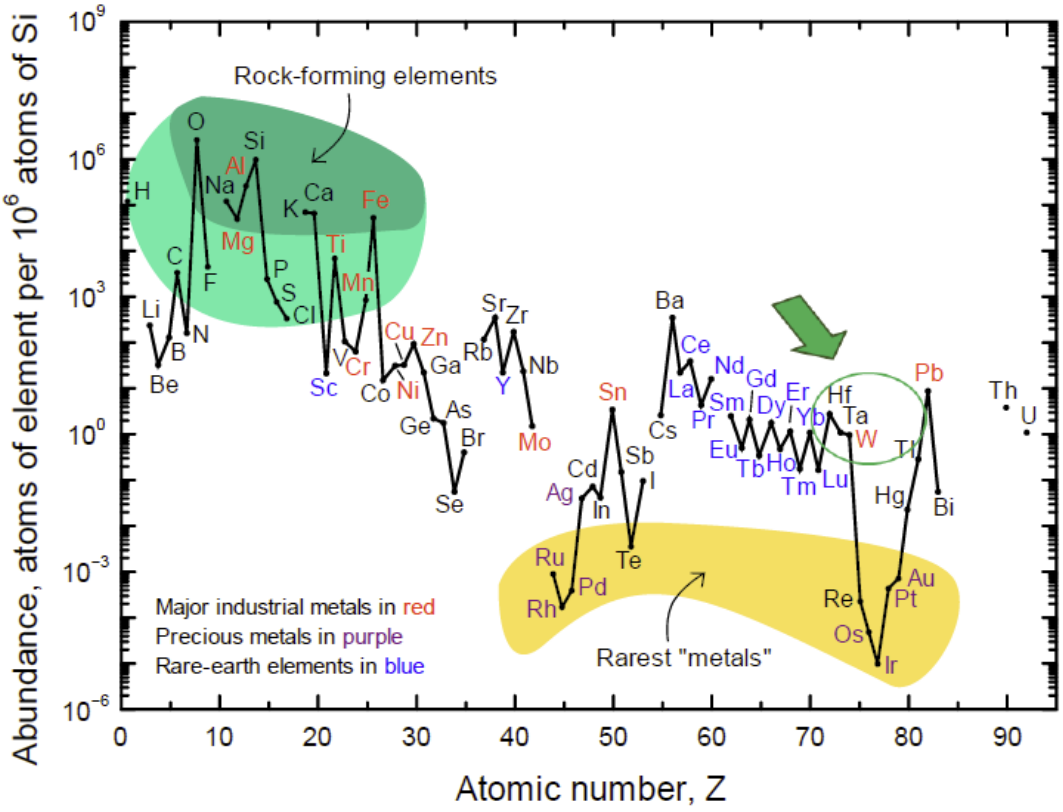

Figure 2.1: Atomic abundance from US Geological Survey Fact Sheet.[17] Early 5d metals (green arrow) circled for emphasis.

This research focuses on complexes of tungsten and an array of important prototypical ligand types involving the 2p elements. The present work focuses on the precision of computed metal-ligand bond strengths most relevant to catalysis: metal-carbon, metal-nitrogen, and metal-oxygen bonds, and their σ- and π-bond strength components. This research seeks to inform

improved theoretical protocols for Earth-abundant 5d metal catalysts that possess higher accuracy and, perhaps more importantly given the paucity of experimental data, which are of known precision. Better understanding of the precision of common DFT levels of theory will facilitate the study of larger, more experimentally relevant organometallic catalysts. Finally, a large computational database is useful in conjunction with emerging machine learning techniques to identify metal-element motifs with desirable thermodynamics to more quickly identify improved catalysts than traditional complex-by-complex quantum mechanical analyses of individual compounds.

The models studied in this research are derived from three interesting Group 6 complexes that display important metal-ligand bond types. The presence within a particular complex of various metal-element (ME, M = W, E = O, N, C) bond types – dative, single, double and triple – is expected to reduce computational errors arising from basis set limits, incomplete electron correlation treatment, *etc.* The crystallographic structures extracted from the papers of Churchill,[19] Beaumier,[20] and Cotton[21] and their coworkers are also used to calibrate calculated geometries (Figs. 2.2, 2.3, and 2.4, respectively).

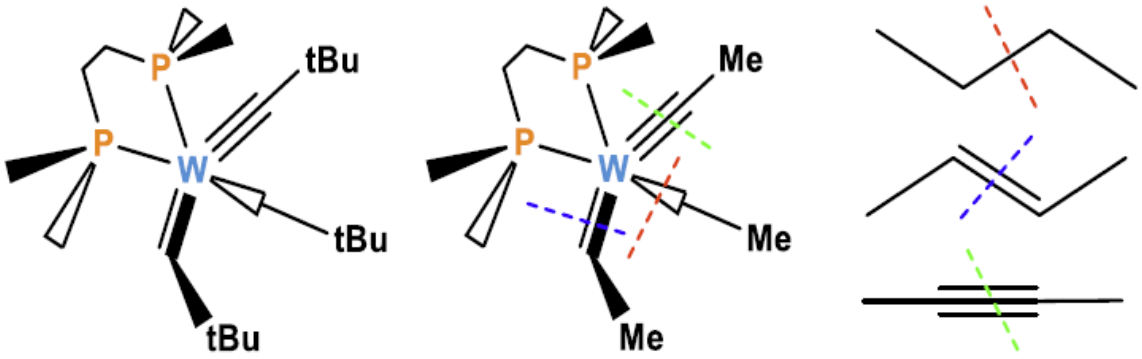

Figure 2.2: Churchill complex[19] (left); computational model used in this work (center), and hydrocarbon analogs (right); color coded dashed lines denote the bond homolysis comparisons.

To facilitate comparisons among models, W replaces Cr for the complex reported by Beaumier *et al.*[20] The empirical atomic radii[22] differ by 10 pm for Cr (145 pm) and W (135 pm).

Of course, replacement of the metal does increase the computed differences between theory and experiment with respect to the crystal structures used to quantify errors in computed geometries. This replacement should be sufficient for this study as the enormous database of results for transition metal complexes[23-28] repeatedly demonstrates that with sufficiently flexible valence basis sets, DFT accurately reproduces/predicts experimental geometries.

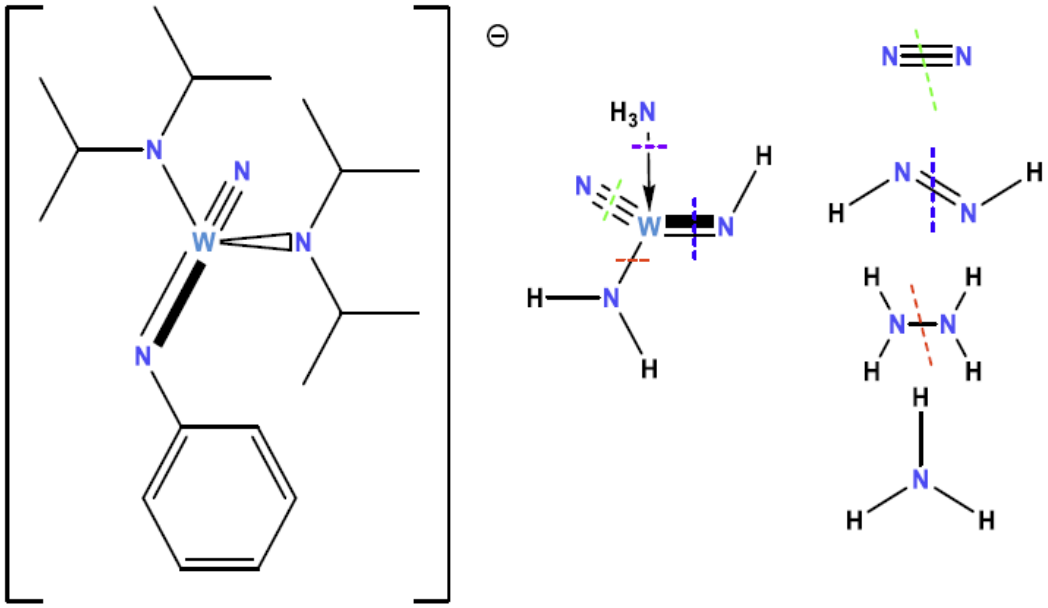

Figure 2.3: Beaumier complex;[20] Cr in the experimental complex has been replaced with W to facilitate comparison with other complexes in this study (left); computational model used (center), and main group analogs. Color coded dashed lines depict the bond cleavage modeling comparisons. Note that the dative W←NH_3 bond is not homolyzed, but cleaved so as to maintain the neutrality of the metal and main group fragments generated.

The levels of theory employed herein are those typically employed in modeling studies for medium to large organometallic and inorganic complexes.[29-31] The methods are also calibrated vis-à-vis relevant bond enthalpy data for small molecule, main group analogs; the latter have either been experimentally determined[32,33] or can be computed via the use of high-accuracy composite *ab initio* techniques. Note that many previous transition metal benchmarking studies have emphasized absolute thermodynamic values such as heats of formation, while the present work focuses on metal-ligand bond enthalpies and the σ- and π-bond enthalpy components thereof.

DeYonker *et al.* use the correlation consistent Composite Approach (ccCA) to compute thermochemical properties such as ΔH_f with greater emphasis on 3d transition metal complexes.[34,35] Other works including Harding *et al.*, focus more on high accuracy thermochemical modeling using coupled cluster approaches, complex basis set extrapolations, etc. to develop HEAT354-(Q) methods that provide excellent predictive thermodynamic data, but with much greater cost than DFT methods.[36] Similarly, Laury and Wilson performance test DFT methods for 4d transition metal thermochemistry and found DFT wanting in comparison to the accuracy and precision of their relativistic pseudopotential-based composite method (rp-ccCA).[37] The present work focuses more on the specifics of the σ- and π- component contributions to heavier transition metal-element BDEs, and the precision in predicted BDEs among the different levels of theory, an excellent primer on which may be found by Frenking and Fröhlich.[29]

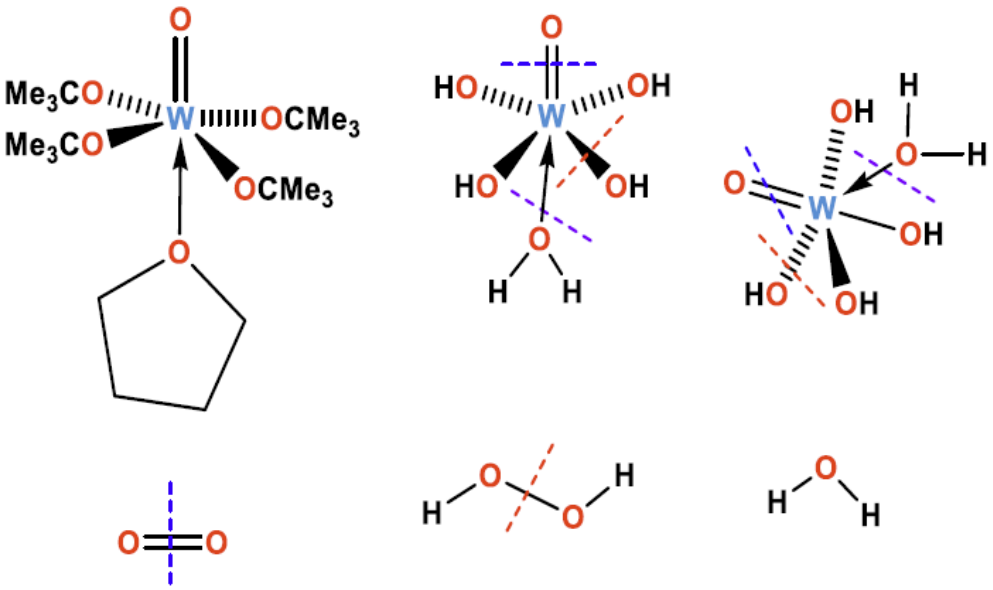

Figure 2.4: Cotton structure[21] (upper left), the cis and trans computational models used (upper center and right, respectively), and main group analogs (bottom). Color-coded dashed lines denote the homolytic bond enthalpies that were computed. Note that the dative W←OH_2 bond is not homolyzed but cleaved so as to maintain the neutrality of the metal and main group fragments thus generated.

The complex of Cotton *et al.*[21] (Fig. 2.4) is octahedral, which provides an opportunity to

assess the impact of the trans influence with respect to metal-ligand bond strengths. As such, while the experimental complex is *trans*, the *cis* isomer is also modeled herein.

For ease of computation of the homolytic bond enthalpies, simplified chemical models are used in which bulky organic substituents are replaced by hydrogen or methyl moieties. Dative W←E bonds are not homolyzed, but calculated by removal of the neutral, Lewis base ligand (water, ammonia, *etc*. depending on the target complex). The bond enthalpy of each unique W–E, W=E, W≡E and W←E bond is modeled by rupture of the bond of interest into two fragments (one main group, one organometallic) broken along the color-coded dashed lines in Figures 2.2, 2.3, and 2.4. The difference in the computed enthalpies between the whole model complexes and the sum of the two fragments yields the homolytic bond dissociation enthalpies (BDEs). Note that the starting complex and any derived fragments used for BDE calculations are fully geometry optimized as neutral species in their appropriate ground spin states.

The same procedure is used to then compare organometallic BDEs with congeneric bond types in small main group molecules for which experimental or high-level *ab initio* thermodynamic data is available. Comparisons are then made based on the calculated bond enthalpies across the computational methods, selected basis sets, pseudopotentials, and bond types. To quote Frenking and Fröhlich, "A model is an abstract of the reality; it cannot be right or wrong; it can only be more or less useful." To this end, the computational design used herein is intended to give a broad overview of the BDEs found in specific WE models. It is expected that error is reduced by using different metal-ligand bond types for related, idealized (but still chemically relevant) models, within a single complex.

2.3 Computational Methods

All calculations, except four MP2 calculations, were run with the Gaussian 09 software

package in the gas phase at standard temperature (298.15 K) and pressure (1 atm).[38] Four MP2 optimizations of the Churchill organometallic fragment generated by cleavage of the W–C single bond (Fig. 2.2) were run with Gaussian 16[39] using the new Opt=RecalcFC=20 option to achieve convergence of these difficult geometry optimizations. A combination of widely used functionals and valence basis sets are used, the latter augmented with d-polarization functions for the associated main group elements. A list of functionals and basis sets employed in this work can be found in Figure 2.5.[40-47]

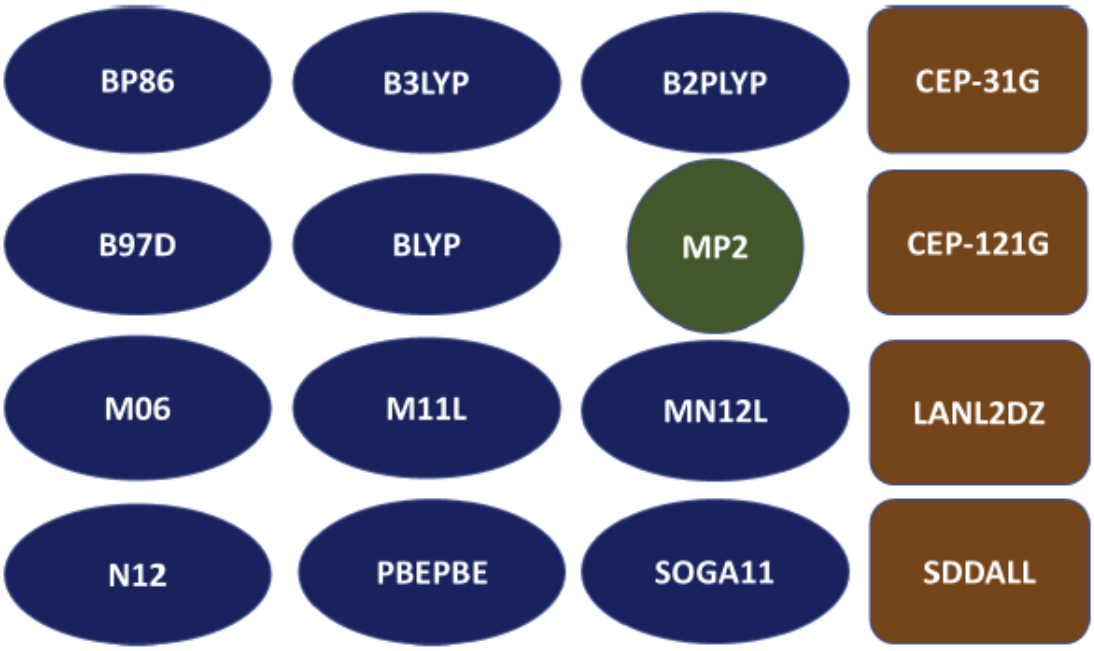

Figure 2.5: The DFT functionals (blue), valence basis sets (brown) explored, and post-Hartree-Fock wavefunction methods (green) examined for this research.[40-47]

Furthermore, the thermodynamic data obtained for the small main group homologs are calibrated with respect to the G4 and W1U levels of theory.[48-51] All complexes and fragments thereof are modeled as neutrals with all appropriate spin multiplicities (low, intermediate and high spin) investigated to determine the lowest energy structure. Enthalpies are reported in kcal/mol. All calculations yield minima upon geometry optimization, defined as having 0 imaginary vibration frequencies via calculation of the energy Hessian. As used herein, accuracy is the extent each BDE

approaches the 'true' value, the evaluation of which is obviously complicated by the paucity of experiments. The reported standard deviations provide a measure of how precise a particular valence basis set and/or functional are.

2.4 Results and Discussion

There are two primary foci in this work: WE (E = C, N, O) prediction of metal-ligand bond dissociation enthalpies, including σ- and π -bond energy components, and assessing the uncertainty of these predictions for commonly used levels of theory in the literature. The first part of the Results and Discussion section presents the results for the BDE models broken out by 2p element (E) for both the ME bonds and EE main group homologs. The second half discusses the computational models, providing insight into their geometric and thermodynamic accuracy and precision as well as any observed eccentricities in the individual methods.

2.4.1 Homolytic Bond Dissociation Enthalpies (BDEs)

This section is divided into three parts to present each of the 2p elements (E = C, N, O) separately. The trends in homolytic bond enthalpies of the entire dataset are discussed in Summary and Conclusions. In this section the data show that for tungsten and 2p nonmetal ligands the σ-bond is always stronger than the π-bond, as expected. Interestingly, it is seen that if a metal-element triple bond is present, the second ME π-bond is stronger than the first π-bond. Interestingly, this trend does not hold for triply-bonded main group homologs.

2.4.1.1 Carbon

The computations for tungsten-carbon bond dissociation enthalpies (BDEs) are derived from the model W(dmpe)(–CH_2Me)(=CHMe)(≡CMe) in Figure 2.6 (center), dmpe = 1,2-(dimethylphosphino)ethane. The W≡C, W=C, W-C bonds have calculated BDEs of 136.5 ± 10.1,

94.0 ± 9.7, and 61.4 ± 11.8 kcal/mol, respectively, for the levels of theory tested (Fig. 2.6). These BDEs are less than the analogous triple, double and single CC bonds in hydrocarbons: but-2-yne, trans-but-2-ene, and butane = 197.8 ± 16.6, 167.2 ± 11.5, and 87.2 ± 15.6 kcal/mol, respectively, for the same suite of methods.

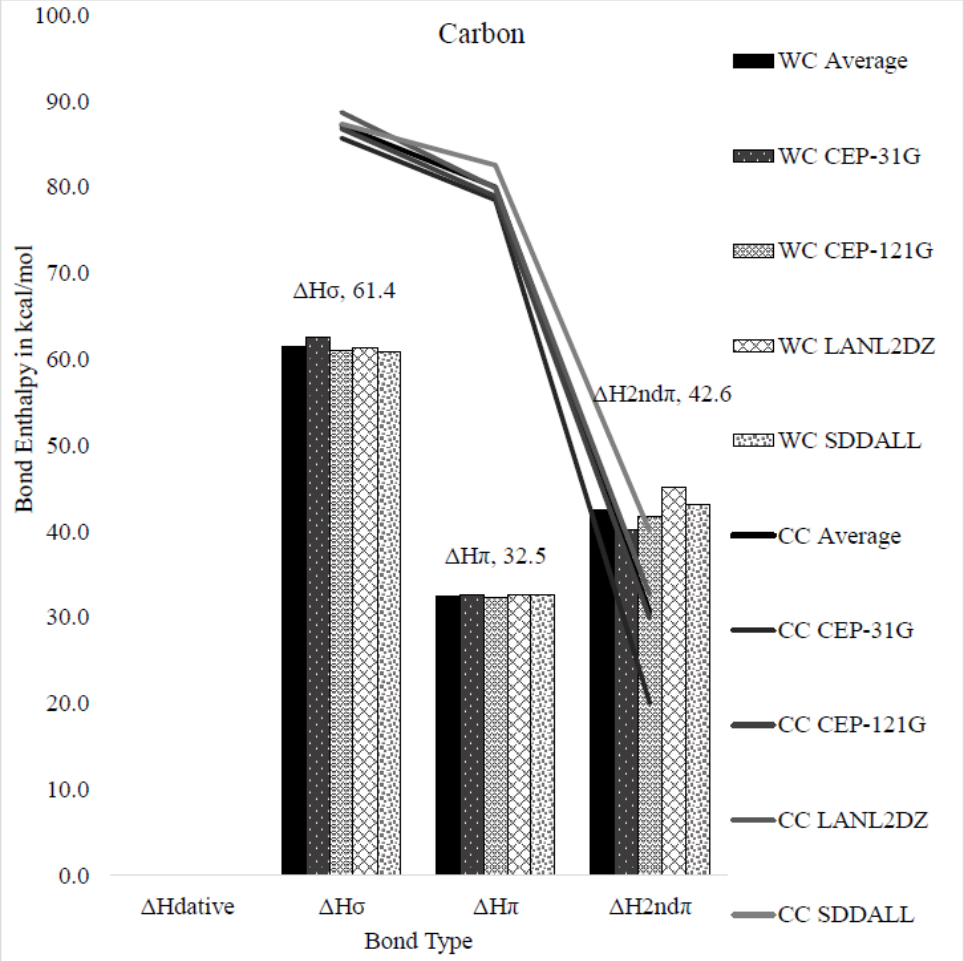

Figure 2.6: Average tungsten-carbon (columns) and carbon-carbon (lines) bond enthalpies by bond type and basis set. Average tungsten-carbon values (left-most solid column) are inset above the columns; the textured columns the average values for each valence basis set.

From these data, BDEs of the WC bond components are 42.6 ± 10.9, 32.5 ± 7.1, and 61.4 ± 11.8 kcal/mol for the 2nd π bond, 1st π bond, and σ bond, respectively (Fig. 2.6). The 1st π bond enthalpy is defined by subtracting the BDE of the WC single bond from the corresponding double bond BDE. The 2nd π bond is defined by subtracting the BDE of the WC double bond from the

corresponding triple bond BDE. Interestingly, the 1st π bond is weaker than the 2nd WC π bond, by ~10.0 kcal/mol; presumably, a shorter bond length (W≡C vs. W=C) and thus better orbital overlap, significantly enhances π-bond strength.

2.4.1.2 Nitrogen

The model utilized for this research is inspired by the fascinating complex of Beaumier *et al.*[20] (Fig. 2.3), W(←NH_3)(–NH_2)(=NH)(≡N) and possesses four different tungsten-nitrogen bond types. The nitrido, imido, amido and ammino tungsten-nitrogen bonds have calculated BDEs of 156.1 ± 12.7, 122.0 ± 14.4, 104.4 ± 10.9 and 47.4 ± 4.0 kcal/mol, respectively, across all 48 levels of theory tested (Fig. 2.7). As a comparison, for the small molecule homologs the computed BDEs of N_2, HN=NH, H_2N–NH_2 are: 217.7 ± 9.8, 120.2 ± 7.3, 64.0 ± 4.9 kcal/mol, respectively, for the same suite of functionals and basis sets. Interestingly, the standard deviations for the main group and organometallic BDEs loosely mirror each other for single, double and triple bond types.

A bit of poetic license was taken with the original experimental structure[20] to convert the anionic complex to a neutral species (to maintain similarity with the other models) – while preserving a coordination number of four – with a dative bond to ammonia replacing one of the amido ligands to yield a W^{VI} model complex. This decision was made to permit additional analysis of WN bond components: 34.1 ± 8.6, 17.6 ± 17.3, 104.4 ± 10.9, and 47.4 ± 4.0 kcal/mol for the 2nd π bond, 1st π bond, σ bond and dative bond, respectively, in the model (Fig. 2.7). As with the WC complex, the 1st π bond is significantly (~16.5 kcal/mol) weaker than the 2nd π bond. This is an intriguing result in that the bonds between transition metals and nitrogen-based ligands such as imides and nitrides may have ambiguous bond orders due to the availability of lone pairs on nitrogen that may or may not participate in bonding with the metal depending on the latter's d-count and ligand field splitting.

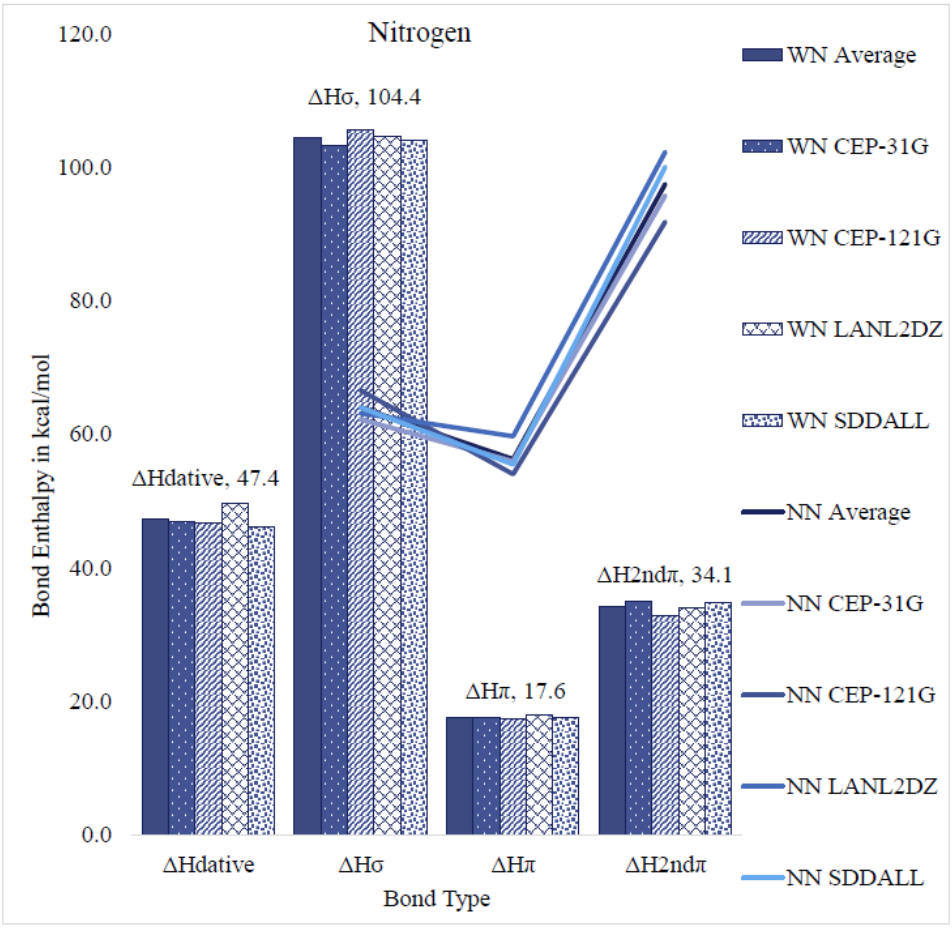

Figure 2.7: Average tungsten-nitrogen (columns) and nitrogen-nitrogen (lines) bond enthalpies by bond type and basis set. Average tungsten-nitrogen (left-most solid column) are inset above the columns; the textured columns are the average values for each valence basis set.

2.4.1.3 Oxygen

The Cotton complex[21] (Fig. 2.4) with its octahedral geometry provides an opportunity to quantify the thermodynamic impact of the trans effect/influence, one of the most important reactivity and structural effects in coordination chemistry.[52-54] Tungsten has a formal d^0 configuration in the model complex, implying that the WO bond is more W≡O in character than W=O.[55]

For the *trans*-$W(O)(OH)_4(OH_2)$ model, the oxo, hydroxyl, and datively bound water have calculated BDEs to tungsten of 161.0 ± 6.0, 93.1 ± 6.1, and 13.6 ± 3.2 kcal/mol, respectively (Fig.

2.8). Thus, for the π and σ bonds in the complex, the computed BDEs are 67.8 ± 6.0 and 93.1 ± 6.1 kcal/mol assuming the W-oxo bond is formally a double bond. The calculated OO bond enthalpies for the main group analogs are 122.3 ± 7.5 kcal/mol for O_2 and 49.9 ± 6.9 kcal/mol for hydrogen peroxide.

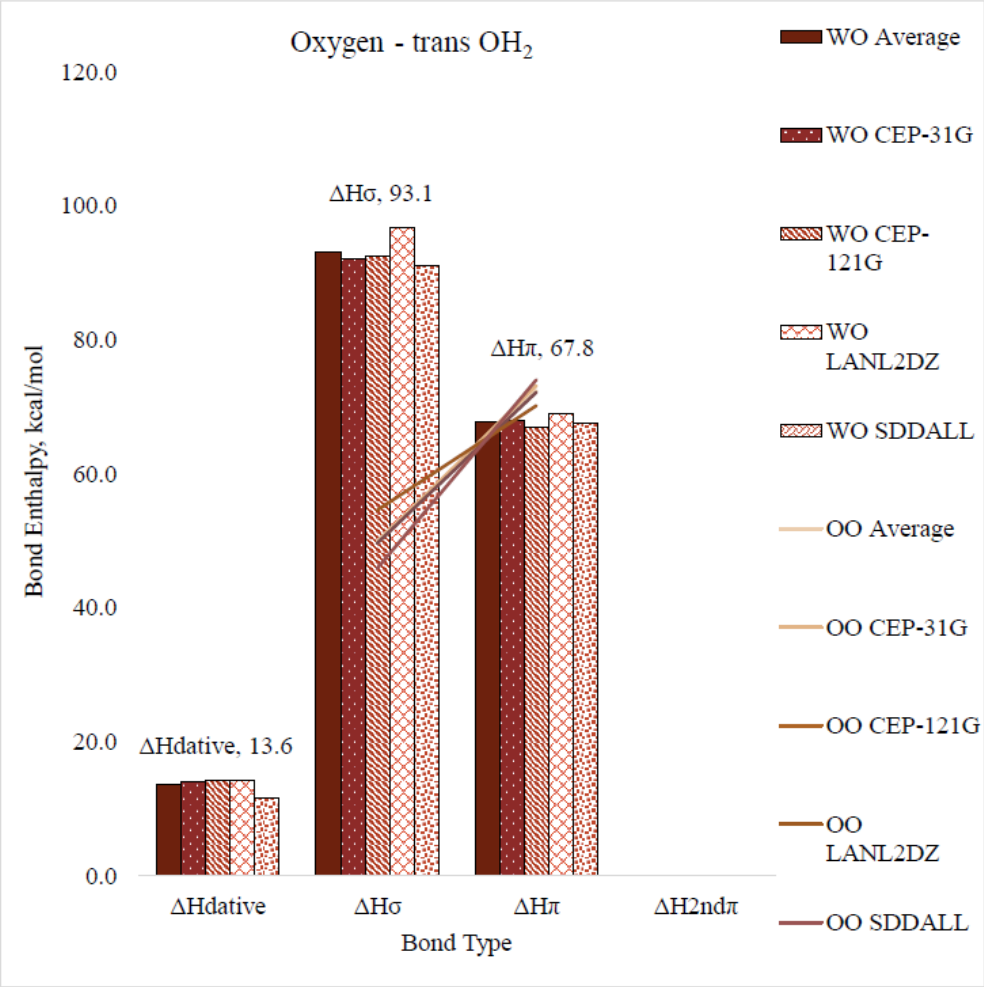

Figure 2.8: Average WO (columns) and OO (lines) bond enthalpies by bond type and basis set for the H_2O trans model complex. Average tungsten-oxygen (left-most solid column) are inset above the columns; the textured columns are the average values for each valence basis set.

For the *cis* tungstenyl model (Figs. 2.4 and 2.9), each W–OH bond homolysis is categorized in reference to the ligand to which it is trans. The dative bond for the water complex weakens from 13.6 ± 3.2 in *trans*-$W(O)(OH)_4(OH_2)$ to 6.3 ± 3.2 kcal/mol in *cis*-$W(O)(OH)_4(OH_2)$. The single bond strengths of the hydroxyls change from 93.1 ± 6.1 kcal/mol for the *trans* model, where all

hydroxyls are chemically equivalent, to 86.2 ± 6.3 kcal/mol for the OH trans to OH, to 85.9 ± 6.0 kcal/mol for the OH trans to water, and 78.5 ± 6.4 kcal/mol for the OH trans to the oxo ligand. Interestingly, these are all less than the W–OH bond strength of the *trans* isomer. Although the higher BDE for the hydroxyl trans to oxo seems counterintuitive, the computations indicate that the impact of trans influence on the W–OH bond strength is ~7 kcal/mol for the $W(=O)(OH)_4(OH_2)$ model.

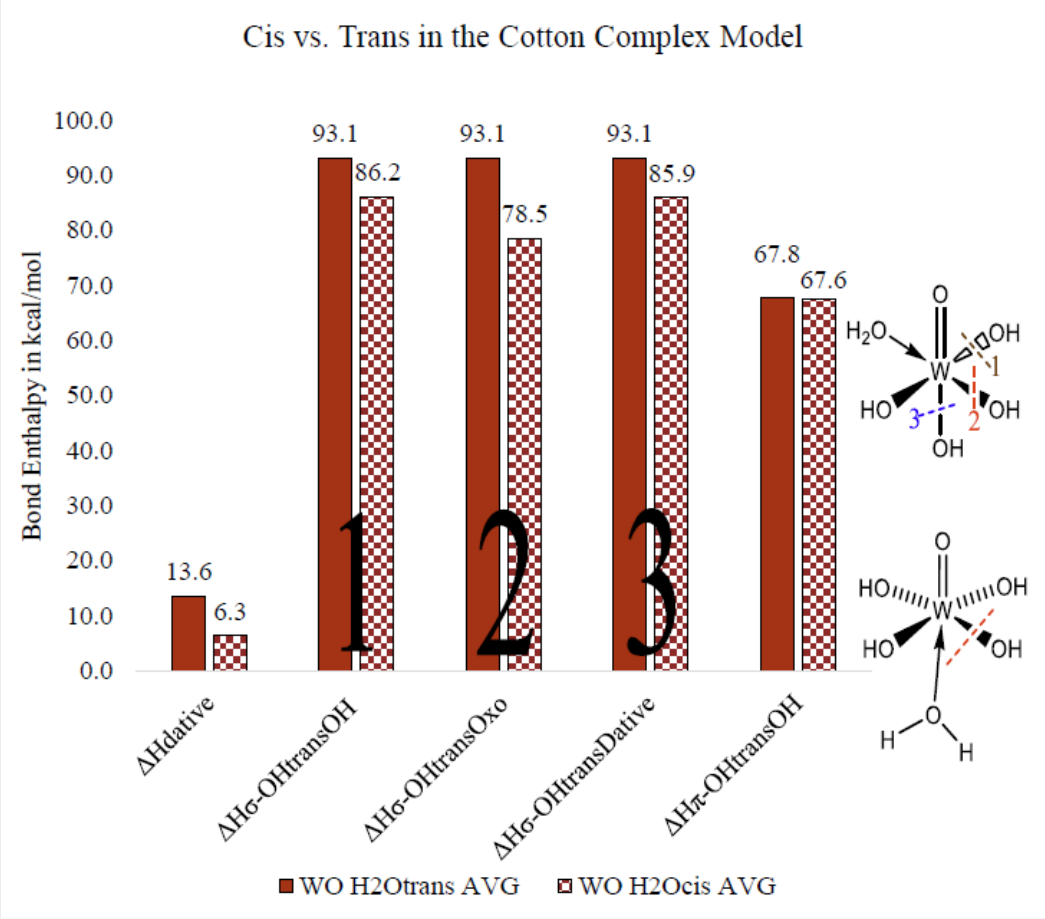

Figure 2.9: Oxygen bond enthalpies for Cotton model[21] complexes with cis and trans structures inset and chemically different hydroxyl ligands chromatically labeled along with the corresponding BDE data: hydroxyl ligand trans to hydroxyl labeled 1 in brown, hydroxyl ligand trans to oxo ligand labeled 3 in blue, and hydroxyl ligand trans to dative bond labeled 2 in red.

The aqua complex models show that the oxo ligand has the greatest labilizing effect on the hydroxyl trans to it, by 14.6 kcal/mol. All of the tungsten-ligand bonds other than the W-oxo bond

in the models are weakened by 7.4 kcal/mol for the dative bond, 6.9 kcal/mol for the OH trans to another OH, 14.6 kcal/mol in the OH trans to the oxo ligand, and 7.2 kcal/mol in the OH trans to the dative bond. As such, the present study helps quantify the thermodynamic extent to which trans influence can alter metal-ligand bond strengths, which can be exploited in catalyst design.

2.4.2 Comparison among Computational Methods

When analyzing bond enthalpy data, it is reasonable to question the accuracy and precision of the methods used.[56,57] Typically, this is difficult to do for d-block organometallic and inorganic complexes given the extreme paucity of experimental data with which to calibrate against. Therefore, to gauge the computed uncertainty in W-element BDEs, in this research forty-eight different combinations of DFT functionals and valence basis sets were applied to the computed BDEs and then compared. This section is divided into three parts, two "global" performance discussions and a section on notable "local" idiosyncrasies in the calculations. The two means of performance testing are geometric analysis referencing the crystal structure data and thermodynamic comparisons against the generally accepted bond enthalpy data. The oddities are included as cautionary notes as to the selection of uncalibrated levels of theory in future modeling studies of organometallics.

2.4.2.1 Accuracy vs. Crystal Structure Data

This study tests twelve functionals with four basis sets and compares the fully optimized structure with experimental values. For each tungsten-ligand bond length the percent error was consistently within 5% across the entire dataset; interestingly, predictions are more sensitive to the functional than the basis sets. Note that the structural data for the nitride model exaggerates the determined errors as the model has W replacing Cr, hence the comparison to the Cambridge Database[58] averages to assess computed WN bond lengths.

For the tungsten-2p element bonds, across the set of four bond types – single, double, triple, dative – for the three ligand types (O, C, N), the mean error for the bond lengths is 3.6% with a standard deviation of 2.5%.

In contrast, bond angles are slightly more sensitive to the wavefunction than the Hamiltonian, as expected given that angular deformation generally takes less energy than bond stretching. Overall, across the set of four ligand types and three 2p elements, the mean error for ligand-metal-ligand bond angles is 6.0% with a standard deviation of 2.7%. For a full heat map of the percent errors found organized by functional and basis set for each 2p element and as aggregates, see Appendix A.

2.4.2.2 Accuracy vs. Higher-level Theory and Experiment for BDEs of Main Group Homologs

Small molecule thermodynamic data for 2p element compounds have generally been experimentally well-established,[31,32,33] which makes these useful reference points in relation to the organometallic complexes studied here. Experimental bond enthalpies for the CC multiple bonds of E-but-2-ene or but-2-yne were not found. Hence, the data available for ethene and acetylene were used as an initial gauge of uncertainties in BDEs one might expect from composite *ab initio* techniques such as G4 and W1U. Calibration against ethene and acetylene suggested that G4 and W1U methods predict C=C and C≡C bond enthalpies to within ± 1 – 2 kcal/mol of experiment (Table 2.1).

The calculated BDEs for the main group homologs reveal variation in the error depending upon which DFT functional and basis sets are used. Overall, the average DFT-predicted values for the homolytic BDEs are quite good when compared to either the G4 or UW1 values (Fig. 2.10). The absolute percent errors in BDEs vary significantly as seen in Figure 2.11. On average, the methods tested are reasonable when compared to experiment or high-level composite *ab initio*

techniques (Table 2.2) but the errors become more pronounced with an increase in EE bond order. The exact values calculated for each E–E, E=E, and E≡E bond organized by functional and basis set are collected in Appendix A. The box-and-whisker plots depict the typical degree of variation among the functionals with respect to the bond type (Fig. 2.11; additional plots are contained in Appendix A).

Table 2.1: Average bond dissociation enthalpies in kcal/mol calculated with standard deviations as compared to the three reference points used for comparision.[32,33]

Small Molecule		DFT		BDE		
		AVG	±	Exp	G4	W1U
Carbon						
triple[a]	$H_3CC{\equiv}CCH_3$	193.1	8.6	229.5[a]	203.6	204.6
double[a]	$H_3CHC{=}CHCH_3$	167.3	9.4	172.2[a]	171.3	171.8
Single	$H_3CH_2C\text{-}CH_2CH_3$	82.9	5.2	86.8	87.1	88.2
Nitrogen						
Triple	N≡N	219.0	6.5	225.9	226.3	225.4
Double	HN=NH	120.8	2.5	129.1	122.2	123.6
Single	$H_2N\text{-}NH_2$	63.8	2.1	67.4	64.9	66
Oxygen						
Double	O=O	120.3	8.2	119.1	118.6	118.9
Single	HO-OH	49.3	6.9	51.0	49.0	50.1

[a] The experimental (exp) values for the CC multiple bonds of E-but-2-ene or but-2-yne could not be found, so values for ethylene and acetylene are provided for comparison.[32] Calibration of G4 and W1U against known bond enthalpies and acetylene suggest that the BDEs given in the table should be accurate to within ± 1 – 2 kcal/mol.

2.4.2.3 Oddities in the Computational Data

In the calculations for the Churchill complex, the rupture of the W=C bond necessitated the calculation of both singlet and triplet methyl carbene as their enthalpies are sufficiently close. It has been experimentally shown that the triplet is the lower energy state,[59-62] which is why all of the present calculations of bond strength use the computed enthalpy of the triplet methyl carbene. However, not all of the functionals used found the triplet spin state to be lower than the

corresponding singlet. Certain functionals, specifically M11L and MN12L, show the methyl carbene fragment as favoring a singlet rather than a triplet state. Specifically, M11L favors the singlet by ~5.1 ± 2.3 kcal/mol and MN12L favors the singlet by ~7.7 ± 3.9 kcal/mol for the different pseudo-potentials/basis sets examined herein.

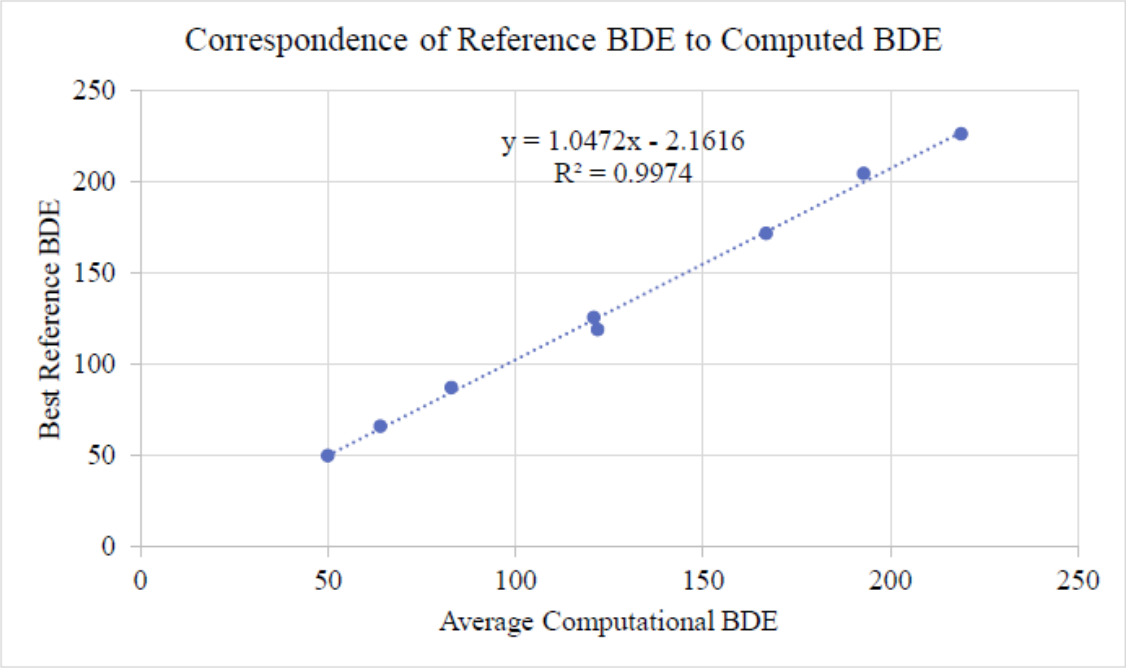

Figure 2.10: Plot of best reference BDEs – average values for G4 and W1U – to overall average DFT-computed BDE data for small main group homonuclear species (H_nEEH_n, n = 0, 1, 2 or 3; E = C, N or O).

Despite the overall consistency found for DFT versus the "best" (average of G4 and W1 values) estimates of main group-main group bond enthalpies, it is interesting that the organometallic bond enthalpies have a narrower standard deviation versus the small molecule congeners for the different levels of theory studied. For example, there is significant variation in the DFT-calculated values for the second π-bond of 2-butyne (std. dev. = ±11.5 kcal/mol) and in the N_2 data for the second π-bond (std. dev. ±6.4 kcal/mol).

It is also worth noting that there is very little consistency in the thermodynamic calibration datasets (Table 2.2). Certain functionals would give large errors for three of the four basis sets, but

relatively small ones for the fourth (e.g., B3LYP, M11L, MN12L). In other cases, a basis set and functional would give low errors for some BDEs and high errors for others. Using the W1U level of theory for comparison, this can be seen in N12/LANL2DZ(d) which has C≡C and O=O in the top ten best performers and both C=C and N=N amongst the poorest. Similarly, M11L/CEP-121G(d) is among the top 10 for C=C and C≡C, and yet among the poorest performers for N≡N and O-O. The best example of this phenomenon is SOGGA11/LANL2DZ(d) with three in each: C–C, C=C, and N=N are among the best, while N-N, O–O and O=O among the lowest performing (Table 2.2). Given the paucity of experimental data available for organometallics, caution is thus needed in ascribing undue significance to results from a specific level of theory without calibration across a series of functionals and basis sets. The present study suggests that evaluation of a range of different functional types must be evaluated for determination of critical bond strengths in transition metal catalysis applications.

Table 2.2: Best- and poorest-performing DFT levels of theory relative to best reference BDE data (experiment[32,33] or high-level ab initio theory) in the absence of experiment) for small main group homonuclear species (H_nEEH_n, n = 0, 1, 2 or 3; E = C, N or O). Note that all basis sets include a d polarization function on E.

Experimental Data		G4		W1	
Best Performing					
2.8%	BD97D/SDDALL	1.7%	PBEPBE/SDDALL	2.1%	PBEPBE/SDDALL
3.3%	PBEPBE/SDDALL	2.3%	B97D/SDDALL	2.2%	B97D/SDDALL
3.0%	MP2/LANL2DZ	2.9%	M11L/LANL2DZ	3.1%	MP2/CEP-121G
Poorest Performing					
13.2%	B3LYP/CEP-121G	11.2%	M11L/SDDALL	11.9%	B3LYP/CEP-121G
13.7%	M11L/SDDALL	7.3%	BLYP/SDDALL	14.3%	BLYP/SDDALL
18.3%	B3LYP/CEP31G	18.4%	B3LYP/CEP-31G	19.1%	B3LYP/CEP-31G

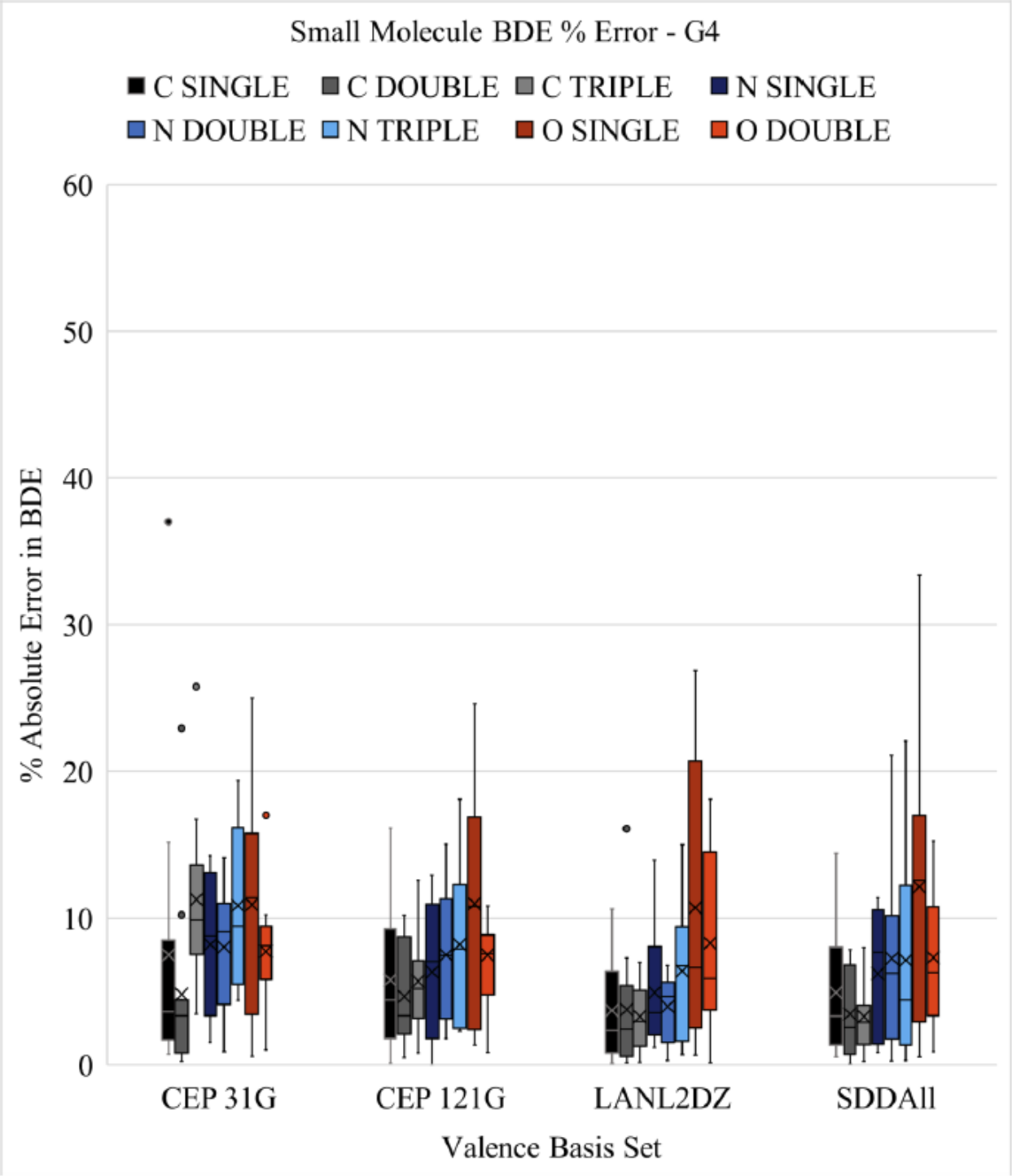

Figure 2.11: Box and whisker plot showing percent absolute error as a function of bond type for the small molecule with respect to the G4 calculation data (similar plots for experiment and W1U calculations are given in Appendix A). The arithmetic mean is indicated with an X, the median depicted with a horizontal line, and the outliers are left as dots. An extreme outlier is not included in this box and whisker plot, the BLYP/SDDAll(d) predicted carbon-carbon triple bond enthalpy has an error versus experiment of 57.9%.

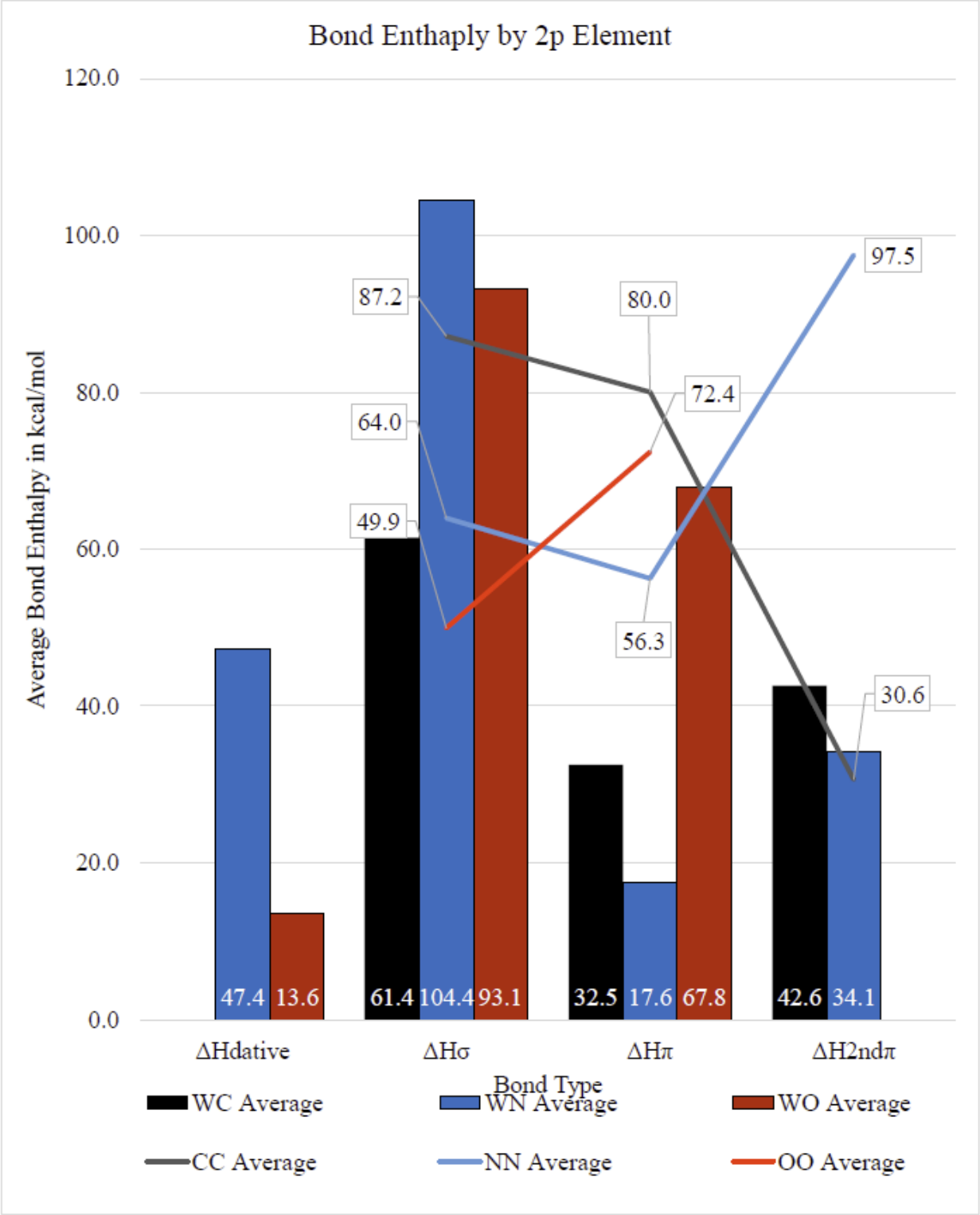

Figure 2.12: Summary of average computed bond enthalpies (kcal/mol) by element and bond type when coordinated to tungsten with bars as WE and lines for EE color coded by element for comparison.

2.5 Summary and Conclusions

In summary, vast portions of predictive chemistry are derived from knowledge, or assumptions, of the (in)stability of various molecular bonds and bond components. Reaction mechanisms are frequently rationalized through an understanding of which bonds are likely to be thermodynamically weaker – and hence more kinetically reactive – based on the chemical characteristics of a particular reagent. For metal complexes and organometallic reactions this knowledge is important in catalysis, but is often unavailable from experiment or of unknown accuracy and precision from calculations, particularly for the near ubiquitous DFT methods. This study of tungsten and a selection of σ- and π-bonding 2p ligand types provides valuable insight into the challenges of bond enthalpy prediction using common DFT/basis set protocols in the literature. While the thermochemistry of compounds of lighter main group compounds have been well studied, it has proven much more difficult to experimentally quantify the strengths of σ and π bonds for transition metals.[29]

The Churchill, Beaumier, Cotton *et al.* crystal structures form the foundation of the computational models used in this research (Figs. 2.2, 2.3, & 2.4).[19-21] The size and scope of these models is restricted to small complexes computed in the gas phase, which thus constitutes a limitation of the models employed herein... Geometric data are accurately predicted as has come to be expected of density functional theory methods in conjunction with sufficiently flexible basis sets. The metal-ligand bond lengths on average have 2.9 ± 2.1% absolute error across the entire suite of 48 levels of theory tested in this work. Furthermore, ligand-metal-ligand bond angles have an average of 5.9 ± 2.7 % absolute error, and so percent errors are roughly double those in relation to predicted bond lengths. Additional details are available in Appendix A for the different computational models evaluated.

The BDEs of small molecule homologs (H_nEEH_n, n = 0, 1, 2 or 3; E = C, N or O) are benchmarked against three different metrics (Table 2.1). First, they are compared against experimental values, where available. The median percent absolute error is 8.0 ± 6.3% with respect to the experimental data. Second, the overall average percent errors are 7.3 ± 6.2% with respect to the high-accuracy G4 composite *ab initio* BDE values. Third, DFT-predicted BDEs differ by 7.2 ± 6.4% with respect to the W1U-calculated BDEs. The overall median percent absolute error rates do rise modestly from carbon to nitrogen to oxygen regardless of which pseudopotential/valence basis set data are used for comparison. However, the correspondence of the "best" reference BDE data vis-à-vis the average DFT-computed BDEs (Fig. 2.10) has an R^2 value of 0.9974, a slope near unity, and an intercept of roughly 2 kcal/mol, thus indicating excellent overall reliability for the DFT techniques.

The DFT-computed enthalpy data show that for tungsten bonded to 2p element ligands, as expected, the σ-bond is always stronger than the π-bond. Interestingly, if a triple bond is present the second π-bond is stronger than the first π-bond (Fig. 2.12). This trend does not hold true for the 2p homologs, which follow the trend of 2^{nd} π > 1^{st} π > σ for nitrogen- and oxygen, and σ > 1^{st} π > 2^{nd} π for carbon.

Table 2.3: Average computed homolytic WE (E = C, N, O) bond dissociation enthalpies in kcal/mol.

Bond	Single	Double	Triple
WC	61.4	94.0	136.5
WN	104.4	122.0	156.1
WO	93.1		161.0

From carbon to nitrogen to oxygen the homolytic bond enthalpy increases with bond order (Table 2.3). The tungsten-nitride BDE (156 kcal/mol) is roughly 20 kcal/mol stronger than a tungsten-alkylidyne (136½ kcal/mol). On the other hand, the tungsten-oxo ligand BDE (161 kcal/mol) is 39 kcal/mol stronger than the tungsten-imido BDE (122 kcal/mol), which in turn is

28 kcal/mol than the tungsten-alkylidene BDE (94.0 kcal/mol). As these are d^0 complexes, the obvious conclusion from the computed thermodynamics is that the W-oxo bond is more akin to a triple bond as discussed by Gray in his seminal paper on metal-oxo bonding.[63] The tungsten-oxo bond is far stronger than any other bond studied in this research, and clearly stands out as a triple bond via the current thermodynamic analyses.

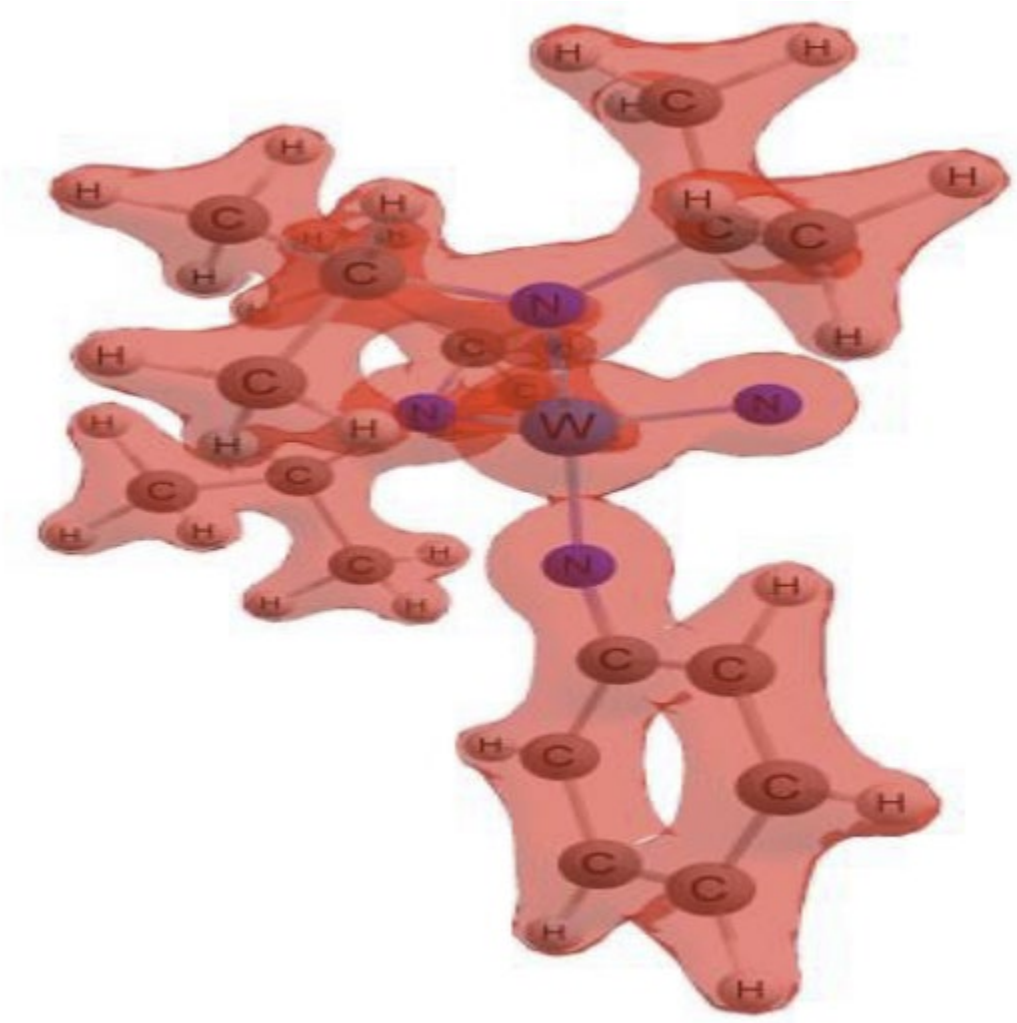

Figure 2.13: Electron density plot of the full model tungsten complex highlighting the electron density on the nitride and imide moieties (PBEPBE/SDDALL, IsoValue = 0.144).

The aforementioned difference in WN 1st and 2nd π-bond strengths may underpin the differences in reactivity for metal-element multiple bonds as compared to the element-element multiple bonds, and the typical stability of metal-element triple bonds versus double bond

congeners. For instance, imide (NR^{2-}) ligands are generally highly π-basic, donating electron density to a metal with low d-electron counts. A formally tri-anionic nitride ligand is expected to be even more π-basic than di-anionic imide. This makes the lack of reactivity of terminal nitrides of early to middle series metals in relation to imides somewhat surprising, for example as is the case in Beaumier *et al.*'s complex[20] and its reactivity with MeI. Kinetic arguments are often made to explain such discrepancies; however, the electron density plots for the tungsten model complex do not fully support such arguments. When the electron density of $[W(N)(=NPh)(N^iPr_2)_2]^-$ is visualized (Fig. 2.13), it becomes apparent that the charge density is in the W≡N internuclear region and in the N lone pair (largely 2s in character). This is consistent with the often-muted reactivity of nitride ligands when coordinated to low d-count transition metal ions. Rather, the BDE data for the model W-complex, $W(NH_3)(NH_2)(=NH)(\equiv N)$, elucidate a possible thermodynamic explanation for why the preferred site for nucleophilic attack by MeI is the imide ligand. For MeI to react with a W=NR moiety, the first π-bond must break, whereas reaction with the M≡N moiety, entails breaking the second π-bond. The latter is significantly stronger (34.1 ± 8.6 kcal/mol) than the former (17.6 ± 17.3 kcal/mol). This thermodynamic penalty is likely reflected in a kinetic penalty for MeI addition. Hence, the computed BDE data provide insight into why the M=NR moiety is nucleophilically attacked while the M≡N is not.

Research that preceded this study indicated that the M=N π-bond strength in imido model complexes[4] was a key descriptor for determining which methane CH activation mechanism is favored. Stronger metal-nitrogen π-bonds directed activation to either the metal (oxidative addition) or ligand (H-atom abstraction) as opposed to 1,2-addition across the metal-imido bond. Hence there is great potential in M=N and M≡N bonds for alkane and aryl CH bond activation in catalysis through understanding the thermodynamic response of metal-nitrogen π-bonds to metal,

supporting ligand and substituent (on both the actor and supporting ligands) modification. By the same chain of reasoning, tungsten-alkylidene bonds with π-bond strengths of ~33 kcal/mol as compared to tungsten-imido bonds at ~17 kcal/mol may be expected to be less reactive, but also be accessible for catalysis as this is roughly half the π-bond strength of a C=C bond. On the other hand, the sheer thermodynamic strength of the tungsten-oxo bond (161.0 kcal/mol) makes it very stable. The 67.8 kcal/mol average calculated BDE_{π} value for the WO tungsten-oxo bond is more than double the WC tungsten-alkylidene value (32.5 kcal/mol) and roughly triple that computed for the WN tungsten-imide (17.6 kcal/mol).

The tungsten-oxo ligand in Cotton *et al.*'s octahedral complex[21] is trans to the dative ligand and has a strong trans influence. Modeling the complex in a cis configuration allowed the trans influence of the oxo ligand to be quantified. A comparison between the trans and cis models demonstrates that the influence of the oxo moiety is observed in the BDE of every bond in the complex. The cis complex has all bonds, except the W-oxo bond, weakened by between 7 and 21 kcal/mol, which suggests a very significant thermodynamic impact, commensurate with some of the π-bond strengths just discussed.

Future work extending this study includes research on W-3p nonmetal ligand bond types. Efforts may be further expanded to include the rest of the p-block in their most common bond formations as well as a far broader set of metals, as well as to assessing how the supporting and actor ligand environment can impact W-element bonds and their σ- and π-bond enthalpy components, in particular those cases in which other π-bonding ligands are coordinated to the same metal, thus competing for M d_{π} – E p_{π} bonding.

2.6 Supporting Information

A detailed accounting of the computed homolytic bond enthalpy and geometric data found

with respect to each functional/valence basis set are available in the supporting information for all models. This material can be found at http://pubs.acs.org and in Appendix A.

2.7 Acknowledgements

K.K. acknowledges the University of North Texas' Texas Academy of Math & Sciences (TAMS) program for a 2018 Undergraduate Research Summer Scholarship. This material is based upon work supported by the National Science Foundation Graduate Research Fellowship Program under Grant No. 1746050. Any opinions, findings, and conclusions or recommendations expressed in this material are those of the author(s) and do not necessarily reflect the views of the National Science Foundation.

2.8 References

1. Simões, J. A. M.; Beauchamp, J. L. Transition Metal–Hydrogen and Metal–Carbon Bond Strengths: The Keys to Catalysis. *Chem. Rev.* **1990**, *90*, 629–688.

2. Ceylan, Y. S.; Cundari, T. R. Computational Analysis of Transition Metal-Terminal Boride Complexes. *J. Phys. Chem. A* **2017**, *121*, 9358–9368.

3. Durand, D.; Fey, N. Computational Ligand Descriptors for Catalyst Design; *Chem. Rev.* **2019**.

4. Moulder, C. A.; Cundari, T. R. A DFT Survey of the Effects of D-Electron Count and Metal Identity on the Activation and Functionalization of C−H Bonds for Mid to Late Transition Metals. *Isr. J. Chem.* **2017**, *57*, 1023–1031.

5. Cundari, T. R. Computational Studies of Transition Metal-Main Group Multiple Bonding. *Chem. Rev.* **2000**, *100*, 807–818.

6. Davies, H. M. L.; Morton, D. Recent Advances in C-H Functionalization. *J. Org. Chem.* **2016**, *81*, 343-350.

7. Mayernick, A. D.; Janik, M. J. Methane Activation and Oxygen Vacancy Formation over CeO_2 and Zr, Pd Substituted CeO 2 Surfaces. *J. Phys. Chem. C* **2008**, *112*, 14955–14964.

8. Tomson, N. C.; Arnold, J.; Bergman, R. G. Halo, Alkyl, Aryl, and Bis(Imido) Complexes of Niobium Supported by the β-Diketiminato Ligand. *Organometallics* **2010**, *29*, 2926–2942.

9. Kriegel, B. M.; Bergman, R. G.; Arnold, J. Nitrene Metathesis and Catalytic Nitrene Transfer Promoted by Niobium Bis(Imido) Complexes. *J. Am. Chem. Soc.* **2016**, *138*, 52–55.

10. Sicilia, E.; Mazzone, G.; Pérez-González, A.; Pirillo, J.; Galano, A.; Heine, T.; Russo, N. Direct and Cluster-Assisted Dehydrogenation of Methane by $Nb^+$and Ta^+: A Theoretical Investigation. *Phys. Chem. Chem. Phys.* **2017**, *19*, 16178–16188.

11. Hirsekorn, K. F.; Hulley, E. B.; Wolczanski, P. T.; Cundari, T. R. Olefin Substitution in $(Silox)_3M(Olefin)$ (Silox = $^tBu_3SiO$; M = Nb, Ta): The Role of Density of States in Second vs Third Row Transition Metal Reactivity. *J. Am. Chem. Soc.* **2008**, *130*, 1183–1196.

12. Cundari, T. R. Methane Activation by Group V Bis(Imido) Complexes. *Organometallics* **1994**, *13*, 2987–2994.

13. Maurya, M. R.; Rana, L.; Avecilla, F. Oxidoperoxidotungsten(VI) and Dioxidotungsten(VI) Complexes Catalyzed Oxidative Bromination of Thymol in Presence of H_2O_2-KBr-$HClO_4$. *Inorg. Chim. Acta* **2016**, *440*, 172–180.

14. Bianchi, S.; Bortoluzzi, M.; Castelvetro, V.; Marchetti, F.; Pampaloni, G.; Pinzino, C.; Zacchini, S. The Reactivity of Tungsten Hexachloride with Tetrahydrofuran and 2-Methoxyethanol. *Polyhedron* **2016***, 117*, 769–776.

15. Paul, S. S.; Selim, M.; Saha, A.; Mukherjea, K. K. Synthesis and Structural Characterization of Dioxomolybdenum and Dioxotungsten Hydroxamato Complexes and Their Function in the Protection of Radiation Induced DNA Damage. *Dalton Trans.* **2014***, 43*, 2835–2848.

16. Hay, P. J. Ab Initio Theoretical Studies of Dihydrogen Coordination vs. Oxidative Addition of H2 to Five-Coordinate Tungsten Complexes. *J. Am. Chem. Soc.* **1987***, 109*, 705–710.

17. Haxel, G. B.; Hedrick, J. B.; Orris, G. J. Rare Earth Elements — Critical Resources for High Technology. United States Geol. Surv. Fact Sheet **2002**, 87, 4 ff. https://pubs.usgs.gov/fs/2002/fs087-02/fs087-02.pdf, (Accessed April 4, 2019).

18. Ziegler, T.; Tschinke, V.; Becke, A. A Theoretical Study on the Relative Strengths of the Metal—Hydrogen and Metal—Methyl Bonds in Complexes of Middle to Late Transition Metals. *J. Am. Chem. Soc.* **1987***, 109*, 1351–1358.

19. Churchill, M. R.; Youngs, W. J. Crystal Structure and Molecular Geometry of $W(.Tplbond.CCMe_3)(:CHCMe_3)(CH_2CMe_3)$(Dmpe), a Mononuclear Tungsten(VI) Complex with Metal-Alkylidyne, Metal-Alkylidene, and Metal-Alkyl Linkages. *Inorg. Chem.* **1979***, 18*, 2454–2458.

20. Beaumier, E. P.; Billow, B. S.; Singh, A. K.; Biros, S. M.; Odom, A. L. A Complex with Nitrogen Single, Double, and Triple Bonds to the Same Chromium Atom: Synthesis, Structure, and Reactivity. *Chem. Sci.* **2016***, 7*, 2532–2536.

21. Cotton, F. A.; Schwotzer, W.; Shamshoum, E. S. Further Studies of the Reactions of Ditungsten Hexa-t- Butoxide with Acetylenes. Isolation and Characterization of $WO(OCMe_3)_4(THF)$, $[W_3(OCMe_3)_5(\mu\text{-}O)(\mu\text{-}CC_3H_7)O]_2$ and $W(CPh)(OCMe_3)_3$. *J. Organomet. Chem.* **1985***, 296*, 55–68.

22. M. Winter. WebElements Periodic Table https://www.webelements.com/tungsten/ (accessed Nov 13, 2018).

23. Laurent, A.; Jacquemin, D. TD-DFT Benchmarks; A Review. *Int. J. Quantum Chem.* **2013***, 113*, 2019-2039.

24. Ghosh, S.; Verma, P.; Cramer, C. J.; Gagliardi, L.; Truhlar, D. G. Combining Wave Function Methods with Density Functional Theory for Excited States. *Chem. Rev.* **2018***, 118*, 7249–7292.

25. Lischka, H.; Nachtigallová, D.; Aquino, A. J. A.; Szalay, P. G.; Plasser, F.; MacHado, F. B. C.; Barbatti, M. Multireference Approaches for Excited States of Molecules. *Chem. Rev.* **2018***, 118*, 7293–7361.

26. Korth, M.; Grimme, S. "Mindless" DFT Benchmarking *J. Chem. Theory Comput.* **2009***, 5*, 993-1003.

27. Bencini, A. Some Considerations on the Proper Use of Computational Tools in Transition Metal Chemistry. *Inorganica Chim. Acta* **2008***, 361*, 3820–3831.

28. Ryu, H.; Park, J.; Kim, H. K.; Park, J. Y.; Kim, S. T.; Baik, M. H. Pitfalls in Computational Modeling of Chemical Reactions and How to Avoid Them. *Organometallics* **2018***, 37*, 3228–3239.

29. Frenking, G.; Fröhlich, N. The Nature of the Bonding in Transition-Metal Compounds. *Chem. Rev.* **2000***, 100*, 717-774.

30. Frenking, G.; Krapp, A. Unicorns in the World of Chemical Bonding. *J. Comput. Chem.* **2007***, 28,* 15-24.

31. Boehme, C.; Frenking, G. Electronic Structure of Stable Carbenes, Silylenes, and Germylenes. *J. Am. Chem. Soc.* **1996***, 118*, 2039-2046.

32. Luo, Y.-R. *Handbook of Bond Dissociation Energies in Organic Compounds*; CRC Press: Boca Raton, FL, **2003**.

33. Haynes, W. M. *CRC Handbook of Chemistry and Physics 2016-2017, 96th ed*.; CRC Press: Boca Raton, FL, **2016**.

34. DeYonker, N. J.; Wilson, B. R.; Pierpont, A. W.; Cundari, T. R.; Wilson, A. K. Towards the Intrinsic Error of the Correlation Consistent Composite Approach (CcCA). *Mol. Phys.* **2009***, 107*, 1107–1121.

35. DeYonker, N. J.; Williams, T. G.; Imel, A. E.; Cundari, T. R.; Wilson, A. K. Accurate Thermochemistry for Transition Metal Complexes from First-Principles Calculations. *J. Chem. Phys.* **2009***, 131*, 24106.

36. Harding, M. E.; Vázquez, J.; Ruscic, B.; Wilson, A. K.; Gauss, J.; Stanton, J. F. High-Accuracy Extrapolated Ab Initio Thermochemistry. III. Additional Improvements and Overview. *J. Chem. Phys.* **2008***, 128*, 114111.

37. Laury, M. L.; Wilson, A. K. Performance of Density Functional Theory for Second Row (4d) Transition Metal Thermochemistry. *J. Chem. Theory Comput.* **2013***, 9,* 3939–3946.

38. Gaussian 09, Revision E.03, Frisch, M. J.; Trucks, G. W.; Schlegel, H. B.; Scuseria, G. E.; Robb, M. A.; Cheeseman, J. R.; Scalmani, G.; Barone, V.; Mennucci, B.; Petersson, G. A.; et al. Gaussian, Inc., Wallingford CT, 2009.

39. Gaussian 16, Revision A.03. Frisch, M. J.; Trucks, G. W.; Schlegel, H. B.; Scuseria, G. E.; Robb, M. A.; Cheeseman, J. R.; Scalmani, G.; Barone, V.; Petersson, G. A.; Nakatsuji, H.; et al. Gaussian, Inc., Wallingford CT, 2016.

40. Becke, A. D. Density-Functional Exchange-Energy Approximation with Correct Asymptotic Behavior. *Phys. Rev. A* **1988***, 38*, 3098–3100.

41. Adamo, C.; Scuseria, G. E.; Barone, V. Accurate Excitation Energies from Time-Dependent Density Functional Theory: Assessing the PBE0 Model. *J. Chem. Phys.* **1999***, 111*, 2889–2899.

42. Adamo, C.; Barone, V. Inexpensive and Accurate Predictions of Optical Excitations in Transition-Metal Complexes: The TDDFT/PBE0 Route. *Theor. Chem. Acc.* **2000***, 105*, 169–172.

43. Møller, C.; Plesset, M. S. Note on an Approximation Treatment for Many-Electron Systems. *Phys. Rev.* **1934***, 46*, 618–622.

44. Bartlett, R. J. Perspective on "on the Correlation Problem in Atomic and Molecular Systems. Calculation of Wavefunction Components in Ursell-Type Expansion Using Quantum-Field Theoretical Methods." *Theor. Chem. Acc.* **2000***, 103*, 273–275.

45. Hay, P. J.; Wadt, W. R. Ab Initio Effective Core Potentials for Molecular Calculations. Potentials for the Transition Metal Atoms Sc to Hg. *J. Chem. Phys.* **1985***, 82*, 270–283.

46. Ma, F.; Xie, H. Bin; Chen, J. Benchmarking of DFT Functionals for the Kinetics and Mechanisms of Atmospheric Addition Reactions of OH Radicals with Phenyl and Substituted Phenyl-Based Organic Pollutants. *Int. J. Quantum Chem.* **2018***, 118*, e25533.

47. Cundari, T. R.; Stevens, W. J. Effective Core Potential Methods for the Lanthanides. *J. Chem. Phys.* **1993***, 98*, 5555–5565.

48. Curtiss, L. A.; Redfern, P. C.; Raghavachari, K. Gaussian-4 Theory. *J. Chem. Phys.* **2007***, 126*, 084108.

49. Curtiss, L. A.; Redfern, P. C.; Raghavachari, K. Gn Theory. *Wiley Interdisciplinary Reviews: Computational Molecular Science*. John Wiley & Sons, Ltd September 1, **2011**, pp 810–825.

50. Martin, J. M. L.; De Oliveira, G. Towards Standard Methods for Benchmark Quality Ab Initio Thermochemistry - W1 and W2 Theory. *J. Chem. Phys.* **1999***, 111*, 1843–1856.

51. Barnes, E. C.; Petersson, G. A.; Montgomery, J. A.; Frisch, M. J.; Martin, J. M. L. Unrestricted Coupled Cluster and Brueckner Doubles Variations of W1 Theory. *J. Chem. Theory Comput.* **2009***, 5*, 2687–2693.

52. Hartwig, J. F. *Organotransition Metal Chemistry: from Bonding to Catalysis*; University Science Books: Mill Valley, CA, **2010**, pp 217-245.

53. Miessler, G. L.; Fischer, P. J.; Tarr, D. A. *Inorganic Chemistry*, 5th ed.; Pearson: Boston, MA, **2014**, p 462.

54. Crabtree, R. H. *The Organometallic Chemistry of the Transition Metals*, 5th ed.; Wiley: Hoboken, NJ, **2009**, p 7.

55. Gray, H. B.; Winkler, J. R. Living with Oxygen. *Acc. Chem. Res.* **2018***, 51*, 1850–1857.

56. Korth, M.; Grimme, S. Mindless DFT Benchmarking. *J. Chem. Theory Comput.* **2009***, 5*, 993–1003.

57. Lupp, D.; Christensen, N. J.; Fristrup, P. Synergy between Experimental and Theoretical Methods in the Exploration of Homogeneous Transition Metal Catalysis. *Dalt. Trans.* **2014***, 43*, 11093–11105.

58. Groom, C. R.; Bruno, I. J.; Lightfoot, M. P.; Ward, S. C.; *Acta Cryst.* **2016***, B72*, 171-179.

59. Montgomery, C. Fischer and Schrock Carbene Complexes: A Molecular Modeling Exercise. *J. Chem. Educ.* **2015***, 92*, 1653-1660.

60. Hahn, F. E. Introduction: Carbene Chemistry. *Chem. Rev.* **2018***, 118*, 9455-9456.

61. Schrock, R. R. High Oxidation State Multiple Metal−Carbon Bonds. *Chem. Rev.* **2002***, 102,* 145-180.

62. Moerdyk, J. P.; Bielawski, C. W. Stable Carbenes. Contemp. Carbene Chem. 2013, 40–74.

63. Ballhausen, C. J.; Gray, H. B. The Electronic Structure of the Vanadyl Ion. Inorg. Chem. 1962, 1, 111–122.

CHAPTER 3

THERMOCHEMISTRY OF TUNGSTEN – 3P ELEMENTS FOR DFT, CAVEAT LECTOR!*

3.1 Abstract

There are two primary foci in this research on WE (E = Si, P, and S) bonds: prediction of their bond dissociation enthalpies, including σ- and π-bond energy components, and assessing the uncertainty of these BDE predictions for levels of theory commonly used in the literature. Internal standards for computational accuracy include metal-element bond lengths (mean absolute error = 1.8 ± 1.2%), main group homolog BDEs vs. higher levels of ab initio theory (W1U and G4 BDEs, R2 = 0.98), and DLPNO-CCSD(T)/def2-QZVPP calculations for metal-ligand BDEs (R2 = 0.88). The W=Si 1st π-bond is underreported for DFT/MP2 methods vs. DLPNO-CCSD(T), while the latter shows negligible strength for the W≡Si 2nd π-bond, consistent with the literature. This research highlights clear issues with the underlying assumptions required for the use of perturbation theory methods for the fragments derived from W–P homolysis. The difficulties associated with modeling the metal thermochemistry with DFT (and MP2) levels of theory are manifest in the broad standard deviations observed. However, average BDEs found using 48 popular DFT and MP2 levels of theory are reliable, 10.8 ± 6.8% mean absolute error (with W–P removed) compared vs. DLPNO-CCSD(T); with the caveat that individual basis set/pseudopotential/valence basis set combination can vary wildly. Analysis of the absolute error percentages with respect to level of theory indicate little benefit to going higher on Jacob's Ladder, as simpler methods have lower error versus high-level ab initio techniques such as G4 and DLPNO-CCSD(T).

* This chapter is reproduced from Moulder, C. A.; Kafle, K.; Zhou, C. X.; Cundari, T. R., Thermochemistry of Tungsten-3p Elements for Density Functional Theory, Caveat Lector! **J Phys Chem A 2021**, 125 (2), 681-690. DOI: 10.1021/acs.jpca.0c05351, with permission from the American Chemical Society.

3.2 Introduction

The thermodynamics of bond formation and cleavage is a key governing principle of chemical reactions. In transition metal catalysis, bond stability is critically important, particularly the σ and π-bond components of a metal-ligand multiple bond. The criticality of metal-carbon and metal-hydrogen bond energies is reflected in their reference as "the keys to catalysis" by Simões and Beauchamp in a classic review on transition metal thermochemistry.[1] Stability, and thereby reactivity, can thus be altered through covalent, electrostatic, steric, *etc*. effects imparted by the supporting ligands upon the metal and substituents on the actor ligand for organometallic catalysts in predictable, albeit typically not quantifiable, ways.[2,3] For example, Moulder and Cundari observed in a methane C–H activation study by imide complexes (LnM=NR, M = Group 8 - 10 metals) that the strength of the metal-imide π-bond – and how this thermodynamic quantity was modulated as a function of metal identity – was a critical factor in determining the preferred activation mechanism: [2+2] vs. oxidative addition vs. hydrogen atom abstraction.[4]

The early 4d and 5d transition metals are "green" in both the economic and ecological senses (Fig. 2.1) and are widely used in industrial catalysis.[5] Many olefin metathesis catalysts have heavy, early transition metal centers like molybdenum and tungsten, Schrock's catalysts being a notable example.[6-9] Some 4d/5d metal catalysts like Grubbs catalysts and myriad iridium and rhodium catalysts may be considered green given the recyclability of the metal.[10] Ziegler-Natta metallocenes classically feature Group 4 metals and are currently widely used for polyolefin production.[11-14]

Despite its critical importance, experimental data for metal-ligand bond thermochemistry, especially for s and p components, is virtually non-existent. It is currently impossible to experimentally dissect the enthalpic contributions of the individual bond components for a general

series of metal-element bond types.[1,15] Theoretical methods can help bridge this gap and provide a means to access homolytic metal-ligand bond enthalpies and assess σ and π components.[16] Such bond enthalpies would be useful in guiding inorganic/organometallic catalytic design.[17,18] This work presents a somewhat naïve approach in that it focuses on a set of popular DFT functionals, as well as second order Møller–Plesset perturbation theory, to model the homolytic cleavage of tungsten – 3p element bonds, although the 11 functional subset chosen (Fig. 2.5) is anticipated be representative of the greater superset of available functionals.[19] Through the use of multiple levels of theory, both density functional theory (DFT) and wavefunction methods, benchmarks for Earth-abundant 5d transition metals are generated to address the question of the precision of such predictions. In the absence of experiment, as is often the case in transition metal thermochemistry for larger, more realistic complexes, the accuracy of DFT is evaluated relative to couple cluster calculations, specifically the DLPNO-CCSD(T) variant of Neese and coworkers, at DFT-optimized geometries.[20,21]

The present research extends a previous study by Moulder *et al.* for tungsten with the 2p main group elements (E = C, N, O).[22] Both works use the same suite of methodologies to permit a solid basis of comparison between W-2p and W-3p databases. By using the same DFT methodologies, the sensitivity of the metal-energy bond enthalpies and their components can be more readily assessed across a set of catalytically relevant bonding motifs for many of the most popular functionals and effective core potentials/valence basis sets. While there are high accuracy methods like HEAT and the correlation consistent Composite Approach (ccCA)[23-26] this work uses these DFT functionals and valence basis sets specifically because they are commonplace in transition metal catalyst modeling.[27] Moreover, apart from the ccCA family of *ab initio* composite methods, composite techniques are not applicable to d-block chemistry; the ccCA composite

method of Wilson and coworkers is very expensive for larger organometallics, and is to our knowledge, not yet available for 5d elements. The precision of the computed metal-ligand bond strengths, including their σ and π components, is thus sought herein to further assess the reliability of DFT studies for transition metal catalysis.[28,29]

The coordination chemistry of 3p main group elements (WE = Si, P, and S) is highly relevant in inorganic and organometallic chemistry and so are studied here to see how they compare and contrast with the reported thermochemistry of the 2p congeners.[2,22,30,31] To this end, the present research takes advantage of the isoelectronic nature of silicon, phosphorus, and sulfur to carbon, nitrogen, and oxygen, respectively, to construct models with similar coordination environments.

For a W-silicon model complex, the Churchill alkyl-alkylidene-alkylidene[32] has been updated to replace ligating C–H functionalities with Si–Me moieties (Fig. 3.1). Capping silicon with methyl groups was found necessary in preliminary studies as Si–H derivatives lead to a-agostic MSiH bonding in the optimized stationary points,[33,34] which was deemed to introduce too much additional ambiguity vis-à-vis the designation of metal-silicon p-bond orders.

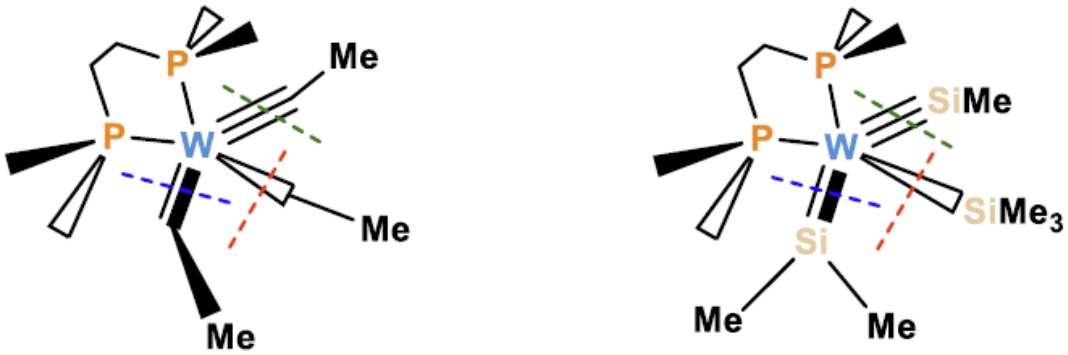

Figure 3.1: Conversion of Churchill's W-carbon computational model[19,29] to a W-silicon variant; color coded dashed lines denote the studied bond homolyses.

While carbon and silicon are isoelectronic, it is of course naïve to believe that their

reactivity and thermochemistry will be similar.[35] Silylene catalysts have long been sought to attempt potential innovations that would take advantage of the similarities and differences between silicon and carbon chemistry.[36] For example, Waterman *et al.* discuss the behavior of silylene ligands acting as a Lewis acid to an electron-rich metal center and being stabilized by effects such as p-backbonding.[37] The thermochemistry of silylene complexes is thus expected to be quite distinct from that of carbene congeners and the model in Figure 3.1 is designed to elucidate and quantify some of the underlying thermochemistry involved.

Transformation of a tungsten-nitrogen complex (Fig. 3.2) derived from the crystal structure of Beaumier *et. al.*[38] to a tungsten-phosphorus model is interesting. Nitrogen- and phosphorus-based ligands are both well studied, but typically have divergent electronic properties in that nitrogen-based ligands are often hard s-donors whereas phosphorus-based congeners, notably phosphines, are soft s-donors and p-acceptors. The ambiguity of lone pairs on ligating pnictogen atoms – in particular the extent to which they may be donated to vacant metal-based orbitals of appropriate symmetry in complexes such as imides and phosphinidenes ($L_nM{=}PR$) – also appears to play a key role in the thermochemistry of such moieties.[30,39-42]

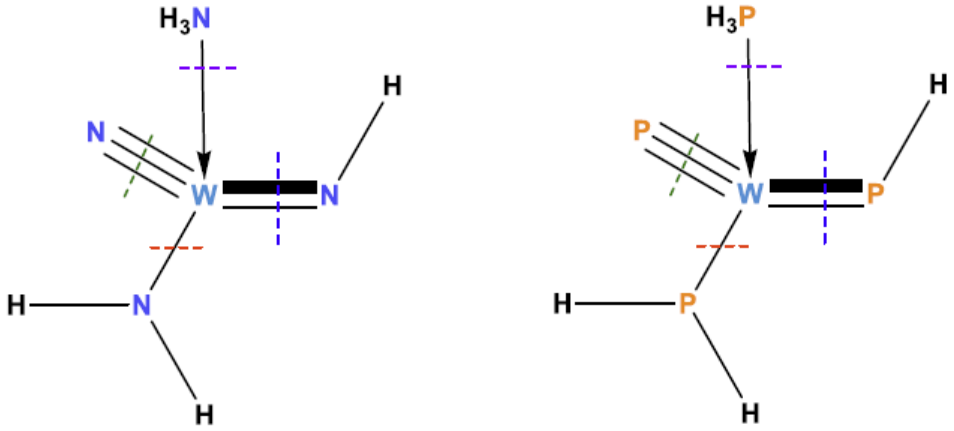

Figure 3.2: Conversion of a reported W-nitrogen computational model[19,35] to a W-phosphorus computational model; color coded dashed lines denote the studied bond homolyses.

For the tungsten-sulfur model employed herein (Fig. 3.3), the tungsten-oxo complex from the Cotton lab[43] is utilized to not only compare sulfur with the lighter chalcogen, but to provide insight into the trans-influence of the sulfido moiety on the d^0 complex.[44-46]

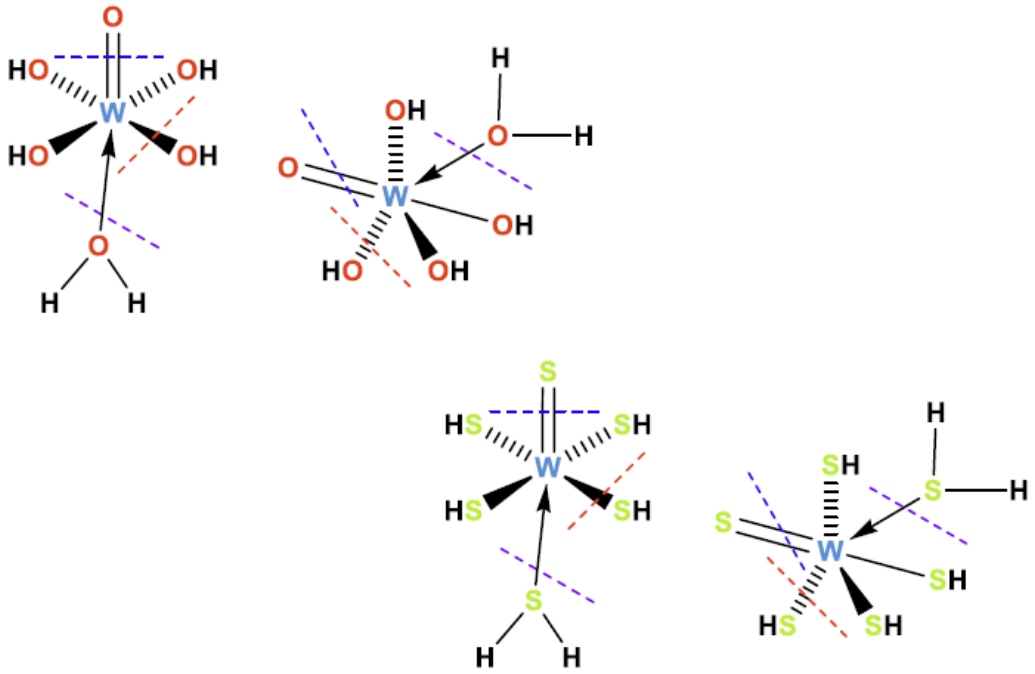

Figure 3.3: Conversion of a reported W-oxygen complex[19,41] to its W-sulfur congener; color coded dashed lines denote the bond homolysis comparisons.

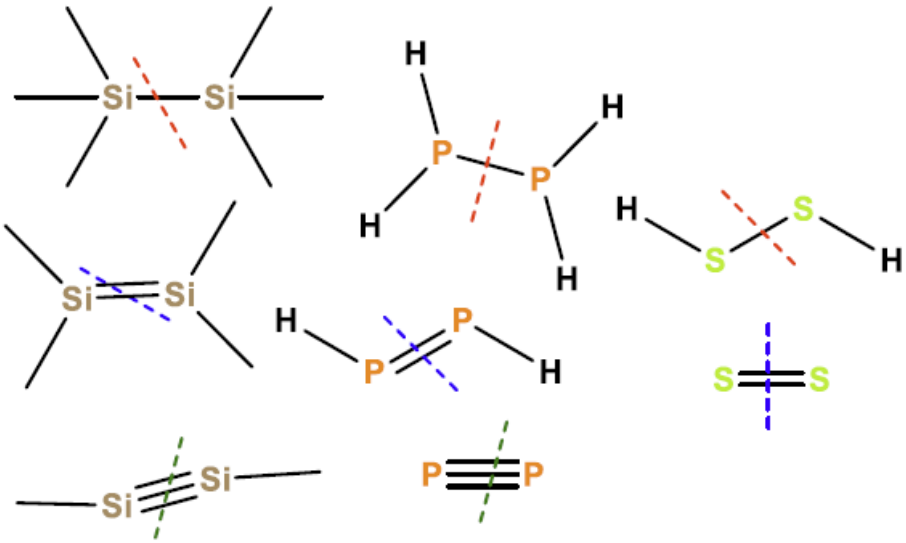

Figure 3.4: Main group homologs for each computational model with color coded dashed lines denote the bond homolysis comparisons.

Small main group homologs in Figure 3.4 are also calibrated with the G4 and, where feasible, W1U levels of theory.[47-50] When the small main group homologs were found insufficient, an additional set of reference data is generated using ORCA[51,52] and DLPNO-CCSD(T)/def2-QZVPP[20,21] single point calculations (at SOGGA11/CEP-31G(d) optimized minima) to provide a high accuracy reference for both the main group homologs and for the organometallic complexes.

The various plots and graphics in the present study are color-coded to facilitate organization and comparison of the datasets. The standard CPK colors for silicon, phosphorus, and sulfur are nude, orange, and yellow, respectively. For the 2p elements, a black, blue, and red color scheme is used for carbon, nitrogen, and oxygen, respectively. Similarly, the homolytic cleavage of the metal-ligand bonds are denoted by dashed lines in red for single bonds, blue for double, and green for triple bonds as well as violet for the dissociation of the dative bond; the latter is, of course, cleaved heterolytically, generating a neutral Lewis base.

3.3 Computational Methods

All calculations save the DLPNO-CCSD(T)[53] simulations have been run with the Gaussian 09 software package in the gas phase at standard temperature (298.15 K) and pressure (1 atm).[54] A selection of widely used functionals and pseudopotentials and valence basis sets, the latter augmented with d-polarization functions for the associated main group elements, form the main body of the computations analyzed. All metal complexes and fragments thereof are modeled as neutrals with all appropriate spin multiplicities (low, intermediate and high spin) investigated to determine the lowest energy structure. Figure 2.5 provides a graphical list of the functionals and basis sets used.[55-61] An additional set of internal standards are generated using ORCA and DLPNO-CCSD(T)/def2-QZVPP single point calculations (at SOGGA11/CEP-31G(d) optimized minima).[20,21,51-53]

All enthalpies are derived from clearly defined minima with no imaginary vibrational frequency from the energy Hessian, and are reported in kcal/mol. The 2nd π-bond enthalpy for a metal-element is defined by subtracting the calculated BDE of the W=E double bond from the corresponding triple bond BDE. The 1st π-bond BDE is defined by the difference between the double bond and the single bond enthalpies. Note that these definitions assume that, for example, the W–E σ-bond is the same strength in the W–E, W=E and W≡E bonds, which can lead to difficulties as discussed later. The standard deviations reported herein quantify how precise each valence basis set and/or functional are for the models used. The accuracy of each BDE as it approaches the "true" value is convoluted by the dearth of experimental data and is therefore reported in this paper with respect to higher-level *ab initio* calculations.

3.4 Results and Discussion

There are two primary foci in this research: (a) for WE (E = Si, P, and S) bonds, prediction of their bond dissociation enthalpies, including σ- and π-bond energy components, and (b) assessing the uncertainty of these BDE predictions for commonly used levels of theory. The first part of the Results and Discussion section presents the results for the calculated BDEs organized by 3p element (E) for both the ME organometallics as well as EE main group homologs. The second half of this section discusses the computational models, providing insight into their geometric and thermodynamic accuracy and precision as well as any observed eccentricities in the individual methods. All pertinent data has been provided in the Supporting Information B.3. There is little valence basis sets dependence for WE BDEs. The DFT/MP2 functional choice provides the greatest variance in the values calculated for BDEs (*vide infra*) as seen in the box-and-whisker plots in Appendix B. The accuracy of each individual bond enthalpy with respect to the DLPNO-

CCSD(T)/def2-QZVPP//SOGGA11/CEP-31G(d) level of theory as shown in Table 3.5 is also provided in Appendix B.

3.4.1 Homolytic Bond Dissociation Enthalpies (BDEs)

The trends in homolytic bond enthalpies for the overall set of 3p elements are discussed in Summary and Conclusions and compared with previous findings[22] for the 2p elements. In this section the data show that for tungsten and 3p nonmetal ligands the σ-bond is always stronger than the π-bond, as expected. Interestingly, it is seen that for a metal-element triple bond, the second WE π-bond is stronger than the first π-bond, akin to the trend computed for W-2p elements.[22] The MP2 results are not included in the averages for the BDE values reported herein, which focus on DFT results, and are instead discussed at length in Appendix B. The Møller–Plesset perturbation theory models had large errors that necessitated their exclusion from the data analysis. Furthermore, the analyses of the small molecule reference homologs are in Appendix B, as well.

3.4.1.1 Silicon

The tungsten-silicon model (Fig. 3.1) for bond dissociation enthalpies (BDEs) is derived from W(dmpe)(–$CH_2{}^tBu$)(=CH^tBu)(≡C^tBu), dmpe = 1,2-(dimethylphosphino)ethane.[32] For silicon ligating atoms all α-H have been replaced with methyl groups to eliminate agostic W(SiH) interactions.[33,34] The model is W(dmpe)(–$SiMe_3$)(=$SiMe_2$)(≡ SiMe), dmpe = 1,2-(dimethyl-phosphino)ethane.

The W≡ Si, W=Si, W–Si bonds have calculated BDEs of 95.1 ± 8.0, 70.7 ± 8.8, and 65.0 ± 12.1 kcal/mol, respectively, for the 48 levels of theory tested (Fig. 3.5). The calculated tungsten-silicon BDEs have a different pattern from the silicon-silicon triple, double and single SiSi bonds in the main group congeners: MeSi≡ SiMe, Me_2Si=$SiMe_2$, and Me_3Si–$SiMe_3$: 69.3 ± 15.4, 53.3 ±

15.3, and 58.2 ± 14.5 kcal/mol, respectively, for the same suite of methods.

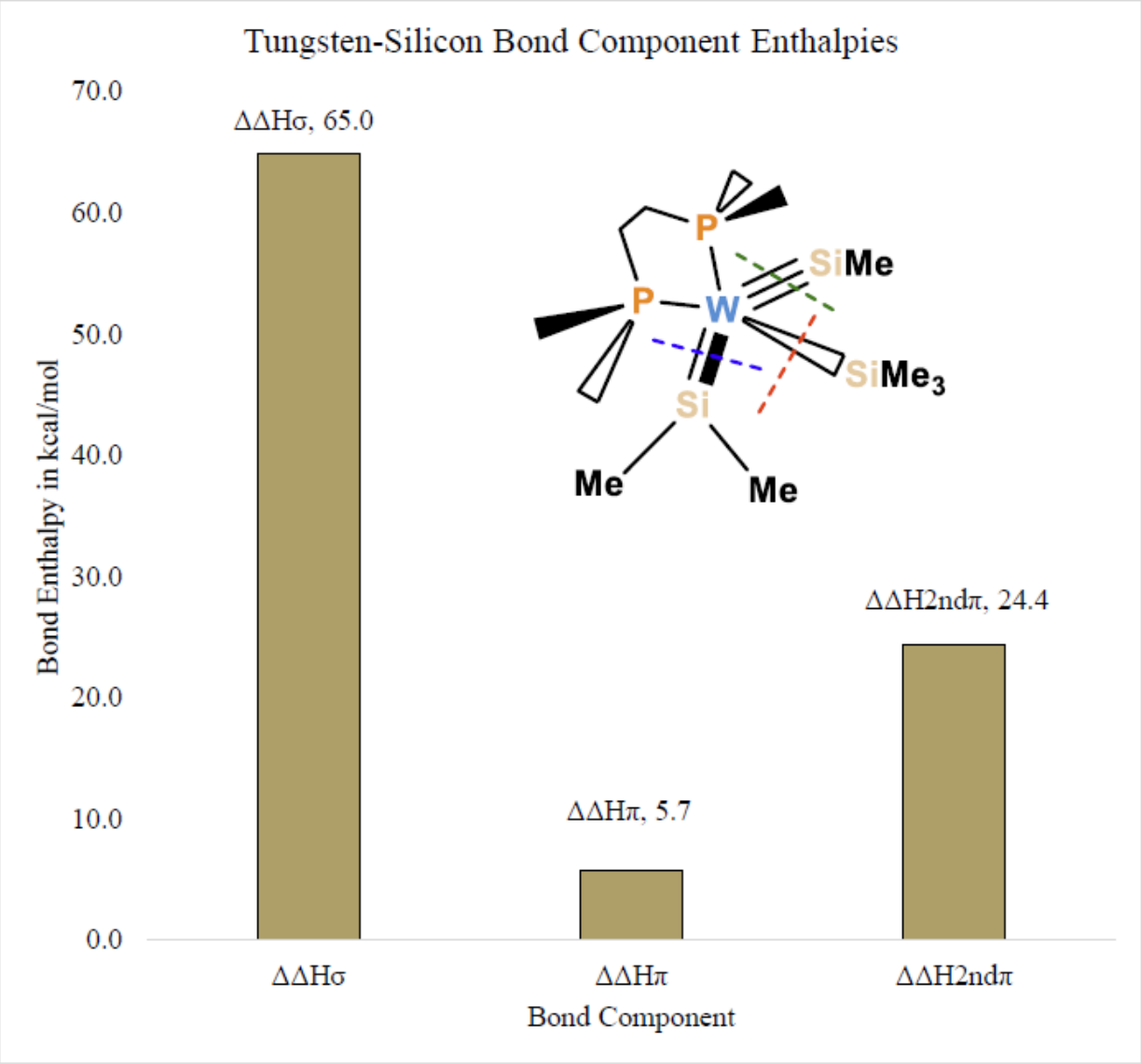

Figure 3.5: Average DFT-/MP2-calculated bond dissociation enthalpies (kcal/mol) for homolytic cleavage of tungsten-silicon bonds organized by basis set with average BDE inset above columns. WSi model is inset.

The 2nd π bond for a metal-element is defined by subtracting the calculated BDE of the W=Si double bond from the corresponding triple bond BDE. The 1st π-bond BDE is defined by the difference between the double bond and the single bond enthalpies. Note that these definitions assume that, for example, the W–Si s-bond is the same strength in W–Si, W=Si and W≡Si bonds,

which can lead to difficulties as discussed below. The WSi bond component BDEs thus defined are 24.4 ± 6.1, 5.7 ± 3.3, and 65.0 ± 12.1 kcal/mol, respectively, for the 2nd π bond, 1st π bond, and σ-bonds. There is a great discrepancy between σ and π bond strengths, supporting literature discussions of the bonding in heavier main group elements in terms of distinguishing the structure and reactivity of light- vs. heavy-main group multiple bonding.[15,34]

Interestingly, the 1st π-bond is considerably weaker than the 2nd WSi π bond, by ~19 kcal/mol; presumably, a shorter bond length (W≡Si vs. W=Si) and thus better orbital overlap, significantly enhances π-bond strength. A similar enhancement of the 2nd π-bond strength of ME *vis-à-vis* the 1st π-bond of M=E was observed for the 2p main group elements.[22]

3.4.1.2 Phosphorous

The tungsten-phosphorus model (Fig. 3.3) is a modification of a previously modeled tungsten-nitrogen complex that is liberally inspired by Beaumier *et al.*'s[38] chromium complex. This model has four different tungsten-phosphorus ligand types: phosphido (≡P), hydrophosphinidene (=PH), dihydrophosphide (–PH_2), and phosphine (←PH_3). The BDEs calculated for W(≡P)(=PH)(–PH_2)(←PH_3) are 116.8 ± 6.3, 90.1 ± 7.1, 97.9 ± 8.0 kcal/mol in decreasing bond order with the dative bond last. It is immediately notable that the tungsten-phosphorus bonds are quite strong regardless of bond type. Also, there is the surprising conclusion that the double and triple bonds between phosphorus and tungsten are actually *weaker* than their singly bonded counterpart (Fig. 3.6)!

For the tungsten-phosphorus model, the 2nd π, 1st π, and σ-bond component enthalpies computed are 26.7 ± 4.4, -7.8 ± 6.3, and 97.9 ± 8.0 kcal/mol respectively (Fig. 3.6). As with WSi bond enthalpies there is a considerable dichotomy in the strength of the s and p bonds, which hints at the paucity of examples of transition metal complexes with M=P and M≡P functionalities. There

is clearly an issue in terms of the negative 1st WP π-bond enthalpy that will be discussed more fully later. This oddity is, however, a first hint that DFT methods may break down for modeling bond enthalpies between 5d metals and 3p elements. Also, it is likely that the underlying assumption of equal WP s bond strengths is leading to the *"negative"* p-bond enthalpy, as are the assumptions of metal-element bond order based on stoichiometry, which worked so well for the 2p elements but may be more suspect for 3p elements.

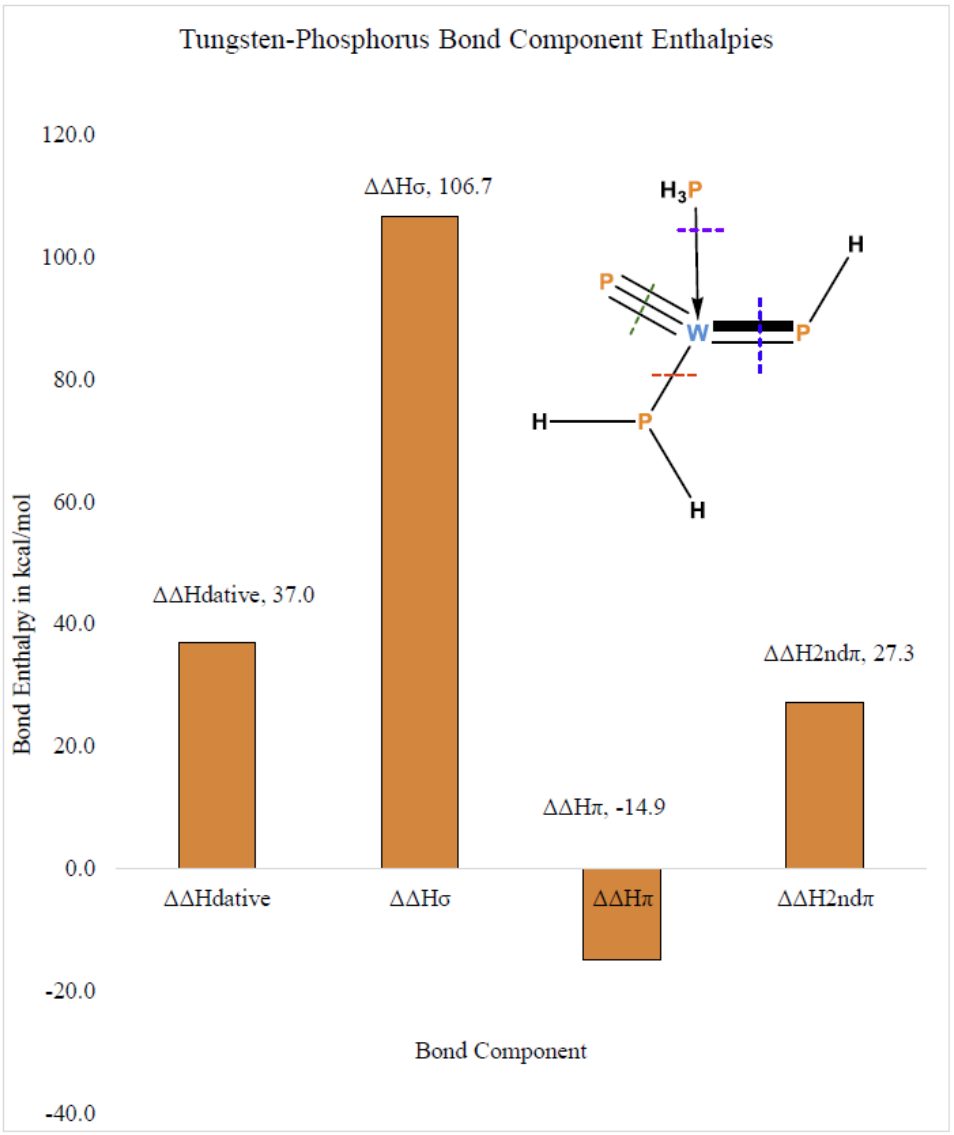

Figure 3.6: Average DFT-/MP2-calculated bond dissociation enthalpies (kcal/mol) for homolytic cleavage of tungsten-phosphorus bonds organized by basis set with average BDE inset above columns. WP model is inset.

3.4.1.3 Sulfur

The tungsten-sulfur model (Fig. 3.3) is a modification of a tungsten-oxygen complex derived from a crystal structure published by Cotton *et al.*[43] This WS model has three different tungsten-sulfur ligand types: sulfide (which can be formulated as either ≡S or =S), thiolate (–SH), and thiol (←SH_2). The BDEs calculated for W(≡S)(–SH)$_4$(←SH_2) are 91.6 ± 0.8, 48.3 ± 1.1, 2.9 ± 0.3 kcal/mol, by decreasing bond order with the dative bond last (Fig 3.7). The bond component enthalpies are 43.4 ± 0.1, 48.3 ± 1.1, and 2.9 ± 0.3, respectively for the π-, σ- and dative bonds in the tungsten complex. As with the prior WO model,[22] the W-sulfido BDE is more consistent with a triple bond formulation than the double bond illustrated in Figure 3.7, as might be expected given the molecular symmetry and d^0 nature of the central W^{VI}.

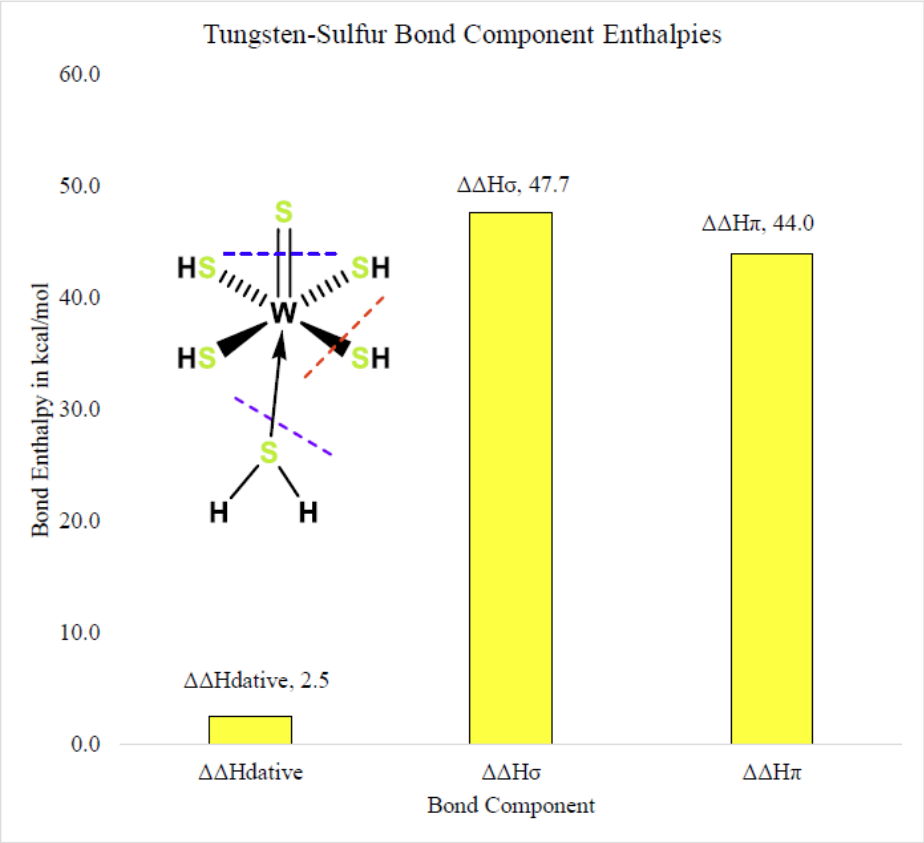

Figure 3.7: Average DFT-/MP2-calculated bond dissociation enthalpies (kcal/mol) for homolytic cleavage of tungsten-sulfur bonds organized by basis set with average BDE inset above columns. WS model is inset.

3.4.2 Comparison among Computational Methods

3.4.2.1 Calculated Bond Lengths vs. Crystal Structure Data

The structural models used in this study are computational homologs to those in a previous study.[19] As such, there are no direct crystal structure comparisons to be made, thus an indirect comparison is made using the mean values for various bond lengths for the assigned bond types found within the Cambridge Crystallographic Database.[62] Several of these bonds – particularly those with formal metal-3p element multiple bonds – are highly reactive; thus, there are generally few examples found of those bond types. The insufficiency is also why no analysis for the reliability of the bond angles could be made; however, it is assumed that the predicted bond angles are not inordinately unreasonable.

The calculated bond lengths of each of the three models are compared to the mean values for the corresponding bonds from the Cambridge Database and reported as a percent error. The fully optimized structural models are found to have a mean absolute error of 1.8 ± 1.2% across a set of four bond types – single, double, triple, and dative – for three ligand types (Si, P, S). A complete breakdown by functional, ECP/valence basis set, 3p element, and bond type may be found in Appendix B.

The WSi model complex has mean bond lengths of 2.57 ± 0.05 Å for the tungsten-silyl bond, 2.39 ± 0.01 Å for the tungsten-silylene bond, and 2.23 ± 0.02 Å for the tungsten-silyne bond. The average from the Cambridge database for these bond types are 2.55 ± 0.08 Å, 2.50 ± 0.09 Å, and 2.37 Å for the tungsten-silyl, -silylene, and -silyne bonds, respectively.[62,63] The overall mean absolute error for tungsten-silicon bonds is 1.7 ± 1.1%. The paucity of structures with these bond types is such that there are only sixty-eight tungsten-silyl structures, eleven tungsten-silylene structures, and only a single unambiguous tungsten-silyne bond published by Fukuda *et al.*[63] The

discrepancy between the model and the crystal structure averages may be a small sample set effect due to the scarcity of crystal structures with unambiguous W=Si double bonding, or differences arising from the formal oxidation state of the metal.

The mean DFT calculated bond lengths are 2.14 ± 0.02 Å, 2.27 ± 0.01 Å, 2.38 ± 0.02 Å, 2.48 ± 0.03 Å for the tungsten-phosphido (≡P), -hydrophosphinidene (=PH), dihydrophosphide (–PH_2), and -phosphine (←PH_3) respectively. There are four explicitly defined W≡P bonds[64-67] with an average length of 2.15 ± 0.02 Å and four W=P bonds with 2.34 ± 0.13 Å in the CCDC.[64,68] For the W–P and the W←P bond motifs, there is a problem of definitions. There are 188 W–P single bonds where the phosphorus is clearly three-coordinate, but there are an additional 229 complexes where tungsten is ligated to a 3-coordinate phosphorus; there is no functional difference in the average bond length of these subsets: 2.49 ± 0.08 Å and 2.48 ± 0.09 Å, respectively. Tungsten-phosphine moieties are quite plentiful with 3335 entries that average 2.50 ± 0.06 Å. The mean absolute error of 2.3 ± 1.6% in the calculated bond lengths from these structural data is respectable, but may be artificially inflated due to the small experimental sample sizes for multiply bonded moieties. However, there is reasonable agreement between theory and experiment for the measurements that do exist.

The WS model complex has a mean absolute difference for the metal-sulfur bond lengths of 1.5 ± 0.8% relative to experimental structural data, excluding the dative moiety (5.1 ± 9.5% with). In the CCDB, terminal W=S bonds average 2.16 ± 0.03 Å for 351 entries whereas tungsten-sulfur single bonds average 2.38 ± 0.11 Å for 1500 entries. The bond lengths for tungsten-thiol (W←SR_2) moieties average 2.42 ± 0.11 Å across 1012 entries. The sheer number of entries with W=S/W≡S motifs speaks to their inherent stability vis-à-vis the WP and WSi congeners, and is reflected by the computed p-bond strength in Figure 3.7. The computed DFT average bond lengths

found are 2.15 ± 0.02 Å, 2.42 ± 0.02 Å, and 3.48 ± 1.06 Å for W=S/W≡S, W–S, and W←S respectively.

3.4.3 Oddities in the Computational Data

In the WSi model calculations, the degree of variability is a concern. Certain basis set and functional combinations yield numbers that are well out of line with the rest of the data. These are often extreme outliers. For the tungsten-silylene π-bond BDE, the LANL2DZ basis set does not yield numbers in line with the other three basis sets in nine out of the twelve functional combinations, the exceptions being SOGGALL, B2PLYP, and MP2. For example, the N12/LANL2DZ(d), tungsten-silylene π-bond BDE is 0.9 kcal/mol whereas the PBEPBE/LANL2DZ(d) tungsten-silylene π-bond BDE is 11.6 kcal/mol both beyond the standard deviation of 3.3 kcal/mol for the mean value of 5.7 kcal/mol. Furthermore, for the organometallic fragments less the single bond, *viz* W(=$SiMe_2$)(≡SiMe)(dmpe), the MN12L functional optimized to a lower minima for the quartet rather than the doublet spin state for each ECP modeled, with the exception of SDDALL; this was also the case with the N12/LANL2DZ(d) combination. The B2PLYP /SDDALL(d), M11L/CEP-121G(d), and M11L/CEP-31G(d) levels of theory found the triplet spin state to be the more stable minima for Si_2Me_2.

In the WP model, as noted above, the MP2 wavefunction – with any of the valence basis set/pseudopotential combinations – yields predicted BDEs so far out of line with the DFT data that it was removed from the averages as an outlier. To wit, the sigma bond enthalpies found with the MP2 method are 203.3 ± 5.9 kcal/mol for the different valence basis set/pseudopotential combinations. This value is more than 100 kcal/mol higher than those predicted via the DFT functionals, and 96 kcal/mol adrift of the DLPNO-CCSD(T)/def2-QZVPP value. The underlying assumptions required for the perturbation theory to be effective are obviously invalid for the

fragments derived from W–P homolysis, possibly due to weaker metal-3p ligand bonding and the potential for low energy states in these fragments. It is worth noting that analysis of the DLPNO-CCSD(T) amplitudes did not indicate any higher than 0.08.

In the WS model complexes, the homolytic cleavage of the W–S single bond from the tungsten frequently resulted in the H_2S ligand dissociating from the organometallic fragment as well. For such simulations, the bond between the tungsten and the dihydrogensulfide was manually enforced through the ModRedundant command in Gaussian. In view of the small calculated W←SH_2 BDE of 2.7 ± 3.0 kcal/mol (DLPNO-CCSD(T)/def2-QZVPP, 3.1 kcal/mol), this is not expected to have a major impact on the other tungsten-sulfur BDEs.

3.5 Summary and Conclusions

3.5.1 Accuracy vs. Higher-level Theory and Experiment for BDEs of Main Group Homologs

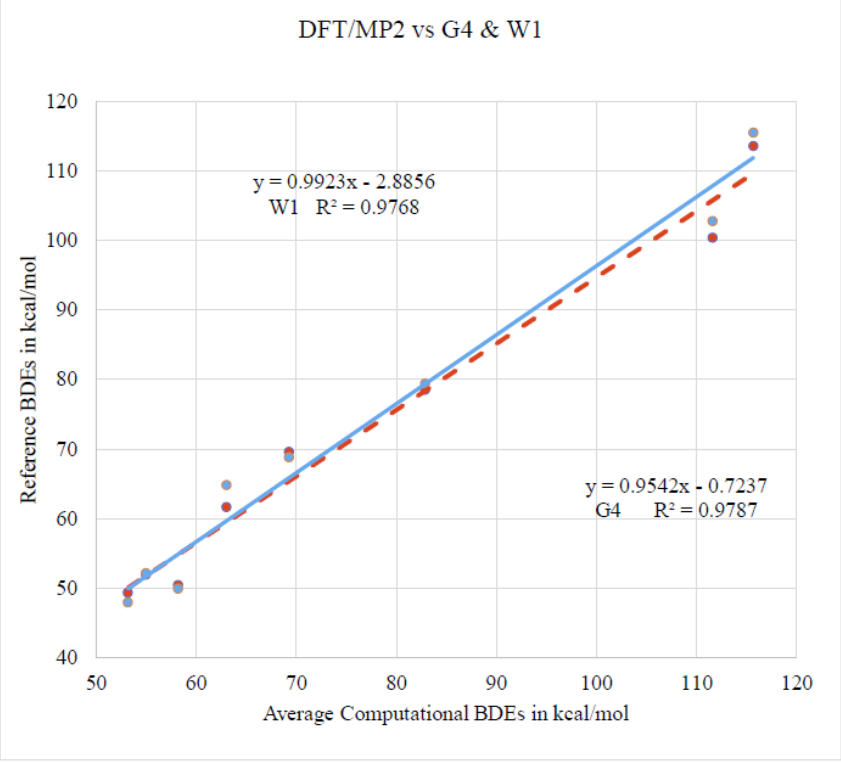

Figure 3.8: Plot of G4 (red) and W1 (blue) calculated BDEs compared to the mean values found using DFT for the main group homologs (R_nEER_n, n = 0, 1, 2, 3; E = Si, P, S; R = Me for Si, H for P and S).

The calculated BDEs for the 3p main group homologs can shed light upon the error variation from each DFT functional and basis set as there is either experimental data or BDEs obtained from high-accuracy G4 and W1U composite *ab initio* techniques (Fig. 3.8).[47-50,62-63] Thus, for each 3p element, main group thermodynamic data may serve as internal standards for the organometallic complexes studied herein.

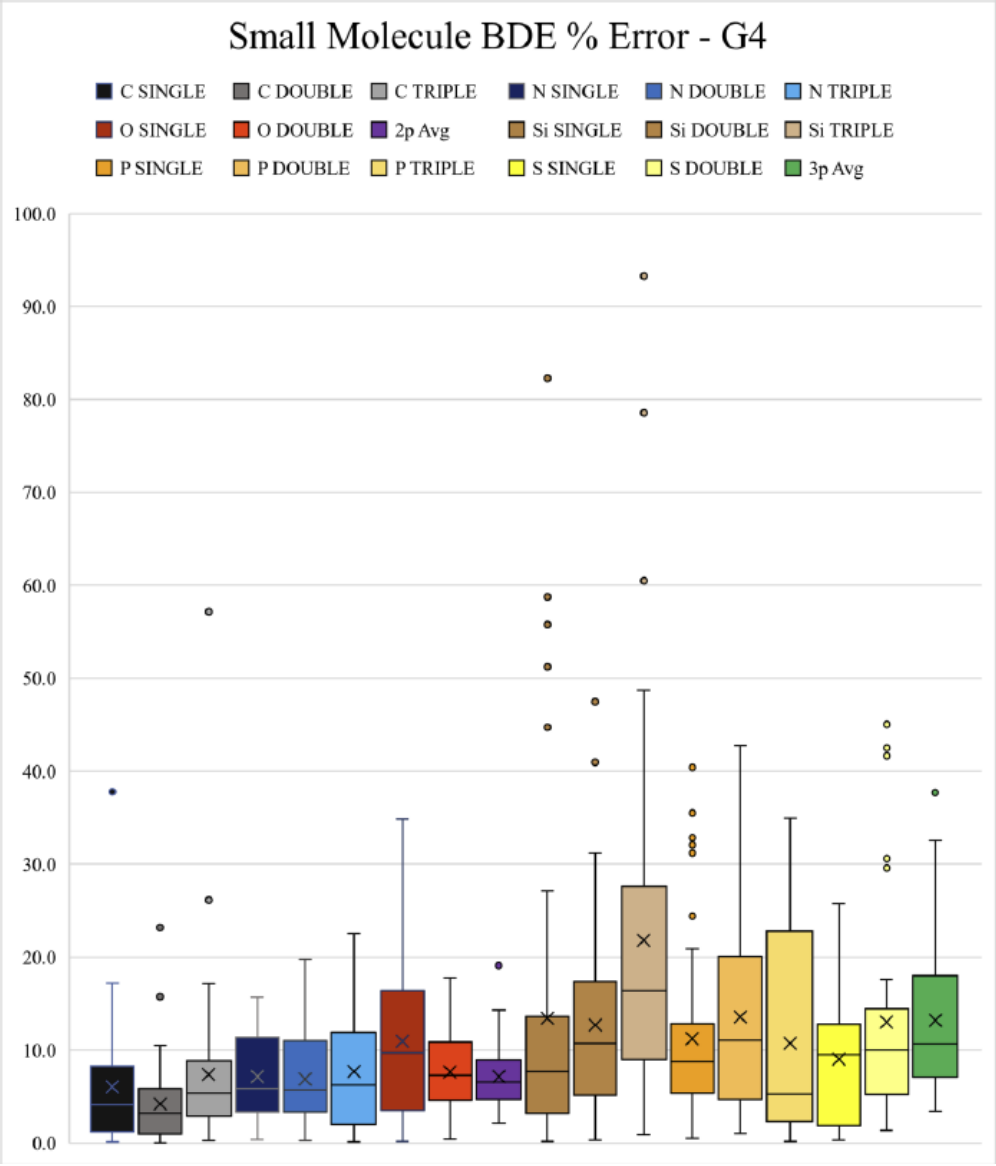

Figure 3.9: Box and whisker plot showing percent absolute error (y-axis) in DFT-predicted BDEs as a function of bond type for main group molecules with respect to G4 calculated BDEs (similar plots for experiment and W1U calculations are given in Appendix B). The arithmetic mean is indicated with an X, the median depicted with a horizontal line, and the outliers are left as dots. More plots may be found in Appendix B.

While the overall average DFT values are well correlated with W1U and G4 BDEs, R^2 = 0.98 for both (Fig. 3.8), the individual BDE absolute errors vary widely (Fig. 3.9). The box-and-whisker plots give a synopsis of the typical degree of variation among the functionals with respect to bond type (Fig. 3.9). Greater care is needed for the basis set/functional selection with 3p elements than with 2p elements as demonstrated by the larger boxes and greater median distance from zero error in Figure 3.9.

3.5.2 Accuracy vs. Higher-level Theory and Experiment for BDEs of Organometallic Models

Ultimately, the distinctly high degree of variation observed for DFT- and MP2-based predictions is worrisome. There are clearly apocryphal predictions for some of the organometallic W-3p bonds, particularly the tungsten-phosphorous complex, which the main group homologs do not adequately illuminate. In the absence of reliable experimental thermodynamic data, theoretical measures are valuable to bridge the gap. However, particularly for ligand sets where lone pairs exist on the 3p element, such complexes can be ambiguous vis-à-vis metal-element bond order. DLPNO-CCSD(T)/def2-QZVPP simulations were thus done as single point calculations for both main group and organometallic models at representative DFT (SOGGA11/CEP-31G(d)) geometries. Enthalpic corrections needed to obtain BDEs are also derived from DFT simulations. The DLPNO-CCSD(T)/def2-QZVPP//SOGGA11/CEP-31G(d) results for small molecule homolog BDEs can be found in Appendix B. As expected, they parallel the G4 and W1u data shown above (Fig. 3.8).

For the organometallic models studied herein, the DFT-/MP2-predicted average BDEs are generally in impressive agreement with the CCSD(T) BDEs (Table 3.1 and Fig. 3.10), akin to what was computed for the main group congeners. The mean absolute error for the average DFT/MP2

BDEs compared to the CCSD(T) BDEs differ by 10.8 ± 6.8% with the W–P single bond removed (14.0 ± 12.8% with this bond included; Fig. 3.10).

Table 3.1: Comparison of DLPNO-CCSD(T)/def2-QZVPP//SOGGA11/CEP-31G(d) predicted BDEs versus mean DFT-/MP2-predicted values for metal-element bond dissociation enthalpies in kcal/mol for organometallic models. Values in parentheses (avg) are the standard deviations for the DFT/MP2 averages' "diff" is the difference = CCSD(T) – DFT average.

Bonds		CCSD(T)	DFT avg		diff
triple	W≡SiMe	83.2	92.5	(±13.8)	-9.3
double	W=$SiMe_2$	84.3	69.6	(±13.5)	14.7
single	W–$SiMe_3$	52.0	64.1	(±13.2)	-12.1
triple	W≡P	113.0	119.2	(±9.8)	6.2
double	W=PH	91.3	91.9	(±7.7)	0.6
single	W–PH_2	73.1	106.7	(±30.4)	33.6
dative	W←PH_3	41.3	37.1	(±4.4)	-4.2
double	W=S	85.8	90.2	(±16.7)	-4.4
single	W–SH	43.0	47.7	(±10.7)	-4.8
dative	W←SH_2	3.1	2.7	(±3.0)	0.5

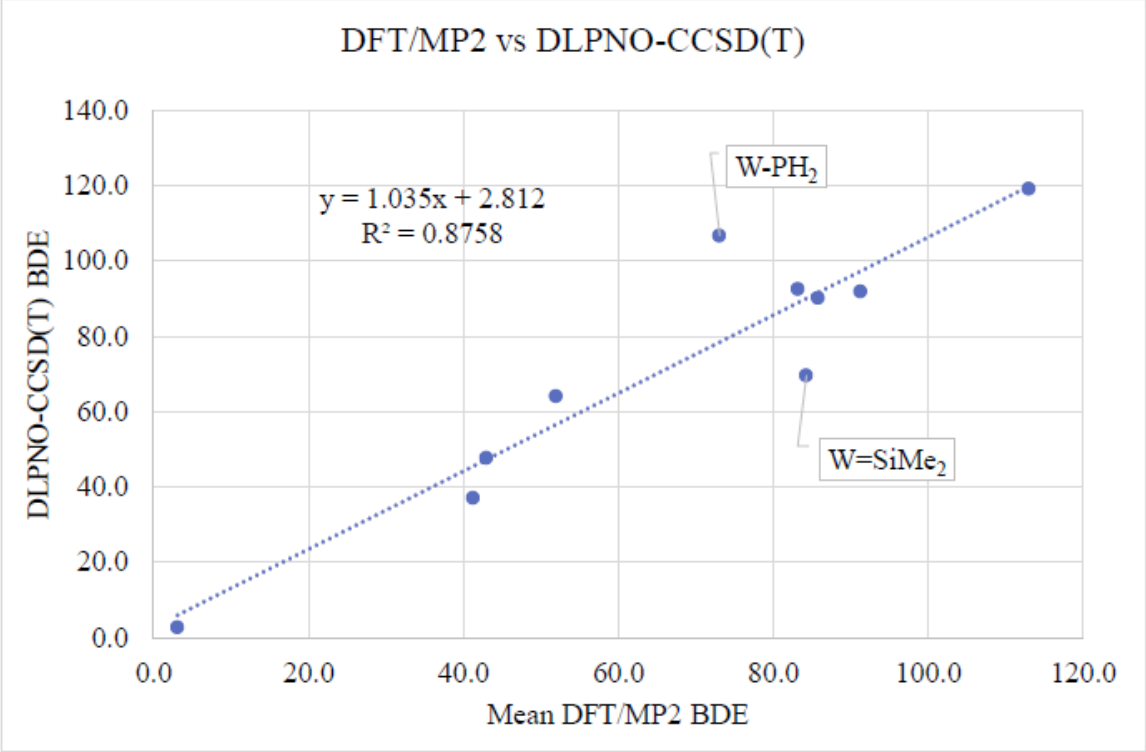

Figure 3.10: Scatter plot of the mean DFT values in comparison to the computed CCSD(T) for the same model, note the W–P single bond bond is an outlier (without the WP single bond the R^2 = 94.9%) and the W=Si double bond is the next largest difference. Original data are given in Table 3.1.

The agreement is less exemplary for the tungsten-silicon model than the WP and WS models, indicating the W=Si 1st π-bond is underreported by the more approximate methods and the W≡Si 2nd π-bond strength is essentially zero, which is consistent with the extremely limited number of structurally characterized silyne complexes.[62,-68] Interestingly, the tungsten-phosphorus model has good agreement among the different theories except for the W–P single bond, which has a massive 33 kcal/mol difference and a very large standard deviation for the DFT averages versus the DLPNO-CCSD(T)/def2-QZVPP//SOGGA11/CEP-31G(d) predicted bond enthalpy! This is obviously indicative of a systematic problem in the calculations for the WP model (Table 3.1).

3.5.3 Jacob's Ladder

For the small main group homologs with respect to the G4 level of theory, there is surprisingly little benefit to moving up Jacob's Ladder (Table 3.2).[69] The best performers were all generalized gradient approach (GGA) functionals with PBEPBE/SDDALL(d) performing the best across the models (4.1 ± 5.0% absolute error). When the double and triple bonds between silicon atoms are removed from the test set the performance of PBEPBE/SDDALL(d) vs. G4 predicted BDEs improves to 2.4 ± 1.7%. The two functionals that include exact exchange (B3LYP and B97D) do perform better than the meta-GGA functionals tested, but not better than the GGA functionals. Correcting for dispersion does seem to improve the hybrid-GGA B97D over B3LYP. Finally, the double hybrid-GGA B2PLYP's performance is disappointing. The MP2 post-HF level of theory has relatively high error rates (17.3 ± 9.7%).

CCSD(T) calculations provide the accuracy standard to discern the performance of DFT/MP2 methods given the experimentally unavailable W-element bond enthalpies. The suite of DFT functionals have a broad range of accuracy that does not correlate strongly to the rungs on Jacob's Ladder. This is largely from the disagreements over the WE dative bonds While the overall

average of DFT/MP2 and pseudopotential combinations correlates quite well to the CCSD(T) values for the BDEs, R^2 = 87.6% (Fig. 3.10), the spread of the percent absolute error is nearly 30%. However, if the dative bonds are removed from the set, the percent absolute error with respect to CCSD(T) BDEs calculations drops to 17.7 ± 16.2%. The MP2 level of theory is again a poor fit for thermochemistry with errors coming in at 41.7 ± 23.1%.

Table 3.2: The precent absolute errors found as each of the DFT functionals in the bright colors is compared to the BDEs calculated G4 for the 3p small molecule homologs, then the 2p and 3p small molecule homologs, then a comparison of the small molecule homolog BDEs to the CCSD(T) BDEs under the SM column, and finally the organometallic complex BDEs compared to the CCSD(T) BDEs presented as a Jacob's Ladder.

Jacob's Ladder	Basis	G4		CCSD(T)	
		3p	2-3p	SM	OM-3p
Double hybrid - GGA	B2PLYP	12.1	10.3	20.0	16.1
w/dispersion	B97D	12.1	10.3	16.3	13.2
hybrid-GGA	B3LYP	7.5	9.7	16.2	13.7
meta-GGA	M06	17.6	11.9	21.8	17.1
	M11L	18.8	13.5	24.1	12.3
	MN12L	33.4	20.6	37.7	26.4
GGA	BLYP	6.2	8.2	14.5	9.9
	BP86	4.8	5.5	12.8	12.9
	N12	14.4	10.0	18.1	16.5
	PBEPBE	6.4	5.6	12.2	11.1
	SOGGALL	10.7	9.0	14.4	16.5
Post-HF	MP2	17.3	12.1	22.9	41.7

There is apparently little benefit to moving “higher” on Jacob’s ladder of DFT functionals when modeling bond dissociation enthalpies for a heavy 5d metal like tungsten. The best performing functionals are the GGA type with BLYP/CEP-31G(d) coming in as the closest match at 6.4 ± 7.7%. For a dataset that includes tungsten and a combination of 2p and 3p elements PBEPBE/SDDALL(d) appears to be the most reliable versus G4 values. Further comparison of performance among the various families of functionals are given Appendix B.

3.5.4 Comparison with W-2p Ligands

Using the same suite of the popular functionals (plus MP2 methods) and valence basis sets/effective core potentials for W-3p complexes as previously used to study W-2p enthalpies by Moulder *et al.*[22] provides a platform for comparison.

Table 3.3: Average DFT Computed Homolytic WE (E = C, N, O, Si, P, S) Bond Enthalpies in kcal/mol.

Element	Dative	σ	π	2nd π
C		61.4	32.5	42.6
N	47.4	104.4	17.6	34.1
O	13.6	93.1	67.8	
Si		65.5	7.2	22.9
P	37.0	106.7	-14.9	27.3
S	2.5	47.7	44.0	

For the 3p elements studied herein, however, there is a fair amount of spread in the overall error (Table 3.1 and Fig. 3.9) for example, indicating a need for careful calibration of the level of theory – indeed multiple levels of theory – before studying thermochemistry with any of these heavier main group elements. The main group homologs do run into curious issues arising from ambiguous bond order as expected given the literature on modeling silenes and silynes.[70-73] Silicon has access to d-orbitals and less propensity to hybridize compared to carbon. For example, the trans-bent geometry of Si_2Me_2 implies a bond order closer to 2 while its stoichiometry suggests a triple bond (Fig. 3.11).[74] This appears to have an impact on the observed bond enthalpies rendering the 3p elements more prone to have the 2nd π-bond component stronger than the 1st π-bond, which is more akin to transition metal complexes than to 2p-based main group compounds.[22]

The pnictogen models have been particularly problematic. The DLPNO-CCSD(T) calculation of the WP σ-bond is revealed to be far weaker at ~73 kcal/mol than implied by DFT (Table 3.1). The coupled cluster value is more consistent with the rest of the data set and with

known experimental reactivity trends.[40-42] Indeed, it is also worth noting that the DLPNO-CCSD(T) calculation of the WSi σ-bond enthalpy is also 13 kcal/mol weaker than the mean BDE for the DFT models at 52 kcal/mol. Interestingly, the W–C and W–Si BDE values are fairly close for all but the tungsten-alkylidyne and the tungsten-silyne bonds, particularly when comparing the mean DFT BDEs for WC to the CCSD(T) BDEs for WSi (Table 3.2).

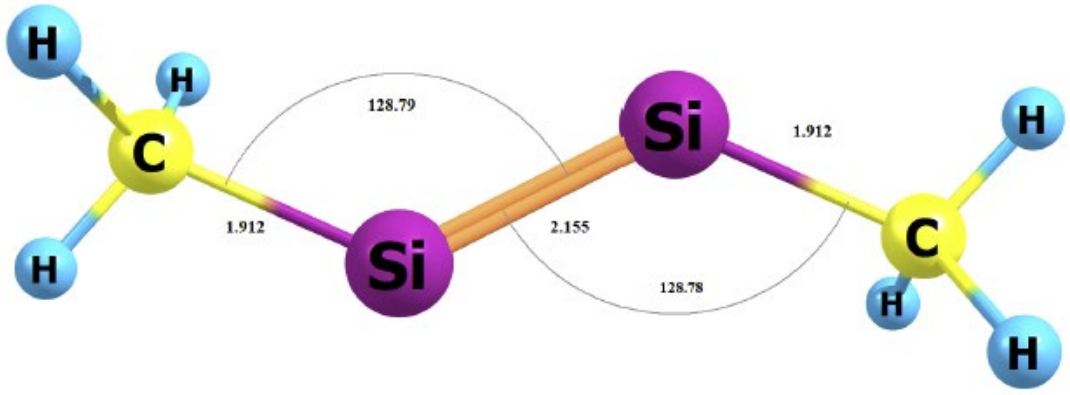

Figure 3.11: Geometry of Si_2Me_2 optimized at the SOGGA11/CEP-31G(d.p) level of theory including all pertinent bond lengths and angles.

This work highlights the need for caution.[75] Tungsten is a heavy metal, which one might infer requires less computational finesse in comparison to 3d metals to model given the large ligand-field splitting expected of a 5d metal. On the contrary, this work demonstrates the difficulties associated with attempting to model the thermochemistry of a heavy metal with DFT (and MP2 as well) levels of theory through the broad standard deviations observed. On average, the values found using these popular DFT levels of theory are reliable (Fig. 3.10), but the box-and-whisker plot (Fig. 3.9) reveals that individual basis set/pseudopotential/valence basis set combination can vary wildly. The supporting information in Appendix B is provided to assist in the decisions on which basis set and functional combination is most applicable. For critical computational thermochemical information in organometallic and inorganic chemistry applications, *caveat lector*!

3.6 Supporting Information

A detailed accounting of the computed homolytic bond enthalpy and geometric data found with respect to each functional/ECP/valence basis set are available in the supporting information for all models. This material can be found at Appendix B and http://pubs.acs.org/ .

3.7 Acknowledgements

K.K. and C.Z. acknowledge the University of North Texas' Texas Academy of Math & Sciences (TAMS) program for Undergraduate Research Summer Scholarships. This material is based upon work supported by the National Science Foundation Graduate Research Fellowship Program under Grant No. 1746050. Any opinions, findings, and conclusions or recommendations expressed in this material are those of the author(s) and do not necessarily reflect the views of the National Science Foundation.

3.8 References

1. Simões, J. A. M.; Beauchamp, J. L. Transition Metal–Hydrogen and Metal–Carbon Bond Strengths: The Keys to Catalysis. *Chem. Rev.* **1990***, 90*, 629–688.

2. Durand, D.; Fey, N. Computational Ligand Descriptors for Catalyst Design; *Chem. Rev.* ***2019****, 119*, 6561-6594.

3. Ceylan, Y. S.; Cundari, T. R. Computational Analysis of Transition Metal-Terminal Boride Complexes. *J. Phys. Chem. A.* ***2017****, 121*, 9358–9368.

4. Moulder, C. A.; Cundari, T. R. A DFT Survey of The Effects of d-Electron Count and Metal Identity on the Activation and Functionalization of C−H Bonds for Mid to Late Transition Metals. *Isr. J. Chem.* ***2017****, 57*, 1023–1031.

5. Haxel, G. B.; Hedrick, J. B.; Orris, G. J. Rare Earth Elements — Critical Resources for High Technology. United States Geol. Surv. Fact Sheet **2002**, 87, 4 ff. https://pubs.usgs.gov/fs/2002/fs087-02/fs087-02.pdf, (Accessed April 4, 2019).

6. Schrock, R. R. High Oxidation State Multiple Metal-Carbon Bonds. *Chem. Rev.* **2002***, 102,* 145–179.

7. Wu, P.; Yap, G. P. A.; Theopold, K. H., Structure nd Reactivity of Chromium(VI) Alkylidenes. *J. Am. Chem. Soc.* **2018***, 140*, 7088-7091.

8. Parveen, R.; Cundari, T. R.; Younker, J. M.; Rodriguez, G.; McCullough, L., DFT And QSAR Studies of Ethylene Polymerization by Zirconocene Catalysts. *ACS Catalysis* ***2019,*** 9339-9349.

9. Messinis, A. M.; Batsanov, A. S.; Wright, W. R. H.; Howard, J. A. K.; Hanton, M. J.; Dyer, P. W., Bis(Imido) Tungsten Complexes: Efficient Precatalysts for the Homogeneous Dimerization of Ethylene. *ACS Catalysis* **2018***, 8*, 11249-11263.

10. Vougioukalakis, G. C.; Grubbs, R. H. Ruthenium-Based Heterocyclic Carbene-Coordinated Olefin Metathesis Catalysts. *Chem. Rev.* **2010***, 110*, 1746–1787.

11. Ziegler, K. Serial No. 232,476 Claims Priority, Application Germany, **1951**.

12. Corradini, P.; Guerra, G.; Cavallo, L., Do New Century Catalysts Unravel the Mechanism of Stereocontrol of Old Ziegler-Natta Catalysts? *Acc. Chem. Res.* **2004***, 37*, 231-241.

13. Kissin, Y. V.; Liu, X.; Pollick, D. J.; Brungard, N. L.; Chang, M. Ziegler-Natta Catalysts for Propylene Polymerization: Chemistry of Reactions Leading to the Formation of Active Centers. *J. Mol. Catal. A Chem.* **2008***, 287*, 45–52.

14. Eisch, J. J., Fifty Years of Ziegler–Natta Polymerization: From Serendipity to Science. A Personal Account. *Organometallics* **2012***, 31*, 4917-4932.

15. Pitzer, K. S., Repulsive Forces in Relation to Bond Energies, Distances and Other Properties. *J. Am. Chem. Soc.* **1948***, 70*, 2140-2145.

16. Cundari, T. R. Computational Studies of Transition Metal-Main Group Multiple Bonding. *Chem. Rev.* **2000***, 100*, 807–818.

17. Davies, H. M. L.; Morton, D. Recent Advances in C-H Functionalization. *J. Org. Chem.* **2016***, 81*, 343-350.

18. Frenking, G.; Frohlich, N.; The Nature of the Bonding in Transition-Metal Compounds. *Chem. Rev.* **2000***, 100*, 717-774.

19. Pople, J. A.; Head-Gordon, M.; Fox, D. J.; Raghavachari, K.; Curtiss, L. A. Gaussian-1 Theory: a General Procedure for Prediction of Molecular Energies. *J. Chem. Phys.* **1989***, 90*, 5622–5629.

20. Guo, Y.; Riplinger, C.; Becker, U.; Liakos, D. G.; Minenkov, Y.; Cavallo, L.; Neese, F. Communication: An Improved Linear Scaling Perturbative Triples Correction for the Domain Based Local Pair-Natural Orbital Based Singles and Doubles Coupled Cluster Method [DLPNO-CCSD(T)]. *J. Chem. Phys.* **2018***, 148*, 11101.

21. Riplinger, C.; Sandhoefer, B.; Hansen, A.; Neese, F. Natural Triple Excitations in Local Coupled Cluster Calculations with Pair Natural Orbitals. *J. Chem. Phys.* **2013***, 139*, 134101.

22. Moulder, C.; A.; Kafle, K.; R. Cundari, T.; Cundari, T. R. Tungsten–Ligand Bond Strengths for 2p Elements Including σ- and π-Bond Strength Components, a Density Functional Theory and ab initio Study. *J. Phys. Chem. A* **2019***, 123*, 7940–7949.

23. Harding, M. E.; Vázquez, J.; Ruscic, B.; Wilson, A. K.; Gauss, J.; Stanton, J. F. High-Accuracy Extrapolated ab initio Thermochemistry. III. Additional Improvements and Overview. *J. Chem. Phys.* **2008***, 128,* 120-128.

24. Laury, M. L.; Wilson, A. K. Performance of Density Functional Theory for Second Row (4d) Transition Metal Thermochemistry. *J. Chem. Theory Comput.* **2013***, 9*, 3939–3946.

25. Laury, M. L.; Deyonker, N. J.; Jiang, W.; Wilson, A. K. A Pseudopotential-Based Composite Method: The Relativistic Pseudopotential Correlation Consistent Composite Approach for Molecules Containing 4d Transition Metals (Y-Cd). *J. Chem. Phys.* **2011***, 135*, 214103.

26. DeYonker, N. J.; Williams, T. G.; Imel, A. E.; Cundari, T. R.; Wilson, A. K. Accurate Thermochemistry for Transition Metal Complexes from First-Principles Calculations. *J. Chem. Phys.* **2009***, 131*, 24106.

27. Mardirossian, N.; Head-Gordon, M., Thirty Years of Density Functional Theory in Computational Chemistry: An Overview and Extensive Assessment of 200 Density Functionals. *Molecular Physics* **2017***, 115*, 2315-2372.

28. Ryu, H.; Park, J.; Kim, H. K.; Park, J. Y.; Kim, S.-T.; Baik, M.-H., Pitfalls in Computational Modeling of Chemical Reactions and How to Avoid Them. *Organometallics* **2018***, 37*, 3228-3239.

29. Lemonick, S. As DFT Matures, Will It Become a Push-Button Technology? *C&EN Glob. Enterp.* **2019***, 97*, 16–18.

30. Waterman, R.; Hillhouse, G. L.; Group Transfer from Nickel Imido, Phosphinidene, and Carbene Complexes to Ethylene with Formation of Aziridine, Phosphirane, and Cyclopropane Products. *J. Am. Chem. Soc.* **2003***, 125*, 13350-13351.

31. Pluth, M. D.; Tonzetich, Z. J., Hydrosulfide Complexes of the Transition Elements: Diverse Roles in Bioinorganic, Cluster, Coordination, and Organometallic Chemistry. *Chem. Soc. Rev.* **2020**, Advance Article.

32. Churchill, M. R.; Youngs, W. J. Crystal Structure and Molecular Geometry of W(.Tplbond.Ccme3)(:Chcme3)(CH2CMe3)(Dmpe), A Mononuclear Tungsten(VI) Complex with Metal-Alkylidyne, Metal-Alkylidene, and Metal-Alkyl Linkages. *Inorg. Chem.* **1979***, 18*, 2454–2458.

33. Kubas, J. G. Molecular Hydrogen Complexes: Coordination of a σ Bond to Transition Metals Acc. *Chem. Res.* **1988** *21*, 120-128.

34. Sadow, A. D.; Tilley, T. D. Activation of Arene C-H Bonds by a Cationic Hafnium Silyl Complex Possessing an α-Agostic Si-H Interaction. *J. Am. Chem. Soc.* **2002***, 124*, 6814–6815.

35. Boehme, C.; Frenking, G. Electronic Structure of Stable Carbenes, Silylenes, and Germylenes. *J. Am. Chem. Soc.* **1996***, 118*, 2039-2046.

36. Price, J. S.; Emslie, D. J. H., Interconversion and Reactivity of Manganese Silyl, Silylene, and Silene Complexes. *Chem. Sci.* **2019***, 10*, 10853-10869.

37. Waterman, R.; Hayes, P. G.; Tilley, T. D.; Synthetic Development and Chemical Reactivity of Transition-Metal Silylene Complexes. *Acc. Chem. Res.* **2007***, 40*, 712–719.

38. Beaumier, E. P.; Billow, B. S.; Singh, A. K.; Biros, S. M.; Odom, A. L. A Complex with Nitrogen Single, Double, and Triple Bonds to the Same Chromium Atom: Synthesis, Structure, and Reactivity. *Chem. Sci.* **2016***, 7*, 2532–2536.

39. Bonanno, J. B.; Wolczanski, P. T.; Lobkovsky, E. B.; Arsinidene, Phosphinidene, and Imide Formation via L,2-H2-Elimination from (Silox)3htaehph (E = N, P, As): Structures Of (Silox)3Ta=EPh (E = As). *J. Am. Chem. Soc.* **1994***, 116*, 11159-11160.

40. Sterenberg, B. T.; Senturk, O. S.; Udachin, K. A.; Carty, A. J., Reactivity of Terminal, Electrophilic Phosphinidene Complexes of Molybdenum and Tungsten. Nucleophilic Addition at Phosphorus and P-P Bond Forming Reactions with Phosphines and Diphosphines. *Organometallics* **2007***, 26*, 925-937.

41. Sterenberg, B. T.; Udachin, K. A.; Carty, A. J., Electrophilic "Fischer Type" Phosphinidene Complexes of Molybdenum, Tungsten, and Ruthenium. *Organometallics* **2001***, 20,* 2657-2659.

42. Grubba, R.; Ordyszewska, A.; Ponikiewski, L.; Gudat, D.; Pikies, J., An Investigation on the Chemistry of the R2P = P Ligand: Reactions of a Phosphanylphosphinidene Complex of Tungsten(VI) with Electrophilic Reagents. *Dalton Trans.* **2016***, 45*, 2172-9.

43. Cotton, F. A.; Schwotzer, W.; Shamshoum, E. S. Further Studies of the Reactions of Ditungsten Hexa-T- Butoxide with Acetylenes. Isolation and Characterization of WO(OCMe3)4(THF), [W3(OCMe3)5(μ-O)(μ-CC3H7)O]2 and W(CPh)(OCMe3)3. *J. Organomet. Chem.* **1985***, 296*, 55–68.

44. Crabtree, R. H. *The Organometallic Chemistry of the Transition Metals*, 5th ed.; Wiley: Hoboken, NJ, **2009**, p 7.

45. Hartwig, J. F. *Organotransition Metal Chemistry: from Bonding to Catalysis*; University Science Books: Mill Valley, CA, **2010**, pp 217-245.

46. Pluth, M. D.; Tonzetich, Z. J., Hydrosulfide Complexes of the Transition Elements: Diverse Roles in Bioinorganic, Cluster, Coordination, and Organometallic Chemistry. *Chem Soc Rev* **2020**.

47. Curtiss, L. A.; Redfern, P. C.; Raghavachari, K. Gaussian-4 Theory. *J. Chem. Phys.* **2007***, 126*, 084108.

48. Curtiss, L. A.; Redfern, P. C.; Raghavachari, K. Gn Theory. *Wiley Interdisciplinary Reviews: Computational Molecular Science*. John Wiley & Sons, Ltd September 1, **2011**, pp 810–825.

49. Martin, J. M. L.; De Oliveira, G. Towards Standard Methods for Benchmark Quality ab initio Thermochemistry - W1 and W2 Theory. *J. Chem. Phys.* **1999***, 111*, 1843–1856.

50. Barnes, E. C.; Petersson, G. A.; Montgomery, J. A.; Frisch, M. J.; Martin, J. M. L. Unrestricted Coupled Cluster and Brueckner Doubles Variations of W1 Theory. *J. Chem. Theory Comput.* **2009***, 5*, 2687–2693.

51. Neese, F. The ORCA Program System. Wiley Interdiscip. Rev. *Comput. Mol. Sci.* **2012***, 2,* 73–78.

52. Neese, F. Software Update: The ORCA Program System, Version 4.0. Wiley Interdiscip. Rev. *Comput. Mol. Sci.* **2018***, 8*.

53. Liakos, D. G.; Sparta, M.; Kesharwani, M. K.; Martin, J. M. L.; Neese, F. Exploring the Accuracy Limits of Local Pair Natural Orbital Coupled-Cluster Theory. *J. Chem. Theory Comput.* **2015***, 11*, 1525–1539.

54. Gaussian 09, Revision E.03, Frisch, M. J.; Trucks, G. W.; Schlegel, H. B.; Scuseria, G. E.; Robb, M. A.; Cheeseman, J. R.; Scalmani, G.; Barone, V.; Mennucci, B.; Petersson, G. A.; et al. Gaussian, Inc., Wallingford CT, 2009.

55. Becke, A. D. Density-Functional Exchange-Energy Approximation with Correct Asymptotic Behavior. *Phys. Rev. A* **1988***, 38*, 3098–3100.

56. Adamo, C.; Scuseria, G. E.; Barone, V. Accurate Excitation Energies from Time-Dependent Density Functional Theory: Assessing the PBE0 Model. *J. Chem. Phys.* **1999***, 111*, 2889–2899.

57. Adamo, C.; Barone, V. Inexpensive and Accurate Predictions of Optical Excitations in Transition-Metal Complexes: the TDDFT/PBE0 Route. Theor. *Chem. Acc.* **2000***, 105*, 169–172.

58. Møller, C.; Plesset, M. S. Note on an Approximation Treatment for Many-Electron Systems. *Phys. Rev.* **1934***, 46*, 618–622.

59. Bartlett, R. J. Perspective On "On the Correlation Problem in Atomic and Molecular Systems. Calculation of Wavefunction Components in Ursell-Type Expansion Using Quantum-Field Theoretical Methods." *Theor. Chem. Acc.* **2000***, 103*, 273–275.

60. Hay, P. J.; Wadt, W. R. Ab Initio Effective Core Potentials for Molecular Calculations. Potentials for the Transition Metal Atoms Sc to Hg. *J. Chem. Phys.* **1985***, 82*, 270–283.

61. Cundari, T. R.; Stevens, W. J. Effective Core Potential Methods for the Lanthanides. *J. Chem. Phys.* **1993***, 98*, 5555–5565.

62. Groom, C. R.; Bruno, I. J.; Lightfoot, M. P.; Ward, S. C.; *Acta Cryst.* **2016***, B72*, 171-179.

63. Luo, Y.-R. *Handbook of Bond Dissociation Energies in Organic Compounds*; CRC Press: Boca Raton, FL, **2003**.

64. Haynes, W. M. *CRC Handbook of Chemistry and Physics 2016-2017*, 96th ed.; CRC Press: Boca Raton, FL, **2016**.

65. Fukuda,T.; Yoshimoto, T.; Hashimoto, H.; Tobita, H.; Synthesis of a Tungsten–Silylyne Complex via Stepwise Proton and Hydride Abstraction from a Hydrido Hydrosilylene Complex. *Organometallics* **2016** *35*, 921-924

66. Balázs, G.; Green, J. C.; Scheer, M. Terminally Coordinated AsS and PS Ligands. Chem. - *A Eur. J.* **2006***, 12*, 8603–8608.

67. Scheer, M.; Kramkowski, P.; Schuster, K. An Approach to Novel Complexes with a Tungsten-Phosphorus Triple Bond. *Organometallics* **1999***, 18*, 2874–2883.

68. Cowley, A. H.; Pellerin, B.; Atwood, J. L.; Bott, S. G. Cleavage of a Phosphorus-Carbon Double Bond and Formation of a Linear Terminal Phosphinidene Complex. *J. Am. Chem. Soc.* **1990***, 112*, 6734–6735.

69. Zanetti, N. C.; Schrock, R. R.; Davis, W. M. Monomeric Molybdenum and Tungsten Complexes that Contain a Metal–Phosphorus Triple Bond. Angew. *Chemie Int. Ed. English* **1995***, 34*, 2044–2046.

70. Perdew, J. P.; Ruzsinszky, A.; Tao, J.; Staroverov, V. N.; Scuseria, G. E.; Csonka, G. I., Prescription for the Design and Selection of Density Functional Approximations: More Constraint Satisfaction with Fewer Fits. *J Chem Phys* **2005***, 123*, 62201.

71. Kobayashi, K.; Nagase, S. Silicon-Silicon Triple Bonds: Do Substituents Make Disilynes Synthetically Accessible? *Organometallics* **1997***, 16*, 2489–2491.

72. Curtiss, L. A.; Raghavachari, K.; Deutsch, P. W.; Pople, J. A. Theoretical Study of Si2Hn (N=0-6) and Si 2Hn+ (N=0-7): Appearance Potentials, Ionization Potentials, and Enthalpies of Formation. *J. Chem. Phys.* **1991***, 95,* 2433–2444.

73. Ruscic, B.; Berkowitz, J. Photoionization Mass Spectrometric Studies of the Transient Species Si 2Hn (N=2-5). *J. Chem. Phys.* **1991***, 95*, 2416–2432.

74. Grev, R. S.; Schaefer, H. F. The Remarkable Monobridged Structure of Si2H2. *J. Chem. Phys.* **1992***, 97*, 7990–7998.

75. Pignedoli, C. A.; Curioni, A.; Andreoni, W., Disproving A Silicon Analog of an Alkyne with the Aid of Topological Analyses of the Electronic Structure and ab initio Molecular Dynamics Calculations. *Chemphyschem* **2005***, 6*, 1795-9.

76. Lupp, D.; Christensen, N. J.; Fristrup, P. Synergy Between Experimental and Theoretical Methods in the Exploration of Homogeneous Transition Metal Catalysis. *Dalt. Trans.* **2014***, 43*, 11093–11105.

CHAPTER 4

ON THE THEORY OF π-LOADING AND TUNGSTEN

4.1 Introduction

A common motif in catalytic design involves more than one multiply bonded ligand coordinated to a metal. This motif is particularly common for early transition metals in high formal oxidation states including Schrock's imide (alkylidene) catalysts, Wolczsanski's poly-imidos, and several others.[1-11] This paradigm has been proposed to exploit the principle of π-loading for enhanced reactivity. First proposed by Wigley,[12] π-loading is defined as the weakening of transition metal π-bonds via competition among the M d_π – E p_π molecular orbitals. There has been some discussion as to whether or not π-loading is a real phenomenon, how significant it may be, and if so, is its influence overstated?[13-18] Moreover, much of the early discussion of π-loading has focused on structural (*i.e.* bond lengths) as opposed to thermochemical data.

This work focuses on how the thermochemistry of π-loaded tungsten complexes might be analyzed to test the veracity of the Wigley's hypothesis. Tungsten is a Group VI transition metal that has been suggested to exhibit the effects of π-loading and was featured in Wigley's initial hypothesis in 1991.[12] This theoretical study uses DFT and coupled cluster methods to analyze the purported bond weakening of π-loaded complexes, thus attempting to quantify the size and scale of π-loading in thermochemical terms.

How then to approach the problem of quantifying and critically analyzing the proposed existence of this M d_π – E p_π molecular orbital competition and what factors may actually modify its strength? Prior work on σ- and π-bond enthalpy components of metal-2p element bonds by Moulder *et al.* (see Chapter 2) provides a starting point.[20,21] Using similar homolytic cleavage models to the prior efforts for W-2p ligands, new models can be designed to provide insight into

π-loaded, multiply bonded catalyst motifs.[20]

The homolytic cleavage provides some insight on the bond dissociation enthalpy for a particular M=E bond; weakening when other π-bonding ligands are present.[21-23] Given the earlier finding that M=E π-bond strengths dictate the mechanism of C–H activation for a three-coordinate metal-imide active site model,[24,25] one may further hypothesize that using π-loading to reduce M=N π-bond strengths would lead to more reactive intermediates.[26-32] This may be particularly interesting for complexes like nitridos, which are generally unreactive in the absence of extremely electron-rich metals.[33-41]

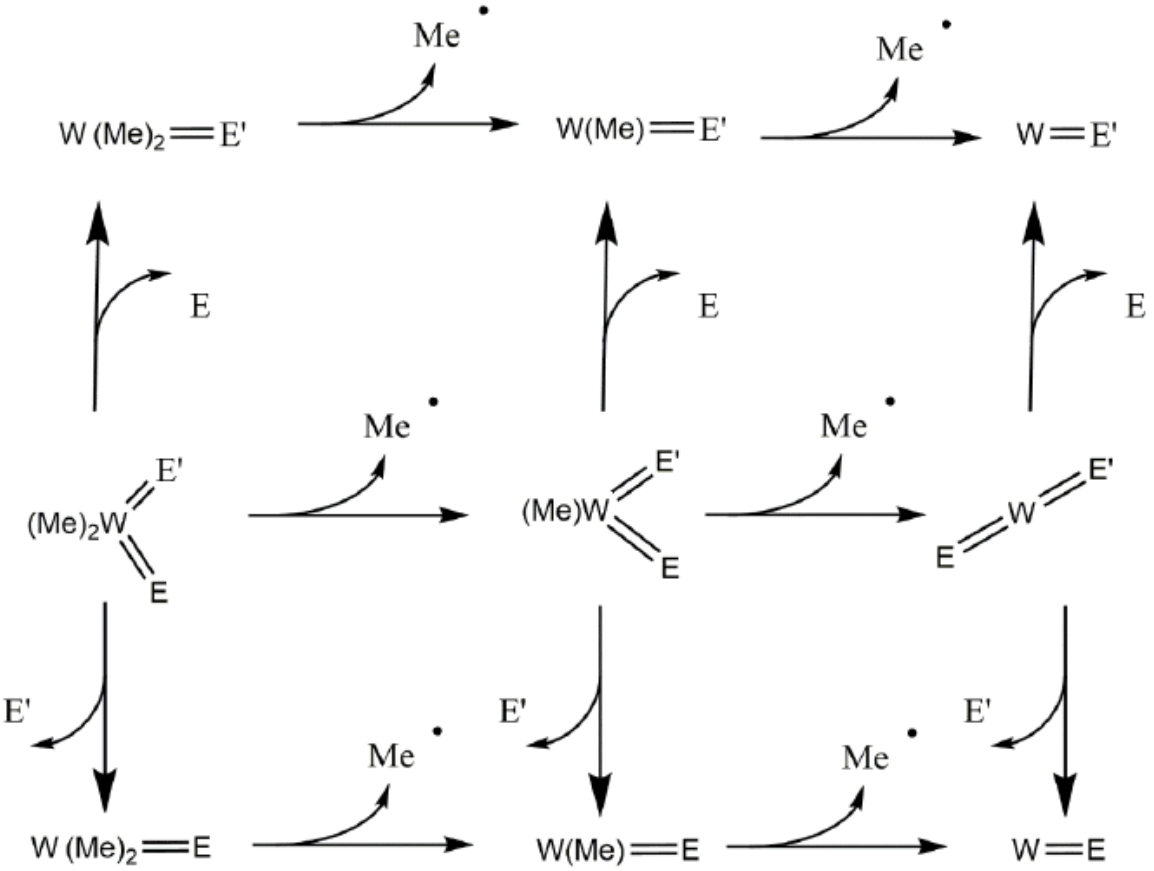

Scheme 4.1: Model of homolytic cleavage between W and E, E' where E, E' = CH_2, CH, NH, N, O for calculating the bond enthalpies of the di-ligated complexes.

The weakening of a M=E bond logically must have some underlying principles.[42] First, does the identity of E matter? To evaluate the impact of the ligand identity, it is worthwhile to

model the most experimentally relevant moieties and those most likely to demonstrate a significant change in the BDEs, for this work, E = CR_2, CR, NR, N, and O *viz* alkylidene, alkylidyne, imide, nitride, and oxo ligands, respectively (Scheme 4.1).[43-51] These are the most common multiply bonded ligand motifs seen in organometallic catalysts. Future work could evaluate, for example, the impact of metal identity within Group VI.

But first, there needs to be a baseline for comparison. The bond strengths of the multiple bonds in question must first be known when there are no other multiple bonds in the complex. Thus, the initial models for W d_π – E p_π, where E = CR_2, CR, NR, N, and O, are modeled within $(Me)_nW{=}E$ complexes, n = 1 - 4. With this baseline, it is then possible to evaluate factors such as the relaxation energy of the fragments upon homolysis, and facets such as those that result from a change in formal oxidation states of the metal.

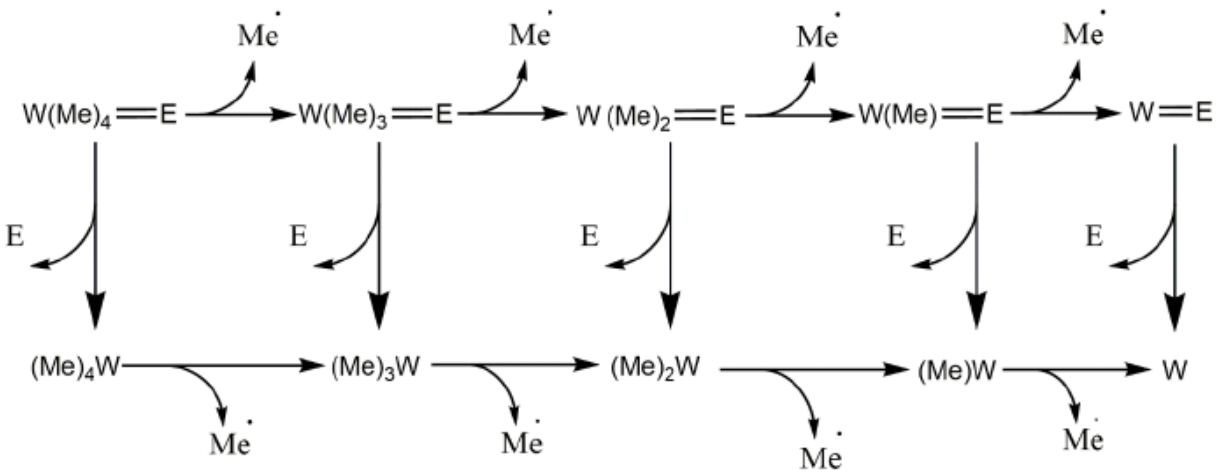

Scheme 4.2: Model of homolytic cleavage between W and E where E = CH_2, CH, NH, N, O for calculating the bond enthalpies of the complexes with a single metal-element multiple bond.

Evaluation of the relaxation energy in the system from the coordination environment may be assessed through the models in Scheme 4.2. This reduction in the number of spectator ligands to the π-bonded E allows for observation of the impact of the d-electron count at the metal, and changes in metal coordination number using typical organometallic counting rules, for example,

while WMe_4O defines a d^0 W(VI) complex, the fragment generated by W—Me homolysis, WMe_3O is formally, d^1 or W(V). The formal oxidation state of the metal is thus anticipated to change with bond homolyses metal coordination numbers.

4.2 Computational Methods

The BDE calculations for Schemes 4.1 and 4.2 are performed with the Gaussian 16 software package[52] in the gas phase at standard temperature (298.15 K) and pressure (1 atm) for the optimized complexes and the fragments generated by homolysis. The PBE0 functional and SDDALL valence basis sets, augmented with d-polarization functions for the associated main group elements have been selected on the basis of having provided the most optimal data in previous work on similar systems.[20] All metal complexes, and fragments thereof, are modeled as neutral species with all appropriate spin multiplicities (low, intermediate and high spin) investigated to determine the lowest energy structure. All enthalpies are derived from clearly defined minima with no imaginary vibrational frequency from the energy Hessian, and are reported in kcal/mol. The lowest energy optimized geometries obtained from DFT optimization are then run as single point coupled clusters calculations using the ORCA software package.

The ORCA software package[52,53] and DLPNO-CCSD(T)/ Def2-SVP, Def2-TZVPP, and Def2-QZVPP single point calculations (at PBE0/SDDALL(d) optimized minima) form a minimal set of calculations to derive a series of complete basis set limits.[54,55] Enthalpic corrections needed to obtain BDEs are also derived from the PBE0/SDDALL(d) DFT simulations. The DLPNO-CCSD(T)/Def2-TZVPP//PBE0/SDDALL(d) level of theory is used for all reported homolytic bond dissociation enthalpies and the snap energy calculations.[56-60]

4.3 Results and Discussion

While unlikely, the use of DFT for these models may misrepresent these BDE values if the

level of theory is inadequate? To discern if the PBE0/SDDALL(d) level of theory is sufficient the complete basis set CCSD(T) limits for a subset of model complexes from the initial research on tungsten bond enthalpies by Moulder *et al.* (Fig. 4.1)[19,20] were calculated. These models allow for not just the current work to be considered, but also for the prior work and are based on known experimental crystal structures.[61-63] All of the bond dissociation enthalpies calculated via DFT methods are within ~10 kcal/mol of CBS/CCSD(T) methods save for the hydrazine double bond which is just over at 11.5 kcal/mol among the small molecule homologs.

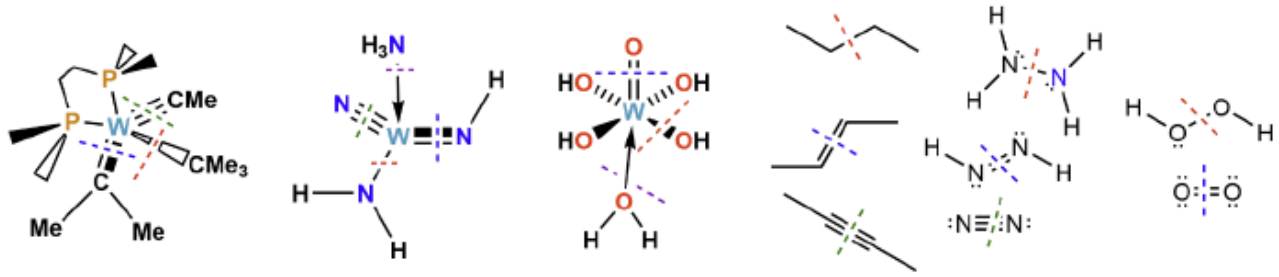

Figure 4.1: D^0 Tungsten-Element models (left) and Element-Element models (right) used to calibrate the level of theory for this research and to model the deformation (snap) enthalpies. Homolytic bond cleavages are color coded with dashed lines to highlight commonalities: red for single bond, blue for double, and green for triple bonds, plus a purple for the disassociation of a dative moiety.

The small molecule main group models are provided as experimentally verifiable homologs of the various bond types modeled. For carbon, the models are butane, *trans*-but-2-ene, and but-2-yne homolytically cleaved between carbons two and three. For nitrogen, the small molecules are hydrazine, *trans*-diazene, and nitrogen gas all cleaved at the bond between the nitrogens. The oxygen models are peroxide and oxygen gas, again homolytically cleaved between the oxygens.

The consistency of the DFT values with the calculated complete basis set limits is impressive (Fig. 4.2). Using the simple formula of double bond BDE – single bond BDE to get the enthalpy difference for the π- bond in the double bond, there is remarkably limited variance in the calculated enthalpies from the DFT to the CCSD(T) complex basis set limit values. The largest

differences are seen in the 2nd π-bonds. This is entirely expected as the errors propagate through the derived BDE values. Regardless, the variances are overall modest and indicative that the PBE0/SDDALL(d) level of theory is a reasonable compromise between computational expense and chemical accuracy for this modeling work with tungsten. However, the small main group models, particularly those involving oxygen, would be better served with the use higher levels of theory both because the variance is higher and because the models are comparatively less computationally expensive even at relatively high levels theory. The difference here illustrates one of the difficulties in modeling heavy metals compared to lighter elements, every compromise between expense and accuracy requires judicious care.

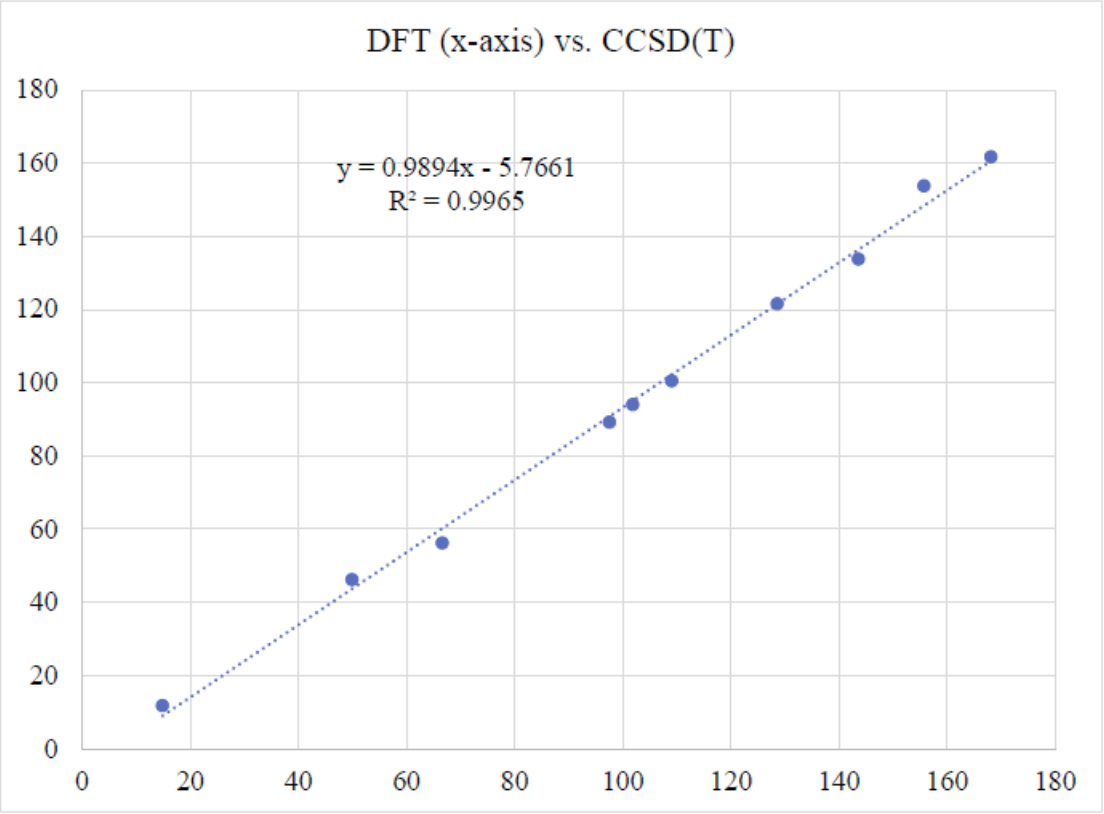

Figure 4.2: Correlation of PBE0/SDDALL(d) DFT calculations to the DLPNO-CCSD(T)/Def2-TZVPP calculations. The coefficient of determination is: R^2 = 99.65%.

The DFT calculations are accurate to the general trend of the homolytic bond cleavages

(Tables 4.1 and 4.2). In most studies, DFT would be sufficient for the modeling (Fig. 4.2), but the preliminary π-loading calculations show small enthalpic differences. (A very high degree of correlation is expected as the higher-level theory calculations use the PBE0/SDDALL(d) geometries.) The complete basis set limits for each of these bonds reveals that the errors from DFT may obscure the π-loading measurements entirely. Thus, this modeling work benefits from the DLPNO-CCSD(T)/def2-TZVPP//PBE0/SDDALL(d) level of theory. Having determined that the CCSD(T) level of theory is necessary and sufficient for this work, the next question is what are the results?

Table 4.1: Complete basis set limits (CBS) in kcal/mol for each bond type as calculated, PBE0/SDDALL(d) (the DFT level of theory for this work), and DFT avg gives the values calculated in Chapter 2.

	Dative	Single	Double	Triple
WC				
CBS		66.7	97.7	143.7
PBE0/SDDALL(d)		56.2	89.2	133.7
DFT avg		61.4	94.0	136.5
WN				
CBS	50.0	109.2	128.7	155.9
PBE0/SDDALL(d)	46.2	100.5	121.5	153.7
DFT avg	47.4	104.4	122.0	156.1
WO				
CBS	14.9	102.0	168.3	
PBE0/SDDALL(d)	11.7	94.0	161.7	
DFT avg	13.6	93.1	161.0	
CC				
CBS		95.1	178.6	212.8
PBE0/SDDALL(d)		81.9	161.2	199.0
DFT avg		87.2	167.2	197.8
NN				
CBS		74.1	130.0	226.5
PBE0/SDDALL(d)		64.9	118.5	217.0
DFT avg		64.0	120.2	217.7

(table continues)

	Dative	Single	Double	Triple
OO				
CBS		55.1	120.1	
PBE0/SDDALL(d)		51.0	125.2	
DFT avg		49.9	122.3	

Table 4.2: The variance between calculated π- bond enthalpies are listed under the Var columns and the π- bond dissociation enthalpies are listed under 1st π- and 2nd π- for each method: complete basis set limits in kcal/mol for each bond type as calculated by CBS complete basis set limit using the energy, PBE0/SDDALL (the level of theory for this work), and DFT avg gives the values calculated in Chapter 2.

	1st π	Var	2nd π	Var
WC				
CBS	31.0	1.2	46.0	2.1
PBE0/SDDALL(d)	33.0		44.5	
DFT avg	32.6		42.5	
WN				
CBS	19.5	1.9	27.2	10.7
PBE0/SDDALL(d)	21.0		32.2	
DFT avg	17.6		34.1	
WO				
CBS	66.3	0.5		n/a
PBE0/SDDALL(d)	67.7			
DFT avg	67.9			
CC				
CBS	83.5	4.8	34.2	9.1
PBE0/SDDALL(d)	79.3		37.8	
DFT avg	80.0		30.6	
NN				
CBS	55.9	2.0	96.5	2.9
PBE0/SDDALL(d)	53.6		98.5	
DFT avg	56.2		97.5	
OO				
CBS	65.0	17.5		n/a
PBE0/SDDALL(d)	74.2			
DFT avg	72.4			

The formal oxidation state and the d-count of the tungsten are frequently convoluted with the coordination number of the metal center given that changes in the latter involve the homolysis of a W—Me bond for the present models; thus, pains have been taken to account for this throughout. The ligands selected for this study are small to minimize the influence of steric factors. Comparing the bond enthalpies of each of the models with respect to their d-counts allows the observation of how they change with different ligand is the primary focus and thus all models are small and optimized to their global minima. The spectator methyl groups function as a model organometallic spectator ligand, which have minimal π-bonding influence of their own, and minimal steric impact, and hence it is expected minimal impact on the strengths of the WE bonds of interest.

The bond dissociation energies in Table 4.3 of WE are modeled according to Scheme 4.1. With this set of homolytic cleavages as a function of d-count, formal oxidation state, and ligand identity, a baseline for the variability of the bond dissociation enthalpies of each of the ligands may be generated.

Table 4.3: Bond dissociation enthalpies of ligands in kcal/mol as a function of the tungsten d-count calculated at the DLPNO-CCSD(T)/Def2-TZVPP//PBE0/SDDALL(d) level of theory for WMe_nE models.

Ligand*	d^0	d^1	d^2
$W{=}CH_2^{2-}$	108.7	136.7	140.0
$W{=}NH^{2-}$	128.4	151.0	156.1
$W{=}O^{2-}$	166.2	191.8	197.3
$W{\equiv}CH^{3-}$	184.4	177.4	
$W{\equiv}N^{3-}$	180.8	173.7	

*Formal charges provided for each ligand using the ionic counting scheme. All ligands that have a formal charge of 2- are modeled as WMe4=E and all with a formal charge of 3- are modeled as WMe3≡E to provide a d^0 tungsten metal center.

The baseline bond dissociation enthalpies allow the observation that every bond dissociation enthalpy for the complexes with multiple-multiple bonds is subtlety different than

those seen for the neutral single multiple bond complexes. The d^0 complexes modeled for Figure 4.3 are $Me_4W{=}E$ (E= CH_2^{2-}, NH^{2-}, divalent O^{2-}) and $Me_3W{\equiv}E$ (E = CH^{3-}, N^{3-}) for the complexes with a single multiply bonded element. The double bonded CH_2^{2-}, NH^{2-} and divalent O^{2-} bonds demonstrate a distinct increase in energy required to homolytically cleave the multiple bond when bonds that are stronger as mono-ligated moieties are present in the complex (Fig. 4.3). For example, the tungsten bisalkylidene model has a + 6.8 kcal/mol greater BDE at 115.5 kcal/mol from the tungsten alkylidene model at 108.7 kcal/mol. All of the alkylidene moieties are stronger, or within error in the case of $MeW(CH_2)(\equiv N)$, when another π-bonded moiety is present in the complex. The tungsten alkylidene alkylidyne model has the BDE of the alkylidene increase slightly by +2.4 kcal/mol to 111.1 kcal/mol. The imide moiety is weaker in the presence of the alkylidyne (by -8.4 kcal/mol to 120.0 kcal/mol) or nitride (by -27.4 kcal/mol to 101.1 kcal/mol) moieties; and distinctly stronger when paired with any of the other three moieties. The imide bond in the tungsten alkylidene imide model is +10.1 kcal/mol stronger at 138.6 kcal/mol. Again, the imide bond in the tungsten bisimide model is +12.9 kcal/mol stronger at 141.3 kcal/mol. This is the exact opposite of π-loading as hypothesized by Wigley![12] Similarly, the imide bond in the tungsten imide oxo model is also strengthened by +7.5 kcal/mol to 135.9 kcal/mol whereas the oxo moiety is strengthened by +10.9 kcal/mol to 177.1 kcal/mol from 166.2 kcal/mol.

The oxo moiety is curious. The two lone pairs on oxygen can make the exact bond order of an oxo ambiguous. To resolve the issue of just how many π-bonds are in the oxo, it is helpful to observe whether or not there is electron spin density on the metal and if there should be. In the d^0 tungsten oxo models there is, of course, no spin density on the central tungsten. Oxygen is a highly electronegative atom which may rationalize why the BDE of the oxo moieties have stronger bond enthalpies compared to the $Me_4W{=}O$ model oxo BDEs when cleaved with another divalent

moiety is present in the $Me_2W(=E)(=O)$ model (E = CH_2, NH, O). Tungsten is an oxophilic metal and this incredible bond strength helps explain why oxygen contamination can so easily kill tungsten catalysts.

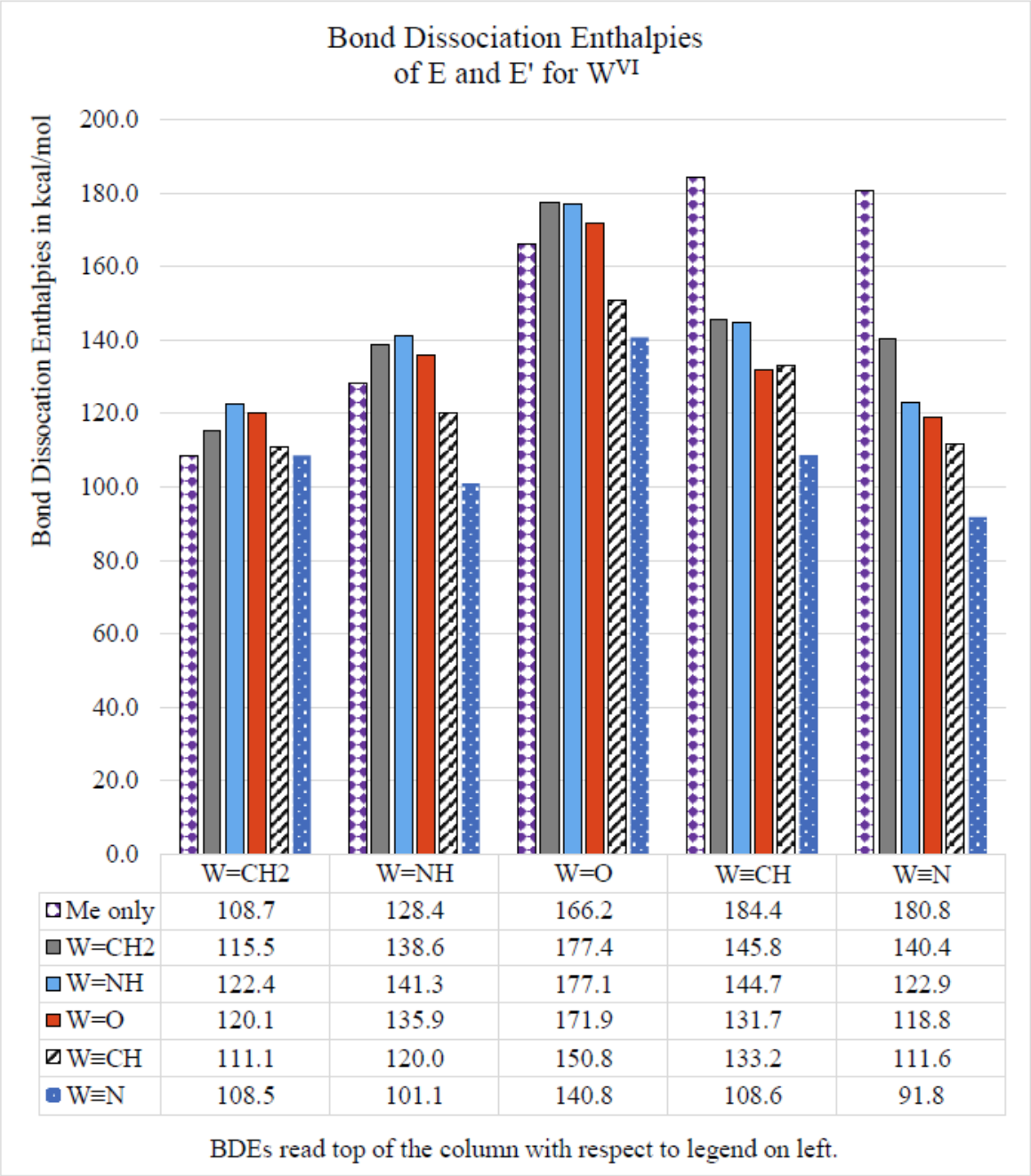

	W=CH2	W=NH	W=O	W≡CH	W≡N
Me only	108.7	128.4	166.2	184.4	180.8
W=CH2	115.5	138.6	177.4	145.8	140.4
W=NH	122.4	141.3	177.1	144.7	122.9
W=O	120.1	135.9	171.9	131.7	118.8
W≡CH	111.1	120.0	150.8	133.2	111.6
W≡N	108.5	101.1	140.8	108.6	91.8

Figure 4.3: Calculated bond dissociation enthalpies in kcal/mol for d^0 W(VI) complexes. Columns are clustered enthalpies for one moiety, the rows are which moiety the enthalpy listed in the column is in respect to. Note, the 'Me Only' in the purple checkerboard is the BDE of the mono-ligated models for that moiety, that is $Me_{n+2}W(E)$ and where the di-ligated species are the $Me_nW(E)(E')$.

For the cleavage of the triple bonds in the d^0 π-loaded models, there is a distinct decrease in the bond dissociation enthalpy consistent with the π-loading hypothesis. For the triple bond cleavages, $Me_2W{\equiv}E$ ($E = CH^{3-}$, N^{3-}) all have strong bond dissociation enthalpies between ~180-184 kcal/mol on their own as mono-ligated species, WMe_3E. The homolytic bond cleavage enthalpies of the triple bonds decrease by 38.6 to 89.0 kcal/mol when any other π-bonded moiety is present. This suggests that π-loading with multiple-multiple bonds only consistently weakens the triple bonds in a d^0 complex, an important nuance and perhaps one that may be exploited for catalysis involving early metal-nitrido moieties, which can be quite inert.[36,64]

The reorganization energy (snap/deformation energy) does point to significant changes in the optimal geometries of the model upon homolytic cleavage.[66-69] Unfortunately, in the absence of a specific catalytic reaction the reorganization energy cannot be conclusively determined to play a significant role in the π-loading hypothesis. Should a π-loaded catalyst be modeled for a specific reaction, the scale of the reorganization enthalpies can be found in the appendices.

Much of the early work assessing π-loading focused on metal-element multiple bond lengths from X-ray crystal structures. Using X-ray crystallography to ascertain structural information is of course logical. It does not, however, give insight into the d-count on the metal and how available lone pairs on a multiply bonded ligating atom, especially O and N which may convolute the issue of bond order and bond enthalpies.

Using the mono-oxo $Me_nW{=}O$ models (Fig. 4.4), the bond lengths between the tungsten and oxygen are static as methyl groups are removed, increasing the d-count on the metal. This example demonstrates how bond order cannot be fully determined by crystal structure alone. Instead, other experimental tests to support the bond order assessment are critical if certainty is needed.

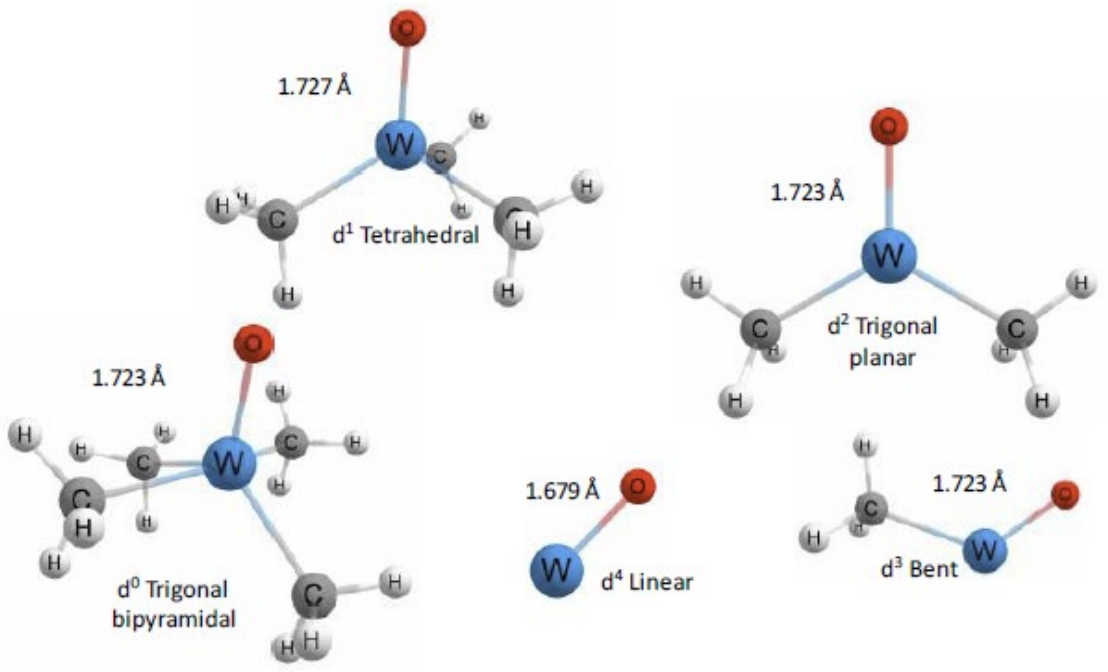

Figure 4.4: Geometry optimized mono-ligated $Me_nW{=}O$ models with their d-counts, geometry at the metal center, and tungsten-oxo bond lengths in angstroms.

To see if the bond lengths changed in any significant manner with respect to the d^0 complexes used for the π-loading models (Fig. 4.5), the WE bond lengths are tabulated based on the PBE0/SDDALL(d) geometries, same as the single point CCSD(T) calcs. DFT predicted metal-element bond lengths generally correlate very well with those derived from experimental crystal structures as observed in prior work from Moulder *et al.*[19,20] Thus, the bond lengths from the models are likely to correspond well to experimental reality.[69]

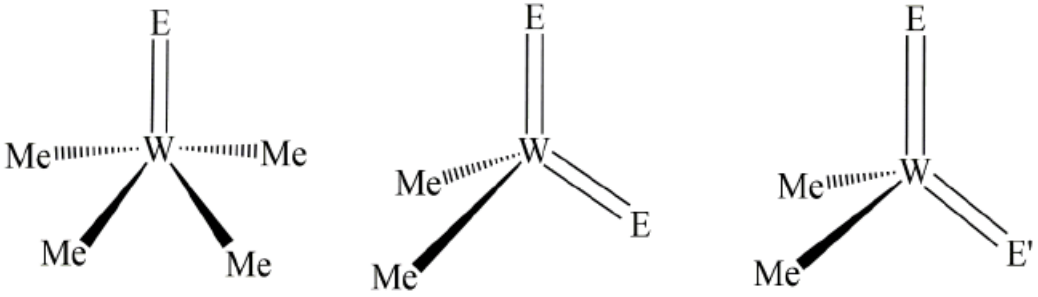

Figure 4.5: The d^0 models used to determine changes in WE bond lengths. Mono-ligated, di-ligated with the same E, and di-ligated with different E'. Note that those models with a triple bond have one fewer methyl groups to remain consistently d^0 tungsten models.

Table 4.4: Mono-ligated $Me_nW{=}E$ bond lengths in Å from Figure 4.5 on left.

Å	W=CH$_2$	W≡CH	W=NH	W≡N	W=O
W=CH$_2$	1.899				
W≡CH		1.763			
W=NH			1.779		
W≡N				1.692	
W=O					1.724

Table 4.5: Percent difference of bond length in Å between the mono-ligated and di-ligated models from Figure 4.5. The percentage reads from the bond on the left with respect to the column above.

E/(E/E') %	W=CH$_2$	W≡CH	W=NH	W≡N	W=O
W=CH$_2$	-0.4	-0.5	-0.2	-1.1	-0.2
W≡CH	-0.1	-7.8	-1.3	-3.9	-1.9
W=NH	1.7	-0.7	0.2	-3.5	-0.1
W≡N	0.1	-1.2	-0.3	-3.6	-1.0
W=O	0.2	-0.9	-0.6	-1.4	-0.6

Table 4.6: Di-ligated $Me_nW{=}E$ bond lengths in Å from Figure 4.5 center and right. The bond length reads from the bond on the left with respect to the column above.

Å	W=CH$_2$	W≡CH	W=NH	W≡N	W=O
W=CH$_2$	1.906	1.909	1.903	1.919	1.903
W≡CH	1.765	1.900	1.786	1.831	1.797
W=NH	1.749	1.792	1.775	1.841	1.780
W≡N	1.690	1.713	1.697	1.752	1.710
W=O	1.721	1.739	1.734	1.748	1.734

Table 4.7: Percent difference of bond length in Å between same and different moiety di-ligated models Figure 4.5 center and right. The percentage reads from the bond on the left with respect to the column above.

E/(E/E') %	W=CH$_2$	W≡CH	W=NH	W≡N	W=O
W=CH$_2$	0.0	-0.2	0.1	-0.7	0.1
W≡CH	7.1	0.0	6.0	3.6	5.4
W=NH	1.4	-1.0	0.0	-3.8	-0.3
W≡N	3.5	2.3	3.2	0.0	2.4
W=O	0.7	-0.3	0.0	-0.8	0.0

The differences in bond lengths do not change significantly for d^0 tungsten metal centers regardless of which ligand is being modeled. Even the greatest percent difference is less than 10%, which translates to a tenth of an angstrom in bond length at most. This may be taken to imply that the ionic radius of the metal center is the dominant factor in the bond length, not the main group element ligated to the metal center. While not unexpected, metal radii are generally larger than main group radii, this does mean that d^0 tungsten centers should have ligands with similar bond lengths for the higher bond orders in any complex. Indeed, the greatest differences are in the alkylidyne and nitride bond lengths that may be defined by alternative resonance structures and thus be ambiguous.[70]

4.4 Summary and Conclusions

This work tests the validity of the π-loading hypothesis and concludes that the π-loading hypothesis is, at best, incomplete. A series of computational models shown in Schemes 4.1 and 4.2 have been created to determine if the mono- or di- ligated complex with the same d-electron count has the stronger tungsten-ligand bond. Several avenues of investigation are pursued to assess what the underlying mechanism might be for potential increase in catalytic activity for W(VI) complexes based on the presence of multiple-multiple bonds.

The calculated complete basis set limits with the DLPNO-CCSD(T)/ Def2-SVP, Def2-TZVPP, and Def2-QZVPP //PBE0/SDDALL(d) levels of theory from the single point geometries show remarkable agreement with the bond enthalpies calculated at the DFT PBE0/SDDALL(d) level of theory. The basis set limits for the bond dissociation enthalpies are calculated in Taable 4.1, and the variances in the π-bond enthalpies are seen in Table 4.2. However, as the scale of the differences in the bond dissociation enthalpies is not necessarily very large, a higher level of theory

than PBE0/SDDALL(d) is needed. All calculations herein are reported at the DLPNO-CCSD(T)/def2-QZVPP//PBE0/SDDALL(d) level of theory except when otherwise specified.

These models provide evidence that the inductive effects of π-bonds do impact the bond strength of other π-bonds within the complex; however, it is not solely in one direction (Fig. 4.6). The divalent bonds in d^0 the tungsten models all have higher homolytic bond dissociation enthalpies when paired together in a di-ligated model than in a mono-ligated model (Fig. 4.1 and Table 4.3). On the other hand, the alkylidyne and nitride bonds have considerably lower homolytic bond enthalpies in the di-ligated d^0 models compared to the d^0 mono-ligated models (Fig. 4.1 and Table 4.3).

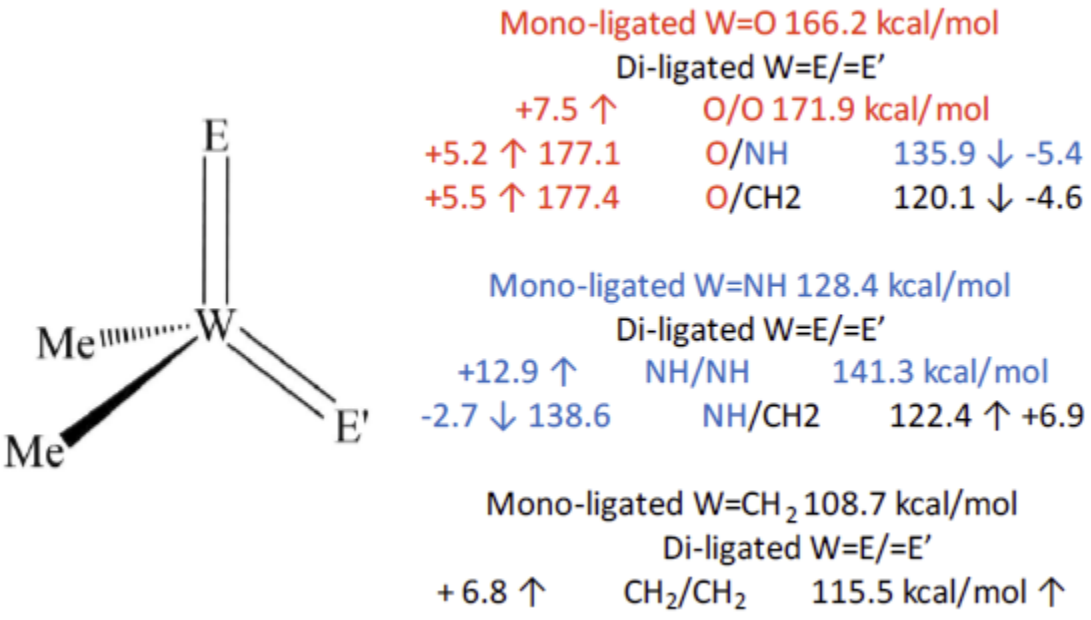

Figure 4.6: Di-ligated d^0 tungsten model with the scale of the impact of π-loading on right in kcal/mol in comparison to di-ligated models with identical E groups.

At higher d-counts, d^1 and d^2, the bond enthalpies in the di-ligated models (Appendix C) decrease consistent with the π-loading hypothesis compared to the mono-ligated models (Table 4.3). Unfortunately, it is far less likely that a catalyst would be synthesized to have access to such

formal oxidation states without, for example, a redox non-innocent ligand donating electrons to the metal which is well beyond the scope of this dissertation.

The snap energies for the homolytic cleavages point to significant molecular orbital strain (see Appendix C). There is significant reorganization occurring in the tungsten fragments at homolytic cleavage of higher bonder orders. In the absence of a specific catalytic reaction, whether this deformation energy plays a significant role in the catalytic activity cannot be determined; nevertheless, it should be considered as an option when studying complexes with multiple-multiple bonds. This work is suggestive, but not conclusive, that snap enthalpy may play a factor in the π-loading hypothesis.

Bond length analysis shows that the multiple bonds are remarkably consistent in length regardless of which ligand or whether mono or di ligated to the tungsten metal center (Fig. 4.5, Tables 4.4 to 4.7). As long as the d-count on the metal is the same, and thus the metal has a consistent ionic radius, the differences in the bond lengths are effectively within error.

There remains a question of the impact of the polarizability of the metal itself on the intramolecular dynamics of the inductive effects on multiple π-bonds. This question could be addressed through interrogating other transition metal complexes with similar features. Future work ideally would involve the rest of the Group VI metals with near identical model complexes to allow the strongest possible basis for comparison with this work.

Ideally, these inductive reasonings would be experimentally confirmed through a combination of spectroscopic techniques. A well deigned experiment with indicator ligands for FTIR has potential to measure the electronic effect of multiple π-bonds through the π-backbonding effects. The shielding and deshielding measurements in NMR also hold some promise to directly measure the influence of the electron densities' proximity to the nuclei.

As there is little evidence in this study to show the existence of π-loading as a thermodynamic effect, there should be some experiments to see if the increase in catalytic activity of a π-loaded system has measurable effect. Systematic experiments that include various π-bonds, coordination numbers, and steric environments should be performed alongside kinetic and buried volume studies.

4.5 Supporting Information

A detailed accounting of the computed homolytic bond enthalpies, snap energies, and complete basis set limits are available in the supporting information for all models. This material can be found in Appendix C.

4.6 Acknowledgements

This material is based upon work supported by the National Science Foundation Graduate Research Fellowship Program under Grant No. 1746050. Any opinions, findings, and conclusions or recommendations expressed in this material are those of the author(s) and do not necessarily reflect the views of the National Science Foundation.

4.7 References

1. Schrock, R. R., High Oxidation State Multiple Metal−Carbon Bonds. *Chem. Rev.* **2002**, *102*, 145−179.

2. Schafer, D. F.; Wolczanski, P. T.; Lobkovsky, E. B., Reactivity Studies of (^{t}Bu$_3$SiNH)(^{t}Bu$_3$SiN═)$_2$WH Including Anionic Derivatives Featuring the Tris-tri-tert-butylsilylimide Tungsten Core. *Organometallics* **2011**, *30*, 6539-6561.

3. Schafer, D. F.; Wolczanski, P. T.; Lobkovsky, E. B., Alkane Binding Implicated in Reactions of (tBu3SiN═)3WHK and Alkyl Halides. *Organometallics* **2011**, *30*, 6518-6538.

4. Corradini, P.; Guerra, G.; Cavallo, L., Do New Century Catalysts Unravel the Mechanism of Stereocontrol of Old Ziegler-Natta Catalysts? *Acc. Chem. Res.* **2004**, *37*, 231-241.

5. Wengrovius, J. H.; Schrock R. R.; Churchill, M. R.; Missert, J. R.; Youngs, W. J., Tungsten-Oxo Alkylidene Complexes as Olefin Metathesis Catalysts and the Crystal Structure of $W(O)(CHCMe_3)(PEt_3)Cl_2$. *J. Am. Chem. Soc.***1980**, *102*, 4515-4516.

6. Georgios C. Vougioukalakis; Grubbs, R. H., Ruthenium-Based Heterocyclic Carbene-Coordinated Olefin Metathesis Catalysts. *Chem. Rev.* **2010**, *110*, 1746–1787.

7. Tomson, N. C.; Arnold, J.; Bergman, R. G., Halo, Alkyl, Aryl, and Bis(imido) Complexes of Niobium Supported by the beta-Diketiminato Ligand. *Organometallics* **2010**, *29*, 2926-2942.

8. Gianetti, T. L.; La Pierre, H. S.; Arnold, J., Group 5 Imides and Bis(imide)s as Selective Hydrogenation Catalysts. *European Journal of Inorganic Chemistry*, **2013**, 3771-3783.

9. Davis-Gilbert, Z. W.; Yao, L. J.; Tonks, I. A., Ti-Catalyzed Multicomponent Oxidative Carboamination of Alkynes with Alkenes and Diazenes. *J. Am. Chem. Soc.* **2016**, *138*, 14570-14573.

10. Davis-Gilbert, Z. W.; Wen, X.; Goodpaster, J. D.; Tonks, I. A., Mechanism of Ti-Catalyzed Oxidative Nitrene Transfer in [2 + 2 + 1] Pyrrole Synthesis from Alkynes and Azobenzene. *J. Am. Chem. Soc.* **2018**, *140*, 7267-7281.

11. Xu, J.; Eagan, J. M.; Kim, S.-S.; Pan, S.; Lee, B.; Klimovica, K.; Jin, K.; Lin, T.-W.; Howard, M. J.; Ellison, C. J.; LaPointe, A. M.; Coates, G. W.; Bates, F. S., Compatibilization of Isotactic Polypropylene (iPP) and High-Density Polyethylene (HDPE) with iPP–PE Multiblock Copolymers. *Macromolecules* **2018**, *51*, 8585-8596.

12. Chao, Y. W.; Rodgers, P. M.; Wigley, D. E.; Alexander, S. J.; Rheingold, A. L. Tris(phenylimido) Complexes of Tungsten: Preparation and Properties of the d0 W(:NR)3 Functional Group. *J. Am. Chem. Soc.* **1991**, *113*, 6326-6328.

13. Helgert, T. R.; Zhang, X.; Box, H. K.; Denny, J. A.; Valle, H. U.; Oliver, A. G.; Akurathi, G.; Webster, C. E.; Hollis, T. K., Extreme π-Loading as a Design Element for Accessing Imido Ligand Reactivity. A CCC-NHC Pincer Tantalum Bis(imido) Complex: Synthesis, Characterization, and Catalytic Oxidative Amination of Alkenes. *Organometallics* **2016**, *35*, 3452-3460.

14. Benson, M. T. B., J. C.; Burrell, A. K.; Cundari, T. R., Bonding and Structure of Heavily π-Loaded Complexes. *Inorg. Chem.* **1995**, *34*, 2348-2355.

15. Wu, P.; Yap, G. P. A.; Theopold, K. H., Structure and Reactivity of Chromium(VI) Alkylidenes. *J. Am. Chem. Soc.* **2018**, *140*, 7088-7091.

16. Wolczanski, P. T. in email correspondence to Theopold, K. H. and Cundari, T. R. May 13, 2019 – Jun 24, 2019.

17. Liang, G.; Hollis, T. K.; Webster, C. E., Computational Analysis of the Intramolecular Oxidative Amination of an Alkene Catalyzed by the Extreme π-Loading N-Heterocyclic Carbene Pincer Tantalum(V) Bis(imido) Complex. *Organometallics* **2018**, *37*, 1671-1681.

18. Messinis, A. M.; Batsanov, A. S.; Wright, W. R. H.; Howard, J. A. K.; Hanton, M. J.; Dyer, P. W., Bis(Imido) Tungsten Complexes: Efficient Precatalysts for the Homogeneous Dimerization of Ethylene. *ACS Catalysis* **2018**, *8*, 11249-11263.

19. Moulder, C. A.; Kafle, K.; Cundari, T. R., Tungsten-Ligand Bond Strengths for 2p Elements Including σ- and π-Bond Strength Components, A Density Functional Theory and *ab Initio* Study. *J Phys Chem A* **2019**, *123*, 7940-7949.

20. Moulder, C. A.; Kafle, K.; Zhou, C. X.; Cundari, T. R., Thermochemistry of Tungsten-3p Elements for Density Functional Theory, *Caveat Lector*! *J Phys Chem A* **2021**, *125*, 681-690.

21. Eikey, R. A.; Abu-Omar, M. M. Nitrido and Imido Transition Metal Complexes of Groups 6−8. *Coord. Chem. Rev.* **2003**, *243*, 83−124.

22. Wang, D.; Loose, F.; Chirik, P. J.; Knowles, R. R., N-H Bond Formation in a Manganese(V) Nitride Yields Ammonia by Light-Driven Proton-Coupled Electron Transfer. *J. Am. Chem. Soc.* **2019**, *141*, 4795-4799.

23. Pappas, I.; Chirik, P. J. Catalytic Proton Coupled Electron Transfer from Metal Hydrides to Titanocene Amides, Hydrazides and Imides: Determination of Thermodynamic Parameters Relevant to Nitrogen Fixation. *J. Am. Chem. Soc.* **2016**, *138*, 13379−13389.

24. Moulder, C. A.; Cundari, T. R., 5d Metal(IV) Imide Complexes. The Impact (or Lack Thereof) of d-Orbital Occupation on Methane Activation and Functionalization. *Inorg Chem* **2017**, *56*, 1823-1829.

25. Moulder, C. A.; Cundari, T. R., A DFT Survey of the Effects of d-Electron Count and Metal Identity on the Activation and Functionalization of C−H Bonds for Mid to Late Transition Metals. *Isr. J. Chem.* **2017**, *57*, 1023-1031.

26. Kriegel, B. M.; Bergman, R. G.; Arnold, J. Nitrene Metathesis and Catalytic Nitrene Transfer Promoted by Niobium Bis(imido) Complexes. *J. Am. Chem. Soc.* **2016**, *138*, 52-55.

27. Webb, J. R.; Burgess, S. A.; Cundari, T. R.; Gunnoe, T. B.; Activation of Carbon–Hydrogen Bonds and Dihydrogen by 1,2-CH-Addition Across Metal–Heteroatom Bonds. *Dalton Trans.* **2013**, *42*, 16646-16665.

28. Billow, B. S.; McDaniel, T. J.; Odom, A. L., Quantifying Ligand Effects in High-Oxidation-State Metal Catalysis. *Nat Chem* **2017**, *9*, 837-842.

29. Clough, B. A.; Mellino, S.; Protchenko, A. V.; Slusarczyk, M.; Stevenson, L. C.; Blake, M. P.; Xie, B.; Clot, E.; Mountford, P., New Titanium Borylimido Compounds: Synthesis, Structure, and Bonding. *Inorg Chem* **2017**, *56*, 10794-10814.

30. Shoaf, A. L.; Bayse, C. A., Trigger Bond Analysis of Nitroaromatic Energetic Materials Using Wiberg Bond Indices. *J Comput Chem* **2018**, *39*, 1236-1248.

31. O'Connor, K. S.; Lamb, J. R.; Vaidya, T.; Keresztes, I.; Klimovica, K.; LaPointe, A. M.; Daugulis, O.; Coates, G. W., Understanding the Insertion Pathways and Chain Walking Mechanisms of α-Diimine Nickel Catalysts for α-Olefin Polymerization: A ^{13}C NMR Spectroscopic Investigation. *Macromolecules* **2017**, *50*, 7010-7027.

32. Berry, J. F. Terminal Nitrido and Imido Complexes of The Late Transition Metals. *Comments Inorg. Chem.* **2009**, *30*, 28−66.

33. Smith, J. M. Smith; Lachicotte, R. J.; Pittard, K. A.; Cundari, T. R.; Lukat-Rodgers, G; Rodgers, K. R.; Holland, P. L., Stepwise Reduction of Dinitrogen Bond Order by a Low-Coordinate Iron Complex. *J. Am. Chem. Soc.* **2001**, *123*, 9222-9223.

34. Davies, D. L.; Macgregor, S. A.; McMullin, C. L., Computational Studies of Carboxylate-Assisted C-H Activation and Functionalization at Group 8-10 Transition Metal Centers. *Chem Rev* **2017**, *117*, 8649-8709.

35. Margulieux, G. W.; Bezdek, M. J.; Turner, Z. R.; Chirik, P. J., Ammonia Activation, H_2 Evolution and Nitride Formation from a Molybdenum Complex with a Chemically and Redox Noninnocent Ligand. *J Am Chem Soc* **2017**, *139*, 6110-6113.

36. Sun, Z.; Hull, O. A.; Cundari, T. R., Computational Study of Methane C-H Activation by Diiminopyridine Nitride/Nitridyl Complexes of 3d Transition Metals and Main-Group Elements. *Inorg Chem* **2018**, *57*, 6807-6815.

37. Shoaf, A. L.; Bayse, C. A., The Effect of Nitro Groups on N_2 Extrusion from Aromatic Azide-based Energetic Materials. *New J. Chem.* **2019**, *43*, 15326-15334.

38. Ashida, Y.; Arashiba, K.; Tanaka, H.; Egi, A.; Nakajima, K.; Yoshizawa, K.; Nishibayashi, Y., Molybdenum-Catalyzed Ammonia Formation Using Simple Monodentate and Bidentate Phosphines as Auxiliary Ligands. *Inorg Chem* **2019**, *58*, 8927-8932.

39. Black, C. C.; Gorden, A. E. V., Oxidative Mannich Reactions of Tertiary Amines Using a Cu(II) 2-Quinoxalinol Salen Catalyst. *J Org Chem* **2019**, *84*, 9806-9810.

40. Najafian, A.; Cundari, T. R., Computational Mechanistic Study of Electro-Oxidation of Ammonia to N_2 by Homogenous Ruthenium and Iron Complexes. *J Phys Chem A* **2019**, *123*, 7973-7982.

41. Bezdek, M. J.; Chirik, P. J. Expanding Boundaries: N_2 Cleavage and Functionalization beyond Early Transition Metals. *Angew. Chem., Int. Ed.* **2016**, *55*, 7892−7896.

42. Schrock, R. R. Catalytic Reduction of Dinitrogen to Ammonia by Molybdenum: Theory versus Experiment. *Angew. Chem., Int. Ed.* **2008**, *47*, 5512−5522.

43. Durand, D. J.; Fey, N., Computational Ligand Descriptors for Catalyst Design. *Chem Rev* **2019**, *119*, 6561-6594.

44. Scheibel, M. G.; Abbenseth, J.; Kinauer, M.; Heinemann, F. W.; Würtele, C.; de Bruin, B.; Schneider, S. Homolytic N−H Activation of Ammonia: Hydrogen Transfer of Parent Iridium Ammine, Amide, Imide, and Nitride Species. *Inorg. Chem.* **2015**, *54*, 9290−9302.

45. Tanaka, H.; Nishibayashi, Y.; Yoshizawa, K. Interplay between Theory and Experiment for Ammonia Synthesis Catalyzed by Transition Metal Complexes. *Acc. Chem. Res.* **2016**, *49*, 987−995.

46. Jakhar, V.; Pal, D.; Ghiviriga, I.; Abboud, K. A.; Lester, D. W.; Sumerlin, B. S.; Veige, A. S., Tethered Tungsten-Alkylidenes for the Synthesis of Cyclic Polynorbornene via Ring Expansion Metathesis: Unprecedented Stereoselectivity and Trapping of Key Catalytic Intermediates. *J Am Chem Soc* **2021**, *143*, 1235-1246.

47. Cundari, T. R., Computational Studies of Transition Metal-Main Group Multiple Bonding. *Chem. Rev.* **2000**, *100*, 807-818.

48. Mindiola, D. J.; Hillhouse, G. L., Terminal Amido and Imido Complexes of Three-Coordinate Nickel. *J. Am. Chem. Soc.* **2001**, *123*, 4623-4624.

49. Buchmeiser, M. R.; Sen, S.; Lienert, C.; Widmann, L.; Schowner, R.; Herz, K.; Hauser, P.; Frey, W.; Wang, D., Molybdenum Imido Alkylidene N-Heterocyclic Carbene Complexes: Structure-Productivity Correlations and Mechanistic Insights. *ChemCatChem* **2016**, *8*, 2710-2723.

50. Wengrovius, J. H. S., R. R.; Churchill, M. R.; Missert, J. R.; Youngs, W. J., Tungsten-Oxo Alkylidene Complexes as Olefin Metathesis Catalysts and the Crystal Structure of $W(O)(CHCMe_3)(PEt_3)Cl_2$. *J. Am. Chem. Soc.* **1980**, *102*, 4515-4516.

51. Gaussian 16, Revision **A.03.** Frisch, M. J.; Trucks, G. W.; Schlegel, H. B.; Scuseria, G. E.; Robb, M. A.; Cheeseman, J. R.; Scalmani, G.; Barone, V.; Petersson, G. A.; Nakatsuji, H.; *et al.* Gaussian, Inc., Wallingford CT, **2016**.

52. Neese, F. The ORCA Program System. Wiley *Interdiscip. Rev. Comput. Mol. Sci.* **2012**, *2*, 73–78.

53. Neese, F. Software Update: The ORCA Program System, Version 4.0. Wiley *Interdiscip. Rev. Comput. Mol. Sci.* **2018**, *8*.

54. Matxain, J. M.; Piris, M.; Lopez, X.; Ugalde, J. M., Complete Basis Set Limit Extrapolation Calculations with $PNOF_3$. *Chemical Physics Letters* **2010**, *499*, 164-167.

55. Feller, D., Benchmarks of Improved Complete Basis Set Extrapolation Schemes Designed for Standard CCSD(T) Atomization Energies. *J Chem Phys* **2013**, *138*, 074103.

56. Rezac, J.; Simova, L.; Hobza, P., CCSD[T] Describes Noncovalent Interactions Better than the CCSD(T), CCSD(TQ), and CCSDT Methods. *J Chem Theory Comput* **2013**, *9*, 364-9.

57. Riplinger, C.; Sandhoefer, B.; Hansen, A.; Neese, F., Natural Triple Excitations in Local Coupled Cluster Calculations with Pair Natural Orbitals. *J Chem Phys* **2013**, *139*, 134101.

58. Liakos, D. G.; Sparta, M.; Kesharwani, M. K.; Martin, J. M.; Neese, F., Exploring the Accuracy Limits of Local Pair Natural Orbital Coupled-Cluster Theory. *J Chem Theory Comput* **2015**, *11*, 1525-39.

59. Feller, D.; Peterson, K. A.; Hill, J. G., On the Effectiveness of CCSD(T) Complete Basis Set Extrapolations for Atomization Energies. *J Chem Phys* **2011**, *135*, 044102.

60. Riplinger, C.; Sandhoefer, B.; Hansen, A.; Neese, F. Natural Triple Excitations in Local Coupled Cluster Calculations with Pair Natural Orbitals. *J. Chem. Phys.* **2013**, *139*, 134101.

61. Churchill, M. R. Y., W. J., Crystal Structure and Molecular Geometry of $W(\equiv CCMe_3)(:CHCMe_3)(CH_2CMe_3)$(Dmpe), a Mononuclear Tungsten(VI) Complex with Metal-Alkylidyne, Metal-Alkylidene, and Metal-Alkyl Linkages. *Inorg. Chem*. **1979**, *18*, 2454-2458.

62. Beaumier, E. P.; Billow, B. S.; Singh, A. K.; Biros, S. M.; Odom, A. L., A Complex with Nitrogen Single, Double, and Triple Bonds to the Same Chromium Atom: Synthesis, Structure, and Reactivity. *Chem Sci* **2016**, *7*, 2532-2536.

63. Cotton, F. A. S., W.; Shamshoum, E. S., Further Studies of the Reactions of Ditungsten Hexa-t- Butoxide with Acetylenes. Isolation and Characterization of $WO(OCMe_3)_4$(THF), $[W_3(OCMe_3)5(\mu\text{-}O)(\mu\text{-}CC_3H_7)O]_2$ and $W(CPh)(OCMe_3)_3$. *J. Organomet. Chem.* **1985**, *296*, 55-68.

64. Lugosan, A.; Cundari, T.; Fleming, K.; Dickie, D.A.; Zeller, M.; Ghannam, J.; Lee, W. Synthesis, characterization, DFT calculations, and reactivity study of a nitrido-bridged dimeric vanadium(iv) complex. *Dalton Trans.*, **2020**, *49*, 1200-1206.

65. van Zeist, W.; Visser, R.; Bickelhaupt, F. M. The Steric Nature of the Bite Angle. *Chem. - Eur. J.* **2009**, *15*, 6112−6115.

66. van Zeist, W. J.; Bickelhaupt, F. M. The Activation Strain Model of Chemical Reactivity. *Org. Biomol. Chem.* **2010**, *8,* 3118−3127.

67. Vermeeren, P.; van der Lubbe, S. C. C.; Fonseca Guerra, C.; Bickelhaupt, F. M.; Hamlin, T. A., Understanding Chemical Reactivity Using the Activation Strain Model. *Nat Protoc* **2020**, *15*, 649-667.

68. Lupp, D.; Christensen, N. J.; Fristrup, P., Synergy between Experimental and Theoretical Methods in the Exploration of Homogeneous Transition Metal Catalysis. *Dalton Trans.,* **2014**, *43*, 11093-105.

69. Beaumier, E. P.; Gordon, C. P.; Harkins, R. P.; McGreal, M. E.; Wen, X.; Coperet, C.; Goodpaster, J. D.; Tonks, I. A., Cp_2Ti(kappa(2)-(^{t})BuNCN(^{t})Bu): A Complex with an Unusual kappa(2) Coordination Mode of a Heterocumulene Featuring a Free Carbene. *J Am Chem Soc* **2020**, *142*, 8006-8018.

CHAPTER 5

SUMMARY, PROSPECTUS, AND FUTURE WORK

5.1 Summary

This body of dissertation research on tungsten-element bond enthalpies is fundamental science, albeit with potential applications in areas such as catalysis where a knowledge of such bond enthalpies is critical. Bond enthalpies are related to a variety of chemical phenomena including chemical reactions, solid state device development, absorption frequencies in spectroscopy, mechanical properties, *etc*. As a physical property of a chemical bond, in theory the bond dissociation enthalpy should be possible to experimentally measure. The difficulty in experimentally measuring bond enthalpies is that they are sensitive to temperature and pressure, not to mention that specific bonds can be impossible to isolate within a molecule. Nevertheless, bond enthalpies are highly useful to predicting, rationalizing, and understand the chemical properties of molecules. This dissertation takes advantage of computational methods to isolate and evaluate the thermochemistry of tungsten-element bonds, filling a knowledge gap. Moreover, this dissertation research seeks to establish accuracy and precision metrics for these metal-element bond enthalpies by comparison of high-level coupled cluster predicted BDES to those obtained from a library of popular functionals and pseudopotentials/valence basis sets.

Tungsten is an early heavy transition metal in Group VI that can be used as the active site in a catalyst, for example, as in the well-known Schrock olefin metathesis catalysts.[1-11] As a Group VI element, tungsten has as many as six electrons in its elemental state and in formally W^{6+} complexes such as $W(CO)_6$. It can also have a formal oxidation state of 6^+ in d^0 complexes. It is the d^0 W(VI) complexes upon which this dissertation focuses most heavily as this high-valent metal state is frequently found in relatively small molecular catalysts. For example, Group VI

elements, including tungsten, have featured as the catalysts in all kinds of olefin metathesis reactions since the 1950s. These catalysts typically involve the metal being ligated to 2p or 3p elements in a variety of different bonding motifs, via both formally single and multiple metal-element bonds. Chapters 2 and 3 provide insight, to our knowledge, for the first time in the literature into metal-ligand bond enthalpies, including the σ and π components, for single, double, and triple bonds between tungsten and these elements.

Quantum chemical methods provide a highly effective tool to access the bond enthalpies of these tungsten-element bonds as isolating the bonds of interest is relatively facile via computations. Like any instrument, to separate the signal from the noise the error needs to be quantified. Using a set of popular DFT functionals and pseudopotentials/valence basis sets a protocol to evaluate the accuracy and precision of the thermochemistry calculations relative to higher levels of *ab initio* theory and, when possible, experimental values. These 'quality control' measurements are reported both in the chapters and in the appendices.

5.2 Prospectus

Furthermore, the computational protocols used herein have been optimized to allow other scientists to reproduce them for other transition metals. It is anticipated that future researchers will expand the BDE database created here to other metals and ligand types. For example, the scripts, datasheets, and files are available with training instructions to allow undergraduate researchers to use for their own work. Moreover, with expansion of the database of metal-ligand bond enthalpies, combined with modern machine learning techniques, there is the potential for a Benson-style group additivity scheme to be developed based on the bond dissociation enthalpies for transition metals that could be used as a means of quickly determining if a potential reaction is worth pursuing

before resorting to quantitative calculations, or at a minimum to prioritize a series of possible calculations.

The ultimate goal of the research on bond dissociation enthalpies is to be highly useful to informing experimental design, for example, of catalysts. To this end, chapter 4 addresses an interesting hypothesis that multiple π-bonds ligated to a metal center would weaken the bond dissociation energies of those bonds and thus increase catalyst reactivity. This π-loading hypothesis was inferred on the basis of analyses of metal-ligand bond lengths, but herein is tested via calculation of bond enthalpies. The effect is found to be likely too subtle to describe the bond enthalpies found with CCSD(T) and especially DFT calculations. While π-loading is shown to affect the bond enthalpies, it is not necessarily weakening the metal-element bonds. Instead, for the d^0 tungsten models, triply bonded ligands weaken other bonds but the double bonds are found to strengthen other double bonds! The analysis presented here suggests that other factors such as the d-count on the metal and the metal's coordination number have a greater impact on the bond enthalpies than π-loading does.

The, at least partial, disconfirmation of the π-loading hypothesis upends a paradigm that has been discussed for 30 years to rationalize experimental catalyst reactivity of $L_nW(E)(E')$ complexes, where E and E' are multiply bond ligands such as imidos, alkylidenes, oxos, *etc.* More needs to be done to validate this disconfirmation. While π-loading does not have a major impact on double bonds in d^0 tungsten, it does have some impact – on the order of less than 10 kcal/mol – that might be useful under the right circumstances for fine-tuning a catalyst.

5.3 Future Work

Does the disconfirmation of π-loading hold for other early transition metals? What about more electron rich late transition metals? The higher d-count tungsten models in the appendices

do show greater impact so might late transition metals show more effect from π-loading? Does the polarizability of the transition metal impact the inductive effects of π-loading? Additionally, given the growing interest in the exploring the reactivity of early – mid series nitrido complexes, and the inference that triply bonded ligands are more susceptible to π-loading in an enthalpic sense, there would seem to be more research worthy in this direction.

It is suspected that the electronegativity match between the central tungsten and the elements that comprise the π-bonded ligands may play a role in the importance – or lack thereof – of so-called π -loading. We posit that with the better electronegativity matches there is less of a "tug of war" over the electrons and more of a covalent sharing than would exist with a large mismatch to use the electroneutrality principles espoused by Pauling. Large electronegativity mismatches (e.g., greater than 1.7 Pauling units difference) lead to metal-ligand interactions that are more ionic in character and pull the electrons more toward the ligands. Tungsten has a similar Pauling electronegativity to carbon (2.36 and 2.55 Pauling units, respectively) compared to nitrogen and oxygen (3.04 and 3.44 Pauling units, respectively). The multiple bonding prevents the correlation from being direct; however, there are computational modeling techniques that visualize the electron density/localization functions that would be informative. These are further avenues for theoretical investigation that are beyond the scope of the work already completed.

Of course, thermochemistry is not the only possible explanation for increased catalyst reactivity. There is the possibility that effect that experimentalists were attributing to π-loading may be manifested not as a ground state but rather a transition state or kinetic effect. This could be simulated using statistical modeling or directly tested experimentally with well-defined kinetic studies. Ideally, a theoretical model would be created using molecular dynamics or the like to simulate the kinetics and then experimentally feasible complexes would be used to confirm the

findings. Systematic experiments that include various π-bonds, coordination numbers, and steric environments, and buried volume studies would be needed before attempting experimental verification.

The body of work that is this dissertation contains significant theoretical work on understanding the electronic structure of tungsten complexes through the analysis bond dissociation enthalpies. It is hoped that these contributions to the field of organometallic theoretical chemistry are widely useful to other inorganic and physical chemists. Moreover, the calibration of popular DFT functionals and pseudopotentials versus coupled cluster techniques should be useful to computational and theoretical chemists.

5.4 References

1. Schrock, R. R., High Oxidation State Multiple Metal−Carbon Bonds. *Chem. Rev.* **2002**, *102*, 145−179.

2. Schafer, D. F.; Wolczanski, P. T.; Lobkovsky, E. B., Reactivity Studies of (tBu3SiNH)(tBu3SiN═)2WH Including Anionic Derivatives Featuring the Tris-tri-tert-butylsilylimide Tungsten Core. *Organometallics* **2011**, *30*, 6539-6561.

3. Schafer, D. F.; Wolczanski, P. T.; Lobkovsky, E. B., Alkane Binding Implicated in Reactions of (tBu3SiN═)3WHK and Alkyl Halides. *Organometallics* **2011**, *30*, 6518-6538.

4. Corradini, P.; Guerra, G.; Cavallo, L., Do New Century Catalysts Unravel the Mechanism of Stereocontrol of Old Ziegler-Natta Catalysts? *Acc. Chem. Res.* **2004**, *37*, 231-241.

5. Wengrovius, J. H.; Schrock R. R.; Churchill, M. R.; Missert, J. R.; Youngs, W. J., Tungsten-Oxo Alkylidene Complexes as Olefin Metathesis Catalysts and the Crystal Structure of W(O)(CHCMe3)(PEt3)Cl2. *J. Am. Chem. Soc.***1980**, *102*, 4515-4516.

6. Georgios C. Vougioukalakis; Grubbs, R. H., Ruthenium-Based Heterocyclic Carbene-Coordinated Olefin Metathesis Catalysts. Chem. Rev. 2010, 110, 1746–1787.

7. Tomson, N. C.; Arnold, J.; Bergman, R. G., Halo, Alkyl, Aryl, and Bis(imido) Complexes of Niobium Supported by the beta-Diketiminato Ligand. *Organometallics* **2010**, *29*, 2926-2942.

8. Gianetti, T. L.; La Pierre, H. S.; Arnold, J., Group 5 Imides and Bis(imide)s as Selective Hydrogenation Catalysts. *European Journal of Inorganic Chemistry,* **2013**, 3771-3783.

9. Davis-Gilbert, Z. W.; Yao, L. J.; Tonks, I. A., Ti-Catalyzed Multicomponent Oxidative Carboamination of Alkynes with Alkenes and Diazenes. *J. Am. Chem. Soc.* **2016***, 138*, 14570-14573.

10. Davis-Gilbert, Z. W.; Wen, X.; Goodpaster, J. D.; Tonks, I. A., Mechanism of Ti-Catalyzed Oxidative Nitrene Transfer in [2 + 2 + 1] Pyrrole Synthesis from Alkynes and Azobenzene. *J. Am. Chem. Soc.* **2018***, 140*, 7267-7281.

11. Xu, J.; Eagan, J. M.; Kim, S.-S.; Pan, S.; Lee, B.; Klimovica, K.; Jin, K.; Lin, T.-W.; Howard, M. J.; Ellison, C. J.; LaPointe, A. M.; Coates, G. W.; Bates, F. S., Compatibilization of Isotactic Polypropylene (iPP) and High-Density Polyethylene (HDPE) with iPP–PE Multiblock Copolymers. *Macromolecules* **2018***, 51*, 8585-8596.

APPENDIX A

SUPPLEMENTAL INFORMATION FOR CHAPTER 2

A.1 BDE Aggregate Data

A.1.1 BDE Aggregate Data vis a vis Experimental Data

Table A.1.1:Percent absolute error of small molecule homolog calculated bond dissociation enthalpies in kcal/mol by functional and valence basis set with respect to experimental reference values.

Basis	Psuedo-potential	Carbon			Nitrogen			Oxygen		Overall	
		Single	Double	Triple	Single	Double	Triple	Single	Double	Avg	Std Dev
BP 86	CEP 31G	8.8			17.4	15.5	8.8	3.0	6.7	10.0	5.4
	CEP 121G	9.7			6.8	8.6	2.2	3.0	6.8	6.2	3.0
	LANL2DZ	5.3			1.5	1.6	1.0	17.1	16.0	7.1	7.5
	SDDAll	8.2			5.2	5.6	1.7	1.5	4.4	4.4	2.6
B3LYP	CEP 31G	36.8			16.8	18.7	12.6	16.1	8.6	18.3	9.8
	CEP 121G	12.1			15.3	17.8	9.9	15.9	8.4	13.2	3.7
	LANL2DZ	7.9			7.1	10.8	6.2	4.6	0.6	6.2	3.4
	SDDAll	10.6			13.9	15.1	6.3	20.7	11.1	13.0	4.9
M06	CEP 31G	1.7			0.6	11.3	19.3	4.5	10.6	8.0	7.1
	CEP 121G	0.5			0.8	13.4	17.4	5.4	11.2	8.1	7.0
	LANL2DZ	1.7			0.5	9.1	9.3	0.7	4.2	4.3	4.1
	SDDAll	0.6			2.8	10.3	19.6	18.3	15.6	11.2	8.1
BLYP	CEP 31G	14.8			17.4	15.5	8.8	5.2	0.6	10.4	6.6
	CEP 121G	15.8			16.1	14.8	6.4	5.2	0.4	9.8	6.7
	LANL2DZ	10.3			5.9	5.6	1.2	9.9	11.3	7.4	3.8
	SDDAll	14.1			14.2	11.5	2.2	10.9	3.3	9.4	5.3
B97D	CEP 31G	3.7			5.2	9.1	6.5	1.3	4.9	5.1	2.6
	CEP 121G	5.2			3.7	8.2	4.0	0.8	4.7	4.4	2.4
	LANL2DZ	6.3			4.9	0.3	0.8	19.8	17.6	8.3	8.4
	SDDAll	3.7			2.4	5.7	0.1	0.1	5.1	2.8	2.4
PBEPBE	CEP 31G	6.0			5.9	7.5	4.2	5.8	8.4	6.3	1.5
	CEP 121G	6.8			5.1	7.3	2.3	5.9	8.6	6.0	2.2
	LANL2DZ	2.2			5.6	9.7	7.0	5.2	6.4	6.0	2.5
	SDDAll	5.6			2.9	4.8	1.2	3.4	1.7	3.3	1.7
M11L	CEP 31G	1.6			13.3	5.2	10.1	26.2	7.9	10.7	8.6
	CEP 121G	2.9			2.6	3.4	13.2	26.2	4.2	8.8	9.4
	LANL2DZ	0.5			6.4	5.0	2.0	6.7	5.3	4.3	2.5
	SDDAll	0.9			13.7	8.4	13.9	36.0	9.4	13.7	11.9

Basis	Psuedo-potential	Carbon			Nitrogen			Oxygen		Overall	
		Single	Double	Triple	Single	Double	Triple	Single	Double	Avg	Std Dev
MN12L	CEP 31G	3.0			11.3	2.6	17.4	16.2	1.9	8.7	7.1
	CEP 121G	2.1			11.0	8.9	18.3	16.1	6.5	10.5	6.0
	LANL2DZ	0.9			2.5	0.2	5.8	4.6	11.2	4.2	4.0
	SDDAll	3.0			12.4	14.6	22.3	25.7	1.3	13.2	9.9
N12	CEP 31G	0.4			2.6	4.5	4.9	12.1	7.6	5.3	4.1
	CEP 121G	1.4			4.3	3.6	2.1	12.5	7.4	5.2	4.1
	LANL2DZ	0.5			5.8	9.8	14.9	12.5	2.5	7.7	5.7
	SDDAll	0.9			7.3	1.1	2.1	8.2	5.9	4.2	3.2
SOGGA11	CEP 31G	3.6			5.7	1.1	4.6	20.1	16.5	8.6	7.8
	CEP 121G	2.0			7.3	0.5	2.6	19.7	16.7	8.1	8.2
	LANL2DZ	1.1			9.7	4.7	10.6	21.9	14.9	10.5	7.4
	SDDAll	1.4			2.4	0.4	1.4	8.2	11.8	4.3	4.6
B2PLYP	CEP 31G	6.4			14.9	18.2	12.9	16.5	10.0	13.1	4.4
	CEP 121G	6.8			12.7	16.5	9.7	14.8	8.7	11.5	3.8
	LANL2DZ	4.1			7.1	11.8	7.4	7.5	4.1	7.0	2.8
	SDDAll	6.1			12.6	14.7	7.0	18.9	11.1	11.7	4.8
MP2	CEP 31G	2.0			7.3	14.6	19.3	6.6	7.8	9.6	6.2
	CEP 121G	2.7			3.7	11.4	9.1	2.5	5.0	5.7	3.7
	LANL2DZ	2.6			2.6	10.7	9.2	1.6	4.9	5.3	3.8
	SDDAll	2.2			5.3	11.0	7.7	6.0	6.7	6.5	2.9
Average	CEP 31G	5.7			0.6	11.3	19.3	-4.1	-1.1	5.3	8.7
	CEP 121G	4.5			0.8	13.4	17.4	-3.7	-0.7	5.3	8.4
	LANL2DZ	2.8			0.5	9.1	9.3	-5.1	-3.2	2.2	6.1
	SDDAll	3.8			2.8	10.3	19.6	-10.4	-0.9	4.2	10.2
Overall	Average	4.2			1.2	11.0	16.4	-5.8	-1.5	8.1	
	Std Dev	6.1			5.1	5.4	6.0	8.5	4.6		
	Q1	1.7			3.3	4.7	2.2	4.9	4.5		
	Q2	3.0			5.9	8.9	7.0	8.2	7.4		
	Q3	6.6			11.8	11.6	11.6	16.8	10.9		
	Q4	36.8			17.4	18.7	22.3	36.0	17.6		
	Median	3.3			5.9	9.0	7.0	8.2	7.1	7.8	
	Max	36.8			17.4	18.7	22.3	36.0	17.6	18.3	
	Min	0.4			0.5	0.2	0.1	0.1	0.4	2.8	

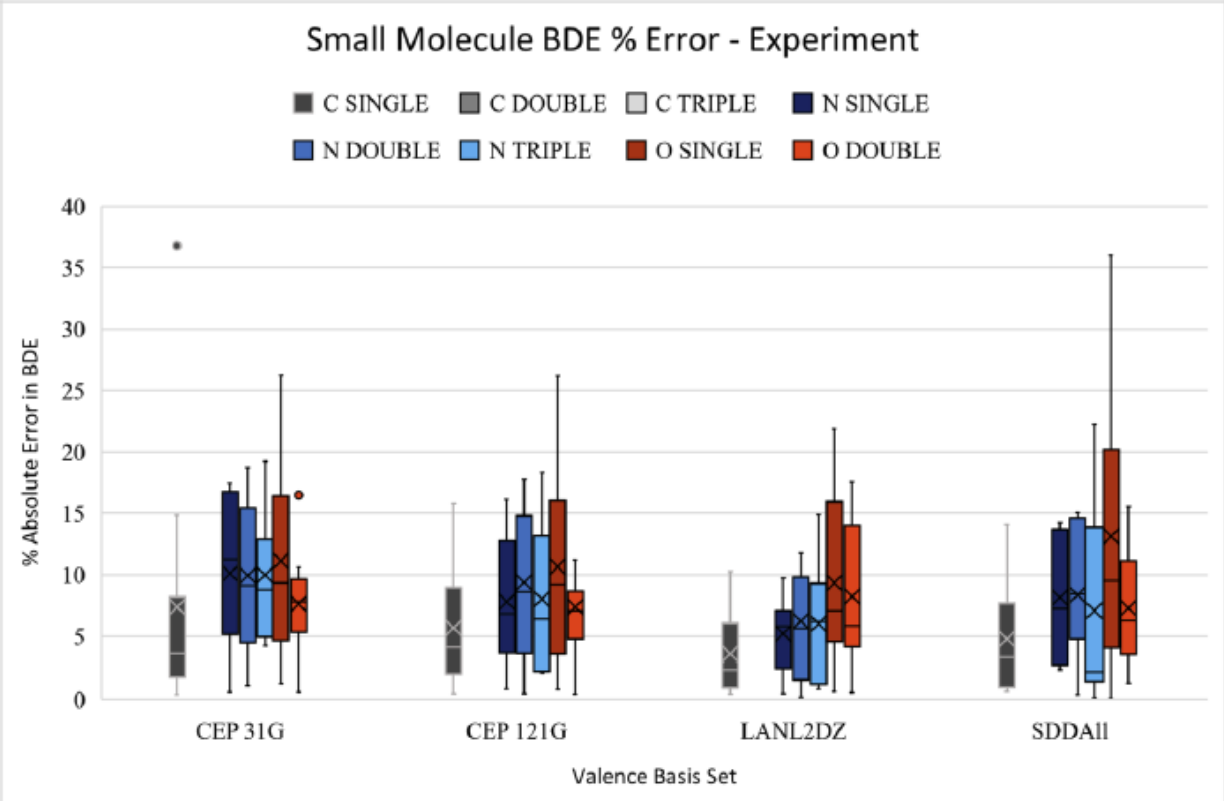

Figure A.1.1: Box and whisker plot showing percent absolute error as a function of bond type for the small molecule with respect to the experimental reference data. The arithmetic mean is indicated with an X, the median depicted with a horizontal line, and the outliers are left as dots.

A.1.2 BDE Aggregate Data vis a vis G4

Table A.1.2: Percent absolute error of small molecule homolog calculated bond dissociation enthalpies in kcal/mol by functional and valence basis set with respect to reference values calculated at the G4 level of theory.

Basis	Psuedo-potential	Carbon			Nitrogen			Oxygen		Overall	
		Single	Double	Triple	Single	Double	Triple	Single	Double	Avg	Std Dev
BP 86	CEP 31G	9.1	0.6	11.5	14.2	10.7	8.9	7.2	7.2	8.7	4.0
	CEP 121G	10.0	4.8	7.2	3.2	3.5	2.4	7.2	7.3	5.7	2.6
	LANL2DZ	5.6	0.1	2.1	5.5	4.0	0.8	21.9	16.5	7.1	7.9
	SDDAll	8.5	2.5	4.1	1.6	0.3	1.5	2.6	4.8	3.2	2.6
B3LYP	CEP 31G	37.0	22.9	25.8	13.6	14.1	12.7	12.6	8.2	18.4	9.5
	CEP 121G	12.4	10.0	10.9	12.0	13.2	10.1	12.5	8.0	11.1	1.7
	LANL2DZ	8.2	5.7	4.6	3.5	5.8	6.3	0.7	0.1	4.4	2.8
	SDDAll	11.0	7.7	8.0	10.6	10.3	6.5	17.4	10.8	10.3	3.3
M06	CEP 31G	1.4	2.6	9.1	3.2	6.3	19.4	0.6	10.2	6.6	6.2
	CEP 121G	0.1	2.0	5.0	3.0	8.5	17.5	1.6	10.8	6.1	5.9
	LANL2DZ	2.1	0.6	3.3	4.4	4.0	9.4	3.4	3.8	3.9	2.6
	SDDAll	1.0	0.0	2.9	1.0	5.3	19.7	15.0	15.2	7.5	7.9
BLYP	CEP 31G	15.1	10.2	16.7	14.2	10.7	8.9	1.3	1.0	9.8	5.9
	CEP 121G	16.1	9.5	12.6	12.9	10.0	6.6	1.3	0.8	8.7	5.5
	LANL2DZ	10.6	3.5	5.2	2.3	0.3	1.4	14.4	11.8	6.2	5.3
	SDDAll	14.4	7.1	57.9	10.9	6.5	2.4	7.2	2.8	13.7	18.3
B97D	CEP 31G	4.0	3.1	10.2	1.5	4.0	6.6	5.4	5.3	5.0	2.6
	CEP 121G	5.6	2.4	6.2	0.0	3.0	4.1	4.9	5.1	3.9	2.0
	LANL2DZ	6.7	1.6	4.8	8.9	5.3	0.7	24.7	18.1	8.9	8.4
	SDDAll	4.0	0.4	2.8	1.3	0.3	0.3	4.0	5.6	2.3	2.0
PBEPBE	CEP 31G	6.4	3.6	9.5	2.2	2.3	4.4	10.1	8.9	5.9	3.2
	CEP 121G	7.1	10.2	5.2	1.4	2.1	2.4	10.2	9.1	6.0	3.7
	LANL2DZ	2.5	1.9	0.2	2.0	4.6	7.1	9.5	6.8	4.3	3.2
	SDDAll	6.0	0.7	2.3	0.8	0.6	1.0	0.5	2.1	1.7	1.8
M11L	CEP 31G	1.9	0.4	14.2	10.0	11.1	10.0	23.2	8.3	9.9	7.1
	CEP 121G	3.3	0.5	0.8	6.5	9.3	13.0	23.2	4.6	7.6	7.6
	LANL2DZ	0.1	3.0	7.0	2.8	0.4	2.2	2.9	4.9	2.9	2.2
	SDDAll	1.2	2.7	3.8	10.4	14.6	13.7	33.4	9.8	11.2	10.3
	CEP 31G	2.7	4.4	8.5	7.8	8.4	17.2	12.8	1.5	7.9	5.2

Basis	Psuedo-potential	Carbon			Nitrogen			Oxygen		Overall	
		Single	Double	Triple	Single	Double	Triple	Single	Double	Avg	Std Dev
MN12L	CEP 121G	1.8	3.7	5.1	7.6	15.0	18.1	16.1	6.1	9.2	6.3
	LANL2DZ	0.5	0.3	2.6	1.2	5.4	6.0	0.7	10.8	3.4	3.7
	SDDAll	2.6	5.8	1.4	9.0	21.1	22.1	22.7	0.9	10.7	9.7
N12	CEP 31G	0.7	0.3	7.2	6.5	0.9	5.1	16.7	8.0	5.7	5.4
	CEP 121G	1.8	1.2	2.4	8.3	1.8	2.3	17.1	7.8	5.3	5.5
	LANL2DZ	0.8	16.1	1.1	9.9	4.7	15.0	17.1	2.9	8.5	6.9
	SDDAll	0.5	3.4	0.2	11.4	6.8	1.9	12.6	6.3	5.4	4.7
SOGGA11	CEP 31G	3.2	1.3	7.2	9.8	4.5	4.7	25.0	17.0	9.1	8.1
	CEP 121G	1.7	2.2	3.1	11.5	5.1	2.7	24.6	17.2	8.5	8.5
	LANL2DZ	0.8	4.5	1.0	14.0	0.7	10.7	26.9	15.4	9.2	9.3
	SDDAll	1.7	2.2	1.1	6.3	5.2	1.3	12.6	12.3	5.3	4.8
B2PLYP	CEP 31G	6.7	4.4	11.8	11.6	13.6	13.0	13.1	9.6	10.5	3.3
	CEP 121G	7.2	3.0	6.6	9.4	11.7	9.8	11.4	8.3	8.4	2.9
	LANL2DZ	4.5	0.6	1.7	3.6	6.8	7.6	3.7	3.7	4.0	2.3
	SDDAll	6.5	0.9	4.1	9.2	9.9	7.2	15.6	10.8	8.0	4.5
MP2	CEP 31G	1.6	3.7	3.5	3.8	9.8	19.4	2.8	7.4	6.5	5.9
	CEP 121G	2.3	6.3	3.3	0.0	6.4	9.3	1.5	4.6	4.2	3.0
	LANL2DZ	2.2	7.3	6.0	1.2	5.7	9.4	2.4	4.5	4.8	2.8
	SDDAll	1.8	7.8	5.5	1.6	6.0	7.8	2.1	6.3	4.9	2.6
Average	CEP 31G	6.0	3.1	11.3	10.7	10.4	10.0	10.9	7.7	8.8	2.9
	CEP 121G	4.8	2.3	5.2	8.5	9.8	8.0	11.0	7.5	7.1	2.9
	LANL2DZ	3.1	1.3	2.3	5.3	6.2	5.7	10.7	8.3	5.4	3.1
	SDDAll	4.1	0.3	3.4	8.7	8.6	6.7	12.1	7.3	6.4	3.7
Overall	Average	4.5	1.8	5.5	8.3	8.8	7.6	11.2	7.7	7.1	
	Std Dev	6.3	4.4	8.9	4.6	4.7	6.0	8.7	4.7		
	Q1	1.7	1.3	2.7	2.1	3.7	2.4	2.8	4.6		
	Q2	3.2	3.0	5.0	6.3	5.7	7.1	11.4	7.4		
	Q3	6.9	5.8	7.6	9.9	9.8	11.7	16.9	10.5		
	Q4	37.0	22.9	57.9	14.2	21.1	22.1	33.4	18.1		
	Median	3.2	3.0	5.0	6.4	5.7	7.1	10.8	7.3	6.5	
	Max	37.0	22.9	57.9	14.2	21.1	22.1	33.4	18.1	18.4	
	Min	0.1	0.0	0.2	0.0	0.3	0.3	0.5	0.1	1.7	

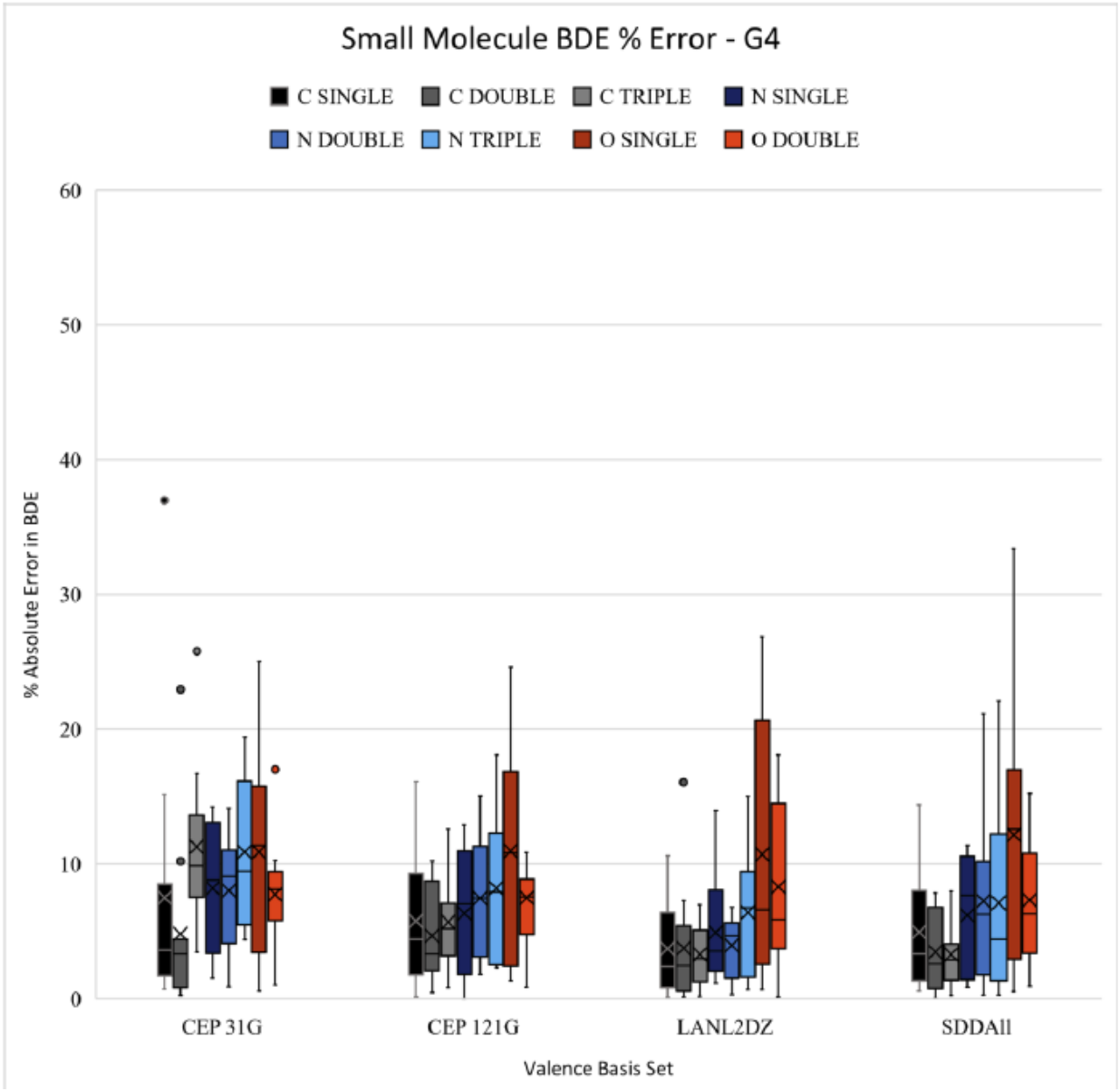

Figure A.1.2: Box and whisker plot showing percent absolute error as a function of bond type for the small molecule with respect to the G4 calculation data. The arithmetic mean is indicated with an X, the median depicted with a horizontal line, and the outliers are left as dots. An extreme outliers is not included in this box and whisker plot, the BLYP/SDDAll(d,p) predicted carbon-carbon triple bond enthalpy has an error versus experiment of 57.9%.

A.1.3 BDE Aggregate Data vis a vis W1u

Table A.1.3: Percent absolute error of small molecule homolog calculated bond dissociation enthalpies in kcal/mol by functional and valence basis set with respect to reference values calculated at the uW1 level of theory.

Basis	Psuedo-potential	Carbon			Nitrogen			Oxygen		Overall	
		Single	Double	Triple	Single	Double	Triple	Single	Double	Avg	Std Dev
BP 86	CEP 31G	10.2	0.9	11.9	15.7	11.7	8.6	4.9	6.9	8.9	4.6
	CEP 121G	11.1	5.1	7.7	4.8	4.5	2.0	4.9	7.0	5.9	2.7
	LANL2DZ	6.8	0.4	2.5	3.7	2.8	1.2	19.2	16.2	6.6	7.1
	SDDAll	9.7	2.8	4.5	3.2	1.4	2.0	0.3	4.6	3.6	2.9
B3LYP	CEP 31G	37.8	23.2	26.1	15.00	15.11	12.4	14.6	8.4	19.1	9.5
	CEP 121G	13.5	10.3	11.3	13.49	14.14	9.7	14.4	8.2	11.9	2.3
	LANL2DZ	9.3	6.0	5.0	5.13	6.84	6.0	2.9	0.4	5.2	2.7
	SDDAll	12.1	8.0	8.4	12.12	11.27	6.1	19.3	11.0	11.0	4.0
M06	CEP 31G	0.1	2.9	9.5	1.48	7.35	19.1	2.7	10.5	6.7	6.3
	CEP 121G	1.1	2.3	5.4	1.26	9.57	17.2	3.7	11.1	6.5	5.7
	LANL2DZ	3.3	0.9	3.8	2.62	5.06	9.1	1.1	4.1	3.7	2.6
	SDDAll	2.2	0.3	3.4	0.70	6.35	19.4	16.9	15.4	8.1	7.9
BLYP	CEP 31G	16.2	10.5	17.1	15.68	11.70	8.6	3.5	0.8	10.5	6.0
	CEP 121G	17.2	9.8	13.0	14.35	11.00	6.2	3.5	0.6	9.5	5.6
	LANL2DZ	11.7	3.8	5.6	3.90	1.43	1.0	11.8	11.5	6.4	4.7
	SDDAll	15.5	7.4	57.1	12.43	7.58	2.0	9.3	3.1	14.3	17.9
B97D	CEP 31G	5.2	3.3	10.7	3.17	5.07	6.2	3.1	5.1	5.2	2.5
	CEP 121G	6.7	2.6	6.6	1.65	4.11	3.7	2.6	4.9	4.1	1.9
	LANL2DZ	7.8	1.9	5.3	7.11	4.13	1.1	22.0	17.8	8.4	7.6
	SDDAll	5.2	0.1	3.3	0.36	1.46	0.1	1.7	5.3	2.2	2.2
PBEPBE	CEP 31G	7.5	3.9	9.9	3.88	3.39	4.0	7.7	8.6	6.1	2.6
	CEP 121G	8.3	10.5	5.7	3.04	3.22	2.0	7.8	8.8	6.2	3.1
	LANL2DZ	3.7	1.6	0.3	3.59	5.67	6.8	7.1	6.6	4.4	2.5
	SDDAll	7.1	0.9	2.7	0.83	0.54	1.4	1.7	1.9	2.1	2.1
M11L	CEP 31G	3.2	0.1	14.6	11.48	9.87	10.4	24.9	8.1	10.3	7.5
	CEP 121G	4.5	0.2	1.3	4.74	8.05	13.5	24.9	4.4	7.7	8.1
	LANL2DZ	1.1	3.3	7.4	4.45	0.75	1.8	5.0	5.1	3.6	2.3
	SDDAll	2.5	2.4	3.3	11.86	13.27	14.1	34.8	9.6	11.5	10.6
	CEP 31G	1.4	4.1	8.9	9.37	7.17	17.7	14.7	1.8	8.1	5.8

Basis	Psuedo-potential	Carbon			Nitrogen			Oxygen		Overall	
		Single	Double	Triple	Single	Double	Triple	Single	Double	Avg	Std Dev
MN12L	CEP 121G	0.5	3.4	5.6	9.10	13.73	18.6	14.6	6.3	9.0	6.2
	LANL2DZ	0.7	0.0	3.1	0.44	4.25	5.6	2.9	11.0	3.5	3.6
	SDDAll	1.4	5.5	1.9	10.52	19.75	22.6	24.4	1.2	10.9	9.9
N12	CEP 31G	2.0	0.0	7.6	4.76	0.24	4.7	14.1	7.8	5.2	4.7
	CEP 121G	3.0	0.9	2.8	6.50	0.65	1.9	14.6	7.6	4.7	4.7
	LANL2DZ	2.1	15.7	1.6	8.04	5.78	14.7	14.5	2.7	8.1	6.1
	SDDAll	0.7	3.1	0.2	9.53	5.61	2.3	10.1	6.0	4.7	3.8
SOGGA11	CEP 31G	1.9	1.0	7.6	7.92	3.28	4.3	22.3	16.7	8.1	7.6
	CEP 121G	0.4	1.9	3.6	9.60	3.94	2.3	21.9	16.9	7.6	7.9
	LANL2DZ	0.5	4.2	1.5	12.06	0.45	10.4	24.1	15.1	8.5	8.4
	SDDAll	2.9	1.9	1.6	4.57	4.06	1.7	10.1	12.0	4.9	4.0
B2PLYP	CEP 31G	7.9	4.7	12.2	13.09	14.54	12.7	15.0	9.9	11.2	3.5
	CEP 121G	8.3	3.3	7.1	10.90	12.75	9.4	13.3	8.5	9.2	3.2
	LANL2DZ	5.6	0.3	2.2	5.17	7.83	7.2	5.8	3.9	4.8	2.5
	SDDAll	7.6	1.2	4.5	10.71	10.90	6.8	17.4	11.0	8.8	4.9
MP2	CEP 31G	0.4	3.4	3.9	5.37	10.78	19.06	4.9	7.6	6.9	5.8
	CEP 121G	1.0	6.0	2.8	1.65	7.46	8.89	0.7	4.9	4.2	3.1
	LANL2DZ	0.9	7.0	5.4	0.53	6.76	9.02	0.2	4.8	4.3	3.4
	SDDAll	0.5	7.5	5.0	3.27	7.02	7.47	4.3	6.5	5.2	2.4
Average	CEP 31G	7.2	3.4	11.7	9.77	8.43	9.77	11.0	7.7	8.6	2.6
	CEP 121G	6.0	2.6	5.6	7.82	8.06	7.7	10.6	7.4	7.0	2.3
	LANL2DZ	4.3	1.0	2.7	5.01	3.87	5.5	9.7	8.3	5.1	2.8
	SDDAll	5.3	0.0	2.9	7.44	7.48	6.7	12.5	7.3	6.2	3.7
Overall	Average	5.7	1.8	5.7	7.5	7.0	7.4	11.0	7.7	7.2	
	Std Dev	6.6	4.4	8.8	4.7	4.7	6.1	8.5	4.6		
	Q1	1.3	1.1	3.0	3.2	3.7	2.2	3.5	4.7		
	Q2	3.7	3.3	5.3	5.1	6.3	6.8	10.1	7.6		
	Q3	8.1	5.7	8.1	10.6	10.3	11.4	15.9	10.7		
	Q4	37.8	23.2	57.1	15.7	19.7	22.6	34.8	17.8		
	Median	4.1	3.2	5.4	5.1	6.6	6.8	9.7	7.3	6.7	
	Max	37.8	23.2	57.1	15.7	19.7	22.6	34.8	17.8	19.1	
	Min	0.1	0.0	0.2	0.4	0.2	0.1	0.2	0.4	2.1	

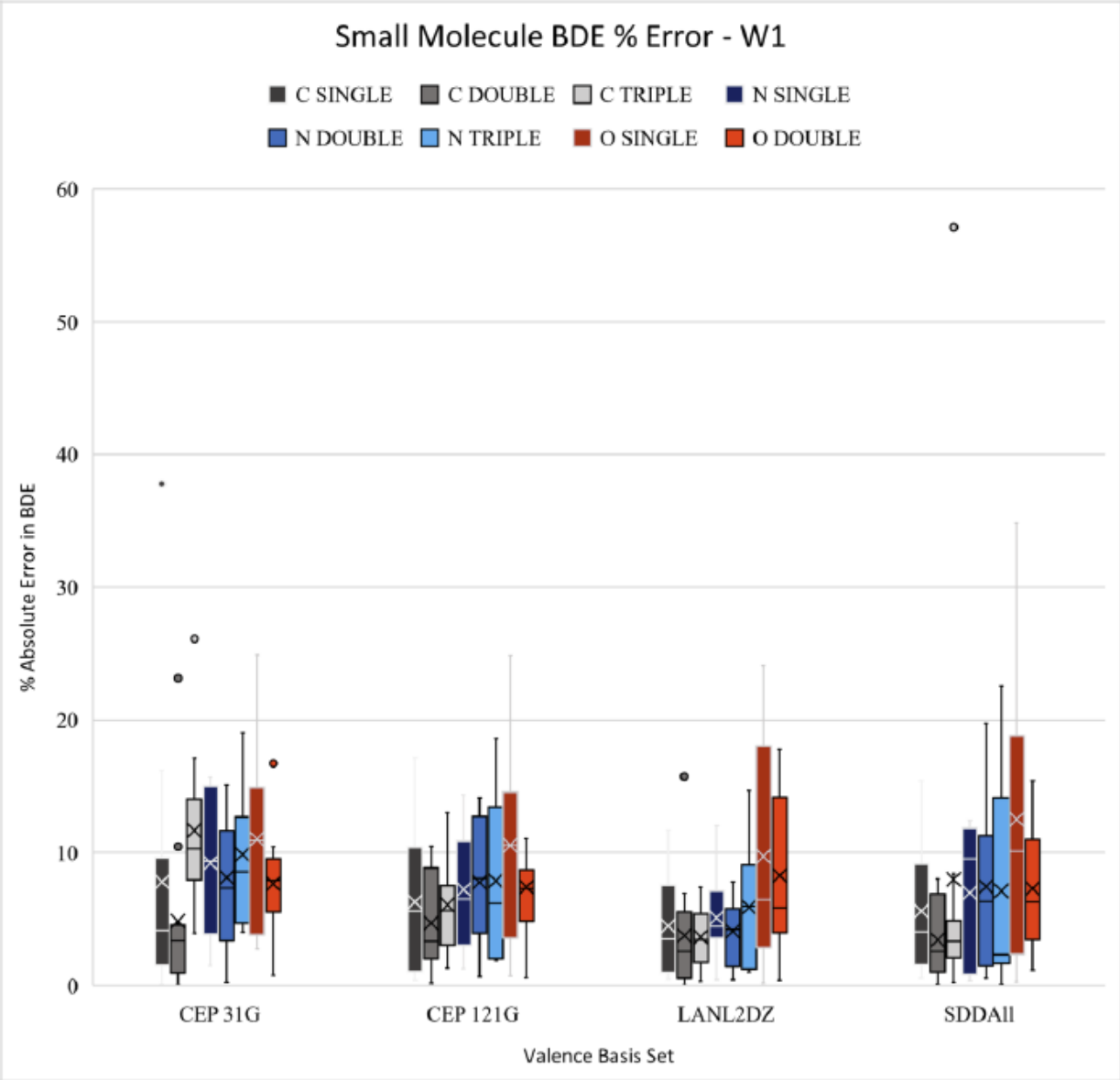

Figure A.1.3: :Box and whisker plot showing percent absolute error as a function of bond type for the small molecule with respect to the uW1 calculation data. The arithmetic mean is indicated with an X, the median depicted with a horizontal line, and the outliers are left as dots.

A.2 Thermochemistry Calculations

A.2.1 Calculated BDEs for WC Bonds, CC Bonds, and Comparison of Optimized Geometries

Table A.2.1: Calculated bond dissociation enthalpies for tungsten-carbon bonds, carbon-carbon bonds, and comparison of optimized geometries to reference crystal structure by functional and valence basis set.

Basis	Psuedo-potential	Churchill Complex						Hydrocarbon Analog						Chuchill Bond Lengths		Churchill Bond Angles	
		σ		π		2nd π		σ		π		2nd π					
		ΔH	ΔG	ΔH	ΔG	ΔH	ΔG	ΔH	ΔG	ΔH	ΔG	ΔH	ΔG	% Error	% Abs Err	% Error	% Abs Err
BP 86	CEP 31G	54.6	39.7	34.1	35.0	41.0	42.3	79.2	61.8	77.2	80.1	23.8	27.2	0.8	1.5	0.9	4.1
	CEP 121G	53.1	39.7	34.0	33.2	41.9	43.9	78.4	63.5	78.9	79.4	31.6	34.8	0.8	1.5	0.9	4.1
	LANL2DZ	55.0	41.4	35.4	34.9	43.3	45.1	82.2	67.0	81.7	82.6	35.5	38.8	0.7	1.5	0.8	3.9
	SDDAll	53.5	39.9	34.6	34.1	42.8	44.1	79.7	64.6	81.4	82.1	34.2	37.2	1.2	1.7	0.5	3.8
	Average	54.0	40.2	34.5	34.3	42.3	43.9	79.9	64.3	79.8	81.1	31.3	34.5	0.9	1.6	0.8	4.0
	Std Dev	0.9	0.8	0.6	0.8	1.0	1.1	1.7	2.2	2.1	1.5	5.2	5.1	0.2	0.1	0.2	0.1
B3LYP	CEP 31G	52.7	38.5	32.7	33.0	37.7	38.0	54.9	39.3	77.1	78.2	19.1	22.3	1.2	1.7	0.9	4.1
	CEP 121G	51.1	37.2	32.7	32.8	38.5	38.3	76.3	61.0	77.8	78.8	27.3	31.9	1.2	1.7	0.9	4.1
	LANL2DZ	53.0	39.5	34.4	33.4	42.3	43.7	80.0	65.0	81.6	82.1	32.8	35.9	1.0	1.8	0.8	3.9
	SDDAll	51.5	37.3	33.4	33.7	39.1	39.4	77.6	61.5	80.5	82.2	29.3	32.4	1.6	2.0	0.9	4.3
	Average	52.1	38.1	33.3	33.2	39.4	39.8	72.2	56.7	79.2	80.3	27.1	30.6	1.3	1.8	0.9	4.1
	Std Dev	0.9	1.1	0.8	0.4	2.0	2.6	11.6	11.7	2.1	2.1	5.8	5.9	0.2	0.1	0.0	0.1
M06	CEP 31G	64.7	50.0	32.6	34.1	38.5	36.8	88.3	72.9	75.0	76.8	21.8	23.3	0.6	1.3	0.6	3.7
	CEP 121G	63.9	49.7	31.3	31.7	39.7	38.4	87.2	73.3	75.1	75.3	31.2	32.4	0.6	1.3	0.6	3.7
	LANL2DZ	61.6	47.0	31.7	32.4	43.4	42.0	85.3	69.9	75.2	76.5	36.4	38.2	0.3	1.3	0.6	3.8
	SDDAll	63.5	49.1	31.2	31.7	41.6	40.2	86.3	70.8	76.9	78.3	34.6	36.1	0.9	1.5	1.1	3.8
	Average	63.4	48.9	31.7	32.5	40.8	39.4	86.8	71.7	75.5	76.7	31.0	32.5	0.6	1.4	0.7	3.7
	Std Dev	1.3	1.4	0.6	1.1	2.2	2.2	1.3	1.7	0.9	1.2	6.5	6.6	0.2	0.1	0.2	0.0
	CEP 31G	51.5	36.6	35.0	36.8	36.6	37.0	73.9	56.6	79.9	83.9	15.7	18.0	2.0	2.3	1.0	4.2
	CEP 121G	49.6	35.2	35.3	36.5	37.4	37.5	73.1	56.4	81.9	85.5	23.0	25.1	2.0	2.3	1.0	4.2

Basis	Psuedo-potential	Churchill Complex						Hydrocarbon Analog						Chuchill Bond Lengths		Churchill Bond Angles	
		σ		π		2nd π		σ		π		2nd π					
		ΔH	ΔG	ΔH	ΔG	ΔH	ΔG	ΔH	ΔG	ΔH	ΔG	ΔH	ΔG	% Error	% Abs Err	% Error	% Abs Err
BLYP	LANL2DZ	52.4	39.1	37.9	37.7	40.6	41.8	77.9	62.9	87.5	88.9	27.8	29.9	1.8	2.4	0.9	4.1
	SDDAll	50.3	36.7	34.8	34.8	39.1	39.8	74.6	59.9	84.5	86.1	162.4	164.2	2.4	2.5	1.0	4.4
	average	51.0	36.9	35.8	36.5	38.4	39.0	74.8	59.0	83.5	86.1	57.2	59.3	2.0	2.4	1.0	4.2
	std dev	1.2	1.6	1.4	1.2	1.8	2.2	2.1	3.1	3.3	2.1	70.3	70.1	0.3	0.1	0.0	0.1
B97D	CEP 31G	64.6	51.1	31.6	31.4	36.8	38.1	83.6	68.8	77.7	77.9	21.5	25.4	0.5	1.0	0.9	4.7
	CEP 121G	62.5	48.3	31.4	30.9	38.2	40.9	82.3	67.7	78.7	78.8	30.1	33.1	0.5	1.0	0.9	4.7
	LANL2DZ	62.4	48.6	31.3	31.5	41.3	42.2	81.3	66.3	78.2	78.8	34.3	38.7	0.4	1.0	0.9	4.7
	SDDAll	63.1	48.9	31.8	32.5	39.6	40.1	83.6	68.2	80.7	81.6	33.5	36.8	0.9	1.2	0.9	4.8
	Average	63.2	49.2	31.5	31.6	39.0	40.3	82.7	67.8	78.8	79.3	29.9	33.5	0.6	1.0	0.9	4.7
	Std Dev	1.0	1.3	0.2	0.7	1.9	1.7	1.1	1.1	1.3	1.6	5.9	5.9	0.2	0.1	0.0	0.0
PBEPBE	CEP 31G	57.4	43.8	32.4	32.3	42.9	44.3	81.6	66.4	75.2	75.9	27.5	31.0	0.6	1.3	0.8	4.1
	CEP 121G	55.7	41.9	32.4	32.1	43.9	45.3	80.9	65.9	64.1	64.8	47.9	51.1	0.6	1.3	0.8	4.1
	LANL2DZ	57.9	44.1	34.3	34.0	46.2	47.9	84.9	70.1	80.8	81.3	38.3	41.5	0.4	1.3	0.8	3.9
	SDDAll	56.2	41.6	33.0	33.5	44.5	45.8	81.9	65.4	79.3	81.4	37.8	40.7	0.9	1.5	0.8	4.3
	Average	56.8	42.9	33.0	33.0	44.4	45.8	82.3	66.9	74.8	75.9	37.9	41.1	0.6	1.4	0.8	4.1
	Std Dev	1.0	1.3	0.9	0.9	1.4	1.5	1.8	2.1	7.5	7.8	8.3	8.2	0.2	0.1	0.0	0.1
M11L	CEP 31G	56.3	42.7	39.6	41.2	34.9	34.5	85.4	69.4	86.6	87.7	2.7	6.6	0.1	1.4	0.7	3.2
	CEP 121G	55.4	41.3	38.2	39.2	36.3	36.0	84.3	69.8	87.8	87.8	29.8	32.5	0.1	1.4	0.7	3.2
	LANL2DZ	55.8	40.9	35.1	36.8	35.7	34.1	87.2	72.5	79.0	79.6	23.2	25.7	-0.2	1.5	-0.2	3.3
	SDDAll	54.9	42.8	38.7	39.5	38.9	38.2	86.0	72.3	89.8	89.0	35.4	37.8	0.4	1.7	0.4	3.5
	Average	55.6	41.9	37.9	39.2	36.4	35.7	85.7	71.0	85.8	86.0	22.8	25.7	0.1	1.5	0.4	3.3
	Std Dev	0.6	1.0	2.0	1.8	1.7	1.8	1.2	1.6	4.7	4.3	14.3	13.6	0.2	0.1	0.4	0.2
MN12L	CEP 31G	61.4	48.3	45.5	46.2	31.5	32.1	89.4	74.2	89.5	90.4	7.5	10.7	0.8	1.5	0.6	4.0
	CEP 121G	61.0	47.3	44.0	44.8	32.2	32.1	88.7	73.6	88.9	89.7	15.6	18.0	0.8	1.5	0.6	4.0
	LANL2DZ	58.9	46.3	40.8	40.9	37.7	37.9	87.5	73.0	84.2	84.5	26.6	29.0	0.4	1.5	0.5	3.8

Basis	Psuedo-potential	Churchill Complex						Hydrocarbon Analog						Chuchill Bond Lengths		Churchill Bond Angles	
		σ		π		2nd π		σ		π		2nd π					
		ΔH	ΔG	ΔH	ΔG	ΔH	ΔG	ΔH	ΔG	ΔH	ΔG	ΔH	ΔG	% Error	% Abs Err	% Error	% Abs Err
	SDDAll	61.4	49.1	44.0	44.5	33.2	33.2	89.4	75.2	91.9	91.8	19.5	21.8	1.0	1.7	0.4	4.5
	Average	60.7	47.7	43.5	44.1	33.7	33.8	88.8	74.0	88.6	89.1	17.3	19.9	0.8	1.5	0.5	4.1
	Std Dev	1.2	1.2	2.0	2.2	2.8	2.8	0.9	0.9	3.2	3.2	8.0	7.6	0.3	0.1	0.1	0.3
N12	CEP 31G	60.3	45.9	30.9	32.1	42.9	43.5	132.7	120.3	79.6	79.9	22.9	25.7	-0.3	1.1	0.7	4.1
	CEP 121G	58.0	43.8	31.1	31.2	44.1	44.4	132.0	119.4	81.6	81.2	31.6	33.9	-0.3	1.1	0.7	4.1
	LANL2DZ	58.5	44.0	29.8	30.9	47.7	48.0	138.4	126.0	78.4	78.7	36.5	39.3	-0.5	0.9	0.7	4.0
	SDDAll	59.1	44.7	32.5	33.8	43.6	44.0	133.7	120.9	84.8	84.7	0.0	33.7	0.1	0.9	0.8	4.2
	Average	59.0	44.6	31.1	32.0	44.6	45.0	134.2	121.6	81.1	81.1	22.8	33.2	-0.3	1.0	0.7	4.1
	Std Dev	1.0	0.9	1.1	1.3	2.1	2.1	2.9	3.0	2.8	2.6	16.2	5.6	0.3	0.1	0.0	0.1
SOGGA11	CEP 31G	68.4	53.0	32.0	32.9	20.8	24.3	89.9	74.5	78.3	79.3	41.6	42.5	0.1	0.9	0.9	6.2
	CEP 121G	64.0	49.5	31.9	33.2	28.5	31.6	88.6	73.4	80.1	80.9	44.6	44.3	0.1	0.9	0.9	6.2
	LANL2DZ	65.4	53.3	28.9	30.8	37.5	40.4	87.8	72.4	76.3	77.2	49.6	49.2	-0.3	1.0	0.7	5.4
	SDDAll	61.5	48.4	32.1	32.4	32.0	34.6	85.6	71.1	83.8	84.0	44.5	44.7	0.6	1.2	0.8	5.8
	Average	64.8	51.1	31.2	32.3	29.7	32.7	88.0	72.8	79.6	80.3	45.1	45.2	0.1	1.0	0.8	5.9
	Std Dev	2.9	2.5	1.5	1.0	7.0	6.7	1.8	1.4	3.2	2.9	3.3	2.9	0.3	0.1	0.1	0.4
B2LYP	CEP 31G	60.1	46.4	33.6	33.7	46.8	47.1	81.3	66.4	75.0	27.3	0.0	0.0	1.2	1.8	0.9	4.2
	CEP 121G	59.3	45.6	33.6	33.6	47.8	48.0	80.9	66.1	77.5	35.4	0.0	0.0	1.2	1.8	0.9	4.2
	LANL2DZ	59.2	46.0	35.8	35.6	50.9	50.8	83.2	68.6	80.3	39.9	0.0	0.0	1.1	1.9	0.8	4.1
	SDDAll	58.3	44.7	34.2	34.2	48.3	48.9	81.5	66.5	80.0	36.9	0.0	0.0	1.6	2.0	0.8	4.1
	Average	59.2	45.7	34.3	34.3	48.5	48.7	81.7	66.9	78.2	34.9	0.0	0.0	1.3	1.8	0.8	4.2
	Std Dev	0.8	0.8	1.1	0.9	1.8	1.6	1.0	1.1	2.5	5.4	0.0	0.0	0.2	0.1	0.0	0.0
MP2	CEP 31G	98.9	87.2	11.5	10.1	71.1	73.3	88.5	74.1	71.5	71.6	36.5	41.1	0.9	1.5	0.7	4.6
	CEP 121G	99.5	87.9	11.6	10.5	72.8	74.6	89.1	74.8	75.4	75.6	45.8	49.8	0.9	1.5	0.7	4.6
	LANL2DZ	95.0	83.3	15.7	14.8	75.2	77.1	89.0	74.7	76.1	76.3	50.6	53.7	0.8	1.7	0.6	4.6
	SDDAll	96.3	84.7	11.6	10.2	75.4	77.6	88.7	74.3	77.4	77.7	48.7	52.3	1.0	1.8	8.6	12.5

Basis	Psuedo-potential	Churchill Complex						Hydrocarbon Analog						Chuchill Bond Lengths		Churchill Bond Angles	
		σ		π		2nd π		σ		π		2nd π					
		ΔH	ΔG	ΔH	ΔG	ΔH	ΔG	ΔH	ΔG	ΔH	ΔG	ΔH	ΔG	% Error	% Abs Err	% Error	% Abs Err
	Average	97.4	85.8	12.6	11.4	73.6	75.6	88.8	74.5	75.1	75.3	45.4	49.2	0.9	1.6	2.6	6.6
	Std Dev	2.2	2.1	2.0	2.3	2.1	2.1	0.3	0.3	2.5	2.6	6.2	5.6	0.1	0.1	3.9	3.9
Overall Averages	CEP 31G	62.6	48.6	32.6	33.2	40.1	40.9	85.7	70.4	78.5	75.8	20.1	22.8	0.7	1.4	0.8	4.3
	CEP 121G	61.1	47.3	32.3	32.5	41.8	42.6	86.8	72.1	79.0	76.1	29.9	32.2	0.7	1.4	0.8	4.3
	LANL2DZ	61.3	47.8	32.6	32.8	45.1	45.9	88.7	74.0	79.9	77.2	32.6	35.0	0.5	1.5	0.7	4.1
	SDDAll	60.8	47.3	32.7	32.9	43.2	43.8	87.4	72.6	82.6	79.7	40.0	44.8	1.1	1.6	1.4	5.0
	Average	61.4	47.7	32.5	32.9	42.6	43.3	87.2	72.3	80.0	77.2	30.6	33.7	0.7	1.5	0.9	4.4
	Std Dev	11.8	12.4	7.1	7.5	10.9	11.2	15.6	16.3	5.1	13.9	23.9	23.6	0.6	0.4	1.1	1.3

A.2.2 Calculated BDEs for WN Bonds, NN Bonds, and Comparison of Optimized Geometries

Table A.2.2: Calculated bond dissociation enthalpies in kcal/mol for tungsten-nitrogen bonds and nitrogen-nitrogen bonds by functional and valence basis set.

DFT Functional	Valence Basis Set	Beaumier Nitrogen Complex								Nitrogen Analog					
		Dative		σ		π		2nd π		σ		π		2nd π	
		ΔH	ΔG	ΔH	ΔG	ΔH	ΔG	ΔH	ΔG	ΔH	ΔG	ΔH	ΔG	ΔH	ΔG
BP 86	CEP 31G	-46.2	-35.8	-98.9	-86.1	-21.5	-23.1	-35.3	-35.5	-61.9	-50.1	-55.0	-56.9	-98.4	-100.1
	CEP-121g	-45.6	-35.1	-102.3	-89.4	-23.3	-24.9	-35.7	-36.0	-68.4	-56.7	-58.6	-60.5	-101.1	-102.8
	LANL2DZ	-49.3	-39.0	-100.9	-88.2	-21.0	-22.5	-43.8	-43.0	-63.9	-52.1	-58.0	-59.9	-107.9	-109.6
	SDDAll	-45.3	-34.9	-99.1	-86.3	-21.6	-23.2	-34.5	-34.7	-62.8	-51.1	-55.2	-57.1	-102.9	-104.6
	Average	-46.6	-36.2	-100.3	-87.5	-21.8	-23.4	-37.3	-37.3	-64.2	-52.5	-56.7	-58.6	-102.6	-104.3
	Std Dev	1.9	1.9	1.6	1.6	1.0	1.0	4.3	3.8	2.9	2.9	1.9	1.9	4.0	4.0
B3LYP	CEP 31G	-46.8	-36.4	-95.1	-82.2	-15.5	-17.4	-27.7	-27.7	-56.1	-44.4	-48.8	-50.7	-92.6	-94.2
	CEP-121g	-46.5	-36.0	-98.8	-85.8	-17.5	-19.2	-28.4	-28.5	-62.6	-50.9	-52.5	-54.4	-96.8	-98.5
	LANL2DZ	-50.1	-39.7	-97.1	-84.3	-14.9	-16.5	-26.2	-26.7	-58.0	-46.2	-51.7	-53.6	-102.0	-102.5
	SDDAll	-45.9	-35.6	-95.3	-82.5	-15.7	-17.5	-26.7	-26.9	-57.1	-45.3	-49.0	-50.9	-97.4	-99.1
	Average	-47.3	-36.9	-96.6	-83.7	-15.9	-17.6	-27.3	-27.4	-58.5	-46.7	-50.5	-52.4	-97.2	-98.6
	Std Dev	1.9	1.9	1.8	1.7	1.1	1.2	1.0	0.8	2.9	2.9	1.9	1.9	3.9	3.4
M06	CEP 31G	-50.0	-39.8	-105.6	-93.3	-11.6	-13.0	-17.6	-17.9	-67.0	-55.2	-47.5	-49.4	-67.9	-69.6
	CEP-121g	-49.0	-38.9	-105.4	-92.9	-13.4	-15.0	-25.3	-26.7	-67.7	-56.0	-49.6	-51.5	-87.6	-89.3
	LANL2DZ	-52.6	-41.2	-106.1	-92.5	-11.5	-12.8	-12.2	-12.4	-65.5	-53.8	-50.2	-52.1	-65.9	-67.6
	SDDAll	-49.0	-39.2	-105.3	-93.2	-10.1	-11.7	-17.3	-18.8	-66.8	-55.1	-44.9	-46.8	-74.8	-76.5
	Average	-50.1	-39.8	-105.6	-92.9	-11.6	-13.1	-18.1	-18.9	-66.8	-55.0	-48.1	-50.0	-74.1	-75.8
	Std Dev	1.7	1.0	0.4	0.4	1.3	1.4	5.4	5.9	0.9	0.9	2.4	2.4	9.8	9.8
BLYP	CEP 31G	-43.6	-33.2	-94.6	-81.8	-18.6	-20.3	-46.7	-45.6	-55.7	-43.9	-53.5	-55.4	-97.0	-98.7
	CEP-121g	-43.1	-32.7	-98.8	-85.8	-21.3	-23.0	-48.1	-46.8	-63.4	-51.7	-58.4	-60.3	-101.3	-103.0
	LANL2DZ	-47.2	-36.9	-96.8	-84.1	-17.9	-19.5	-45.0	-45.7	-57.8	-46.1	-56.4	-58.3	-106.7	-108.4

DFT Functional	Valence Basis Set	Beaumier Nitrogen Complex								Nitrogen Analog					
		Dative		σ		π		2nd π		σ		π		2nd π	
		ΔH	ΔG	ΔH	ΔG	ΔH	ΔG	ΔH	ΔG	ΔH	ΔG	ΔH	ΔG	ΔH	ΔG
	SDDAll	-42.4	-32.1	-94.6	-81.9	-18.9	-20.6	-33.9	-34.1	-56.5	-44.8	-53.5	-55.3	-101.4	-103.1
	Average	-44.1	-33.7	-96.2	-83.4	-19.2	-20.8	-43.4	-43.1	-58.4	-46.6	-55.5	-57.3	-101.6	-103.3
	Std Dev	2.2	2.2	2.0	1.9	1.5	1.5	6.4	6.0	3.5	3.5	2.4	2.4	4.0	4.0
PBEPBE	CEP 31G	-47.2	-36.8	-100.3	-87.5	-20.8	-22.4	-33.0	-33.3	-63.9	-52.1	-53.4	-55.6	-94.0	-95.5
	CEP-121g	-46.6	-36.1	-103.8	-90.9	-23.2	-24.8	-34.8	-35.1	-70.7	-58.9	-58.0	-60.0	-99.1	-100.8
	LANL2DZ	-50.6	-40.3	-102.3	-89.6	-20.1	-21.6	-31.5	-33.1	-65.8	-54.0	-56.0	-58.1	-103.9	-105.4
	SDDAll	-46.2	-35.9	-100.5	-87.8	-21.0	-22.6	-32.2	-32.5	-64.9	-53.1	-53.6	-55.5	-98.5	-100.2
	Average	-47.7	-37.3	-101.7	-88.9	-21.3	-22.9	-32.9	-33.5	-66.3	-54.5	-55.3	-57.3	-98.9	-100.4
	Std Dev	2.0	2.0	1.6	1.6	1.4	1.4	1.4	1.1	3.0	3.0	2.2	2.1	4.0	4.0
B97D	CEP 31G	-47.1	-36.8	-102.5	-89.7	-19.0	-20.8	-32.5	-32.6	-63.4	-51.7	-56.0	-57.9	-97.0	-98.6
	CEP-121g	-45.9	-35.5	-101.8	-88.8	-17.9	-19.6	-30.2	-30.1	-63.6	-51.9	-53.0	-54.8	-93.6	-95.3
	LANL2DZ	-50.6	-40.3	-104.9	-92.2	-17.8	-19.4	-31.0	-31.5	-65.4	-53.8	-57.5	-59.2	-105.7	-107.4
	SDDAll	-46.1	-35.9	-102.4	-89.2	-18.9	-21.2	-49.9	-49.7	-64.0	-52.3	-55.6	-57.5	-101.2	-102.9
	Average	-47.4	-37.1	-102.9	-90.0	-18.4	-20.2	-35.9	-36.0	-64.1	-52.4	-55.5	-57.4	-99.3	-101.1
	Std Dev	2.2	2.2	1.4	1.5	0.7	0.9	9.4	9.2	0.9	0.9	1.9	1.8	5.2	5.3
M111	CEP 31G	-47.3	-37.2	-98.2	-85.8	-28.3	-29.3	-36.7	-37.6	-58.4	-46.6	-77.4	-79.3	-113.1	-114.8
	CEP-121g	-46.1	-35.6	-100.3	-87.7	-18.4	-19.4	-28.1	-29.2	-63.1	-51.3	-59.6	-61.4	-98.6	-100.4
	LANL2DZ	-47.3	-37.2	-98.2	-85.8	-28.3	-29.3	-36.7	-37.6	-58.4	-46.6	-77.4	-79.3	-113.1	-114.8
	SDDAll	-46.5	-37.0	-103.6	-86.8	-21.9	-28.0	-38.2	-39.0	-69.1	-47.2	-64.4	-76.5	-122.2	-123.9
	average	-46.8	-36.8	-100.1	-86.5	-24.2	-26.5	-34.9	-35.9	-62.3	-47.9	-69.7	-74.1	-111.8	-113.5
	std dev	0.6	0.8	2.5	0.9	4.9	4.8	4.6	4.5	5.1	2.3	9.1	8.6	9.7	9.7
MN12L	CEP 31G	-48.5	-38.0	-96.6	-83.6	-31.0	-36.5	-41.6	-37.3	-59.8	-48.1	-72.6	-87.0	-132.8	-122.0
	CEP-121g	-50.1	-39.5	-102.5	-89.5	-27.0	-26.7	-15.9	-18.2	-65.7	-53.9	-63.1	-65.0	-83.9	-85.6
	LANL2DZ	-50.6	-40.1	-97.4	-84.5	-37.5	-39.2	-38.8	-38.5	-59.1	-47.4	-88.9	-90.2	-128.2	-130.5

DFT Functional	Valence Basis Set	Beaumier Nitrogen Complex								Nitrogen Analog					
		Dative		σ		π		2nd π		σ		π		2nd π	
		ΔH	ΔG	ΔH	ΔG	ΔH	ΔG	ΔH	ΔG	ΔH	ΔG	ΔH	ΔG	ΔH	ΔG
	SDDAll	-47.7	-37.2	-96.4	-83.4	-35.2	-35.2	-39.3	-41.3	-60.0	-48.3	-80.6	-82.4	-126.7	-128.4
	Average	-49.2	-38.7	-98.2	-85.3	-32.7	-34.4	-33.9	-33.8	-61.1	-49.4	-76.3	-81.2	-117.9	-116.6
	Std Dev	1.4	1.3	2.9	2.9	4.6	5.4	12.1	10.6	3.1	3.0	11.0	11.2	22.8	21.0
N12	CEP 31G	-46.2	-35.9	-105.7	-93.2	-18.8	-20.3	-34.5	-35.1	-69.1	-57.4	-54.2	-56.1	-91.5	-93.2
	CEP-121g	-45.6	-35.3	-107.0	-94.3	-14.9	-16.3	-25.5	-26.0	-71.3	-59.5	-45.1	-47.1	-75.9	-77.6
	LANL2DZ	-49.7	-39.5	-108.0	-95.6	-18.9	-20.1	-31.8	-32.5	-72.3	-60.5	-58.2	-60.1	-100.1	-101.8
	SDDAll	-44.9	-34.9	-105.7	-93.4	-19.0	-20.4	-33.6	-34.2	-70.3	-58.6	-54.1	-56.0	-96.7	-98.4
	Average	-46.6	-36.4	-106.6	-94.1	-17.9	-19.3	-31.3	-31.9	-70.8	-59.0	-52.9	-54.8	-91.0	-92.7
	Std Dev	2.1	2.1	1.1	1.1	2.0	2.0	4.1	4.1	1.4	1.3	5.5	5.5	10.7	10.7
SOGGA11	CEP 31G	-37.7	-27.4	-104.7	-91.4	-23.0	-24.8	-36.2	-36.6	-71.2	-59.5	-56.4	-58.3	-88.0	-89.7
	CEP-121g	-40.1	-29.6	-108.4	-95.5	-17.4	-18.7	-29.0	-29.4	-74.0	-62.1	-49.1	-51.0	-78.9	-80.6
	LANL2DZ	-38.9	-29.1	-103.4	-91.3	-22.2	-23.2	-33.8	-34.4	-69.0	-57.3	-59.6	-61.5	-100.6	-102.3
	SDDAll	-37.0	-26.7	-105.3	-92.5	-24.1	-25.5	-35.0	-35.4	-72.3	-60.6	-56.1	-58.0	-91.7	-93.4
	Average	-38.4	-28.2	-105.4	-92.7	-21.7	-23.0	-33.5	-34.0	-71.6	-59.9	-55.3	-57.2	-89.8	-91.5
	Std Dev	1.3	1.4	2.1	2.0	3.0	3.1	3.2	3.2	2.1	2.1	4.4	4.4	9.0	9.0
B2PLYP	CEP 31G	-48.6	-38.2	-99.6	-87.0	-14.9	-16.6	-33.2	-33.3	-57.4	-45.6	-48.3	-50.2	-91.2	-92.9
	CEP-121g	-47.8	-37.4	-102.2	-89.4	-18.0	-19.8	-48.2	-49.0	-62.6	-50.8	-51.3	-53.2	-95.3	-97.0
	LANL2DZ	-51.8	-41.4	-101.6	-89.0	-14.6	-16.1	-31.9	-32.3	-58.9	-47.2	-51.2	-53.1	-100.0	-101.6
	SDDAll	-48.1	-37.8	-100.4	-87.5	-15.3	-17.4	-32.7	-32.9	-58.8	-47.1	-49.0	-50.9	-96.3	-97.9
	Average	-49.1	-38.7	-101.0	-88.2	-15.7	-17.5	-36.5	-36.9	-59.4	-47.7	-50.0	-51.9	-95.7	-97.3
	Std Dev	1.9	1.8	1.2	1.2	1.6	1.6	7.8	8.1	2.2	2.2	1.5	1.5	3.6	3.6
MP2	CEP 31G	-54.6	-44.4	-137.8	-126.2	11.6	10.6	-44.9	-45.0	-62.5	-50.7	-47.8	-49.7	-86.0	-87.7
	LANL2DZ	-53.0	-42.9	-137.1	-125.5	5.4	4.6	-43.4	-43.5	-65.7	-53.9	-49.6	-51.5	-89.8	-91.5
	SDDAll	-57.3	-47.0	-138.0	-126.4	10.2	9.6	-44.1	-44.4	-63.8	-52.1	-51.1	-53.0	-93.6	-95.3

DFT Functional	Valence Basis Set	Beaumier Nitrogen Complex								Nitrogen Analog					
		Dative		σ		π		2nd π		σ		π		2nd π	
		ΔH	ΔG	ΔH	ΔG	ΔH	ΔG	ΔH	ΔG	ΔH	ΔG	ΔH	ΔG	ΔH	ΔG
	CEP-121g	-54.8	-44.7	-139.3	-128.0	10.4	9.7	-44.5	-44.8	-64.9	-54.0	-49.5	-50.6	-91.0	-92.6
	Average	-54.9	-44.7	-138.0	-126.5	9.4	8.6	-44.2	-44.4	-64.2	-52.7	-49.5	-51.2	-90.1	-91.8
	Std Dev	1.8	1.7	0.9	1.1	2.7	2.7	0.6	0.6	1.4	1.6	1.3	1.4	3.2	3.1
Overall Averages	CEP 31G	-47.0	-36.7	-103.3	-90.6	-17.6	-19.5	-35.0	-34.8	-62.2	-50.5	-55.9	-58.9	-95.8	-96.4
	CEP-121g	-46.6	-36.2	-105.7	-93.0	-17.2	-18.6	-32.7	-33.2	-66.6	-54.8	-54.0	-55.9	-91.8	-93.5
	LANL2DZ	-49.7	-39.3	-104.6	-92.0	-17.9	-19.2	-33.9	-34.3	-63.2	-51.4	-59.7	-61.5	-102.3	-103.9
	SDDAll	-46.2	-36.0	-104.0	-91.0	-17.6	-19.5	-34.8	-35.4	-64.0	-51.4	-55.5	-58.1	-100.1	-101.8
	Average	-47.4	-37.0	-104.4	-91.7	-17.6	-19.2	-34.1	-34.4	-64.0	-52.0	-56.3	-58.6	-97.5	-98.9
	Std Dev	4.0	4.0	10.9	11.3	17.3	17.3	8.6	8.2	4.9	4.9	9.2	10.1	13.5	12.9

A.2.3 Calculated BDEs for WO Bonds, OO Bonds, and Comparison of Optimized Geometries

Table A.2.3-1: Calculated bond dissociation enthalpies in kcal/mol for tungsten-oxygen bonds and oxygen-oxygen bonds by functional and valence basis set for both the Cotton model with tetrahydrofuran and the Cotton model with water trans to the oxo moiety.

Basis	Pseudo-Potential	Cotton Complex - Trans THF						Cotton Complex - Trans H_2O						Oxygen Analogs			
		Dative Bond		σ		π		Dative Bond		σ		π		Peroxide		O_2	
		ΔH	ΔG	ΔH	ΔG	ΔH	ΔG	ΔH	ΔG	ΔH	ΔG	ΔH	ΔG	ΔH	ΔG	ΔH	ΔG
BP 86	CEP 31G	-9.0	3.5	-94.3	-82.4	-60.5	-61.3	-12.7	-1.6	-93.4	-81.7	-69.7	-70.7	-52.5	-43.8	-74.6	-76.3
	CEP 121G	-8.0	2.8	-94.8	-82.8	-60.0	-60.9	-13.0	-2.0	-93.8	-82.0	-69.1	-70.2	-52.5	-43.8	-74.7	-76.4
	LANL2DZ	-8.5	2.4	-100.3	-89.4	-65.3	-67.9	-13.0	-2.0	-98.3	-86.5	-74.4	-75.6	-59.7	-50.9	-78.5	-80.2
	SDDAll	-8.0	3.9	-94.2	-82.2	-59.6	-60.9	-10.1	0.7	-92.8	-81.2	-68.8	-70.0	-50.3	-41.5	-74.1	-75.8
	Average	-8.4	3.1	-95.9	-84.2	-61.4	-62.7	-12.2	-1.2	-94.6	-82.9	-70.5	-71.6	-53.8	-45.0	-75.5	-77.2
	Std Dev	0.5	0.7	2.9	3.5	2.7	3.4	1.4	1.3	2.5	2.5	2.6	2.6	4.1	4.1	2.0	2.0
B3LYP	CEP 31G	-10.0	2.3	-85.1	-72.6	-48.8	-50.4	-12.6	-1.7	-83.9	-72.0	-59.1	-60.0	-42.8	-34.0	-66.1	-67.8
	CEP 121G	-9.4	2.9	-85.6	-73.5	-48.4	-49.9	-12.9	-2.0	-84.5	-72.4	-58.6	-59.7	-42.9	-34.1	-66.3	-67.9
	LANL2DZ	-9.3	2.6	-91.2	-78.7	-54.1	-55.8	-12.8	-1.8	-89.1	-77.2	-64.0	-65.1	-48.7	-39.9	-69.8	-71.5
	SDDAll	-8.9	2.7	-85.3	-73.3	-47.6	-49.0	-10.1	0.6	-83.7	-72.0	-58.1	-59.0	-40.5	-31.7	-65.4	-67.1
	Average	-9.4	2.6	-86.8	-74.6	-49.7	-51.3	-12.1	-1.2	-85.3	-73.4	-59.9	-61.0	-43.7	-34.9	-66.9	-68.6
	Std Dev	0.4	0.3	3.0	2.8	3.0	3.1	1.3	1.2	2.6	2.5	2.8	2.8	3.5	3.5	2.0	2.0
M06	CEP 31G	-17.1	-3.4	-94.6	-82.9	-46.3	-46.9	-16.7	-5.4	-93.4	-81.4	-56.0	-57.1	-48.7	-39.9	-57.7	-59.5
	CEP 121G	-16.8	-2.7	-94.8	-82.8	-45.6	-45.9	-17.2	-6.0	-93.8	-81.8	-55.4	-56.6	-48.2	-39.4	-57.5	-59.3
	LANL2DZ	-16.4	-3.1	-96.6	-84.1	-52.2	-53.5	-16.9	-5.7	-95.0	-83.2	-61.5	-62.5	-50.7	-41.8	-63.4	-65.1
	SDDAll	-16.1	-2.7	-93.3	-80.9	-48.0	-46.9	-14.5	-3.3	-91.6	-79.5	-57.0	-58.3	-41.7	-32.8	-58.9	-60.6
	Average	-16.6	-3.0	-94.8	-82.7	-48.0	-48.3	-16.3	-5.1	-93.5	-81.5	-57.5	-58.6	-47.3	-38.5	-59.4	-61.1
	Std Dev	0.5	0.3	1.3	1.3	3.0	3.5	1.2	1.2	1.4	1.5	2.8	2.7	3.9	3.9	2.7	2.7
BLYP	CEP 31G	-8.5	3.5	-90.4	-78.5	-59.3	-60.6	-11.4	-0.5	-89.2	-77.5	-68.4	-69.4	-48.4	-39.6	-71.5	-73.1
	CEP 121G	-8.0	3.6	-90.8	-79.2	-58.8	-60.3	-11.7	-0.9	-89.5	-77.8	-67.6	-68.7	-48.3	-39.6	-71.3	-72.9
	LANL2DZ	-8.2	3.0	-97.4	-85.5	-65.8	-67.2	-11.9	-1.1	-94.9	-83.2	-74.1	-75.2	-56.0	-47.3	-76.6	-78.3

Basis	Pseudo-Potential	Cotton Complex - Trans THF						Cotton Complex - Trans H_2O						Oxygen Analogs			
		Dative Bond		σ		π		Dative Bond		σ		π		Peroxide		O_2	
		ΔH	ΔG	ΔH	ΔG	ΔH	ΔG	ΔH	ΔG	ΔH	ΔG	ΔH	ΔG	ΔH	ΔG	ΔH	ΔG
	SDDAll	-10.2	0.1	-92.0	-81.4	-57.9	-59.4	-8.2	2.4	-87.5	-75.8	-67.2	-68.5	-45.5	-36.7	-69.8	-71.4
	Average	-8.7	2.6	-92.6	-81.1	-60.4	-61.9	-10.8	0.0	-90.3	-78.6	-69.3	-70.5	-49.5	-40.8	-72.3	-73.9
	Std Dev	1.0	1.6	3.2	3.2	3.6	3.6	1.8	1.6	3.2	3.2	3.2	3.2	4.5	4.5	3.0	3.0
B97D	CEP 31G	-17.6	-4.6	-94.9	-83.8	-56.9	-57.8	-14.5	-3.4	-94.0	-82.1	-67.1	-67.9	-51.6	-42.9	-73.3	-75.0
	CEP 121G	-17.2	-3.5	-95.3	-83.9	-56.4	-57.6	-14.8	-3.7	-94.3	-82.3	-66.5	-67.5	-51.4	-42.6	-73.3	-74.9
	LANL2DZ	-17.1	-4.0	-96.3	-84.5	-58.3	-59.6	-14.5	-3.4	-94.3	-82.0	-68.2	-69.5	-53.7	-44.9	-73.0	-74.7
	SDDAll	-16.5	-3.5	-95.6	-83.6	-55.5	-56.6	-11.9	-0.9	-94.0	-81.9	-65.6	-66.5	-49.3	-40.5	-71.9	-73.5
	Average	-17.1	-3.9	-95.5	-83.9	-56.8	-57.9	-13.9	-2.9	-94.1	-82.1	-66.8	-67.9	-51.5	-42.7	-72.9	-74.5
	Std Dev	0.5	0.5	0.6	0.4	1.2	1.2	1.3	1.3	0.2	0.1	1.1	1.3	1.8	1.8	0.7	0.7
PBEPBE	CEP 31G	-11.3	0.8	-96.2	-84.9	-60.1	-60.6	-14.5	-3.4	-95.3	-83.5	-68.9	-69.9	-54.0	-45.2	-75.2	-76.9
	CEP 121G	-10.8	1.3	-96.8	-84.9	-59.7	-60.4	-14.8	-3.7	-95.7	-83.9	-68.3	-69.5	-54.0	-45.2	-75.3	-77.0
	LANL2DZ	-10.8	1.0	-101.9	-90.1	-65.8	-66.8	-14.8	-3.7	-99.8	-88.1	-73.9	-75.1	-61.1	-52.3	-78.9	-80.7
	SDDAll	-10.6	1.6	-95.6	-83.5	-58.8	0.0	-11.7	-0.9	-94.0	-82.4	-67.6	0.0	-51.0	-42.2	-74.2	-75.9
	Average	-10.9	1.2	-97.6	-85.9	-61.1	-47.0	-13.9	-2.9	-96.2	-84.5	-69.7	-53.6	-55.0	-46.2	-75.9	-77.6
	Std Dev	0.3	0.3	2.9	2.9	3.2	31.4	1.5	1.4	2.5	2.5	2.9	35.8	4.3	4.3	2.1	2.1
M11L	CEP 31G	-15.6	-2.4	-90.1	-78.8	-62.3	-60.9	-17.9	-6.5	-89.6	-78.0	-69.7	-70.6	-37.6	-28.8	-90.8	-92.5
	CEP 121G	-15.5	-0.7	-91.2	-79.8	-58.8	-59.3	-18.3	-6.7	-90.9	-79.2	-66.8	-67.7	-37.6	-28.8	-86.5	-88.2
	LANL2DZ	-15.6	-2.4	-98.2	-86.6	-54.2	-53.2	-17.7	-6.1	-96.9	-85.1	-61.6	-62.8	-47.6	-38.7	-65.2	-66.9
	SDDAll	-14.2	-1.1	-90.6	-78.6	-63.6	-63.1	-16.3	-4.8	-89.3	-77.8	-71.8	-72.6	-32.6	-23.8	-97.6	-99.3
	Average	-15.2	-1.7	-92.5	-80.9	-59.7	-59.1	-17.5	-6.0	-91.7	-80.0	-67.5	-68.4	-38.9	-30.0	-85.0	-86.7
	Std Dev	0.7	0.9	3.8	3.8	4.2	4.2	0.9	0.8	3.5	3.4	4.4	4.3	6.3	6.3	14.0	14.0
MN12L	CEP 31G	-20.6	-6.6	-87.3	-75.6	-66.1	-75.4	-18.3	-7.2	-87.4	-75.7	-70.3	-82.5	-42.7	-33.9	-74.1	-97.5
	CEP 121G	-20.2	-6.2	-88.2	-76.5	-62.9	-61.3	-18.7	-7.5	-88.3	-76.6	-67.0	-68.3	-42.8	-34.0	-68.6	-70.3
	LANL2DZ	-19.5	-5.7	-100.1	-88.3	-60.4	-59.8	-18.9	-7.6	-98.2	-86.6	-65.1	-66.3	-48.7	-39.8	-57.1	-58.9
	SDDAll	-19.5	-5.5	-88.8	-77.2	-67.7	-66.5	-16.7	-5.3	-88.1	-76.4	-72.4	-73.5	-37.9	-29.1	-79.6	-81.4

Basis	Pseudo-Potential	Cotton Complex - Trans THF						Cotton Complex - Trans H_2O						Oxygen Analogs			
		Dative Bond		σ		π		Dative Bond		σ		π		Peroxide		O_2	
		ΔH	ΔG	ΔH	ΔG	ΔH	ΔG	ΔH	ΔG	ΔH	ΔG	ΔH	ΔG	ΔH	ΔG	ΔH	ΔG
	Average	-19.9	-6.0	-91.1	-79.4	-64.3	-65.8	-18.1	-6.9	-90.5	-78.8	-68.7	-72.7	-43.0	-34.2	-69.9	-77.0
	Std Dev	0.5	0.5	6.0	6.0	3.3	7.1	1.0	1.1	5.1	5.2	3.3	7.2	4.4	4.4	9.6	16.5
N12	CEP 31G	-9.3	4.3	-98.5	-85.0	-60.9	-62.5	-13.5	-2.3	-97.4	-85.9	-71.4	-72.2	-57.2	-48.4	-71.0	-72.6
	CEP 121G	-8.3	6.5	-98.6	-85.3	-60.2	-61.7	-13.6	-2.3	-97.5	-85.8	-70.5	-71.4	-57.4	-48.7	-70.5	-72.1
	LANL2DZ	-8.5	4.2	-103.1	-90.5	-58.6	-59.9	-14.1	-2.9	-100.6	-88.2	-68.7	-70.4	-57.4	-48.6	-64.7	-66.4
	SDDAll	-8.3	4.4	-97.6	-84.9	-60.6	-60.5	-10.1	1.0	-96.4	-85.0	-70.8	-71.4	-55.2	-46.4	-70.9	-72.6
	Average	-8.6	4.8	-99.5	-86.4	-60.1	-61.1	-12.8	-1.6	-98.0	-86.2	-70.4	-71.3	-56.8	-48.0	-69.3	-70.9
	Std Dev	0.5	1.1	2.4	2.7	1.0	1.2	1.8	1.8	1.8	1.4	1.2	0.7	1.1	1.1	3.1	3.0
SOGGA11	CEP 31G	-10.7	0.3	-96.4	-84.8	-78.6	-80.4	-8.4	2.2	-96.9	-84.2	-78.6	-80.1	-61.3	-52.4	-77.5	-79.3
	CEP 121G	-10.3	0.7	-96.7	-84.0	-78.8	-81.8	-8.2	2.3	-96.8	-84.0	-79.0	-80.9	-61.1	-52.2	-77.9	-79.6
	LANL2DZ	-4.4	7.9	-95.6	-82.9	-79.8	-80.9	-8.9	1.8	-101.4	-88.0	-79.2	-81.6	-62.2	-53.3	-74.7	-76.4
	SDDAll	-4.1	7.8	-88.5	-62.0	-76.5	-78.3	-6.5	4.2	-94.0	-62.7	-75.5	-77.3	-55.2	-46.3	-78.0	-79.7
	Average	-7.4	4.2	-94.3	-78.4	-78.4	-80.4	-8.0	2.6	-97.3	-79.7	-78.1	-80.0	-59.9	-51.1	-77.0	-78.8
	Std Dev	3.6	4.2	3.9	11.0	1.4	1.5	1.1	1.1	3.0	11.5	1.7	1.9	3.2	3.2	1.6	1.6
B2LYP	CEP 31G	-15.3	-2.3	-90.5	-78.7	-53.9	-54.4	-15.1	-4.0	-89.5	-77.7	-64.0	-65.0	-42.6	-33.8	-64.6	-66.3
	CEP 121G	-15.0	-1.9	-92.0	-80.4	-54.0	-54.5	-15.6	-4.5	-91.0	-79.1	-64.2	-65.2	-43.4	-34.7	-65.3	-67.0
	LANL2DZ	-14.1	-1.7	-96.0	-84.1	-58.0	-58.6	-14.8	-3.8	-93.9	-82.1	-68.1	-69.2	-47.2	-38.4	-67.0	-68.7
	SDDAll	-13.6	-1.3	-92.2	-80.3	-53.5	-54.4	-12.7	-1.8	-90.6	-78.9	-64.0	-65.0	-41.4	-32.6	-64.5	-66.1
	Average	-14.5	-1.8	-92.7	-80.9	-54.9	-55.5	-14.6	-3.5	-91.3	-79.5	-65.1	-66.1	-43.6	-34.9	-65.4	-67.0
	Std Dev	0.8	0.4	2.3	2.3	2.1	2.1	1.3	1.2	1.9	1.8	2.0	2.1	2.5	2.5	1.2	1.2
MP2	CEP 31G	-23.7	-10.4	-108.1	-96.8	-64.5	-63.8	-18.5	-7.3	-107.3	-95.7	-73.8	-74.6	-47.6	-38.9	-62.2	-63.9
	CEP 121G	-24.3	-10.8	-110.9	-99.8	-65.8	-64.9	-19.7	-8.4	-110.1	-98.5	-75.1	-75.9	-49.7	-41.0	-63.4	-65.1
	LANL2DZ	-21.7	-8.8	-111.3	-100.0	-67.7	-67.1	-17.5	-6.4	-109.6	-97.8	-77.0	-78.1	-50.2	-41.4	-63.0	-64.7
	SDDAll	-20.2	-7.5	-110.0	-98.7	-65.8	-65.6	-15.9	-5.0	-108.7	-97.2	-75.8	-76.6	-48.0	-39.2	-63.2	-64.9
	Average	-22.5	-9.4	-110.1	-98.8	-65.9	-65.3	-17.9	-6.8	-108.9	-97.3	-75.4	-76.3	-48.9	-40.1	-62.9	-64.6

Basis	Pseudo-Potential	Cotton Complex - Trans THF						Cotton Complex - Trans H_2O						Oxygen Analogs			
		Dative Bond		σ		π		Dative Bond		σ		π		Peroxide		O_2	
		ΔH	ΔG	ΔH	ΔG	ΔH	ΔG	ΔH	ΔG	ΔH	ΔG	ΔH	ΔG	ΔH	ΔG	ΔH	ΔG
	Std Dev	1.9	1.5	1.5	1.4	1.3	1.4	1.6	1.4	1.2	1.2	1.3	1.5	1.3	1.3	0.5	0.5
Overall Averages	CEP 31G	-13.0	-0.2	-92.8	-80.9	-60.0	-61.7	-14.1	-3.0	-92.1	-80.2	-67.9	-70.0	-49.7	-40.9	-73.2	-77.0
	CEP 121G	-12.5	0.5	-93.3	-81.3	-59.0	-59.9	-14.3	-3.2	-92.5	-80.6	-66.9	-68.1	-49.6	-40.9	-72.2	-73.9
	LANL2DZ	-11.8	0.6	-98.1	-86.1	-61.5	-62.5	-14.3	-3.3	-96.8	-84.8	-69.1	-70.4	-54.6	-45.7	-70.2	-71.9
	SDDAll	-11.6	0.8	-92.2	-78.8	-59.6	-54.1	-11.6	-0.6	-91.1	-77.5	-67.5	-61.7	-45.9	-37.1	-74.0	-75.7
	Average	-12.2	0.4	-94.1	-81.8	-60.0	-59.5	-13.6	-2.5	-93.1	-80.8	-67.8	-67.6	-49.9	-41.1	-72.4	-74.6
	Std Dev	5.0	4.5	6.1	6.9	8.0	12.1	3.2	3.0	6.1	6.7	6.0	11.9	6.9	6.9	8.2	8.9

Table A.2.3-2: Calculated bond dissociation enthalpies in kcal/mol for tungsten-oxygen bonds by functional and valence basis set for the Cotton model with tetrahydrofuran cis to the oxo moiety.

Basis	Pseudo-Potential	Dative Bond		σ						π					
				OHtransOH		OHtransOxo		OHtransTHF		OHtransOH		OHtransOxo		OHtransTHF	
		ΔH	ΔG	ΔH	ΔG	ΔH	ΔG	ΔH	ΔG	ΔH	ΔG	ΔH	ΔG	ΔH	ΔG
BP 86	CEP 31G	-2.1	10.2	-76.0	-64.6	-76.5	-65.5	-87.7	-75.8	-71.9	-72.3	-71.4	-71.4	-60.1	-61.2
	CEP 121G	-0.9	9.7	-76.6	-65.5	-77.1	-66.4	-88.1	-76.6	-71.0	-71.3	-70.6	-70.4	-59.6	-60.2
	LANL2DZ	-1.0	10.8	-82.5	-71.2	-83.0	-71.9	-89.6	-76.1	-75.5	-77.7	-75.1	-77.0	-68.5	-72.8
	SDDAll	-1.0	10.7	-75.6	-64.8	-76.7	-65.7	-86.8	-75.3	-71.2	-71.5	-70.1	-70.5	-60.0	-61.0
	Average	-1.2	10.4	-77.7	-66.5	-78.3	-67.4	-88.0	-75.9	-72.4	-73.2	-71.8	-72.3	-62.1	-63.8
	Std Dev	0.6	0.5	3.3	3.1	3.1	3.0	1.1	0.5	2.1	3.1	2.3	3.1	4.3	6.0
B3LYP	CEP 31G	-2.5	9.4	-64.1	-53.1	-64.8	-54.2	-77.9	-65.9	-62.3	-62.7	-61.6	-61.7	-48.5	-50.0
	CEP 121G	-4.3	8.7	-67.3	-55.7	-68.0	-56.6	-80.8	-68.0	-61.5	-62.0	-60.8	-61.0	-48.1	-49.6
	LANL2DZ	-1.4	10.1	-70.8	-60.1	-71.6	-60.8	-83.2	-71.9	-66.5	-67.0	-65.8	-66.3	-54.2	-55.1
	SDDAll	-3.4	8.5	-66.1	-55.0	-67.5	-55.9	-79.4	-67.0	-61.4	-61.5	-60.0	-70.5	-48.0	-49.5
	Average	-2.9	9.2	-67.1	-56.0	-68.0	-56.9	-80.3	-68.2	-62.9	-63.3	-62.0	-64.9	-49.7	-51.1
	Std Dev	1.3	0.7	2.8	2.9	2.8	2.8	2.3	2.6	2.4	2.5	2.6	4.4	3.0	2.7

Basis	Pseudo-Potential	Dative Bond		σ						π					
				OHtransOH		OHtransOxo		OHtransTHF		OHtransOH		OHtransOxo		OHtransTHF	
		ΔH	ΔG	ΔH	ΔG	ΔH	ΔG	ΔH	ΔG	ΔH	ΔG	ΔH	ΔG	ΔH	ΔG
M06	CEP 31G	-9.1	4.8	-74.0	-62.1	-73.9	-62.6	-86.9	-74.1	-58.9	-59.5	-59.0	-58.9	-46.0	-47.4
	CEP 121G	-10.2	1.3	-76.1	-66.7	-75.9	-66.9	-88.5	-78.2	-57.8	-58.0	-57.9	-57.8	-45.4	-46.6
	LANL2DZ	-8.2	5.4	-76.5	-64.5	-76.7	-65.4	-88.3	-75.5	-64.1	-64.7	-63.9	-63.8	-52.3	-53.7
	SDDAll	-8.0	5.1	-72.4	-60.6	-72.9	-62.0	-85.0	-72.7	-60.9	-59.3	-60.3	-58.0	-48.3	-47.3
	Average	-8.9	4.1	-74.8	-63.5	-74.9	-64.2	-87.2	-75.1	-60.4	-60.4	-60.3	-59.6	-48.0	-48.7
	Std Dev	1.0	1.9	1.9	2.7	1.7	2.3	1.6	2.3	2.8	2.9	2.6	2.8	3.1	3.3
BLYP	CEP 31G	-1.3	10.5	-71.9	-61.1	-72.5	-61.6	-83.6	-72.0	-70.5	-71.0	-70.0	-70.4	-58.8	-60.0
	CEP 121G	-2.6	10.0	-74.9	-63.2	-75.4	-63.6	-86.1	-74.0	-69.4	-69.9	-68.9	-69.5	-58.2	-59.1
	LANL2DZ	-0.4	11.0	-79.9	-69.0	-80.2	-69.5	-85.7	-73.4	-75.5	-75.6	-75.1	-75.1	-69.6	-71.2
	SDDAll	-2.5	9.8	-72.8	-61.4	-72.8	-61.3	-80.7	-66.6	-69.4	-69.7	-69.4	-69.8	-61.5	-64.5
	Average	-1.7	10.3	-74.9	-63.7	-75.2	-64.0	-84.1	-71.5	-71.2	-71.5	-70.8	-71.2	-62.0	-63.7
	Std Dev	1.1	0.5	3.5	3.7	3.6	3.8	2.5	3.4	2.9	2.8	2.9	2.6	5.3	5.5
B97D	CEP 31G	-10.6	3.3	-76.7	-64.4	-75.8	-64.2	-88.5	-75.7	-68.1	-69.2	-68.9	-69.4	-56.2	-57.9
	CEP 121G	-10.0	4.2	-77.5	-65.3	-76.5	-65.0	-88.9	-76.4	-67.1	-68.6	-68.1	-68.9	-55.6	-57.5
	LANL2DZ	-9.7	4.0	-78.7	-66.1	-77.9	-66.2	-88.8	-76.1	-68.5	-70.0	-69.3	-69.8	-58.4	-59.9
	SDDAll	-9.3	4.2	-76.8	-64.3	-76.4	-64.8	-88.4	-75.7	-67.0	-68.3	-67.4	-67.8	-55.4	-56.9
	Average	-9.9	3.9	-77.4	-65.0	-76.6	-65.1	-88.7	-76.0	-67.7	-69.0	-68.4	-69.0	-56.4	-58.0
	Std Dev	0.6	0.4	0.9	0.8	0.9	0.9	0.2	0.4	0.7	0.7	0.9	0.9	1.4	1.3
PBEPBE	CEP 31G	-4.1	8.6	-77.9	-66.1	-78.3	-67.1	-89.7	-77.4	-71.2	-71.7	-70.9	-70.7	-59.4	-60.4
	CEP 121G	-3.4	9.0	-78.7	-67.3	-79.0	-68.1	-90.0	-78.1	-70.3	-70.4	-70.0	-69.6	-59.0	-59.6
	LANL2DZ	-3.0	9.4	-84.3	-72.3	-84.6	-73.0	-91.4	-78.4	-75.6	-76.3	-75.3	-75.6	-68.6	-70.2
	SDDAll	-3.2	8.8	-76.9	-65.8	-77.9	-66.9	-88.1	-76.0	-70.1	-70.3	-69.1	-69.2	-58.9	-60.0
	Average	-3.4	8.9	-79.5	-67.9	-79.9	-68.8	-89.8	-77.5	-71.8	-72.2	-71.3	-71.3	-61.5	-62.6
	Std Dev	0.5	0.3	3.3	3.0	3.1	2.9	1.4	1.0	2.6	2.8	2.8	3.0	4.7	5.1

Basis	Pseudo-Potential	Dative Bond		σ						π					
				OHtransOH		OHtransOxo		OHtransTHF		OHtransOH		OHtransOxo		OHtransTHF	
		ΔH	ΔG	ΔH	ΔG	ΔH	ΔG	ΔH	ΔG	ΔH	ΔG	ΔH	ΔG	ΔH	ΔG
M11L	CEP 31G	-9.4	4.3	-72.4	-60.1	-72.4	-60.6	-84.6	-72.2	-73.7	-72.9	-73.7	-72.4	-61.5	-60.9
	CEP 121G	-9.2	5.6	-73.6	-61.0	-73.6	-61.8	-86.0	-73.9	-70.0	-71.9	-69.9	-71.1	-57.6	-59.0
	LANL2DZ	-9.0	4.6	-80.4	-67.6	-80.8	-69.1	-91.9	-79.3	-65.4	-65.1	-65.0	-63.7	-53.9	-53.5
	SDDAll	-7.7	5.3	-71.9	-58.6	-72.5	-61.1	-84.5	-71.8	-75.7	-76.7	-75.1	-74.2	-63.1	-63.5
	Average	-8.8	5.0	-74.6	-61.8	-74.9	-63.1	-86.7	-74.3	-71.2	-71.7	-70.9	-70.3	-59.0	-59.2
	Std Dev	0.8	0.6	4.0	4.0	4.0	4.0	3.5	3.4	4.5	4.8	4.5	4.6	4.1	4.2
MN12L	CEP 31G	-14.8	-0.7	-73.1	-60.6	-72.5	-60.0	-82.8	-70.5	-74.5	-84.5	-75.2	-85.1	-64.9	-74.7
	CEP 121G	-14.4	-0.3	-74.1	-60.7	-73.5	-61.5	-83.7	-71.3	-71.2	-71.2	-71.8	-70.4	-61.6	-60.6
	LANL2DZ	-12.8	1.4	-84.6	-72.0	-84.6	-72.2	-93.3	-81.1	-69.2	-69.0	-69.2	-68.8	-60.5	-59.9
	SDDAll	-13.4	0.6	-73.4	-61.0	-73.1	-61.2	-83.2	-71.2	-77.0	-76.6	-77.3	-76.4	-67.2	-66.3
	Average	-13.9	0.3	-76.3	-63.6	-75.9	-63.7	-85.7	-73.5	-73.0	-75.3	-73.3	-75.2	-63.5	-65.4
	Std Dev	0.9	1.0	5.6	5.6	5.8	5.7	5.1	5.1	3.5	6.9	3.6	7.4	3.1	6.8
N12	CEP 31G	-2.9	8.9	-78.8	-67.8	-79.7	-70.3	-92.0	-80.7	-74.2	-75.0	-73.3	-72.6	-61.0	-62.1
	CEP 121G	-2.9	11.1	-80.3	-68.8	-81.4	-71.0	-93.1	-81.3	-73.1	-73.7	-72.0	-71.4	-60.3	-61.1
	LANL2DZ	-3.9	8.8	-86.5	-73.8	-87.5	-76.5	-95.1	-81.2	-70.5	-72.0	-69.4	-69.3	-61.9	-64.6
	SDDAll	-3.8	8.4	-80.0	-68.9	-80.9	-69.2	-92.5	-80.2	-73.7	-72.4	-72.9	-72.1	-61.2	-61.1
	Average	-3.4	9.3	-81.4	-69.8	-82.4	-71.7	-93.2	-80.9	-72.9	-73.3	-71.9	-71.4	-61.1	-62.2
	Std Dev	0.6	1.2	3.5	2.7	3.5	3.2	1.3	0.5	1.7	1.4	1.7	1.5	0.7	1.6
SOGGA11	CEP 31G	4.1	16.7	-80.2	-68.7	-80.2	-68.9	-90.9	-78.5	-80.0	-80.1	-79.9	-79.8	-69.2	-70.3
	CEP 121G	4.4	17.3	-81.9	-70.6	-82.1	-70.7	-92.4	-79.9	-78.9	-78.7	-78.7	-78.6	-68.4	-69.4
	LANL2DZ	4.9	17.4	-85.8	-73.1	-86.0	-74.6	-95.9	-83.5	-80.3	-81.3	-80.1	-79.7	-70.3	-70.8
	SDDAll	4.5	16.0	-78.8	-67.8	-79.9	-68.6	-90.0	-79.0	-77.6	-77.5	-76.5	-76.7	-66.4	-66.3
	Average	4.5	16.8	-81.7	-70.1	-82.0	-70.7	-92.3	-80.2	-79.2	-79.4	-78.8	-78.7	-68.6	-69.2
	Std Dev	0.4	0.6	3.1	2.3	2.8	2.7	2.6	2.3	1.2	1.6	1.7	1.5	1.6	2.0

Basis	Pseudo-Potential	Dative Bond		σ						π					
				OHtransOH		OHtransOxo		OHtransTHF		OHtransOH		OHtransOxo		OHtransTHF	
		ΔH	ΔG	ΔH	ΔG	ΔH	ΔG	ΔH	ΔG	ΔH	ΔG	ΔH	ΔG	ΔH	ΔG
B2LYP	CEP 31G	-8.1	4.7	-70.2	-58.3	-70.6	-59.3	-84.1	-71.3	-67.1	-67.8	-66.7	-66.7	-53.2	-54.7
	CEP 121G	-7.8	5.2	-71.9	-60.2	-72.3	-61.1	-85.4	-72.3	-66.9	-67.6	-66.5	-66.6	-53.4	-55.5
	LANL2DZ	-6.4	6.0	-75.7	-63.9	-76.4	-65.0	-88.3	-75.6	-70.5	-71.1	-69.9	-70.0	-58.0	-59.4
	SDDAll	-6.3	5.9	-71.4	-60.2	-72.6	-61.6	-84.7	-72.2	-67.0	-67.3	-65.8	-65.9	-53.7	-55.2
	Average	-7.1	5.4	-72.3	-60.6	-73.0	-61.8	-85.6	-72.8	-67.9	-68.4	-67.2	-67.3	-54.6	-56.2
	Std Dev	1.0	0.6	2.4	2.4	2.4	2.4	1.9	1.9	1.8	1.8	1.8	1.8	2.3	2.2
MP2	CEP 31G	-16.4	-3.0	-87.9	-76.0	-88.0	-76.8	-102.3	-89.2	-77.3	-77.2	-77.2	-76.4	-63.0	-64.1
	CEP 121G	-16.9	-3.5	-91.1	-79.2	-91.0	-79.9	-103.9	-92.3	-78.2	-78.2	-78.4	-77.5	-65.4	-65.1
	LANL2DZ	-13.8	-0.7	-91.3	-79.3	-91.7	-80.3	-104.1	-91.4	-79.8	-79.7	-79.4	-78.7	-67.0	-67.6
	SDDAll	-12.6	0.0	-89.7	-78.2	-90.6	-79.5	-102.7	-90.4	-78.6	-78.6	-77.6	-77.3	-65.6	-66.4
	Average	-14.9	-1.8	-90.0	-78.2	-90.3	-79.1	-103.2	-90.8	-78.5	-78.5	-78.2	-77.5	-65.2	-65.8
	Std Dev	2.1	1.7	1.6	1.5	1.6	1.6	0.9	1.3	1.0	1.0	1.0	0.9	1.7	1.5
Overall Averages	CEP 31G	-5.3	7.6	-74.5	-62.9	-74.7	-63.5	-86.5	-74.3	-70.5	-71.9	-70.4	-71.3	-58.6	-60.5
	CEP 121G	-5.4	7.6	-76.1	-64.5	-76.3	-65.2	-87.7	-75.8	-69.0	-69.6	-68.9	-68.9	-57.4	-58.3
	LANL2DZ	-4.4	8.3	-81.0	-69.0	-81.3	-69.9	-90.3	-77.6	-71.1	-71.9	-70.8	-70.9	-61.8	-63.2
	SDDAll	-4.8	7.7	-74.5	-62.8	-75.1	-63.7	-85.8	-73.6	-70.4	-70.4	-69.8	-70.5	-59.0	-59.6
	Average	-5.0	7.8	-76.5	-64.8	-76.8	-65.6	-87.6	-75.3	-70.3	-70.9	-70.0	-70.4	-59.2	-60.4
	Std Dev	5.5	5.0	6.2	6.1	6.1	6.2	5.9	6.0	5.7	6.0	5.8	5.9	6.6	6.9

Table A.2.3-3: Calculated bond dissociation enthalpies in kcal/mol for tungsten-oxygen bonds by functional and valence basis set for the Cotton model with water cis to the oxo moiety.

Basis	Pseudo-Potential	Dative Bond		σ						π					
				OHtransOH		OHtransOxo		OHtransTHF		OHtransOH		OHtransOxo		OHtransTHF	
		ΔH	ΔG	ΔH	ΔG	ΔH	ΔG	ΔH	ΔG	ΔH	ΔG	ΔH	ΔG	ΔH	ΔG
BP 86	CEP 31G	-6.0	5.4	-87.0	-74.7	-78.9	-67.3	-86.7	-74.7	-69.3	-70.7	-77.4	-78.0	-69.7	-70.7
	CEP 121G	-6.2	5.2	-87.4	-75.1	-79.4	-67.8	-87.0	-74.9	-68.7	-70.0	-76.7	-77.4	-69.1	-70.2
	LANL2DZ	-6.1	5.2	-92.3	-80.2	-84.8	-73.2	-91.4	-79.3	-73.4	-74.7	-80.9	-81.7	-74.4	-75.6
	SDDAll	-2.8	8.3	-85.7	-73.6	-78.3	-67.0	-85.5	-73.7	-68.6	-70.1	-76.0	-76.7	-68.8	-70.0
	Average	-5.3	6.0	-88.1	-75.9	-80.4	-68.8	-87.6	-75.7	-70.0	-71.4	-77.8	-78.5	-70.5	-71.6
	Std Dev	1.6	1.5	2.9	2.9	3.0	2.9	2.6	2.5	2.3	2.2	2.2	2.2	2.6	2.6
B3LYP	CEP 31G	-5.2	6.2	-75.7	-63.2	-67.2	-55.7	-76.4	-64.2	-59.8	-61.0	-68.3	-68.6	-59.1	-60.0
	CEP 121G	-5.4	5.9	-76.3	-63.8	-67.9	-56.3	-76.9	-64.6	-59.1	-60.4	-67.6	-67.9	-58.6	-59.7
	LANL2DZ	-5.2	6.0	-81.6	-69.2	-73.4	-61.8	-81.5	-69.3	-64.0	-65.3	-72.2	-72.7	-64.0	-65.1
	SDDAll	-2.2	8.9	-75.0	-62.6	-67.1	-55.7	-75.8	-63.8	-58.8	-60.1	-66.7	-76.7	-58.0	-58.9
	Average	-4.5	6.8	-77.1	-64.7	-68.9	-57.4	-77.7	-65.5	-60.4	-61.7	-68.7	-71.5	-59.9	-60.9
	Std Dev	1.5	1.4	3.0	3.0	3.0	2.9	2.6	2.6	2.4	2.4	2.4	4.1	2.8	2.8
M06	CEP 31G	-8.4	3.1	-84.9	-72.6	-75.9	-64.4	-84.9	-72.6	-56.3	-57.5	-65.3	-65.6	-56.2	-57.4
	CEP 121G	-8.8	2.7	-85.3	-73.0	-76.2	-64.6	-85.3	-73.3	-55.4	-56.7	-64.5	-65.0	-55.4	-56.4
	LANL2DZ	-8.6	2.8	-86.9	-74.5	-78.3	-66.7	-86.4	-73.7	-61.3	-62.7	-70.0	-70.5	-61.8	-63.5
	SDDAll	-5.9	5.4	-82.5	-70.1	-74.2	-62.7	-83.1	-71.0	-57.6	-59.0	-65.9	-66.4	-57.0	-58.1
	Average	-7.9	3.5	-84.9	-72.5	-76.1	-64.6	-85.0	-72.6	-57.6	-59.0	-66.4	-66.9	-57.6	-58.9
	Std Dev	1.4	1.3	1.8	1.8	1.6	1.6	1.4	1.2	2.6	2.7	2.4	2.5	2.9	3.2
BLYP	CEP 31G	-4.7	6.5	-82.5	-70.2	-75.0	-63.4	-82.5	-70.4	-68.4	-69.6	-75.9	-76.4	-68.4	-69.4
	CEP 121G	-4.9	6.3	-82.7	-70.4	-75.4	-63.8	-82.7	-70.8	-67.6	-68.9	-74.9	-75.5	-67.6	-68.5
	LANL2DZ	-5.1	6.1	-89.0	-76.7	-82.0	-70.3	-88.1	-76.0	-73.3	-74.5	-80.3	-80.9	-74.1	-75.2
	SDDAll	-1.0	10.0	-80.1	-67.8	-73.4	-62.1	-80.3	-68.3	-67.4	-68.9	-74.1	-74.6	-67.1	-68.4
	Average	-3.9	7.2	-83.6	-71.3	-76.4	-64.9	-83.4	-71.4	-69.2	-70.5	-76.3	-76.9	-69.3	-70.4

Basis	Pseudo-Potential	Dative Bond		σ						π					
				OHtransOH		OHtransOxo		OHtransTHF		OHtransOH		OHtransOxo		OHtransTHF	
		ΔH	ΔG	ΔH	ΔG	ΔH	ΔG	ΔH	ΔG	ΔH	ΔG	ΔH	ΔG	ΔH	ΔG
	Std Dev	2.0	1.9	3.8	3.8	3.8	3.7	3.3	3.3	2.8	2.7	2.7	2.8	3.3	3.3
B97D	CEP 31G	-7.0	4.4	-86.3	-73.9	-78.8	-67.1	-86.5	-74.1	-67.3	-68.3	-74.8	-75.2	-67.1	-68.2
	CEP 121G	-7.3	4.1	-86.7	-74.3	-79.2	-67.5	-87.2	-75.2	-66.6	-67.5	-74.0	-74.4	-66.1	-66.7
	LANL2DZ	-7.0	4.4	-87.5	-75.1	-80.5	-68.7	-86.8	-74.0	-67.5	-68.5	-74.5	-75.0	-68.3	-69.6
	SDDAll	-4.1	7.3	-85.8	-73.5	-78.8	-67.1	-86.1	-73.8	-65.8	-66.8	-72.9	-73.3	-65.6	-66.6
	Average	-6.4	5.0	-86.6	-74.2	-79.3	-67.6	-86.6	-74.3	-66.8	-67.8	-74.1	-74.5	-66.8	-67.8
	Std Dev	1.5	1.5	0.7	0.7	0.8	0.8	0.5	0.6	0.8	0.8	0.9	0.9	1.2	1.4
PBEPBE	CEP 31G	-7.7	3.7	-88.8	-76.5	-80.8	-69.1	-88.4	-76.4	-68.6	-69.9	-76.6	-77.3	-68.9	-69.9
	CEP 121G	-7.9	3.5	-89.2	-76.9	-81.3	-69.6	-88.8	-76.8	-67.9	-69.3	-75.9	-76.6	-68.4	-69.4
	LANL2DZ	-7.8	3.5	-93.9	-81.8	-86.5	-74.8	-92.9	-80.8	-72.9	-74.1	-80.3	-81.1	-73.9	-75.1
	SDDAll	-4.4	6.7	-86.9	-74.8	-79.6	-68.3	-86.7	-74.8	-67.5	-68.9	-74.8	-75.5	-67.6	-68.9
	Average	-7.0	4.3	-89.7	-77.5	-82.0	-70.5	-89.2	-77.2	-69.2	-70.6	-76.9	-77.6	-69.7	-70.9
	Std Dev	1.7	1.6	3.0	3.0	3.1	3.0	2.6	2.6	2.5	2.4	2.4	2.4	2.9	2.8
M11L	CEP 31G	-10.9	0.6	-83.1	-70.5	-74.0	-62.4	-82.5	-70.8	-69.2	-71.0	-78.4	-79.1	-69.8	-70.7
	CEP 121G	-11.5	0.1	-84.6	-72.2	-75.3	-63.7	-84.6	-72.4	-66.2	-67.8	-75.6	-76.4	-66.2	-67.7
	LANL2DZ	-10.7	1.1	-91.1	-78.9	-91.1	-78.9	-89.6	-77.8	-60.3	-61.8	-60.3	-61.8	-61.8	-62.9
	SDDAll	-9.2	2.3	-82.5	-70.2	-73.4	-61.9	-82.1	-70.7	-71.5	-73.0	-80.5	-81.4	-71.8	-72.6
	Average	-10.5	1.0	-85.3	-73.0	-78.4	-66.7	-84.7	-72.9	-66.8	-68.4	-73.7	-74.7	-67.4	-68.5
	Std Dev	1.0	0.9	4.0	4.1	8.5	8.2	3.4	3.4	4.8	4.9	9.2	8.8	4.4	4.2
MN12L	CEP 31G	-11.5	-0.1	-82.5	-70.4	-74.1	-62.5	-80.6	-68.9	-68.4	-80.6	-76.8	-88.5	-70.3	-82.2
	CEP 121G	-12.0	-0.8	-83.6	-71.6	-75.1	-63.6	-81.6	-69.6	-65.1	-66.6	-73.6	-74.6	-67.1	-68.5
	LANL2DZ	-11.6	-0.2	-93.9	-81.8	-85.6	-74.1	-90.9	-79.2	-62.2	-63.8	-70.5	-71.5	-65.2	-66.3
	SDDAll	-9.8	1.8	-82.6	-70.4	-74.5	-62.7	-81.3	-69.5	-71.1	-72.5	-79.2	-80.1	-72.4	-73.3
	Average	-11.2	0.2	-85.6	-73.5	-77.3	-65.7	-83.6	-71.8	-66.7	-70.9	-75.0	-78.7	-68.8	-72.6

Basis	Pseudo-Potential	Dative Bond		σ						π					
				OHtransOH		OHtransOxo		OHtransTHF		OHtransOH		OHtransOxo		OHtransTHF	
		ΔH	ΔG	ΔH	ΔG	ΔH	ΔG	ΔH	ΔG	ΔH	ΔG	ΔH	ΔG	ΔH	ΔG
	Std Dev	1.0	1.1	5.5	5.5	5.5	5.6	4.9	5.0	3.9	7.5	3.8	7.5	3.2	7.0
N12	CEP 31G	-6.7	4.7	-89.9	-77.4	-81.9	-70.4	-90.5	-78.7	-72.1	-73.6	-80.1	-80.6	-71.5	-72.4
	CEP 121G	-6.8	4.6	-90.1	-77.3	-82.2	-70.3	-90.9	-79.0	-71.1	-73.1	-79.1	-80.1	-70.4	-71.4
	LANL2DZ	-6.9	4.4	-94.3	-82.1	-86.6	-75.2	-93.8	-82.0	-67.9	-69.2	-75.5	-76.1	-68.4	-69.2
	SDDAll	-2.7	8.3	-88.1	-76.1	-80.8	-69.7	-88.9	-77.6	-71.7	-73.1	-78.9	-79.5	-70.9	-71.6
	Average	-5.8	5.5	-90.6	-78.2	-82.9	-71.4	-91.0	-79.3	-70.7	-72.3	-78.4	-79.1	-70.3	-71.2
	Std Dev	2.0	1.8	2.6	2.7	2.6	2.5	2.0	1.9	1.9	2.1	2.0	2.0	1.4	1.3
SOGGA11	CEP 31G	-1.5	9.8	-89.3	-76.5	-83.0	-71.2	-90.0	-76.5	-79.3	-80.2	-85.7	-85.6	-78.6	-80.2
	CEP 121G	-1.1	10.2	-89.4	-76.5	-83.1	-71.2	-91.5	-79.4	-79.4	-80.5	-85.7	-85.8	-77.2	-77.6
	LANL2DZ	-1.6	9.6	-94.2	-81.4	-87.9	-76.1	-94.2	-80.8	-79.2	-80.5	-85.5	-85.7	-79.2	-81.0
	SDDAll	1.3	12.0	-86.8	-74.2	-80.4	-68.8	-86.3	-73.2	-75.0	-76.2	-81.4	-81.5	-75.6	-77.2
	Average	-0.8	10.4	-89.9	-77.1	-83.6	-71.8	-90.5	-77.5	-78.2	-79.3	-84.5	-84.6	-77.6	-79.0
	Std Dev	1.4	1.1	3.1	3.0	3.1	3.1	3.3	3.4	2.1	2.1	2.1	2.1	1.6	1.9
B2LYP	CEP 31G	-7.6	3.6	-82.0	-69.7	-73.0	-61.7	-82.1	-70.1	-64.1	-65.4	-73.1	-73.4	-64.0	-65.0
	CEP 121G	-8.2	3.1	-83.7	-71.2	-74.7	-63.2	-83.5	-71.4	-64.0	-65.4	-73.1	-73.4	-64.2	-65.3
	LANL2DZ	-7.2	4.1	-87.0	-74.7	-78.2	-66.7	-86.3	-74.2	-67.3	-68.7	-76.1	-76.6	-68.1	-69.2
	SDDAll	-4.9	6.2	-82.9	-70.6	-74.3	-63.1	-82.8	-70.9	-64.0	-65.3	-72.5	-72.8	-64.0	-65.0
	Average	-7.0	4.2	-83.9	-71.5	-75.1	-63.7	-83.7	-71.6	-64.8	-66.2	-73.7	-74.1	-65.1	-66.1
	Std Dev	1.4	1.3	2.2	2.2	2.2	2.2	1.8	1.8	1.7	1.7	1.7	1.7	2.0	2.0
MP2	CEP 31G	-10.8	0.3	-99.8	-87.7	-90.2	-79.2	-99.6	-88.0	-73.6	-75.0	-83.1	-83.5	-73.8	-74.7
	CEP 121G	-11.9	-0.7	-103.0	-90.8	-93.2	-82.1	-102.3	-90.7	-74.5	-75.9	-84.2	-84.6	-75.1	-76.0
	LANL2DZ	-9.4	1.7	-102.7	-90.5	-93.3	-82.1	-101.5	-89.8	-75.8	-77.3	-85.2	-85.7	-77.0	-78.1
	SDDAll	-7.9	3.0	-101.6	-89.6	-92.3	-81.3	-100.7	-89.1	-74.8	-76.2	-84.1	-84.5	-75.8	-76.7
	Average	-10.0	1.1	-101.8	-89.6	-92.3	-81.2	-101.0	-89.4	-74.7	-76.1	-84.2	-84.5	-75.4	-76.4

Basis	Pseudo-Potential	Dative Bond		σ						π					
				OHtransOH		OHtransOxo		OHtransTHF		OHtransOH		OHtransOxo		OHtransTHF	
		ΔH	ΔG	ΔH	ΔG	ΔH	ΔG	ΔH	ΔG	ΔH	ΔG	ΔH	ΔG	ΔH	ΔG
	Std Dev	1.7	1.6	1.5	1.4	1.4	1.4	1.2	1.1	0.9	1.0	0.9	0.9	1.3	1.4
Overall Averages	CEP 31G	-7.0	4.4	-85.0	-72.6	-77.0	-65.4	-84.9	-72.7	-67.9	-70.2	-75.9	-77.5	-68.0	-70.1
	CEP 121G	-7.2	4.2	-85.5	-73.1	-77.5	-65.8	-85.7	-73.6	-66.7	-68.1	-74.8	-75.4	-66.6	-67.6
	LANL2DZ	-7.1	4.3	-90.5	-78.2	-83.7	-72.0	-89.5	-77.3	-68.2	-69.5	-75.0	-75.7	-69.1	-70.4
	SDDAll	-4.1	7.1	-83.6	-71.3	-76.1	-64.6	-83.6	-71.6	-67.5	-68.9	-75.0	-76.6	-67.5	-68.6
	Average	-6.3	5.0	-86.2	-73.8	-78.5	-66.9	-85.9	-73.8	-67.6	-69.2	-75.2	-76.3	-67.8	-69.2
	Std Dev	3.2	3.1	6.3	6.3	6.4	6.5	6.0	6.1	5.9	6.1	5.9	6.0	5.9	6.2

Table A.2.3-4: Difference between the calculated bond dissociation enthalpies in kcal/mol for the trans-Cotton complex and cis-Cotton complex with THF as the dative ligand by functional and valence basis set.

Basis	Pseudo-Potential	Dative Bond		σ						π					
				OHtransOH		OHtransOxo		OHtransTHF		OHtransOH		OHtransOxo		OHtransTHF	
		ΔH	ΔG	ΔH	ΔG	ΔH	ΔG	ΔH	ΔG	ΔH	ΔG	ΔH	ΔG	ΔH	ΔG
BP 86	CEP 31G	-6.9	-6.8	-18.4	-17.8	-17.9	-16.9	-6.6	-6.7	11.4	11.0	10.9	10.2	-0.3	-0.1
	CEP 121G	-7.1	-6.9	-18.2	-17.4	-17.7	-16.4	-6.8	-6.3	11.0	10.4	10.5	9.5	-0.4	-0.7
	LANL2DZ	-7.5	-8.4	-17.7	-18.3	-17.3	-17.5	-10.7	-13.3	10.2	9.8	9.8	9.1	3.1	4.9
	SDDAll	-7.0	-6.8	-18.7	-17.4	-17.5	-16.4	-7.4	-6.9	11.6	10.5	10.5	9.6	0.4	0.0
	Average	-7.2	-7.2	-18.2	-17.7	-17.6	-16.8	-7.9	-8.3	11.1	10.5	10.4	9.6	0.7	1.1
	Std Dev	0.3	0.8	0.4	0.4	0.2	0.5	1.9	3.4	0.6	0.5	0.5	0.4	1.7	2.6
B3LYP	CEP 31G	-7.4	-7.2	-21.0	-19.5	-20.3	-18.4	-7.1	-6.7	13.5	12.3	12.8	11.3	-0.3	-0.5
	CEP 121G	-5.2	-5.8	-18.3	-17.9	-17.5	-16.9	-4.8	-5.5	13.1	12.1	12.4	11.1	-0.4	-0.3
	LANL2DZ	-8.0	-7.5	-20.4	-18.7	-19.6	-17.9	-8.0	-6.8	12.4	11.2	11.6	10.5	0.0	-0.7
	SDDAll	-5.5	-5.8	-19.2	-18.3	-17.8	-17.4	-5.9	-6.3	13.7	12.5	12.3	21.5	0.4	0.5
	Average	-6.5	-6.6	-19.7	-18.6	-18.8	-17.7	-6.4	-6.3	13.2	12.0	12.3	13.6	-0.1	-0.2

Basis	Pseudo-Potential	Dative Bond		σ						π					
				OHtransOH		OHtransOxo		OHtransTHF		OHtransOH		OHtransOxo		OHtransTHF	
		ΔH	ΔG	ΔH	ΔG	ΔH	ΔG	ΔH	ΔG	ΔH	ΔG	ΔH	ΔG	ΔH	ΔG
	Std Dev	1.4	0.9	1.2	0.7	1.3	0.7	1.4	0.6	0.6	0.6	0.5	5.3	0.3	0.5
M06	CEP 31G	-8.0	-8.3	-20.6	-20.8	-20.7	-20.2	-7.8	-8.8	12.6	12.5	12.7	12.0	-0.2	0.5
	CEP 121G	-6.6	-4.0	-18.7	-16.2	-18.9	-15.9	-6.3	-4.7	12.2	12.2	12.3	11.9	-0.2	0.7
	LANL2DZ	-8.2	-8.4	-20.1	-19.6	-19.9	-18.7	-8.3	-8.6	11.8	11.2	11.7	10.3	0.1	0.2
	SDDAll	-8.1	-7.9	-20.9	-20.3	-20.4	-19.0	-8.4	-8.2	12.8	12.4	12.3	11.1	0.3	0.4
	Average	-7.7	-7.1	-20.1	-19.2	-20.0	-18.4	-7.7	-7.6	12.4	12.1	12.2	11.3	0.0	0.4
	Std Dev	0.8	2.1	1.0	2.1	0.8	1.8	0.9	2.0	0.4	0.6	0.4	0.8	0.2	0.2
BLYP	CEP 31G	-7.2	-7.0	-18.5	-17.4	-17.9	-16.8	-6.7	-6.4	11.3	10.4	10.7	9.8	-0.5	-0.6
	CEP 121G	-5.3	-6.4	-15.9	-15.9	-15.3	-15.5	-4.7	-5.2	10.6	9.6	10.0	9.2	-0.6	-1.1
	LANL2DZ	-7.8	-8.0	-17.5	-16.5	-17.1	-16.0	-11.6	-12.1	9.7	8.4	9.3	7.9	3.8	4.1
	SDDAll	-7.7	-9.7	-19.3	-20.0	-19.2	-20.1	-11.3	-14.8	11.6	10.3	11.5	10.5	3.6	5.2
	Average	-7.0	-7.8	-17.8	-17.5	-17.4	-17.1	-8.6	-9.6	10.8	9.7	10.4	9.4	1.6	1.9
	Std Dev	1.2	1.4	1.5	1.8	1.6	2.1	3.4	4.6	0.8	0.9	0.9	1.1	2.5	3.2
B97D	CEP 31G	-7.1	-7.9	-18.3	-19.3	-19.1	-19.6	-6.4	-8.1	11.2	11.4	12.1	11.6	-0.6	0.2
	CEP 121G	-7.2	-7.7	-17.8	-18.7	-18.8	-18.9	-6.4	-7.5	10.7	11.0	11.7	11.2	-0.8	-0.2
	LANL2DZ	-7.4	-8.1	-17.6	-18.4	-18.4	-18.2	-7.5	-8.3	10.2	10.3	11.0	10.2	0.1	0.3
	SDDAll	-7.3	-7.7	-18.8	-19.3	-19.2	-18.8	-7.2	-7.9	11.5	11.6	11.9	11.2	-0.1	0.2
	Average	-7.2	-7.8	-18.1	-18.9	-18.9	-18.9	-6.9	-8.0	10.9	11.1	11.7	11.0	-0.4	0.1
	Std Dev	0.2	0.2	0.5	0.5	0.4	0.5	0.6	0.3	0.6	0.6	0.5	0.6	0.4	0.2
PBEPBE	CEP 31G	-7.2	-7.7	-18.3	-18.8	-17.9	-17.8	-6.5	-7.5	11.0	11.0	10.7	10.1	-0.7	-0.2
	CEP 121G	-7.5	-7.6	-18.1	-17.6	-17.7	-16.8	-6.8	-6.9	10.6	10.0	10.3	9.2	-0.7	-0.8
	LANL2DZ	-7.8	-8.3	-17.6	-17.9	-17.3	-17.2	-10.5	-11.8	9.8	9.5	9.5	8.8	2.7	3.4
	SDDAll	-7.4	-7.3	-18.6	-17.7	-17.7	-16.6	-7.5	-7.4	11.3	70.3	10.3	69.2	0.2	60.0
	Average	-7.5	-7.7	-18.1	-18.0	-17.7	-17.1	-7.8	-8.4	10.7	25.2	10.2	24.3	0.4	15.6

Basis	Pseudo-Potential	Dative Bond		σ						π					
				OHtransOH		OHtransOxo		OHtransTHF		OHtransOH		OHtransOxo		OHtransTHF	
		ΔH	ΔG	ΔH	ΔG	ΔH	ΔG	ΔH	ΔG	ΔH	ΔG	ΔH	ΔG	ΔH	ΔG
	Std Dev	0.2	0.4	0.4	0.5	0.3	0.5	1.9	2.3	0.7	30.0	0.5	29.9	1.6	29.7
M11L	CEP 31G	-6.3	-6.7	-17.7	-18.7	-17.6	-18.1	-5.5	-6.6	11.4	12.0	11.4	11.5	-0.8	-0.1
	CEP 121G	-6.4	-6.2	-17.6	-18.8	-17.5	-18.0	-5.2	-5.9	11.2	12.6	11.2	11.8	-1.2	-0.3
	LANL2DZ	-6.5	-7.1	-17.8	-19.0	-17.4	-17.5	-6.3	-7.4	11.2	11.9	10.8	10.5	-0.2	0.3
	SDDAll	-6.5	-6.5	-18.6	-20.0	-18.0	-17.5	-6.1	-6.8	12.1	13.6	11.5	11.1	-0.5	0.4
	Average	-6.4	-6.6	-17.9	-19.1	-17.6	-17.8	-5.8	-6.7	11.5	12.5	11.2	11.2	-0.7	0.1
	Std Dev	0.1	0.4	0.5	0.6	0.3	0.3	0.5	0.6	0.4	0.8	0.3	0.6	0.4	0.3
MN12L	CEP 31G	-5.8	-5.9	-14.2	-15.0	-14.8	-15.6	-4.5	-5.1	8.4	9.1	9.0	9.7	-1.2	-0.8
	CEP 121G	-5.8	-5.9	-14.1	-15.9	-14.7	-15.1	-4.5	-5.2	8.3	9.9	8.9	9.2	-1.3	-0.7
	LANL2DZ	-6.6	-7.1	-15.4	-16.3	-15.4	-16.1	-6.7	-7.2	8.8	9.2	8.8	9.0	0.1	0.1
	SDDAll	-6.1	-6.1	-15.5	-16.2	-15.8	-16.0	-5.7	-6.0	9.4	10.1	9.6	9.9	-0.5	-0.2
	Average	-6.1	-6.3	-14.8	-15.9	-15.2	-15.7	-5.4	-5.9	8.7	9.6	9.1	9.4	-0.7	-0.4
	Std Dev	0.4	0.6	0.8	0.6	0.5	0.5	1.1	1.0	0.5	0.5	0.4	0.4	0.7	0.4
N12	CEP 31G	-6.4	-4.6	-19.7	-17.2	-18.8	-14.8	-6.5	-4.3	13.3	12.6	12.4	10.1	0.1	-0.3
	CEP 121G	-5.4	-4.6	-18.3	-16.5	-17.2	-14.3	-5.5	-4.0	12.9	11.9	11.8	9.7	0.1	-0.6
	LANL2DZ	-4.6	-4.6	-16.5	-16.7	-15.5	-14.1	-8.0	-9.4	11.9	12.1	10.9	9.4	3.3	4.7
	SDDAll	-4.5	-4.0	-17.6	-15.9	-16.8	-15.7	-5.1	-4.7	13.1	11.9	12.3	11.7	0.7	0.6
	Average	-5.2	-4.5	-18.0	-16.6	-17.1	-14.7	-6.3	-5.6	12.8	12.1	11.8	10.2	1.0	1.1
	Std Dev	0.9	0.3	1.3	0.5	1.4	0.7	1.3	2.5	0.6	0.3	0.7	1.0	1.6	2.5
SOGGA11	CEP 31G	-14.8	-16.4	-16.2	-16.1	-16.1	-15.8	-5.5	-6.3	1.4	-0.3	1.3	-0.6	-9.3	-10.1
	CEP 121G	-14.7	-16.5	-14.8	-13.4	-14.6	-13.3	-4.3	-4.1	0.0	-3.2	-0.1	-3.2	-10.5	-12.4
	LANL2DZ	-9.3	-9.5	-9.8	-9.8	-9.6	-8.3	0.3	0.6	0.5	0.3	0.3	-1.2	-9.6	-10.1
	SDDAll	-8.6	-8.2	-9.8	5.8	-8.6	6.6	1.5	17.0	1.1	-0.8	0.0	-1.6	-10.1	-12.0
	Average	-11.9	-12.7	-12.6	-8.4	-12.3	-7.7	-2.0	1.8	0.8	-1.0	0.4	-1.7	-9.9	-11.2

Basis	Pseudo-Potential	Dative Bond		σ						π					
				OHtransOH		OHtransOxo		OHtransTHF		OHtransOH		OHtransOxo		OHtransTHF	
		ΔH	ΔG	ΔH	ΔG	ΔH	ΔG	ΔH	ΔG	ΔH	ΔG	ΔH	ΔG	ΔH	ΔG
	Std Dev	3.4	4.4	3.4	9.8	3.7	10.1	3.4	10.5	0.6	1.5	0.7	1.1	0.5	1.2
B2LYP	CEP 31G	-7.1	-7.0	-20.4	-20.4	-19.9	-19.3	-6.5	-7.3	13.3	13.4	12.8	12.3	-0.6	0.3
	CEP 121G	-7.2	-7.2	-20.1	-20.2	-19.7	-19.3	-6.6	-8.1	12.9	13.0	12.5	12.1	-0.6	0.9
	LANL2DZ	-7.7	-7.7	-20.2	-20.2	-19.6	-19.1	-7.6	-8.6	12.5	12.5	11.9	11.4	-0.1	0.8
	SDDAll	-7.3	-7.2	-20.8	-20.1	-19.5	-18.7	-7.5	-8.1	13.5	12.9	12.2	11.5	0.2	0.9
	Average	-7.3	-7.3	-20.4	-20.2	-19.7	-19.1	-7.0	-8.0	13.0	13.0	12.4	11.8	-0.3	0.7
	Std Dev	0.3	0.3	0.3	0.1	0.2	0.3	0.6	0.5	0.4	0.4	0.4	0.5	0.4	0.3
MP2	CEP 31G	-7.3	-7.3	-20.2	-20.8	-20.0	-20.0	-5.8	-7.7	12.8	13.5	12.7	12.7	-1.5	0.4
	CEP 121G	-7.4	-7.4	-19.8	-20.6	-20.0	-19.9	-7.0	-7.5	12.4	13.2	12.6	12.6	-0.3	0.2
	LANL2DZ	-7.9	-8.1	-20.1	-20.7	-19.7	-19.7	-7.3	-8.6	12.2	12.7	11.8	11.6	-0.6	0.5
	SDDAll	-7.6	-7.5	-20.3	-20.5	-19.4	-19.2	-7.3	-8.3	12.7	13.0	11.8	11.7	-0.3	0.8
	Average	-7.6	-7.6	-20.1	-20.7	-19.8	-19.7	-6.9	-8.0	12.5	13.1	12.2	12.1	-0.7	0.5
	Std Dev	0.3	0.3	0.2	0.1	0.3	0.4	0.7	0.5	0.3	0.4	0.5	0.6	0.6	0.3
Overall Averages	CEP 31G	-7.7	-7.8	-18.3	-18.1	-18.1	-17.4	-6.3	-6.6	10.6	10.2	10.4	9.6	-1.4	-1.2
	CEP 121G	-7.1	-7.2	-17.2	-16.8	-17.0	-16.1	-5.5	-5.5	10.1	9.7	9.9	9.0	-1.6	-1.6
	LANL2DZ	-7.4	-7.7	-17.0	-17.1	-16.8	-16.2	-7.7	-8.4	9.7	9.4	9.4	8.5	0.4	0.7
	SDDAll	-6.9	-7.0	-17.7	-15.9	-17.1	-15.1	-6.3	-5.2	10.8	16.2	10.2	16.4	-0.6	5.5
	Average	-7.3	-7.4	-17.5	-17.0	-17.2	-16.2	-6.5	-6.4	10.3	11.4	10.0	10.8	-0.8	0.8
	Std Dev	1.9	2.3	2.5	4.1	2.4	4.1	2.3	4.3	3.3	9.4	3.2	9.5	3.0	9.4

Table A.2.3-5: Difference between the calculated bond dissociation enthalpies in kcal/mol for the trans-Cotton complex and cis-Cotton complex with water as the dative ligand by functional and valence basis set.

Basis	Pseudo-Potential	Dative Bond		σ						π					
				OHtransOH		OHtransOxo		OHtransTHF		OHtransOH		OHtransOxo		OHtransTHF	
		ΔH	ΔG	ΔH	ΔG	ΔH	ΔG	ΔH	ΔG	ΔH	ΔG	ΔH	ΔG	ΔH	ΔG
BP 86	CEP 31G	-6.8	-7.0	-6.4	-7.0	-18.8	-5.4	-6.8	-87.1	17.4	0.0	7.8	7.4	0.0	0.0
	CEP 121G	-6.9	-7.1	-6.4	-6.9	-19.1	-5.7	-6.9	-87.2	18.3	-0.2	7.6	7.1	0.0	0.0
	LANL2DZ	-6.9	-7.2	-5.9	-6.3	-19.8	-6.3	-6.9	-91.7	18.0	-0.9	6.6	6.1	0.0	0.0
	SDDAll	-7.3	-7.6	-7.1	-7.6	-18.7	-5.4	-7.2	-89.5	16.9	0.0	7.2	6.6	0.0	0.0
	Average	-6.9	-7.2	-6.5	-6.9	-19.1	-5.7	-7.0	-88.9	17.6	-0.3	7.3	6.8	0.0	0.0
	Std Dev	0.2	0.2	0.5	0.5	0.5	0.4	0.2	2.2	0.6	0.4	0.5	0.6	0.0	0.0
B3LYP	CEP 31G	-7.5	-7.8	-8.2	-8.8	-17.8	-4.3	-7.5	-78.2	16.6	1.0	9.2	8.5	0.0	0.0
	CEP 121G	-7.5	-7.9	-8.1	-8.6	-18.2	-4.5	-7.5	-78.4	17.8	0.7	9.0	8.2	0.0	0.0
	LANL2DZ	-7.6	-7.9	-7.5	-8.0	-19.4	-5.7	-7.6	-83.2	17.6	0.1	8.2	7.6	0.0	0.0
	SDDAll	-7.9	-8.3	-8.7	-9.4	-18.3	-4.9	-7.9	-80.9	16.9	1.1	8.6	17.7	0.0	-0.1
	Average	-7.6	-8.0	-8.1	-8.7	-18.4	-4.9	-7.6	-80.2	17.2	0.7	8.8	10.5	0.0	0.0
	Std Dev	0.2	0.2	0.5	0.6	0.7	0.7	0.2	2.4	0.5	0.4	0.5	4.8	0.0	0.1
M06	CEP 31G	-8.3	-8.5	-8.6	-8.8	-35.7	-21.9	-8.5	-84.5	28.9	0.3	9.2	8.5	0.2	0.3
	CEP 121G	-8.4	-8.7	-8.5	-8.9	-36.2	-22.6	-8.4	-84.5	30.0	0.1	9.2	8.5	0.0	-0.2
	LANL2DZ	-8.3	-8.5	-8.1	-8.7	-31.6	-18.1	-8.6	-86.0	25.4	0.2	8.5	7.9	0.3	1.0
	SDDAll	-8.6	-8.7	-9.1	-9.4	-32.8	-18.8	-8.5	-84.8	25.5	0.7	8.8	8.1	-0.1	-0.2
	Average	-8.4	-8.6	-8.5	-8.9	-34.1	-20.3	-8.5	-85.0	27.4	0.3	8.9	8.2	0.1	0.2
	Std Dev	0.1	0.1	0.4	0.3	2.2	2.2	0.1	0.7	2.3	0.3	0.4	0.3	0.2	0.5
BLYP	CEP 31G	-6.7	-7.0	-6.7	-7.3	-17.7	-4.3	-6.7	-84.0	14.1	0.3	7.5	7.0	0.0	0.0
	CEP 121G	-6.8	-7.2	-6.8	-7.4	-18.2	-4.9	-6.8	-84.1	15.1	0.2	7.3	6.8	0.0	-0.2
	LANL2DZ	-6.8	-7.1	-6.0	-6.4	-18.3	-4.9	-6.8	-89.2	14.9	-0.7	6.2	5.7	0.0	0.0
	SDDAll	-7.2	-7.6	-7.5	-8.0	-17.8	-4.4	-7.2	-85.9	12.9	0.4	6.9	6.2	0.0	-0.1

Basis	Pseudo-Potential	Dative Bond		σ						π					
				OHtransOH		OHtransOxo		OHtransTHF		OHtransOH		OHtransOxo		OHtransTHF	
		ΔH	ΔG	ΔH	ΔG	ΔH	ΔG	ΔH	ΔG	ΔH	ΔG	ΔH	ΔG	ΔH	ΔG
	Average	-6.9	-7.3	-6.7	-7.3	-18.0	-4.6	-6.9	-85.8	14.2	0.0	7.0	6.4	0.0	-0.1
	Std Dev	0.2	0.3	0.6	0.7	0.3	0.3	0.2	2.5	1.0	0.5	0.6	0.6	0.0	0.1
B97D	CEP 31G	-7.4	-7.8	-7.6	-8.1	-20.7	-7.1	-7.5	-86.4	19.3	0.4	7.8	7.2	0.1	0.2
	CEP 121G	-7.5	-7.9	-7.6	-7.9	-21.1	-7.3	-7.1	-86.4	20.2	0.1	7.6	6.9	-0.4	-0.8
	LANL2DZ	-7.4	-7.8	-6.7	-6.8	-21.2	-7.2	-7.5	-86.4	19.3	-1.0	6.3	5.5	0.0	0.1
	SDDAll	-7.9	-8.1	-8.1	-8.4	-22.1	-8.4	-7.9	-89.2	20.3	0.3	7.3	6.7	0.0	0.0
	Average	-7.6	-7.9	-7.5	-7.8	-21.3	-7.5	-7.5	-87.1	19.8	-0.1	7.2	6.6	-0.1	-0.1
	Std Dev	0.2	0.2	0.6	0.7	0.6	0.6	0.3	1.4	0.6	0.6	0.7	0.8	0.2	0.5
PBEPBE	CEP 31G	-6.8	-7.0	-6.5	-7.0	-20.1	-6.6	-6.8	-87.2	19.8	0.0	7.7	7.3	0.0	0.0
	CEP 121G	-6.9	-7.2	-6.5	-7.0	-20.4	-6.9	-6.9	-87.4	20.9	-0.2	7.5	7.1	0.0	0.0
	LANL2DZ	-7.0	-7.3	-5.9	-6.3	-20.9	-7.4	-7.0	-91.6	20.0	-1.0	6.4	6.0	0.0	0.0
	SDDAll	-7.3	-7.6	-7.1	-7.6	-19.8	-6.4	-7.3	-89.1	19.3	68.9	7.1	75.5	0.0	68.9
	Average	-7.0	-7.3	-6.5	-6.9	-20.3	-6.8	-7.0	-88.8	20.0	16.9	7.2	24.0	0.0	17.2
	Std Dev	0.2	0.2	0.5	0.5	0.5	0.4	0.2	2.0	0.7	34.7	0.6	34.4	0.0	34.5
M11L	CEP 31G	-7.0	-7.1	-6.5	-7.5	1.3	14.5	-7.1	-78.6	13.4	0.4	8.6	8.5	0.1	0.1
	CEP 121G	-6.8	-6.7	-6.3	-6.9	-4.4	9.0	-6.2	-79.2	17.8	0.2	8.8	8.7	-0.6	0.1
	LANL2DZ	-7.0	-7.1	-5.7	-6.2	-31.7	-18.1	-7.3	-86.1	29.5	-1.0	-1.3	-1.0	0.2	0.1
	SDDAll	-7.1	-7.1	-6.8	-7.6	8.3	21.5	-7.2	-80.1	10.7	0.5	8.7	8.8	0.0	0.0
	Average	-7.0	-7.0	-6.3	-7.0	-6.6	6.7	-6.9	-81.0	17.9	0.0	6.2	6.3	-0.1	0.1
	Std Dev	0.1	0.2	0.4	0.6	17.5	17.4	0.5	3.5	8.3	0.7	5.0	4.8	0.4	0.0
MN12L	CEP 31G	-6.8	-7.1	-4.9	-5.3	-13.3	21.8	-6.8	-75.6	12.2	-1.8	6.4	6.1	0.0	-0.3
	CEP 121G	-6.7	-6.8	-4.7	-5.0	-19.7	-6.3	-6.7	-75.9	16.5	-1.7	6.5	6.3	0.0	0.2
	LANL2DZ	-7.2	-7.4	-4.3	-4.8	-41.1	-27.8	-7.3	-86.4	28.7	-2.5	5.3	5.2	0.1	0.0
	SDDAll	-6.9	-7.1	-5.5	-6.1	-8.5	4.9	-6.8	-78.2	10.1	-1.1	6.8	6.6	0.0	-0.2

Basis	Pseudo-Potential	Dative Bond		σ						π					
				OHtransOH		OHtransOxo		OHtransTHF		OHtransOH		OHtransOxo		OHtransTHF	
		ΔH	ΔG	ΔH	ΔG	ΔH	ΔG	ΔH	ΔG	ΔH	ΔG	ΔH	ΔG	ΔH	ΔG
	Average	-6.9	-7.1	-4.9	-5.3	-20.7	-1.8	-6.9	-79.0	16.9	-1.8	6.3	6.0	0.0	-0.1
	Std Dev	0.2	0.2	0.5	0.5	14.4	20.8	0.3	5.1	8.3	0.6	0.6	0.6	0.0	0.2
N12	CEP 31G	-6.8	-7.1	-7.5	-8.5	-26.5	-13.3	-7.0	-90.7	18.5	1.5	8.7	8.4	0.1	0.2
N12	CEP 121G	-6.8	-6.8	-7.4	-8.5	-27.0	-13.6	-6.7	-90.3	19.6	1.6	8.6	8.6	-0.1	0.0
N12	LANL2DZ	-7.1	-7.3	-6.3	-6.1	-35.9	-21.8	-6.8	-92.7	25.6	-1.2	6.8	5.8	-0.3	-1.1
N12	SDDAll	-7.4	-7.2	-8.3	-8.9	-25.5	-12.5	-7.5	-93.3	17.4	1.7	8.2	8.1	0.1	0.2
N12	Average	-7.0	-7.1	-7.4	-8.0	-28.7	-15.3	-7.0	-91.7	20.3	0.9	8.1	7.7	-0.1	-0.2
N12	Std Dev	0.3	0.2	0.8	1.3	4.8	4.4	0.4	1.5	3.7	1.4	0.9	1.3	0.2	0.6
SOGGA11	CEP 31G	-6.9	-7.6	-7.6	-7.7	-19.4	-5.0	-7.0	-94.0	10.7	0.1	7.1	5.5	0.1	0.2
SOGGA11	CEP 121G	-7.1	-7.9	-7.4	-7.5	-18.9	-4.3	-5.2	-94.2	10.3	-0.4	6.6	4.9	-1.8	-3.3
SOGGA11	LANL2DZ	-7.3	-7.7	-7.2	-6.6	-26.7	-11.5	-7.2	-97.5	14.9	-1.2	6.2	4.1	-0.1	-0.6
SOGGA11	SDDAll	-7.7	-7.8	-7.2	11.5	-16.0	17.0	-7.8	-74.7	11.2	-1.2	5.8	4.2	0.0	-0.1
SOGGA11	Average	-7.2	-7.7	-7.4	-2.6	-20.3	-1.0	-6.8	-90.1	11.8	-0.6	6.4	4.7	-0.5	-1.0
SOGGA11	Std Dev	0.4	0.1	0.2	9.4	4.5	12.4	1.1	10.4	2.1	0.6	0.5	0.6	0.9	1.6
B2LYP	CEP 31G	-7.5	-7.6	-7.5	-8.0	-25.0	-11.4	-7.5	-81.3	18.0	0.4	9.0	8.4	0.0	0.1
B2LYP	CEP 121G	-7.5	-7.7	-7.3	-7.9	-25.7	-12.2	-7.5	-82.3	19.5	0.3	8.9	8.3	0.0	0.1
B2LYP	LANL2DZ	-7.6	-7.8	-6.9	-7.4	-26.9	-13.3	-7.6	-86.1	19.0	-0.4	8.1	7.5	0.0	0.0
B2LYP	SDDAll	-7.8	-8.0	-7.7	-8.4	-26.1	-12.8	-7.8	-85.1	18.8	0.4	8.4	7.8	0.0	0.1
B2LYP	Average	-7.6	-7.8	-7.4	-7.9	-25.9	-12.4	-7.6	-83.7	18.8	0.1	8.6	8.0	0.0	0.1
B2LYP	Std Dev	0.2	0.2	0.4	0.4	0.8	0.8	0.2	2.3	0.6	0.4	0.4	0.4	0.0	0.0
MP2	CEP 31G	-7.7	-7.6	-7.6	-8.0	-45.2	-31.8	-7.7	-96.0	26.0	0.4	9.4	8.8	0.0	0.1
MP2	CEP 121G	-7.8	-7.7	-7.1	-7.7	-46.7	-33.4	-7.8	-97.8	27.8	0.0	9.1	8.6	0.0	0.1
MP2	LANL2DZ	-8.0	-8.1	-6.9	-7.3	-46.5	-33.1	-8.0	-99.5	25.7	-0.8	8.2	7.6	0.0	-0.1
MP2	SDDAll	-8.0	-8.0	-7.1	-7.6	-45.5	-32.3	-8.1	-100.2	25.9	-0.4	8.4	7.8	0.0	0.1

Basis	Pseudo-Potential	Dative Bond		σ						π					
				OHtransOH		OHtransOxo		OHtransTHF		OHtransOH		OHtransOxo		OHtransTHF	
		ΔH	ΔG	ΔH	ΔG	ΔH	ΔG	ΔH	ΔG	ΔH	ΔG	ΔH	ΔG	ΔH	ΔG
	Average	-7.9	-7.9	-7.2	-7.6	-46.0	-32.6	-7.9	-98.4	26.4	-0.2	8.8	8.2	0.0	0.1
	Std Dev	0.2	0.2	0.3	0.3	0.8	0.7	0.2	1.9	1.0	0.5	0.6	0.6	0.0	0.1
Overall Averages	CEP 31G	-7.1	-7.4	-7.0	-7.6	-18.9	-3.2	-7.2	-84.6	17.1	0.2	8.0	7.4	0.1	0.1
	CEP 121G	-7.1	-7.4	-7.0	-7.5	-20.3	-6.7	-6.8	-84.8	18.7	0.0	7.9	7.3	-0.3	-0.4
	LANL2DZ	-7.3	-7.5	-6.4	-6.6	-26.7	-12.9	-7.3	-89.1	21.4	-0.9	5.9	5.3	0.0	-0.1
	SDDAll	-7.5	-7.7	-7.5	-6.1	-17.1	-1.7	-7.5	-84.6	16.1	7.1	7.6	14.8	0.0	6.9
	Average	-7.3	-7.5	-7.0	-7.0	-20.7	-6.1	-7.2	-85.8	18.3	1.6	7.3	8.7	0.0	1.6
	Std Dev	0.5	0.5	1.0	2.9	11.2	12.5	0.6	6.3	5.4	10.0	1.7	10.1	0.3	10.0

A.3 Geometry Optimization Statistics

A.3.1 Geometry Optimization Bond Length and Angles Comparison Statistics Beaumier WN Model

Table A.3.1: Comparison of optimized geometries to average bond lengths and angles in the Cambridge Crystallographic Database and the reference chromium anion crystal structure by functional and valence basis set.

DFT Functional	Valence Basis Set	Beaumier Bond Lengths				Beaumier Bond Angles			
		Database		Article		Database		Article	
		% Error	% Abs Err	% Error	% Abs Err	% Error	% Abs Err	% Error	% Abs Err
BP 86	CEP 31G	-1.1	6.0	8.6	8.6	-1.1	5.6	8.6	2.1
	CEP-121g	-1.5	5.9	6.4	6.4	0.2	10.2	0.6	4.6
	LANL2DZ	-0.7	5.8	7.3	7.3	0.2	10.2	0.6	5.0
	SDDAll	-1.0	5.9	6.9	6.9	0.2	10.1	0.5	4.6
	Average	-1.1	5.9	7.3	7.3	-0.1	9.0	2.6	4.1
	Std Dev	0.3	0.1	0.9	0.9	0.7	2.3	4.0	1.3
B3LYP	CEP 31G	-1.4	6.0	8.3	8.3	0.2	10.1	0.6	4.9
	CEP-121g	-1.8	5.9	6.1	6.1	0.2	10.1	0.6	5.0
	LANL2DZ	-0.9	5.8	7.0	7.0	0.2	10.1	0.5	5.2
	SDDAll	-1.3	5.9	6.6	6.6	0.2	10.1	0.5	5.0
	Average	-1.3	5.9	7.0	7.0	0.2	10.1	0.5	5.0
	Std Dev	0.4	0.1	1.0	1.0	0.0	0.0	0.0	0.2
M06	CEP 31G	-1.7	6.2	8.0	8.0	0.2	9.9	0.5	3.8
	CEP-121g	-2.2	6.2	5.6	5.6	0.2	9.8	0.4	4.0
	LANL2DZ	-1.4	6.2	6.4	6.4	0.2	10.1	0.5	4.0
	SDDAll	-1.7	6.1	6.2	6.2	0.2	9.9	0.6	3.8
	Average	-1.8	6.2	6.5	6.5	0.2	9.9	0.5	3.9
	Std Dev	0.3	0.0	1.0	1.0	0.0	0.1	0.1	0.1
BLYP	CEP 31G	-0.6	5.9	9.3	9.3	0.2	10.1	0.6	4.5
	CEP-121g	-0.9	5.8	7.1	7.1	0.2	10.2	0.7	4.5
	LANL2DZ	0.0	6.1	8.0	8.0	0.2	10.2	0.6	5.1
	SDDAll	-0.4	5.8	7.6	7.6	0.2	10.1	0.6	4.7
	Average	-0.5	5.9	8.0	8.0	0.2	10.1	0.6	4.7
	Std Dev	0.4	0.1	0.9	0.9	0.0	0.1	0.0	0.3
PBEPBE	CEP 31G	-1.3	6.0	8.4	8.4	0.2	9.9	0.6	4.5
	CEP-121g	-1.6	5.9	6.3	6.3	0.2	10.0	0.6	4.5
	LANL2DZ	-0.9	5.8	7.1	7.1	0.2	10.1	0.6	4.8
	SDDAll	-1.2	5.9	6.7	6.7	0.2	10.0	0.6	4.5

DFT Functional	Valence Basis Set	Beaumier Bond Lengths				Beaumier Bond Angles			
		Database		Article		Database		Article	
		% Error	% Abs Err	% Error	% Abs Err	% Error	% Abs Err	% Error	% Abs Err
	Average	-1.2	5.9	7.1	7.1	0.2	10.0	0.6	4.6
	Std Dev	0.3	0.1	0.9	0.9	0.0	0.1	0.0	0.2
B97D	CEP 31G	-1.6	6.1	8.1	8.1	0.3	9.8	0.9	3.5
	CEP-121g	-1.9	6.2	6.0	6.0	0.3	9.7	0.9	3.6
	LANL2DZ	-1.2	6.0	6.7	6.7	0.3	10.0	1.0	3.7
	SDDAll	-1.6	6.1	6.3	6.3	0.3	9.8	0.9	3.5
	Average	-1.6	6.1	6.8	6.8	0.3	9.8	0.9	3.6
	Std Dev	0.3	0.1	0.9	0.9	0.0	0.1	0.0	0.1
M111	CEP 31G	-2.4	6.0	7.2	7.2	0.2	10.2	0.7	4.4
	CEP-121g	-2.7	6.0	5.0	5.0	0.2	10.3	0.6	4.7
	LANL2DZ	-2.0	5.9	5.8	5.8	0.2	10.3	0.7	4.4
	SDDAll	-2.3	6.0	5.5	5.5	0.2	10.2	0.6	4.4
	Average	-2.3	6.0	5.9	5.9	0.2	10.3	0.6	4.5
	Std Dev	0.3	0.0	1.0	1.0	0.0	0.1	0.0	0.1
MN12L	CEP 31G	-1.3	6.5	8.5	8.5	0.2	9.4	0.1	2.9
	CEP-121g	-2.3	6.3	5.6	5.6	0.2	9.3	0.2	3.2
	LANL2DZ	-1.0	6.5	7.0	7.0	0.2	9.4	0.1	2.8
	SDDAll	-1.2	6.4	6.7	6.7	0.2	9.4	0.1	2.8
	Average	-1.4	6.4	6.9	6.9	0.2	9.4	0.1	2.9
	Std Dev	0.6	0.1	1.2	1.2	0.0	0.0	0.1	0.2
N12	CEP 31G	-2.1	6.0	7.6	7.6	0.2	10.0	0.6	4.7
	CEP-121g	-2.5	5.9	5.3	5.3	0.2	10.1	0.6	4.8
	LANL2DZ	-1.6	5.8	6.3	6.3	0.1	10.2	0.6	5.2
	SDDAll	-2.0	5.9	5.9	5.9	0.2	10.1	0.6	4.9
	Average	-2.1	5.9	6.3	6.3	0.2	10.1	0.6	4.9
	Std Dev	0.4	0.1	1.0	1.0	0.0	0.1	0.0	0.2
SOGGA11	CEP 31G	-1.6	5.7	8.1	8.1	0.2	9.5	0.9	5.5
	CEP-121g	-2.3	5.7	5.6	5.6	0.2	9.6	0.9	5.2
	LANL2DZ	-1.1	5.4	6.8	6.8	0.1	9.5	0.8	6.0
	SDDAll	-1.5	5.5	6.5	6.5	0.2	9.4	0.6	5.3
	Average	-1.6	5.6	6.7	6.7	0.2	9.5	0.8	5.5
	Std Dev	0.5	0.1	1.0	1.0	0.1	0.1	0.1	0.4
	CEP 31G	-1.0	1.0	8.7	8.7	0.3	10.9	1.1	4.7
	CEP-121g	-1.4	1.4	3.2	11.8	0.2	9.6	0.2	9.6
	LANL2DZ	-0.6	0.6	7.3	7.3	0.3	10.8	0.9	4.8

DFT Functional	Valence Basis Set	Beaumier Bond Lengths				Beaumier Bond Angles			
		Database		Article		Database		Article	
		% Error	% Abs Err	% Error	% Abs Err	% Error	% Abs Err	% Error	% Abs Err
B2PLYP	SDDAll	-0.9	0.9	6.9	6.9	0.4	10.7	1.0	4.7
	Average	-1.0	1.0	6.5	8.7	0.3	10.5	0.8	6.0
	Std Dev	0.3	0.3	2.4	2.2	0.1	0.6	0.4	2.4
MP2	CEP 31G								
	LANL2DZ								
	SDDAll								
	CEP-121g								
	Average								
	Std Dev								
Overall Averages	CEP 31G	-1.5	5.6	8.2	8.2	0.1	9.6	1.4	4.1
	CEP-121g	-1.9	5.6	5.6	6.4	0.2	9.9	0.6	4.9
	LANL2DZ	-1.0	5.4	6.9	6.9	0.2	10.1	0.6	4.7
	SDDAll	-1.4	5.5	6.5	6.5	0.2	10.0	0.6	4.4
	Average	-1.4	5.5	6.8	7.0	0.2	9.9	0.8	4.5
	Std Dev	27.5	26.4	29.9	26.0	32.5	8.6	6.3	2.9

A.3.2 Geometry Optimization Bond Length and Angles Comparison Statistics Cotton WO Model

Table A.3.2: Comparison of optimized geometries to the reference crystal structure by functional and valence basis set.

Basis	Pseudo-potential	Cotton Bond Lengths		Cotton Bond Angles	
		% Error	% Abs Err	% Error	% Abs Err
BP 86	CEP 31G	1.9	2.6	-5.5	5.7
	CEP-121g	1.9	2.6	-5.4	5.7
	LANL2DZ	1.7	2.4	-5.1	5.6
	SDDAll	2.1	2.6	-4.8	5.4
	Average	1.9	2.6	-5.2	5.6
	Std Dev	0.2	0.1	0.3	0.2
B3LYP	CEP 31G	1.4	2.4	-5.3	5.3
	CEP-121g	1.5	2.4	-5.1	5.4
	LANL2DZ	1.1	2.1	-4.8	5.1
	SDDAll	1.7	2.5	-4.6	5.0
	Average	1.4	2.3	-5.0	5.2
	Std Dev	0.3	0.1	0.3	0.2

Basis	Pseudo-potential	Cotton Bond Lengths		Cotton Bond Angles	
		% Error	% Abs Err	% Error	% Abs Err
M06	CEP 31G	0.9	1.9	-5.8	6.0
	CEP-121g	0.8	1.9	-5.7	6.0
	LANL2DZ	0.3	1.6	-5.5	5.7
	SDDAll	0.9	1.8	-5.4	5.7
	Average	0.7	1.8	-5.6	5.8
	Std Dev	0.3	0.2	0.2	0.2
BLYP	CEP 31G	2.7	3.3	-5.4	5.4
	CEP-121g	2.8	3.4	-5.2	5.5
	LANL2DZ	2.5	3.2	-4.9	5.4
	SDDAll	3.1	3.5	-4.7	5.0
	Average	2.8	3.3	-5.1	5.3
	Std Dev	0.2	0.1	0.3	0.2
B97D	CEP 31G	1.8	2.6	-5.7	5.9
	CEP-121g	1.8	2.7	-5.5	5.9
	LANL2DZ	1.7	2.4	-5.2	5.7
	SDDAll	2.1	2.7	-5.0	5.5
	Average	1.9	2.6	-5.3	5.7
	Std Dev	0.2	0.1	0.3	0.2
PBEPBE	CEP 31G	1.9	2.6	-4.7	5.8
	CEP-121g	1.9	2.6	-5.5	5.8
	LANL2DZ	1.7	2.6	-5.3	5.7
	SDDAll	1.9	2.5	-5.0	5.4
	Average	1.8	2.6	-5.1	5.7
	Std Dev	0.1	0.0	0.3	0.2
M11	CEP 31G	-0.9	1.8	-3.5	5.6
	CEP-121g	-0.8	0.9	-4.9	5.0
	LANL2DZ	-1.4	1.4	-4.7	5.5
	SDDAll	-0.9	1.3	-4.2	5.4
	Average	-1.0	1.3	-4.3	5.4
	Std Dev	0.3	0.3	0.6	0.2
MN12L	CEP 31G	2.1	2.8	-5.8	7.1
	CEP-121g	1.5	2.2	-6.6	6.7
	LANL2DZ	-0.2	1.0	-5.3	5.8
	SDDAll	2.1	2.1	-5.9	6.7
	Average	1.4	2.0	-5.9	6.6
	Std Dev	1.1	0.8	0.5	0.5

Basis	Pseudo-potential	Cotton Bond Lengths		Cotton Bond Angles	
		% Error	% Abs Err	% Error	% Abs Err
N12	CEP 31G	0.8	1.7	-5.2	5.4
	CEP-121g	0.8	1.8	-5.1	5.5
	LANL2DZ	0.2	1.5	-4.6	5.1
	SDDAll	1.1	1.8	-4.6	5.2
	Average	0.7	1.7	-4.9	5.3
	Std Dev	0.4	0.2	0.3	0.2
SOGGA11	CEP 31G	1.6	2.5	-4.7	4.6
	CEP-121g	1.6	2.5	-4.4	4.9
	LANL2DZ	0.8	1.9	-4.0	4.2
	SDDAll	1.5	2.3	-3.5	4.0
	Average	1.4	2.3	-4.2	4.4
	Std Dev	0.4	0.3	0.5	0.4
B2PLYP	CEP 31G	1.5	2.1	-5.6	5.7
	CEP-121g	1.4	2.1	-5.6	5.7
	LANL2DZ	1.1	1.8	-5.4	5.4
	SDDAll	1.8	2.2	-5.1	5.3
	Average	1.4	2.1	-5.4	5.6
	Std Dev	0.3	0.2	0.2	0.2
MP2	CEP 31G	1.6	2.0	-5.8	6.2
	LANL2DZ	1.5	2.0	-5.9	6.1
	SDDAll	1.1	1.6	-5.4	5.7
	CEP-121g	1.8	2.0	-5.5	5.7
	Average	1.5	1.9	-5.6	5.9
	Std Dev	0.3	0.2	0.3	0.3
Overall Averages	CEP 31G	-5.5	5.7	-5.5	5.7
	CEP-121g	-5.4	5.7	-5.4	5.7
	LANL2DZ	-5.1	5.6	-5.1	5.6
	SDDAll	-4.8	5.4	-4.8	5.4
	Average	-5.2	5.6	-5.2	5.6
	Std Dev	1.0	0.6	0.6	0.6

A.3.3 Geometry Optimization Bond Length Comparison Statistics

Table A.3.3: Bond length comparison of optimized geometries to the reference crystal structures by functional and valence basis set for tungsten-element bonds (elements = carbon, nitrogen, and oxygen).

Basis	Pseudo-potential	Churchill – C Bond Lengths		Beaumier – N Bond Lengths		Cotton – O Bond Lengths		Average Bond Lengths	
		% Error	% Abs Err	% Error	% Abs Err	% Error	% Abs Err	% Error	% Abs Err
BP 86	CEP 31G	0.8	1.5	8.6	8.6	1.9	2.6	3.8	4.2
	CEP-121g	0.8	1.5	6.4	6.4	1.9	2.6	3.1	3.5
	LANL2DZ	0.7	1.5	7.3	7.3	1.7	2.4	3.2	3.7
	SDDAll	1.2	1.7	6.9	6.9	2.1	2.6	3.4	3.7
	Average	0.9	1.6	7.3	7.3	1.9	2.6	3.4	3.8
	Std Dev	0.2	0.1	0.9	0.9	0.2	0.1	3.0	2.7
B3LYP	CEP 31G	1.2	1.7	8.3	8.3	1.4	2.4	3.7	4.1
	CEP-121g	1.2	1.7	6.1	6.1	1.5	2.4	2.9	3.4
	LANL2DZ	1.0	1.8	7.0	7.0	1.1	2.1	3.0	3.7
	SDDAll	1.6	2.0	6.6	6.6	1.7	2.5	3.3	3.7
	Average	1.3	1.8	7.0	7.0	1.4	2.3	3.2	3.7
	Std Dev	0.2	0.1	1.0	1.0	0.3	0.1	2.8	2.5
M06	CEP 31G	0.6	1.3	8.0	8.0	0.9	1.9	3.2	3.7
	CEP-121g	0.6	1.3	5.6	5.6	0.8	1.9	2.3	2.9
	LANL2DZ	0.3	1.3	6.4	6.4	0.3	1.6	2.4	3.1
	SDDAll	0.9	1.5	6.2	6.2	0.9	1.8	2.7	3.2
	Average	0.6	1.4	6.5	6.5	0.7	1.8	2.6	3.2
	Std Dev	0.2	0.1	1.0	1.0	0.3	0.2	2.9	2.5
BLYP	CEP 31G	2.0	2.3	9.3	9.3	2.7	3.3	4.7	4.9
	CEP-121g	2.0	2.3	7.1	7.1	2.8	3.4	3.9	4.2
	LANL2DZ	1.8	2.4	8.0	8.0	2.5	3.2	4.1	4.5
	SDDAll	2.4	2.5	7.6	7.6	3.1	3.5	4.4	4.5
	Average	2.0	2.4	8.0	8.0	2.8	3.3	4.3	4.6
	Std Dev	0.3	0.1	0.9	0.9	0.2	0.1	2.8	2.6
B97D	CEP 31G	0.5	1.0	8.4	8.4	1.8	2.6	3.6	4.0
	CEP-121g	0.5	1.0	6.3	6.3	1.8	2.7	2.9	3.3
	LANL2DZ	0.4	1.0	7.1	7.1	1.7	2.4	3.1	3.5
	SDDAll	0.9	1.2	6.7	6.7	2.1	2.7	3.2	3.5
	Average	0.6	1.0	7.1	7.1	1.9	2.6	3.2	3.6
	Std Dev	0.2	0.1	0.9	0.9	0.2	0.1	3.0	2.8
	CEP 31G	0.6	1.3	8.1	8.1	1.9	2.6	3.5	4.0
	CEP-121g	0.6	1.3	6.0	6.0	1.9	2.6	2.8	3.3

Basis	Pseudo-potential	Churchill – C Bond Lengths		Beaumier – N Bond Lengths		Cotton – O Bond Lengths		Average Bond Lengths	
		% Error	% Abs Err	% Error	% Abs Err	% Error	% Abs Err	% Error	% Abs Err
PBEPBE	LANL2DZ	0.4	1.3	6.7	6.7	1.7	2.6	2.9	3.5
	SDDAll	0.9	1.5	6.3	6.3	1.9	2.5	3.0	3.5
	Average	0.6	1.4	6.8	6.8	1.8	2.6	3.1	3.6
	Std Dev	0.2	0.1	0.9	0.9	0.1	0.0	2.8	2.5
M11	CEP 31G	0.1	1.4	7.2	7.2	-0.9	1.8	2.2	3.5
	CEP-121g	0.1	1.4	5.0	5.0	-0.8	0.9	1.5	2.5
	LANL2DZ	-0.2	1.5	5.8	5.8	-1.4	1.4	1.4	2.9
	SDDAll	0.4	1.7	5.5	5.5	-0.9	1.3	1.7	2.8
	Average	0.1	1.5	5.9	5.9	-1.0	1.3	1.7	2.9
	Std Dev	0.2	0.1	1.0	1.0	0.3	0.3	3.2	2.3
MN12L	CEP 31G	0.8	1.5	8.5	8.5	2.1	2.8	3.8	4.2
	CEP-121g	0.8	1.5	5.6	5.6	1.5	2.2	2.6	3.1
	LANL2DZ	0.4	1.5	7.0	7.0	-0.2	1.0	2.4	3.1
	SDDAll	1.0	1.7	6.7	6.7	2.1	2.1	3.3	3.5
	Average	0.8	1.5	6.9	6.9	1.4	2.0	3.0	3.5
	Std Dev	0.3	0.1	1.2	1.2	1.1	0.8	3.0	2.7
N12	CEP 31G	-0.3	1.1	7.6	7.6	0.8	1.7	2.7	3.4
	CEP-121g	-0.3	1.1	5.3	5.3	0.8	1.8	1.9	2.7
	LANL2DZ	-0.5	0.9	6.3	6.3	0.2	1.5	2.0	2.9
	SDDAll	0.1	0.9	5.9	5.9	1.1	1.8	2.4	2.9
	Average	-0.3	1.0	6.3	6.3	0.7	1.7	2.2	3.0
	Std Dev	0.3	0.1	1.0	1.0	0.4	0.2	3.0	2.5
SOGGA11	CEP 31G	0.1	0.9	8.1	8.1	1.6	2.5	3.3	3.8
	CEP-121g	0.1	0.9	5.6	5.6	1.6	2.5	2.4	3.0
	LANL2DZ	-0.3	1.0	6.8	6.8	0.8	1.9	2.5	3.2
	SDDAll	0.6	1.2	6.5	6.5	1.5	2.3	2.9	3.3
	Average	0.1	1.0	6.7	6.7	1.4	2.3	2.7	3.3
	Std Dev	0.3	0.1	1.0	1.0	0.4	0.3	3.1	2.6
B2PLYP	CEP 31G	1.2	1.8	8.7	8.7	1.5	2.1	3.8	4.2
	CEP-121g	1.2	1.8	3.2	11.8	1.4	2.1	1.9	5.2
	LANL2DZ	1.1	1.9	7.3	7.3	1.1	1.8	3.2	3.7
	SDDAll	1.6	2.0	6.9	6.9	1.8	2.2	3.4	3.7
	Average	1.3	1.8	6.5	8.7	1.4	2.1	3.1	4.2
	Std Dev	0.2	0.1	2.4	2.2	0.3	0.2	2.8	3.5
	CEP 31G	0.9	1.5			1.6	2.0	1.2	1.8
	LANL2DZ	0.9	1.5			1.5	2.0	1.2	1.8

Basis	Pseudo-potential	Churchill – C Bond Lengths		Beaumier – N Bond Lengths		Cotton – O Bond Lengths		Average Bond Lengths	
		% Error	% Abs Err	% Error	% Abs Err	% Error	% Abs Err	% Error	% Abs Err
MP2	SDDAll	0.8	1.7			1.1	1.6	0.9	1.7
	CEP-121g	1.0	1.8			1.8	2.0	1.4	1.9
	Average	0.9	1.6			1.5	1.9	1.2	1.8
	Std Dev	0.1	0.1			0.3	0.2	0.4	0.2
Overall Averages	CEP 31G	0.7	1.4	8.2	8.2	-5.5	5.7	1.1	5.1
	CEP-121g	0.7	1.4	5.6	6.4	-5.4	5.7	0.3	4.5
	LANL2DZ	0.5	1.5	6.9	6.9	-5.1	5.6	0.7	4.7
	SDDAll	1.1	1.6	6.5	6.5	-4.8	5.4	0.9	4.5
	Average	0.7	1.5	6.8	7.0	-5.2	5.6	0.8	4.7
	Std Dev	0.6	0.4	29.9	26.0	1.0	0.6	5.2	2.5

A.3.4 Geometry Optimization Bond Angle Comparison Statistics

Table A.3.4: Bond angle comparison of optimized geometries to the reference crystal structures by functional and valence basis set for tungsten-element bonds (elements = carbon, nitrogen, and oxygen).

Basis	Pseudo-potential	Churchill – C Bond Lengths		Beaumier – N Bond Lengths		Cotton – O Bond Lengths		Average Bond Lengths	
		% Error	% Abs Err	% Error	% Abs Err	% Error	% Abs Err	% Error	% Abs Err
BP 86	CEP 31G	0.9	4.1	8.6	2.1	-5.5	5.7	1.3	4.0
	CEP-121g	0.9	4.1	0.6	4.6	-5.4	5.7	-1.3	4.8
	LANL2DZ	0.8	3.9	0.6	5.0	-5.1	5.6	-1.2	4.8
	SDDAll	0.5	3.8	0.5	4.6	-4.8	5.4	-1.3	4.6
	Average	0.8	4.0	2.6	4.1	-5.2	5.6	-0.6	4.5
	Std Dev	0.2	0.1	4.0	1.3	0.3	0.2	4.1	1.0
B3LYP	CEP 31G	0.9	4.1	0.6	4.9	-5.3	5.3	-1.3	4.8
	CEP-121g	0.9	4.1	0.6	5.0	-5.1	5.4	-1.2	4.8
	LANL2DZ	0.8	3.9	0.5	5.2	-4.8	5.1	-1.1	4.8
	SDDAll	0.9	4.3	0.5	5.0	-4.6	5.0	-1.1	4.7
	Average	0.9	4.1	0.5	5.0	-5.0	5.2	-1.2	4.8
	Std Dev	0.0	0.1	0.0	0.2	0.3	0.2	2.8	0.5
M06	CEP 31G	0.6	3.7	0.5	3.8	-5.8	6.0	-1.5	4.5
	CEP-121g	0.6	3.7	0.4	4.0	-5.7	6.0	-1.6	4.6
	LANL2DZ	0.6	3.8	0.5	4.0	-5.5	5.7	-1.4	4.5
	SDDAll	1.1	3.8	0.6	3.8	-5.4	5.7	-1.3	4.4
	Average	0.7	3.7	0.5	3.9	-5.6	5.8	-1.5	4.5

Basis	Pseudo-potential	Churchill – C Bond Lengths		Beaumier – N Bond Lengths		Cotton – O Bond Lengths		Average Bond Lengths	
		% Error	% Abs Err	% Error	% Abs Err	% Error	% Abs Err	% Error	% Abs Err
	Std Dev	0.2	0.0	0.1	0.1	0.2	0.2	3.1	1.0
BLYP	CEP 31G	1.0	4.2	0.6	4.5	-5.4	5.4	-1.3	4.7
	CEP-121g	1.0	4.2	0.7	4.5	-5.2	5.5	-1.2	4.7
	LANL2DZ	0.9	4.1	0.6	5.1	-4.9	5.4	-1.1	4.8
	SDDAll	1.0	4.4	0.6	4.7	-4.7	5.0	-1.0	4.7
	Average	1.0	4.2	0.6	4.7	-5.1	5.3	-1.2	4.8
	Std Dev	0.0	0.1	0.0	0.3	0.3	0.2	2.9	0.5
B97D	CEP 31G	0.9	4.7	0.6	4.5	-5.7	5.9	-1.4	5.0
	CEP-121g	0.9	4.7	0.6	4.5	-5.5	5.9	-1.3	5.0
	LANL2DZ	0.9	4.7	0.6	4.8	-5.2	5.7	-1.2	5.1
	SDDAll	0.9	4.8	0.6	4.5	-5.0	5.5	-1.2	4.9
	Average	0.9	4.7	0.6	4.6	-5.3	5.7	-1.3	5.0
	Std Dev	0.0	0.0	0.0	0.2	0.3	0.2	3.0	0.6
PBEPBE	CEP 31G	0.8	4.1	0.9	3.5	-4.7	5.8	-1.0	4.5
	CEP-121g	0.8	4.1	0.9	3.6	-5.5	5.8	-1.3	4.5
	LANL2DZ	0.8	3.9	1.0	3.7	-5.3	5.7	-1.2	4.5
	SDDAll	0.8	4.3	0.9	3.5	-5.0	5.4	-1.1	4.4
	Average	0.8	4.1	0.9	3.6	-5.1	5.7	-1.1	4.5
	Std Dev	0.0	0.1	0.0	0.1	0.3	0.2	3.0	0.9
M111	CEP 31G	0.7	3.2	0.7	4.4	-3.5	5.6	-0.7	4.4
	CEP-121g	0.7	3.2	0.6	4.7	-4.9	5.0	-1.2	4.3
	LANL2DZ	-0.2	3.3	0.7	4.4	-4.7	5.5	-1.4	4.4
	SDDAll	0.4	3.5	0.6	4.4	-4.2	5.4	-1.1	4.5
	Average	0.4	3.3	0.6	4.5	-4.3	5.4	-1.1	4.4
	Std Dev	0.4	0.2	0.0	0.1	0.6	0.2	2.4	0.9
MN12L	CEP 31G	0.6	4.0	0.1	2.9	-5.8	7.1	-1.7	4.6
	CEP-121g	0.6	4.0	0.2	3.2	-6.6	6.7	-2.0	4.6
	LANL2DZ	0.5	3.8	0.1	2.8	-5.3	5.8	-1.6	4.2
	SDDAll	0.4	4.5	0.1	2.8	-5.9	6.7	-1.8	4.7
	Average	0.5	4.1	0.1	2.9	-5.9	6.6	-1.8	4.5
	Std Dev	0.1	0.3	0.1	0.2	0.5	0.5	3.1	1.6
N12	CEP 31G	0.7	4.1	0.6	4.7	-5.2	5.4	-1.3	4.7
	CEP-121g	0.7	4.1	0.6	4.8	-5.1	5.5	-1.2	4.8
	LANL2DZ	0.7	4.0	0.6	5.2	-4.6	5.1	-1.1	4.8
	SDDAll	0.8	4.2	0.6	4.9	-4.6	5.2	-1.1	4.7
	Average	0.7	4.1	0.6	4.9	-4.9	5.3	-1.2	4.8

Basis	Pseudo-potential	Churchill – C Bond Lengths		Beaumier – N Bond Lengths		Cotton – O Bond Lengths		Average Bond Lengths	
		% Error	% Abs Err	% Error	% Abs Err	% Error	% Abs Err	% Error	% Abs Err
	Std Dev	0.0	0.1	0.0	0.2	0.3	0.2	2.7	0.5
SOGGA11	CEP 31G	0.9	6.2	0.9	5.5	-4.7	4.6	-1.0	5.4
	CEP-121g	0.9	6.2	0.9	5.2	-4.4	4.9	-0.8	5.4
	LANL2DZ	0.7	5.4	0.8	6.0	-4.0	4.2	-0.9	5.2
	SDDAll	0.8	5.8	0.6	5.3	-3.5	4.0	-0.7	5.0
	Average	0.8	5.9	0.8	5.5	-4.2	4.4	-0.8	5.3
	Std Dev	0.1	0.4	0.1	0.4	0.5	0.4	2.5	0.7
B2PLYP	CEP 31G	0.9	4.2	1.1	4.7	-5.6	5.7	-1.2	4.9
	CEP-121g	0.9	4.2	0.2	9.6	-5.6	5.7	-1.5	6.5
	LANL2DZ	0.8	4.1	0.9	4.8	-5.4	5.4	-1.2	4.8
	SDDAll	0.8	4.1	1.0	4.7	-5.1	5.3	-1.1	4.7
	Average	0.8	4.2	0.8	6.0	-5.4	5.6	-1.3	5.2
	Std Dev	0.0	0.0	0.4	2.4	0.2	0.2	3.1	1.5
MP2	CEP 31G	0.7	4.6			-5.8	6.2	-2.6	5.4
	LANL2DZ	0.7	4.6			-5.9	6.1	-2.6	5.4
	SDDAll	0.6	4.6			-5.4	5.7	-2.4	5.1
	CEP-121g	8.6	12.5			-5.5	5.7	1.5	9.1
	Average	2.6	6.6			-5.6	5.9	-1.5	6.3
	Std Dev	3.9	3.9			0.3	0.3	5.1	2.6
Overall Averages	CEP 31G	0.8	4.3	1.4	4.1	-5.5	5.7	-1.1	4.7
	CEP-121g	0.8	4.3	0.6	4.9	-5.4	5.7	-1.3	5.0
	LANL2DZ	0.7	4.1	0.6	4.7	-5.1	5.6	-1.3	4.8
	SDDAll	1.4	5.0	0.6	4.4	-4.8	5.4	-0.9	4.9
	Average	0.9	4.4	0.8	4.5	-5.2	5.6	-1.2	4.8
	Std Dev	1.1	1.3	6.3	2.9	0.6	0.6		

APPENDIX B

SUPPLEMENTAL INFORMATION FOR CHAPTER 3

B.1 Comparisons of Percent Error for Small Molecule Homologs

B.1.1 Comparisons of Percent Error for Silicon Small Molecule Homologs

Table B.1.1: Comparisons of percent error for silicon small molecule main group homolog bond dissociation energies with respect to experimental, G4 level of theory, and W1u level of theory calculations.

Basis	Pseudo-Potential	Small Molecule Experimental Thermodynamic Data				Small Molecule G4 Thermodynamic Data				Small Molecule W1U Thermodynamic Data			
		% Error		% Abs Error		% Error		% Abs Error		% Error		% Abs Error	
		Avg	Std Dev	Avg	Std Dev	Avg	Std Dev	Avg	Std Dev	Avg	Std Dev	Avg	Std Dev
BP 86	CEP 31G	16.9	64.0	43.5	41.1	3.9	6.3	5.6	3.8	5.6	6.5	6.7	4.7
	CEP 121G	16.0	63.8	43.6	40.1	3.1	6.2	5.4	3.1	4.8	6.5	6.4	3.8
	LANL2DZ	34.9	81.6	51.2	67.5	18.1	14.2	18.1	14.2	20.1	15.0	20.1	15.0
	SDDAll	21.0	67.5	44.8	47.0	7.1	6.2	7.1	6.2	8.9	6.7	8.9	6.7
	Average	22.2		45.8		8.0		9.1		9.8		10.5	
	Std Dev		59.9		42.9		9.9		8.9		10.3		9.5
B3LYP	CEP 31G	7.2	58.3	41.6	29.7	-5.0	2.8	5.0	2.8	-3.5	2.9	3.5	2.9
	CEP 121G	6.3	58.1	41.8	28.7	-5.9	2.7	5.9	2.7	-4.4	2.9	4.4	2.9
	LANL2DZ	26.0	76.3	49.8	55.8	9.6	7.5	9.6	7.5	11.5	8.6	11.5	8.6
	SDDAll	12.2	62.6	43.3	36.5	-1.1	2.9	1.9	2.2	0.6	3.5	2.8	0.8
	Average	12.9		44.1		-0.6		5.6		1.1		5.5	
	Std Dev		55.4		33.6		7.5		4.7		7.9		5.5
M06	CEP 31G	20.9	56.8	37.1	42.5	9.7	8.0	9.7	8.0	11.5	7.1	11.5	7.1
	CEP 121G	0.7	79.3	58.8	33.2	-14.1	38.9	25.0	29.6	-12.6	39.7	26.2	28.0
	LANL2DZ	21.1	99.6	67.7	61.0	1.7	45.8	35.8	13.4	3.5	46.9	37.3	11.6
	SDDAll	4.7	80.8	58.5	37.7	-10.2	39.9	26.9	25.7	-8.7	40.7	28.2	24.0
	Average	11.8		55.5		-3.3		24.4		-1.6		25.8	
	Std Dev		69.4		40.0		32.5		20.5		33.1		19.4
	CEP 31G	5.0	54.5	39.9	24.9	-6.1	3.1	6.1	3.1	-4.5	2.7	4.5	2.7
	CEP 121G	3.7	54.2	40.1	23.4	-7.2	3.1	7.2	3.1	-5.7	2.7	5.7	2.7

Basis	Pseudo-Potential	Small Molecule Experimental Thermodynamic Data				Small Molecule G4 Thermodynamic Data				Small Molecule W1U Thermodynamic Data			
		% Error		% Abs Error		% Error		% Abs Error		% Error		% Abs Error	
		Avg	Std Dev	Avg	Std Dev	Avg	Std Dev	Avg	Std Dev	Avg	Std Dev	Avg	Std Dev
BLYP	LANL2DZ	22.8	71.8	47.6	50.3	8.0	9.6	10.0	6.1	9.8	10.3	11.2	7.9
	SDDAll	10.2	59.3	41.9	32.3	-1.9	2.6	2.5	1.7	-0.3	2.7	1.9	1.5
	Average	10.4		42.4		-1.8		6.5		-0.2		5.8	
	Std Dev		52.1		29.6		7.8		4.3		8.0		5.2
B97D	CEP 31G	18.1	58.6	38.4	41.3	6.4	4.6	6.4	4.6	8.1	3.7	8.1	3.7
	CEP 121G	17.2	58.4	38.6	40.2	5.5	4.4	5.5	4.4	7.2	3.4	7.2	3.4
	LANL2DZ	36.4	75.9	46.1	67.5	20.8	7.5	20.8	7.5	22.8	7.9	22.8	7.9
	SDDAll	22.5	62.2	39.7	47.5	10.0	3.8	10.0	3.8	11.8	2.8	11.8	2.8
	Average	23.5		40.7		10.7		10.7		12.5		12.5	
	Std Dev		55.3		43.1		7.8		7.8		7.7		7.7
PBEPBE	CEP 31G	22.3	68.9	45.5	48.9	8.1	7.4	8.3	7.2	9.9	7.9	9.9	7.9
	CEP 121G	21.4	68.7	45.6	47.8	7.3	7.4	8.0	6.3	9.1	7.9	9.1	7.9
	LANL2DZ	39.9	86.2	53.1	74.8	22.0	15.6	22.0	15.6	24.1	16.5	24.1	16.5
	SDDAll	26.8	73.0	47.1	55.5	11.7	7.8	11.7	7.8	13.5	8.4	13.5	8.4
	Average	27.6		47.8		12.3		12.5		14.2		14.2	
	Std Dev		64.0		49.4		10.6		10.4		11.1		11.1
M11L	CEP 31G	18.9	54.8	35.8	40.2	8.8	12.1	9.0	11.9	10.5	11.6	10.5	11.6
	CEP 121G	-7.3	82.5	60.4	37.6	-20.7	54.7	35.3	42.0	-19.2	55.5	35.5	41.8
	LANL2DZ	37.2	74.3	44.8	67.7	22.8	16.2	22.8	16.2	24.8	16.4	24.8	16.4
	SDDAll	26.3	63.0	39.6	51.5	14.3	11.0	14.3	11.0	16.1	10.7	16.1	10.7
	Average	18.8		45.2		6.3		20.3		8.1		21.7	
	Std Dev		61.7		44.3		30.5		22.9		30.9		22.6
MN12L	CEP 31G	23.2	34.3	23.2	34.3	19.5	29.5	26.7	19.3	21.2	29.0	26.8	21.1
	CEP 121G	21.5	32.8	21.7	32.6	18.1	29.8	26.7	17.8	19.9	29.3	26.8	19.4
	LANL2DZ	45.7	50.8	45.7	50.8	39.2	35.0	39.2	35.0	41.3	34.6	41.3	34.6

Basis	Pseudo-Potential	Small Molecule Experimental Thermodynamic Data				Small Molecule G4 Thermodynamic Data				Small Molecule W1U Thermodynamic Data			
		% Error		% Abs Error		% Error		% Abs Error		% Error		% Abs Error	
		Avg	Std Dev	Avg	Std Dev	Avg	Std Dev	Avg	Std Dev	Avg	Std Dev	Avg	Std Dev
	SDDAll	28.6	33.0	28.6	33.0	25.8	34.6	31.6	26.4	27.6	34.1	31.7	28.3
	Average	29.8		29.8		25.6		31.0		27.5		31.6	
	Std Dev		34.3		34.2		28.9		22.4		28.6		23.5
N12	CEP 31G	26.3	67.7	43.2	53.0	12.7	8.5	12.7	8.5	14.6	8.5	14.6	8.5
	CEP 121G	29.0	64.2	39.8	54.9	17.2	17.8	17.2	17.8	19.1	17.7	19.1	17.7
	LANL2DZ	6.7	99.8	70.3	51.1	-18.1	65.5	44.1	43.3	-16.6	66.7	45.5	41.8
	SDDAll	31.9	71.5	44.3	60.8	17.7	9.8	17.7	9.8	19.6	10.0	19.6	10.0
	Average	23.5		49.4		7.4		22.9		9.2		24.7	
	Std Dev		66.6		48.7		33.3		24.4		33.8		23.8
SOGGA11	CEP 31G	26.6	65.6	41.3	53.0	13.5	5.8	13.5	5.8	15.4	5.5	15.4	5.5
	CEP 121G	26.6	66.1	41.8	53.1	13.4	6.7	13.4	6.7	15.3	6.5	15.3	6.5
	LANL2DZ	37.7	77.2	46.8	69.3	22.0	9.8	22.0	9.8	24.0	10.2	24.0	10.2
	SDDAll	31.1	70.9	44.1	59.7	16.9	8.8	16.9	8.8	18.8	9.0	18.8	9.0
	Average	30.5		43.5		16.5		16.5		18.4		18.4	
	Std Dev		60.0		50.5		7.7		7.7		7.8		7.8
B2LYP	CEP 31G	12.4	60.6	41.6	36.2	-0.3	2.9	2.2	1.2	1.3	2.9	2.6	1.2
	CEP 121G	-29.6	23.9	29.6	23.9	-31.3	25.6	31.3	25.6	-30.3	25.6	30.3	25.6
	LANL2DZ	32.5	79.8	50.3	64.5	15.5	7.6	15.5	7.6	17.4	8.7	17.4	8.7
	SDDAll	15.8	67.5	45.5	42.8	1.1	7.2	5.9	1.2	2.8	7.8	6.9	1.0
	Average	7.8		41.7		-3.8		13.7		-2.2		14.3	
	Std Dev		57.7		38.7		21.4		16.4		21.8		16.1
MP2	CEP 31G	25.8	77.5	50.2	56.8	8.8	8.0	8.8	8.0	10.6	9.2	10.6	9.2
	CEP 121G	39.2	71.2	42.5	68.3	26.1	20.6	26.1	20.6	28.2	20.6	28.2	20.6
	LANL2DZ	46.9	95.9	57.9	86.5	25.9	13.7	25.9	13.7	28.1	15.3	28.1	15.3
	SDDAll	31.2	81.8	52.0	64.0	13.2	8.6	13.2	8.6	15.1	10.0	15.1	10.0

Basis	Pseudo-Potential	Small Molecule Experimental Thermodynamic Data				Small Molecule G4 Thermodynamic Data				Small Molecule W1U Thermodynamic Data			
		% Error		% Abs Error		% Error		% Abs Error		% Error		% Abs Error	
		Avg	Std Dev	Avg	Std Dev	Avg	Std Dev	Avg	Std Dev	Avg	Std Dev	Avg	Std Dev
	Average	35.8		50.7		18.5		18.5		20.5		20.5	
	Std Dev		70.5		59.8		14.2		14.2		14.8		14.8
Overall Averages	CEP 31G	18.6	51.0	40.1	36.1	6.7	11.5	9.5	9.3	8.4	11.5	10.4	9.7
	CEP 121G	12.1	54.8	42.0	36.5	1.0	26.0	17.3	19.3	2.6	26.3	17.8	19.3
	LANL2DZ	32.3	68.7	52.6	54.2	15.6	26.5	23.8	19.2	17.6	27.0	25.7	19.2
	SDDAll	21.9	56.3	44.1	40.8	8.7	17.0	13.3	13.5	10.5	17.2	14.6	13.7
	Average	21.2		43.5		8.0		10.4		9.8		11.8	
	Std Dev		57.9		42.4		21.6		16.6		21.9		16.8

B.1.2 Comparisons of Percent Error for Phosphorus Small Molecule Homologs

Table B.1.2: Comparisons of percent error for phosphorus small molecule main group homolog bond dissociation energies with respect to experimental, G4 level of theory, and W1u level of theory calculations.

Basis	Pseudo-Potential	Beaumier Thermodynamic Small Molecule Data - Experimental				Beaumier Thermodynamic Small Molecule Data - G4				Beaumier Thermodynamic Small Molecule Data - W1			
		% Error		% Abs Error		% Error		% Abs Error		% Error		% Abs Error	
		Avg	Std Dev	Avg	Std Dev	Avg	Std Dev	Avg	Std Dev	Avg	Std Dev	Avg	Std Dev
BP 86	CEP 31G	-4.5	8.9	5.8	7.7	1.5	0.8	1.5	0.8	0.5	0.2	0.5	0.2
	CEP 121G	-4.5	8.9	5.7	7.8	1.5	0.9	1.5	0.9	0.5	0.2	0.5	0.2
	LANL2DZ	-3.6	8.6	5.4	7.0	2.6	0.5	2.6	0.5	1.5	0.2	1.5	0.2
	SDDAll	-6.8	-6.8	6.8	8.2	-0.9	0.5	0.9	0.5	-1.9	0.3	1.9	0.3
	Average	-4.9		5.9		1.2		1.6		0.2		1.1	
	Std Dev		7.5		6.6		1.5		0.9		1.3		0.7
B3LYP	CEP 31G	-13.5	6.6	13.5	6.6	-7.9	0.9	7.9	0.9	-8.9	1.5	8.9	1.5
	CEP 121G	-13.5	6.6	13.5	6.6	-7.9	1.0	7.9	1.0	-8.8	1.5	8.8	1.5
	LANL2DZ	-12.6	6.3	12.6	6.3	-7.0	1.3	7.0	1.3	-7.9	1.9	7.9	1.9

Basis	Pseudo-Potential	Beaumier Thermodynamic Small Molecule Data - Experimental				Beaumier Thermodynamic Small Molecule Data - G4				Beaumier Thermodynamic Small Molecule Data - W1			
		% Error		% Abs Error		% Error		% Abs Error		% Error		% Abs Error	
		Avg	Std Dev	Avg	Std Dev	Avg	Std Dev	Avg	Std Dev	Avg	Std Dev	Avg	Std Dev
	SDDAll	-15.7	-15.7	15.7	6.0	-10.2	1.4	10.2	1.4	-11.2	1.8	11.2	1.8
	Average	-13.8		13.8		-8.3		8.3		-9.2		9.2	
	Std Dev		5.6		5.6		1.6		1.6		1.9		1.9
M06	CEP 31G	5.8	12.4	8.9	9.2	12.8	12.8	14.1	10.6	11.7	13.3	14.1	9.2
M06	CEP 121G	4.8	12.5	9.1	8.2	11.8	13.5	14.3	9.2	10.7	14.0	14.3	8.0
M06	LANL2DZ	6.7	13.0	10.5	8.5	13.9	14.7	15.9	11.4	12.9	15.2	15.9	10.2
M06	SDDAll	4.6	4.6	8.0	7.8	11.6	12.1	13.1	9.6	10.6	12.7	13.1	8.3
M06	Average	5.5		9.1		12.5		14.3		11.5		14.3	
M06	Std Dev		10.5		7.2		11.4		8.8		11.8		7.7
BLYP	CEP 31G	-10.7	10.1	10.7	10.1	-5.2	3.1	5.2	3.1	-6.1	2.5	6.1	2.5
BLYP	CEP 121G	-10.8	10.1	10.8	10.1	-5.3	3.2	5.3	3.2	-6.2	2.5	6.2	2.5
BLYP	LANL2DZ	-9.8	9.8	9.8	9.8	-4.1	2.8	4.1	2.8	-5.1	2.1	5.1	2.1
BLYP	SDDAll	-12.8	-12.8	12.8	9.6	-7.4	2.9	7.4	2.9	-8.3	2.3	8.3	2.3
BLYP	Average	-11.0		11.0		-5.5		5.5		-6.5		6.5	
BLYP	Std Dev		8.5		8.5		2.9		2.9		2.3		2.3
PBEPBE	CEP 31G	-4.9	6.8	5.9	5.5	1.3	2.4	2.1	1.3	0.3	3.1	2.2	1.6
PBEPBE	CEP 121G	-4.9	6.8	5.8	5.6	1.3	2.3	2.0	1.4	0.3	3.0	2.1	1.6
PBEPBE	LANL2DZ	-4.0	6.5	5.4	4.8	2.3	2.7	2.5	2.4	1.3	3.4	2.6	2.0
PBEPBE	SDDAll	-7.2	-7.2	7.2	6.1	-1.2	2.7	2.3	1.2	-2.1	3.4	3.1	2.0
PBEPBE	Average	-5.2		6.1		0.9		2.2		-0.1		2.5	
PBEPBE	Std Dev		5.7		4.8		2.9		1.4		3.0		1.6
B97D	CEP 31G	8.5	9.2	8.5	9.2	16.6	20.6	16.6	20.6	15.5	21.2	15.5	21.2
B97D	CEP 121G	-2.8	9.6	6.5	6.4	3.4	1.7	3.4	1.7	2.3	1.0	2.3	1.0
B97D	LANL2DZ	-1.0	9.8	7.2	4.5	5.2	1.9	5.2	1.9	4.2	1.1	4.2	1.1
B97D	SDDAll	11.1	11.1	21.5	7.0	17.3	15.7	17.7	15.2	16.1	15.0	16.6	14.1

Basis	Pseudo-Potential	Beaumier Thermodynamic Small Molecule Data - Experimental				Beaumier Thermodynamic Small Molecule Data - G4				Beaumier Thermodynamic Small Molecule Data - W1			
		% Error		% Abs Error		% Error		% Abs Error		% Error		% Abs Error	
		Avg	Std Dev	Avg	Std Dev	Avg	Std Dev	Avg	Std Dev	Avg	Std Dev	Avg	Std Dev
	Average	4.0		10.9		10.6		10.7		9.5		9.6	
	Std Dev		13.8		8.8		13.0		12.9		12.8		12.8
M11L	CEP 31G	13.4	17.3	17.7	9.9	20.2	8.6	20.2	8.6	18.9	7.8	18.9	7.8
	CEP 121G	12.2	17.2	17.3	8.5	18.9	8.6	18.9	8.6	17.7	7.8	17.7	7.8
	LANL2DZ	14.4	16.4	17.3	11.4	21.2	7.4	21.2	7.4	20.0	6.6	20.0	6.6
	SDDAll	11.1	11.1	16.8	7.3	17.7	8.6	17.7	8.6	16.5	7.8	16.5	7.8
	Average	12.8		17.3		19.5		19.5		18.3		18.3	
	Std Dev		14.5		8.0		7.2		7.2		6.6		6.6
MN12L	CEP 31G	27.5	13.8	27.5	13.8	35.5	3.9	35.5	3.9	34.1	3.8	34.1	3.8
	CEP 121G	26.8	13.6	26.8	13.6	34.8	3.6	34.8	3.6	33.4	3.4	33.4	3.4
	LANL2DZ	29.6	13.9	29.6	13.9	37.7	4.4	37.7	4.4	36.3	4.4	36.3	4.4
	SDDAll	25.4	25.4	25.4	13.3	33.3	3.8	33.3	3.8	31.9	3.8	31.9	3.8
	Average	27.3		27.3		35.3		35.3		33.9		33.9	
	Std Dev		11.7		11.7		3.8		3.8		3.7		3.7
N12	CEP 31G	2.8	7.7	5.6	4.9	9.5	4.4	9.5	4.4	8.4	5.0	8.4	5.0
	CEP 121G	2.4	7.7	5.6	4.5	9.0	4.0	9.0	4.0	8.0	4.7	8.0	4.7
	LANL2DZ	4.5	7.4	5.7	6.0	11.3	5.0	11.3	5.0	10.2	5.7	10.2	5.7
	SDDAll	1.6	1.6	5.1	4.2	8.3	4.1	8.3	4.1	7.2	4.8	7.2	4.8
	Average	2.8		5.5		9.5		9.5		8.4		8.4	
	Std Dev		6.5		4.2		3.9		3.9		4.5		4.5
SOGGA11	CEP 31G	1.3	7.1	4.8	4.3	8.0	5.1	8.0	5.1	6.9	5.8	6.9	5.8
	CEP 121G	1.5	6.9	4.6	4.3	8.1	5.3	8.1	5.3	7.1	6.0	7.1	6.0
	LANL2DZ	-0.1	7.9	5.4	4.3	6.3	2.4	6.3	2.4	5.2	3.1	5.2	3.1
	SDDAll	-1.5	-1.5	5.2	2.4	4.9	4.5	4.9	4.5	3.9	5.2	4.9	3.6
	Average	0.3		5.0		6.8		6.8		5.8		6.0	

Basis	Pseudo-Potential	Beaumier Thermodynamic Small Molecule Data - Experimental				Beaumier Thermodynamic Small Molecule Data - G4				Beaumier Thermodynamic Small Molecule Data - W1			
		% Error		% Abs Error		% Error		% Abs Error		% Error		% Abs Error	
		Avg	Std Dev	Avg	Std Dev	Avg	Std Dev	Avg	Std Dev	Avg	Std Dev	Avg	Std Dev
	Std Dev		6.2		3.4		4.1		4.1		4.6		4.2
B2LYP	CEP 31G	-16.2	4.7	16.2	4.7	-10.7	2.9	10.7	2.9	-11.6	3.5	11.6	3.5
	CEP 121G	-15.0	5.1	15.0	5.1	-9.5	2.5	9.5	2.5	-10.4	3.1	10.4	3.1
	LANL2DZ	-15.1	4.3	15.1	4.3	-9.5	3.6	9.5	3.6	-10.4	4.1	10.4	4.1
	SDDAll	-18.1	-18.1	18.1	4.2	-12.6	3.2	12.6	3.2	-13.5	3.7	13.5	3.7
	Average	-16.1		16.1		-10.6		10.6		-11.5		11.5	
	Std Dev		4.1		4.1		3.0		3.0		3.4		3.4
MP2	CEP 31G	-23.5	3.6	23.5	3.6	-18.2	8.4	18.2	8.4	-19.0	8.9	19.0	8.9
	CEP 121G	-20.4	3.4	20.4	3.4	-15.0	7.4	15.0	7.4	-15.8	8.0	15.8	8.0
	LANL2DZ	-21.6	4.1	21.6	4.1	-16.1	9.7	16.1	9.7	-16.9	10.2	16.9	10.2
	SDDAll	-24.9	-24.9	24.9	3.3	-19.6	8.5	19.6	8.5	-20.4	9.0	20.4	9.0
	Average	-22.6		22.6		-17.2		17.2		-18.0		18.0	
	Std Dev		3.6		3.6		7.5		7.5		7.9		7.9
Overall Averages	CEP 31G	-0.1	12.8	11.3	6.9	6.4	13.6	11.4	9.7	5.3	13.5	11.1	9.3
	CEP 121G	-1.2	12.1	11.0	7.0	5.1	12.8	10.0	9.6	4.0	12.7	9.7	9.3
	LANL2DZ	-0.1	12.9	11.1	7.4	6.3	13.6	10.6	10.5	5.3	13.5	10.4	10.2
	SDDAll	-1.8	13.2	13.0	7.0	4.5	13.9	11.3	9.1	3.4	13.8	11.4	8.4
	Average	-1.7		5.5		4.6		11.8		3.5		11.6	
	Std Dev		15.7		9.5		15.1		10.5		15.1		10.2

B.1.3 Comparisons of Percent Error for Sulfur Small Molecule Homologs

Table B.1.3: Comparisons of percent error for sulfur small molecule main group homolog bond dissociation energies with respect to experimental, G4 level of theory, and W1u level of theory calculations.

Basis	Pseudo-Potential	Small Molecule Experimental Thermodynamic Data				Small Molecule G4 Thermodynamic Data				Small Molecule W1U Thermodynamic Data			
		% Error		% Abs Error		% Error		% Abs Error		% Error		% Abs Error	
		Avg	Std Dev	Avg	Std Dev	Avg	Std Dev	Avg	Std Dev	Avg	Std Dev	Avg	Std Dev
BP 86	CEP 31G	-1.3		5.1		1.7		3.4		-1.9		4.6	
	CEP 121G	-0.9		5.0		2.1		3.2		-1.6		4.5	
	LANL2DZ	-1.1		4.9		1.9		3.2		-1.8		4.4	
	SDDAll	-2.0		4.9		1.0		3.2		-2.7		4.4	
	Average	-1.3		5.0		1.7		3.3		-2.0		4.5	
	Std Dev		5.3		1.5		3.5		1.9		4.8		2.2
B3LYP	CEP 31G	-12.0		12.0		-9.3		9.3		-12.5		12.5	
	CEP 121G	-11.6		11.6		-8.9		8.9		-12.2		12.2	
	LANL2DZ	-12.0		12.0		-9.3		9.3		-12.5		12.5	
	SDDAll	-12.8		12.8		-10.1		10.1		-13.4		13.4	
	Average	-12.1		12.1		-9.4		9.4		-12.7		12.7	
	Std Dev		4.7		4.7		3.0		3.0		4.2		4.2
M06	CEP 31G	8.8		8.8		12.2		12.2		8.1		8.1	
	CEP 121G	9.2		9.2		12.6		12.6		8.5		8.5	
	LANL2DZ	9.6		9.6		13.0		13.0		8.8		8.8	
	SDDAll	8.6		8.6		12.0		12.0		7.9		7.9	
	Average	9.0		9.0		12.4		12.4		8.3		8.3	
	Std Dev		2.6		2.6		0.8		0.8		2.1		2.1
BLYP	CEP 31G	-9.0		9.0		-6.2		6.2		-9.6		9.6	
	CEP 121G	-8.6		8.6		-5.8		5.8		-9.2		9.2	
	LANL2DZ	-8.8		8.8		-6.1		6.1		-9.4		9.4	

Basis	Pseudo-Potential	Small Molecule Experimental Thermodynamic Data				Small Molecule G4 Thermodynamic Data				Small Molecule W1U Thermodynamic Data			
		% Error		% Abs Error		% Error		% Abs Error		% Error		% Abs Error	
		Avg	Std Dev	Avg	Std Dev	Avg	Std Dev	Avg	Std Dev	Avg	Std Dev	Avg	Std Dev
	SDDAll	-10.0		10.0		-7.3		7.3		-10.6		10.6	
	Average	-9.1		9.1		-6.4		6.4		-9.7		9.7	
	Std Dev		6.5		6.5		4.9		4.9		6.0		6.0
B97D	CEP 31G	-2.8		5.5		0.2		3.8		-3.4		5.0	
	CEP 121G	-2.5		5.2		0.5		3.5		-3.1		4.7	
	LANL2DZ	0.6		4.1		3.7		3.7		-0.1		3.5	
	SDDAll	-0.4		4.1		2.6		2.6		-1.1		3.6	
	Average	-1.3		4.7		1.8		3.4		-1.9		4.2	
	Std Dev		5.3		2.1		3.6		1.8		4.8		2.6
PBEPBE	CEP 31G	0.6		4.3		3.7		3.7		-0.1		3.8	
	CEP 121G	0.9		4.1		4.1		4.1		0.3		3.6	
	LANL2DZ	-1.7		5.3		1.3		3.6		-2.4		4.8	
	SDDAll	-3.7		5.3		-0.7		3.6		-4.3		4.8	
	Average	-1.0		4.7		2.1		3.7		-1.6		4.2	
	Std Dev		5.5		2.3		3.9		2.0		5.0		2.7
M11L	CEP 31G	12.5		16.8		15.7		15.7		11.7		16.2	
	CEP 121G	12.4		16.6		15.6		15.6		11.6		15.9	
	LANL2DZ	11.3		16.7		14.5		15.1		10.5		16.0	
	SDDAll	11.9		16.0		15.2		15.2		11.2		15.4	
	Average	12.0		16.5		15.3		15.4		11.2		15.9	
	Std Dev		17.7		12.9		16.0		15.8		17.0		12.0
MN12L	CEP 31G	29.7		29.7		33.6		33.6		28.9		28.9	
	CEP 121G	29.8		29.8		33.7		33.7		28.9		28.9	
	LANL2DZ	31.5		31.5		35.4		35.4		30.6		30.6	
	SDDAll	29.1		29.1		33.0		33.0		28.2		28.2	

Basis	Pseudo-Potential	Small Molecule Experimental Thermodynamic Data				Small Molecule G4 Thermodynamic Data				Small Molecule W1U Thermodynamic Data			
		% Error		% Abs Error		% Error		% Abs Error		% Error		% Abs Error	
		Avg	Std Dev	Avg	Std Dev	Avg	Std Dev	Avg	Std Dev	Avg	Std Dev	Avg	Std Dev
	Average	30.0		30.0		33.9		33.9		29.2		29.2	
	Std Dev		12.0		12.0		9.7		9.7		11.2		11.2
N12	CEP 31G	5.9		5.9		9.2		9.2		5.2		5.2	
	CEP 121G	6.1		6.1		9.4		9.4		5.4		5.4	
	LANL2DZ	5.8		5.8		9.0		9.0		5.1		5.1	
	SDDAll	4.7		4.7		7.9		7.9		4.0		4.0	
	Average	5.6		5.6		8.9		8.9		4.9		4.9	
	Std Dev		3.8		3.8		1.8		1.8		3.2		3.2
SOGGA11	CEP 31G	6.0		6.0		9.3		9.3		5.3		5.3	
	CEP 121G	6.3		6.3		9.6		9.6		5.6		5.6	
	LANL2DZ	1.3		5.3		4.4		4.4		0.6		4.8	
	SDDAll	4.3		4.3		7.6		7.6		3.7		3.7	
	Average	4.5		5.5		7.7		7.7		3.8		4.8	
	Std Dev		4.5		3.0		3.1		3.1		4.0		2.4
B2LYP	CEP 31G	-15.0		15.0		-12.3		12.3		-15.5		15.5	
	CEP 121G	-13.7		13.7		-11.0		11.0		-14.3		14.3	
	LANL2DZ	-14.9		14.9		-12.3		12.3		-15.5		15.5	
	SDDAll	-15.2		15.2		-12.6		12.6		-15.8		15.8	
	Average	-14.7		14.7		-12.1		12.1		-15.3		15.3	
	Std Dev		3.4		3.4		1.8		1.8		2.9		2.9
MP2	CEP 31G	Avg	std dev	Avg	std dev	Avg	std dev	Avg	std dev	Avg	std dev	Avg	std dev
	CEP 121G	-19.2		19.2		-16.6		16.6		-19.7		19.7	
	LANL2DZ	-16.2		16.2		-13.6		13.6		-16.8		16.8	
	SDDAll	-18.6		18.6		-16.0		16.0		-19.1		19.1	
	Average	-18.5		18.5		-16.0		16.0		-19.0		19.0	

Basis	Pseudo-Potential	Small Molecule Experimental Thermodynamic Data				Small Molecule G4 Thermodynamic Data				Small Molecule W1U Thermodynamic Data			
		% Error		% Abs Error		% Error		% Abs Error		% Error		% Abs Error	
		Avg	Std Dev	Avg	Std Dev	Avg	Std Dev	Avg	Std Dev	Avg	Std Dev	Avg	Std Dev
	Std Dev	-18.1		18.1		-15.5		15.5		-18.7		18.7	
Overall Averages	CEP 31G		1.3		1.3		1.8		1.8		1.2		1.2
	CEP 121G	1.5	15.1	11.4	9.8	4.6	14.9	11.5	10.3	0.8	14.8	11.1	9.6
	LANL2DZ	2.1	14.6	11.0	9.5	5.2	14.3	11.1	10.2	1.4	14.3	10.7	9.3
	SDDAll	1.3	15.3	11.4	9.9	4.4	15.0	11.1	10.8	0.7	15.0	11.1	9.8
	Average	0.8	14.8	11.0	9.7	3.9	14.6	11.0	10.1	0.1	14.5	10.7	9.6
	Std Dev	0.3		11.3		3.2		10.4		-0.4		11.0	
			14.6		9.2		13.8		9.6		14.3		9.1

B.2 DFT/MP2 BDEs Comparisons to CCSD(T) BDEs

B.2.1 Comparisons of SiSi and WSi BDEs to CCSD(T) BDEs

Table B.2.1: Comparisons of silicon-silicon bond enthalpies and tungsten-silicon bond enthalpies by functional and valence basis set to the DLPNO-CCSD(T)/def2-QZVPP//SOGGA11/CEP-31(d) results.

Basis	Pseudo-potential	Small Molecule Orca QZ				Organometallic Orca QZ			
		% Error		% Abs Err		% Error		% Abs Err	
		Avg	Std Dev	Avg	Std Dev	Avg	Std Dev	Avg	Std Dev
BP 86	CEP 31G	-9.9	44.3	35.4	15.1	-2.6	18.6	13.4	9.2
	CEP-121g	-10.7	43.8	35.3	14.7	41.3	44.2	41.3	44.2
	LANL2DZ	-0.2	41.8	29.8	20.4	0.2	18.1	13.9	6.2
	SDDAll	-7.2	45.3	35.4	15.8	-11.7	18.3	11.7	18.3
	Average	-7.0		34.0		6.8		20.1	
	Std Dev		37.6		14.4		31.5		24.5
B3LYP	CEP 31G	-15.6	48.3	41.5	10.9	-7.6	17.9	11.1	14.9
	CEP-121g	-16.4	47.7	41.3	11.1	-9.1	44.2	10.6	15.9
	LANL2DZ	-5.6	45.4	35.6	14.3	-4.9	17.0	11.4	11.4
	SDDAll	-12.4	49.3	41.2	10.7	-6.9	17.7	11.2	14.1
	Average	-12.5		39.9		-7.1		11.1	
	Std Dev		40.9		10.4		15.0		12.1
M06	CEP 31G	-0.9	60.0	44.8	24.4	17.4	25.4	23.0	17.4
	CEP-121g	-35.9	16.8	35.9	16.8	17.2	23.9	22.0	17.0
	LANL2DZ	-24.5	16.9	24.5	16.9	19.7	23.2	23.1	18.0
	SDDAll	-32.6	17.9	32.6	17.9	9.5	23.0	19.2	10.4
	Average	-23.5		34.5		16.0		21.8	
	Std Dev		31.9		18.1		20.8		13.7
BLYP	CEP 31G	-17.2	44.3	38.3	14.6	-12.6	18.5	12.6	18.5
	CEP-121g	-18.4	43.5	38.0	15.1	-14.2	18.2	14.2	18.2
	LANL2DZ	-7.6	41.8	32.7	15.1	-10.0	18.0	11.9	16.1
	SDDAll	-14.0	45.2	37.9	13.3	-11.7	18.3	11.7	18.3
	Average	-14.3		36.8		-12.1		12.6	
	Std Dev		37.6		12.7		15.7		15.2
B97D	CEP 31G	-5.4	53.2	40.9	19.0	7.1	25.0	18.7	13.3
	CEP-121g	-6.2	52.5	40.7	18.2	4.2	23.8	17.2	12.2
	LANL2DZ	4.6	50.8	35.4	27.1	10.1	23.1	19.1	11.7
	SDDAll	-2.5	54.0	40.6	21.3	7.3	25.0	18.7	13.4

Basis	Pseudo-potential	Small Molecule Orca QZ				Organometallic Orca QZ			
		% Error		% Abs Err		% Error		% Abs Err	
		Avg	Std Dev	Avg	Std Dev	Avg	Std Dev	Avg	Std Dev
	Average	-2.4		39.4		7.2		18.4	
	Std Dev		45.1		18.7		20.8		10.8
PBEPBE	CEP 31G	-6.7	44.5	34.5	16.2	2.4	18.6	15.0	4.1
	CEP-121g	-7.5	44.1	34.5	15.6	1.1	18.1	14.3	5.0
	LANL2DZ	2.8	42.1	29.0	22.8	5.3	17.8	15.5	0.5
	SDDAll	-3.9	45.5	34.4	17.7	3.0	18.4	15.0	3.8
	Average	-3.8		33.1		3.0		14.9	
	Std Dev		37.8		15.8		15.6		3.2
M11	CEP 31G	-4.3	49.8	36.3	23.0	-8.9	20.1	13.2	16.1
	CEP-121g	-45.6	32.7	45.6	32.7	-9.7	19.5	12.9	16.5
	LANL2DZ	4.7	46.0	31.5	25.8	-6.2	18.0	11.8	13.2
	SDDAll	-0.5	49.5	35.0	24.7	-9.1	18.5	12.3	15.4
	Average	-11.4		37.1		-8.5		12.6	
	Std Dev		43.7		23.5		16.3		13.1
MN12L	CEP 31G	8.2	64.1	45.7	32.7	12.2	28.4	24.5	11.3
	CEP-121g	7.3	64.2	45.4	33.2	11.3	28.1	24.0	10.6
	LANL2DZ	22.3	63.4	52.4	25.3	16.9	27.4	26.4	11.6
	SDDAll	13.7	66.8	50.5	30.3	11.7	26.8	23.8	8.6
	Average	12.9		48.5		13.0		24.7	
	Std Dev		55.5		26.2		23.7		9.1
N12	CEP 31G	-2.3	47.5	34.8	21.1	3.8	21.2	17.6	2.7
	CEP-121g	0.7	46.0	31.0	26.0	3.7	22.3	18.2	4.6
	LANL2DZ	-19.9	90.5	73.6	25.6	-0.5	33.1	25.3	11.5
	SDDAll	1.6	48.3	33.9	24.7	5.2	21.1	18.0	1.2
	Average	-5.0		43.3		3.1		19.8	
	Std Dev		52.8		27.8		21.4		6.4
SOGGA11	CEP 31G	-0.5	51.7	37.7	23.2	10.9	21.8	19.6	8.9
	CEP-121g	-0.9	50.5	36.8	22.7	8.6	20.6	18.4	5.1
	LANL2DZ	5.0	49.2	33.7	27.5	10.8	20.9	19.3	7.3
	SDDAll	1.2	48.8	34.6	24.2	8.0	20.1	17.9	4.4
	Average	1.2		35.7		9.6		18.8	
	Std Dev		42.8		21.0		17.8		5.7
	CEP 31G	-11.3	50.9	42.0	12.0	11.0	22.5	20.8	6.1
	CEP-121g	-41.1	28.8	41.1	28.8	-9.1	17.3	10.6	15.9

Basis	Pseudo-potential	Small Molecule Orca QZ				Organometallic Orca QZ			
		% Error		% Abs Err		% Error		% Abs Err	
		Avg	Std Dev	Avg	Std Dev	Avg	Std Dev	Avg	Std Dev
B2PLYP	LANL2DZ	-0.5	48.0	35.8	19.4	11.8	20.8	19.9	6.7
	SDDAll	-10.2	52.4	43.3	10.0	15.8	22.6	22.5	11.4
	Average	-15.8		40.5		7.4		18.5	
	Std Dev		42.4		16.5		20.5		10.4
MP2	CEP 31G	-5.0	50.9	40.3	13.9	58.0	32.8	58.0	32.8
	CEP-121g	7.6	47.3	34.7	22.8	60.0	32.3	60.0	32.3
	LANL2DZ	7.1	48.6	34.1	26.3	54.8	29.0	54.8	29.0
	SDDAll	-1.9	50.2	38.6	17.0	53.5	29.3	53.5	29.3
	Average	2.0		36.9		56.6		56.6	
	Std Dev		42.4		17.8		26.5		26.5
Overall Averages	CEP 31G	-5.9	42.9	39.4	16.8	7.6	26.1	20.6	17.4
	CEP-121g	-13.9	41.0	38.4	19.2	8.8	29.8	22.0	21.7
	LANL2DZ	-1.0	27.0	37.3	22.8	9.0	25.2	21.0	16.2
	SDDAll	-5.7	42.0	38.2	17.2	6.2	25.0	19.6	16.3
	Average	-6.6		38.3		7.9		20.8	
	Std Dev		42.3		19.0		26.3		17.9

B.2.2 Comparisons of PP and WP BDEs to CCSD(T) BDEs

Table B.2.2: Comparisons of phosphorus-phosphorus bond enthalpies and tungsten-phosphorus bond enthalpies by functional and valence basis set to the DLPNO-CCSD(T)/def2-QZVPP//SOGGA11/CEP-31(d) results.

Basis	Pseudo-potential	Beaumier Thermodynamic Small Molecule CCSD(T) Orca Calcs				Beaumier Thermodynamic Organometallic CCSD(T) Orca Calcs			
		% Error		% Abs Err		% Error		% Abs Err	
		Avg	Std Dev	Avg	Std Dev	Avg	Std Dev	Avg	Std Dev
BP 86	CEP 31G	-2.1	6.5	5.1	3.0	5.0	15.9	10.6	11.6
	CEP-121g	-2.1	6.6	5.3	2.9	3.9	16.8	11.5	11.3
	LANL2DZ	-1.1	6.3	4.8	2.7	5.0	16.2	11.4	11.1
	SDDAll	-4.4	6.1	5.8	4.0	3.0	16.6	11.3	10.7
	Average	-2.4		5.2		4.2		11.2	
	Std Dev		5.6		2.8		14.7		10.0
	CEP 31G	-11.2	4.7	11.2	4.7	-1.9	18.9	15.0	7.7

Basis	Pseudo-potential	Beaumier Thermodynamic Small Molecule CCSD(T) Orca Calcs				Beaumier Thermodynamic Organometallic CCSD(T) Orca Calcs			
		% Error		% Abs Err		% Error		% Abs Err	
		Avg	Std Dev	Avg	Std Dev	Avg	Std Dev	Avg	Std Dev
B3LYP	CEP-121g	-11.2	4.9	11.2	4.9	-3.0	19.8	16.1	7.5
	LANL2DZ	-10.4	4.6	10.4	4.6	-2.3	18.8	14.9	8.1
	SDDAll	-13.5	4.6	13.5	4.6	-3.8	19.2	16.1	6.4
	Average	-11.6		11.6		-2.8		15.5	
	Std Dev		4.2		4.2		14.7		6.7
M06	CEP 31G	8.3	7.1	8.3	7.1	11.1	21.1	13.2	19.4
	CEP-121g	7.3	7.7	8.3	6.1	9.2	21.8	13.1	18.9
	LANL2DZ	9.3	8.6	9.7	8.0	11.6	21.6	14.9	18.7
	SDDAll	7.2	6.3	7.2	6.3	9.4	21.7	13.4	18.7
	Average	8.0		8.9		10.3		13.6	
	Std Dev		6.4		6.9		19.3		17.0
BLYP	CEP 31G	-8.4	8.4	8.5	8.3	-2.1	17.7	12.6	10.3
	CEP-121g	-8.5	8.5	8.6	8.4	-3.2	19.2	13.8	11.2
	LANL2DZ	-7.5	8.1	8.1	7.2	-2.5	18.7	13.4	10.8
	SDDAll	-10.6	8.1	10.6	8.1	-3.9	18.5	13.7	10.6
	Average	-8.8		8.9		-2.9		13.4	
	Std Dev		7.1		6.9		16.6		9.6
PBEPBE	CEP 31G	-2.4	3.4	3.2	2.3	6.5	15.5	9.5	13.2
	CEP-121g	-2.4	3.5	3.3	2.2	5.6	16.3	10.8	12.4
	LANL2DZ	-1.5	3.3	2.9	1.2	6.3	15.5	10.2	12.4
	SDDAll	-4.8	3.0	4.8	3.0	4.3	16.0	10.2	11.9
	Average	-2.8		3.5		5.7		10.2	
	Std Dev		3.1		2.1		14.2		11.2
B97D	CEP 31G	11.8	14.6	12.2	14.2	7.8	23.8	15.1	18.6
	CEP-121g	-0.3	7.5	5.3	3.9	3.2	18.5	12.5	12.1
	LANL2DZ	1.5	7.8	5.4	4.5	4.5	17.8	12.5	11.6
	SDDAll	13.5	19.9	19.8	9.1	4.2	18.3	13.9	10.0
	Average	6.7		9.8		5.0		15.9	
	Std Dev		13.1		9.8		17.8		12.1
M111	CEP 31G	16.1	14.2	16.1	14.2	5.8	21.9	15.2	14.6
	CEP-121g	14.9	14.3	15.4	13.6	-1.2	23.3	16.9	12.8
	LANL2DZ	17.1	13.0	17.1	13.0	5.1	21.9	15.7	13.6
	SDDAll	13.8	14.3	15.0	12.3	2.9	22.5	15.9	13.4
	Average	15.5		15.9		3.1		15.9	

Basis	Pseudo-potential	Beaumier Thermodynamic Small Molecule CCSD(T) Orca Calcs				Beaumier Thermodynamic Organometallic CCSD(T) Orca Calcs			
		% Error		% Abs Err		% Error		% Abs Err	
		Avg	Std Dev	Avg	Std Dev	Avg	Std Dev	Avg	Std Dev
	Std Dev		12.0		11.4		20.2		12.2
MN12L	CEP 31G	30.6	8.4	30.6	8.4	15.0	17.5	15.2	17.2
	CEP-121g	30.0	8.5	30.0	8.5	13.3	17.8	15.3	15.5
	LANL2DZ	32.8	8.1	32.8	8.1	15.8	17.2	17.3	15.3
	SDDAll	28.5	7.8	28.5	7.8	12.2	17.9	15.1	14.6
	Average	30.5		30.5		14.1		15.7	
	Std Dev		7.2		7.2		15.8		14.1
N12	CEP 31G	5.4	2.3	5.4	2.3	10.6	19.0	13.8	16.0
	CEP-121g	5.0	2.5	5.0	2.5	9.1	20.4	14.1	16.3
	LANL2DZ	7.1	1.6	7.1	1.6	9.5	19.6	14.2	15.4
	SDDAll	4.3	2.2	4.3	2.2	9.7	19.7	14.8	15.0
	Average	5.5		5.5		9.7		14.2	
	Std Dev		2.2		2.2		17.6		14.0
SOGGA11	CEP 31G	3.9	1.3	3.9	1.3	5.0	20.0	13.0	14.4
	CEP-121g	4.1	1.1	4.1	1.1	3.8	20.5	13.6	14.0
	LANL2DZ	2.4	3.8	3.5	2.3	3.8	21.7	15.2	13.5
	SDDAll	1.0	1.6	1.4	1.0	1.7	21.2	14.2	13.4
	Average	2.9		3.2		3.6		14.0	
	Std Dev		2.3		1.7		18.7		12.4
B2PLYP	CEP 31G	-14.0	3.0	14.0	3.0	16.7	30.9	18.5	29.5
	CEP-121g	-12.8	3.5	12.8	3.5	16.3	31.9	19.6	29.4
	LANL2DZ	-12.8	2.8	12.8	2.8	13.3	29.5	18.1	25.9
	SDDAll	-15.9	3.1	15.9	3.1	13.8	29.1	18.0	25.8
	Average	-13.9		13.9		15.0		18.5	
	Std Dev		3.0		3.0		27.2		24.8
MP2	CEP 31G	-21.4	3.8	21.4	3.8	62.8	78.5	62.8	78.5
	CEP-121g	-18.3	2.8	18.3	2.8	63.6	79.6	63.6	79.6
	LANL2DZ	-19.4	4.9	19.4	4.9	55.7	73.9	55.7	73.9
	SDDAll	-22.8	4.1	22.8	4.1	62.4	80.6	62.4	80.6
	Average	-20.5		20.5		61.1		61.1	
	Std Dev		3.9		3.9		70.0		70.0
Overall Averag	CEP 31G	2.5	13.1	10.6	7.8	6.4	6.0	13.7	2.4
	CEP-121g	1.3	12.4	9.8	7.7	4.5	6.4	14.3	2.5
	LANL2DZ	2.5	13.1	10.2	8.5	5.6	5.8	14.3	2.4

Basis	Pseudo-potential	Beaumier Thermodynamic Small Molecule CCSD(T) Orca Calcs				Beaumier Thermodynamic Organometallic CCSD(T) Orca Calcs			
		% Error		% Abs Err		% Error		% Abs Err	
		Avg	Std Dev	Avg	Std Dev	Avg	Std Dev	Avg	Std Dev
	SDDAll	0.7	13.5	11.4	8.0	4.1	5.9	14.2	2.2
	Average	0.8		11.5		10.5		18.1	
	Std Dev		14.9		9.5		30.7		26.9

B.2.3 Comparisons of SS and WS BDEs to CCSD(T) BDEs

Table B.2.3: Comparisons of sulfur-sulfur bond enthalpies and tungsten-sulfur bond enthalpies by functional and valence basis set to the DLPNO-CCSD(T)/def2-QZVPP//SOGGA11/CEP-31(d) results.

Basis	Pseudo-potential	Small Molecule Orca QZ				Organometallic Orca QZ			
		% Error		% Abs Err		% Error		% Abs Err	
		Avg	Std Dev	Avg	Std Dev	Avg	Std Dev	Avg	Std Dev
BP 86	CEP 31G	1.2		5.3		4.6		4.6	
	CEP-121g	1.6		5.1		4.3		4.3	
	LANL2DZ	1.3		5.0		5.7		5.7	
	SDDAll	0.4		5.0		5.4		5.4	
	Average	1.1		5.1		5.0		5.0	
	Std Dev		5.5		1.3		3.3		3.3
B3LYP	CEP 31G	-9.8		9.8		-14.1		14.1	
	CEP-121g	-9.4		9.4		-14.4		14.4	
	LANL2DZ	-9.7		9.7		-17.8		17.8	
	SDDAll	-10.6		10.6		-13.4		13.4	
	Average	-9.9		9.9		-14.9		14.9	
	Std Dev		4.8		4.8		2.5		2.5
M06	CEP 31G	11.6		11.6		11.0		11.0	
	CEP-121g	11.9		11.9		11.2		11.2	
	LANL2DZ	12.3		12.3		12.2		12.2	
	SDDAll	11.3		11.3		12.0		12.0	
	Average	11.8		11.8		11.6		11.6	
	Std Dev		2.7		2.7		6.3		6.3
BLYP	CEP 31G	-6.7		6.7		-2.5		3.8	
	CEP-121g	-6.3		6.3		-3.1		4.2	
	LANL2DZ	-6.5		6.5		-11.6		11.6	

Basis	Pseudo-potential	Small Molecule Orca QZ				Organometallic Orca QZ			
		% Error		% Abs Err		% Error		% Abs Err	
		Avg	Std Dev	Avg	Std Dev	Avg	Std Dev	Avg	Std Dev
	SDDAll	-7.8		7.8		4.2		4.2	
	Average	-6.8		6.8		-3.2		6.0	
	Std Dev		6.7		6.7		7.7		5.5
B97D	CEP 31G	-0.3		5.6		2.3		2.3	
	CEP-121g	0.0		5.3		1.9		1.9	
	LANL2DZ	3.1		4.2		9.9		9.9	
	SDDAll	2.1		4.2		8.7		8.7	
	Average	1.2		4.8		5.7		5.7	
	Std Dev		5.4		2.1		5.5		5.5
PBEPBE	CEP 31G	3.1		4.4		8.6		8.6	
	CEP-121g	3.5		4.2		8.2		8.2	
	LANL2DZ	0.7		5.4		2.2		2.2	
	SDDAll	-1.3		5.4		2.4		2.4	
	Average	1.5		4.9		5.3		5.3	
	Std Dev		5.6		2.7		5.3		5.3
M111	CEP 31G	15.3		17.3		10.9		10.9	
	CEP-121g	15.2		17.0		10.2		10.2	
	LANL2DZ	14.1		17.1		5.4		5.4	
	SDDAll	14.8		16.4		9.8		9.8	
	Average	14.8		17.0		9.1		9.1	
	Std Dev		18.1		15.9		5.8		5.8
MN12L	CEP 31G	33.0		33.0		38.8		38.8	
	CEP-121g	33.1		33.1		38.4		38.4	
	LANL2DZ	34.8		34.8		39.9		39.9	
	SDDAll	32.3		32.3		37.9		37.9	
	Average	33.3		33.3		38.7		38.7	
	Std Dev		12.3		12.3		6.7		6.7
N12	CEP 31G	8.5		8.5		12.1		12.1	
	CEP-121g	8.8		8.8		11.7		11.7	
	LANL2DZ	8.4		8.4		13.7		13.7	
	SDDAll	7.3		7.3		12.2		12.2	
	Average	8.3		8.3		12.4		12.4	
	Std Dev		3.9		3.9		3.9		3.9
	CEP 31G	8.7		8.7		21.3		21.3	

Basis	Pseudo-potential	Small Molecule Orca QZ				Organometallic Orca QZ			
		% Error		% Abs Err		% Error		% Abs Err	
		Avg	Std Dev	Avg	Std Dev	Avg	Std Dev	Avg	Std Dev
SOGGA11	CEP-121g	8.9		8.9		20.5		20.5	
	LANL2DZ	3.9		5.4		14.8		14.8	
	SDDAll	7.0		7.0		18.8		18.8	
	Average	7.1		7.5		18.9		18.9	
	Std Dev		4.6		3.8		7.3		7.3
B2PLYP	CEP 31G	-12.8		12.8		-1.7		3.6	
	CEP-121g	-11.5		11.5		-0.3		3.7	
	LANL2DZ	-12.8		12.8		-3.1		3.1	
	SDDAll	-13.1		13.1		0.9		3.1	
	Average	-12.6		12.6		-1.1		3.4	
	Std Dev		3.5		3.5		3.8		1.6
MP2	CEP 31G	-17.1		17.1		34.6		34.6	
	CEP-121g	-14.1		14.1		38.7		38.7	
	LANL2DZ	-16.5		16.5		33.9		33.9	
	SDDAll	-16.5		16.5		40.3		40.3	
	Average	-16.1		16.1		36.9		36.9	
	Std Dev		1.3		1.3		14.0		14.0
Overall Averages	CEP 31G	4.0	15.5	11.9	10.5	12.7	14.8	13.8	13.7
	CEP-121g	4.6	14.9	11.5	10.3	12.9	15.3	13.9	14.3
	LANL2DZ	3.9	15.7	11.7	10.9	11.2	15.7	13.9	13.2
	SDDAll	3.3	15.2	11.5	10.2	13.9	14.3	14.1	14.1
	Average	2.8		11.5		10.4		14.0	
	Std Dev		15.0		10.0		16.1		13.1

B.3 Calculated BDEs

B.3.1 Calculated BDEs for WSi Bonds, SiSi Bonds, and Comparison of Optimized Geometries

Table B.3.1 Calculated bond dissociation enthalpies for tungsten-silicon bonds, silicon-silicon bonds, and comparison of optimized geometries to average tungsten-silicon bond lengths found in the Cambridge Crystallographic Database by functional and valence basis set.

Basis	Psuedo-potential	Churchill Si Complex						Silicon Analog						Chuchill Bond Lengths			
		σ		π		2nd π		σ		π		2nd π					
		ΔH	ΔG	ΔH	ΔG	ΔH	ΔG	ΔH	ΔG	ΔH	ΔG	ΔH	ΔG	% Error	Std Dev	% Abs Error	Std Dev
BP 86	CEP 31G	56.5	42.0	7.6	8.2	25.5	27.2	-67.7	-55.2	16.3	16.2	-3.9	-7.1	-2.9	4.1	4.0	2.2
	CEP 121G	55.4	40.8	8.1	8.6	25.6	27.3	-67.1	-54.6	16.0	16.0	-3.7	-6.8	-2.9	4.2	4.1	2.2
	LANL2DZ	56.2	41.4	10.8	11.2	27.0	28.8	-70.7	-57.9	8.9	8.4	-2.2	-5.0	-3.4	4.4	4.4	2.7
	SDDAll	56.8	42.2	7.8	8.4	25.1	27.0	-69.7	-57.1	16.1	16.0	-3.0	-5.5	-2.7	4.2	4.0	2.1
	Average	56.2	41.6	8.6	9.1	25.8	27.6	-68.8	-56.2	14.3	14.2	-3.2	-6.1	-3.0		4.1	
	Std Dev	0.6	0.7	1.6	1.5	2.0	1.9	1.7	1.5	4.0	4.1	4.4	4.5		3.6		2.0
B3LYP	CEP 31G	54.7	39.2	5.9	7.6	22.6	24.1	-68.0	-55.3	21.3	21.2	0.3	-3.2	-2.8	4.6	4.4	2.0
	CEP 121G	53.1	38.5	6.8	7.3	22.9	24.7	-67.2	-54.7	20.7	21.0	0.5	-3.9	-2.8	4.7	4.5	1.9
	LANL2DZ	54.3	39.2	9.3	10.2	24.0	26.0	-71.0	-58.0	13.3	12.8	2.4	-0.6	-3.3	4.9	4.8	2.5
	SDDAll	55.1	39.9	6.4	7.8	22.1	23.7	-70.1	-57.3	20.7	20.7	1.3	-1.7	-2.6	4.7	4.4	1.8
	Average	54.3	39.2	7.1	8.2	22.9	24.6	-69.1	-56.3	19.0	18.9	1.1	-2.4	-2.9		4.5	
	Std Dev	0.8	0.6	1.8	1.4	2.1	1.8	1.8	1.6	4.2	4.4	4.6	4.8		4.0		1.8
M06	CEP 31G	73.9	56.8	3.3	4.1	21.3	24.7	-81.2	-68.0	31.4	30.2	-6.2	-7.5	-4.6	1.4	4.6	1.4
	CEP 121G	73.0	56.7	5.2	6.5	20.3	23.0	-28.7	-15.2	-22.4	-23.8	-5.7	-8.2	-4.6	1.4	4.6	1.4
	LANL2DZ	73.2	56.0	6.9	8.3	22.6	25.6	-33.9	-21.7	-29.0	-29.2	-2.2	-5.0	-5.0	1.9	5.0	1.9
	SDDAll	68.1	53.5	3.9	4.4	21.1	24.5	-30.7	-18.0	-21.8	-22.4	-7.0	-8.4	-3.6	3.7	4.0	3.0
	Average	72.1	55.7	4.8	5.8	21.3	24.5	-43.6	-30.7	-10.5	-11.3	-5.3	-7.3	-4.4		4.5	
	Std Dev	2.7	1.5	3.1	2.5	4.2	3.1	25.1	25.0	37.7	37.4	45.4	45.0		2.1		1.8
	CEP 31G	51.1	36.3	4.5	5.2	25.8	27.5	-64.4	-51.8	19.2	19.1	-3.9	-7.1	-1.3	4.9	4.2	0.5
	CEP 121G	49.6	35.2	5.1	6.0	26.1	27.7	-63.4	-50.7	18.7	18.7	-3.8	-7.5	-2.0	4.7	4.2	1.2

Basis	Psuedo-potential	Churchill Si Complex						Silicon Analog						Chuchill Bond Lengths			
		σ		π		2nd π		σ		π		2nd π					
		ΔH	ΔG	ΔH	ΔG	ΔH	ΔG	ΔH	ΔG	ΔH	ΔG	ΔH	ΔG	% Error	Std Dev	% Abs Error	Std Dev
BLYP	LANL2DZ	50.7	36.6	7.9	8.0	27.1	29.0	-67.4	-54.6	11.9	11.6	-2.2	-5.2	-2.6	4.9	4.6	1.7
	SDDAll	51.7	37.2	4.9	5.1	25.2	27.6	-66.6	-53.8	18.5	18.3	-2.7	-6.5	-1.1	5.0	4.2	0.6
	average	50.8	36.3	5.6	6.1	26.1	28.0	-65.5	-52.7	17.1	16.9	-3.2	-6.6	-1.7		4.3	
	std dev	0.9	0.8	1.8	1.6	2.2	2.0	1.9	1.8	3.9	4.0	4.4	4.5		4.2		1.0
B97D	CEP 31G	68.9	53.6	0.7	2.6	18.6	20.0	-75.1	-63.1	25.2	25.8	-5.6	-8.3	-4.3	2.1	4.3	2.1
	CEP 121G	66.6	52.8	1.3	2.8	18.8	20.3	-74.3	-62.8	24.7	25.8	-5.3	-8.6	-3.7	3.5	3.8	3.3
	LANL2DZ	68.9	54.0	4.0	6.0	19.6	20.1	-78.3	-65.8	17.9	18.0	-3.8	-6.8	-4.8	2.7	4.8	2.7
	SDDAll	69.0	54.7	0.9	1.4	18.4	19.2	-76.9	-64.5	24.7	25.1	-4.9	-7.9	-4.2	2.2	4.2	2.2
	Average	68.3	53.8	1.7	3.2	18.9	19.9	-76.2	-64.1	23.1	23.7	-4.9	-7.9	-4.2		4.3	
	Std Dev	1.2	0.8	2.0	2.1	2.4	2.4	1.8	1.4	3.9	4.0	4.4	4.3		2.3		2.3
PBEPBE	CEP 31G	60.0	46.2	8.4	8.9	23.7	25.8	-69.4	-57.0	15.0	15.0	-3.0	-6.1	-3.1	3.9	3.9	2.5
	CEP 121G	58.7	44.5	9.0	9.7	23.9	25.8	-68.8	-56.5	14.7	14.9	-2.9	-6.2	-3.1	4.0	4.0	2.4
	LANL2DZ	59.9	45.8	11.6	11.7	25.2	27.8	-72.3	-59.5	7.7	7.2	-1.3	-3.8	-3.6	4.2	4.3	3.0
	SDDAll	60.4	46.6	8.7	9.2	23.1	25.8	-71.4	-58.9	14.5	14.5	-1.9	-4.4	-3.0	4.0	4.0	2.4
	Average	59.8	45.8	9.4	9.9	23.9	26.3	-70.5	-58.0	13.0	12.9	-2.3	-5.1	-3.2		4.1	
	Std Dev	0.7	0.9	1.6	1.5	2.0	2.0	1.6	1.4	3.9	4.1	4.3	4.5		3.4		2.2
M11L	CEP 31G	55.4	39.9	2.3	3.0	24.3	26.7	-72.5	-60.5	23.3	22.9	-12.6	-14.3	-1.4	3.8	3.4	0.4
	CEP 121G	54.5	40.6	3.0	2.9	24.1	27.1	-12.3	-1.5	-36.2	-35.0	-12.9	-15.3	-1.4	3.9	3.5	0.5
	LANL2DZ	54.5	38.0	7.1	10.7	24.6	25.0	-74.4	-62.2	14.2	14.2	-10.0	-11.4	-2.0	4.1	3.8	0.9
	SDDAll	54.5	39.7	4.5	3.8	22.5	26.0	-74.4	-63.5	20.6	21.4	-10.2	-11.4	-1.1	3.9	3.4	0.3
	Average	54.7	39.6	4.2	5.1	23.9	26.2	-58.4	-46.9	5.5	5.9	-11.4	-13.1	-1.5		3.5	
	Std Dev	0.4	1.1	2.2	3.9	2.4	4.2	30.7	30.3	41.6	40.9	51.7	50.9		3.4		0.5
MN12L	CEP 31G	71.5	55.9	-2.7	-0.3	29.1	32.2	-84.2	-71.9	40.2	39.6	-30.7	-32.7	-2.9	3.6	3.7	2.3
	CEP 121G	70.8	54.7	-2.6	0.7	29.0	30.9	-83.8	-71.6	40.8	40.3	-30.9	-32.5	-3.0	3.6	3.7	2.4
	LANL2DZ	71.4	56.3	0.9	2.8	34.0	37.4	-88.4	-74.9	33.4	32.1	-34.9	-37.2	-3.4	4.0	4.1	2.7

Basis	Psuedo-potential	Churchill Si Complex						Silicon Analog						Chuchill Bond Lengths			
		σ		π		2nd π		σ		π		2nd π					
		ΔH	ΔG	ΔH	ΔG	ΔH	ΔG	ΔH	ΔG	ΔH	ΔG	ΔH	ΔG	% Error	Std Dev	% Abs Error	Std Dev
	SDDAll	69.5	56.0	-0.5	0.0	30.5	33.2	-87.3	-75.0	42.3	41.2	-35.8	-37.1	-2.9	3.6	3.7	2.3
	Average	70.8	55.7	-1.2	0.8	30.6	33.4	-85.9	-73.3	39.2	38.3	-33.1	-34.9	-3.0		3.8	
	Std Dev	0.9	0.7	2.0	1.6	2.6	2.4	2.3	1.9	4.6	4.6	5.4	5.2		3.2		2.1
N12	CEP 31G	60.7	47.0	6.3	6.8	29.0	31.2	-72.9	-60.0	17.7	17.4	-6.1	-7.3	-3.9	3.6	4.0	3.4
	CEP 121G	58.7	44.8	7.3	7.7	33.9	36.0	-71.7	-58.9	16.9	16.9	-14.3	-16.3	-3.8	3.8	4.1	3.3
	LANL2DZ	71.4	56.3	0.9	2.8	-9.3	-6.1	-88.4	-74.9	33.4	32.1	51.7	49.9	-4.3	4.0	4.4	3.8
	SDDAll	61.3	47.3	6.8	8.1	29.1	30.8	-75.1	-62.7	17.2	17.7	-6.4	-8.5	-3.7	3.7	4.0	3.2
	Average	63.0	48.8	5.3	6.3	20.7	23.0	-77.0	-64.1	21.3	21.0	6.2	4.4	-3.9		4.1	
	Std Dev	5.7	5.1	6.4	5.6	9.7	8.8	7.7	7.4	11.2	10.4	14.7	13.9		3.2		3.0
SOGGA11	CEP 31G	67.4	53.9	6.0	7.2	23.3	25.3	-76.3	-63.7	21.8	22.2	-6.1	-8.2	-3.6	4.0	4.2	3.0
	CEP 121G	64.5	50.2	7.4	8.2	24.9	26.8	-75.3	-62.4	20.6	20.3	-6.2	-8.6	-3.5	4.3	4.4	2.7
	LANL2DZ	66.1	51.5	7.5	9.3	24.7	26.4	-77.4	-66.4	16.2	18.1	-4.6	-6.1	-4.1	4.2	4.5	3.5
	SDDAll	63.9	49.4	7.9	9.5	24.8	26.0	-75.3	-61.7	17.8	17.0	-6.0	-8.3	-3.5	4.1	4.2	3.0
	Average	65.5	51.2	7.2	8.5	24.4	26.1	-76.1	-63.5	19.1	19.4	-5.7	-7.8	-3.7		4.3	
	Std Dev	1.6	2.0	1.8	2.3	2.5	3.1	1.0	2.1	2.7	3.1	3.0	3.8		3.6		2.6
B2LYP	CEP 31G	66.0	53.1	5.9	6.4	28.5	31.3	-71.5	-58.8	22.6	22.3	-0.1	-3.1	-2.4	4.1	3.9	1.7
	CEP 121G	69.3	53.9	6.6	6.5	28.8	31.5	-38.5	-26.2	12.5	12.6	-23.6	-26.9	-3.8	1.7	3.8	1.7
	LANL2DZ	64.3	50.0	9.7	10.4	29.1	32.2	-74.9	-61.8	14.4	13.3	2.1	-0.2	-3.1	4.6	4.5	2.3
	SDDAll	68.7	53.0	7.2	7.5	28.4	31.2	-73.3	-60.5	21.5	21.3	5.1	46.8	-3.7	1.8	3.7	1.8
	Average	67.0	52.5	7.4	7.7	28.7	31.6	-64.5	-51.8	17.8	17.4	-4.1	4.1	-3.3		4.0	
	Std Dev	2.3	1.7	2.9	2.6	3.7	3.1	17.4	17.1	18.2	17.9	25.4	25.4		2.9		1.6
MP2	CEP 31G	99.3	84.5	6.6	5.1	25.0	27.9	-74.9	-62.5	17.1	16.6	6.8	4.7	-3.4	1.0	3.4	1.0
	CEP 121G	100.2	85.3	7.9	6.0	24.0	27.5	-75.4	-62.9	15.7	15.5	6.2	3.5	-3.8	1.1	3.8	1.1
	LANL2DZ	94.7	80.3	10.2	8.8	26.3	30.2	-79.3	-65.8	9.8	8.3	7.6	5.8	-4.2	1.7	4.2	1.7
	SDDAll	94.4	79.8	9.4	7.7	25.9	29.2	-76.0	-63.2	15.3	15.0	6.6	4.2	-3.9	1.3	3.9	1.3

Basis	Psuedo-potential	Churchill Si Complex						Silicon Analog						Chuchill Bond Lengths			
		σ		π		2nd π		σ		π		2nd π					
		ΔH	ΔG	ΔH	ΔG	ΔH	ΔG	ΔH	ΔG	ΔH	ΔG	ΔH	ΔG	% Error	Std Dev	% Abs Error	Std Dev
	Average	97.2	82.5	8.5	6.9	25.3	28.7	-76.4	-63.6	14.5	13.8	6.8	4.5	-3.8		3.8	
	Std Dev	3.0	2.8	3.4	3.3	4.7	4.4	2.0	1.5	3.8	4.1	4.3	4.4		1.2		1.2
Overall Averages	CEP 31G	65.4	50.7	4.6	5.4	24.7	27.0	-73.2	-60.7	22.6	22.4	-5.9	-8.4	-3.0	3.2	4.0	1.8
	CEP 121G	64.5	49.8	5.4	6.1	25.2	27.4	-60.6	-48.2	11.9	11.9	-8.6	-11.4	-3.2	3.1	4.0	1.8
	LANL2DZ	65.5	50.5	7.2	8.3	22.9	25.2	-73.0	-60.3	12.7	12.2	0.2	-2.1	-3.6	3.4	4.5	2.2
	SDDAll	64.4	49.9	5.7	6.1	24.7	27.0	-70.6	-58.0	17.3	17.1	-5.4	-4.1	-3.0	3.2	4.0	1.8
	Average	65.0	50.2	5.7	6.5	24.4	26.7	-69.3	-56.8	16.1	15.9	-4.9	-6.5	-3.2		4.1	
	Std Dev	12.1	12.0	3.3	3.0	6.1	6.1	15.4	15.2	15.4	15.3	13.0	15.0		3.2		1.9

B.3.2 Calculated BDEs for WP Bonds, PP Bonds, and Comparison of Optimized Geometries

Table B.3.2: Calculated bond dissociation enthalpies for tungsten-phosphorus bonds, phosphorus-phosphorus bonds, and comparison of optimized geometries to average tungsten-phosphorus bond lengths found in the Cambridge Crystallographic Database by functional and valence basis set.

Basis	Pseudo-Potential	Dative Bond		Beaumier Phosphorus Complex						Phosphorus Analog						Beaumier Bond Lengths CCDB			
				σ		π		2nd π		σ		π		2nd π					
		ΔH	ΔG	ΔH	ΔG	ΔH	ΔG	ΔH	ΔG	ΔH	ΔG	ΔH	ΔG	ΔH	ΔG	% Error	Std Dev	% Abs Error	Std Dev
BP 86	CEP 31G	-37.5	-26.8	-93.2	-80.9	3.8	4.4	-28.0	-29.0	-52.2	-40.6	-27.7	-29.2	-36.0	-38.5	-2.1	1.9	2.1	1.9
	CEP 121G	-31.1	-20.3	-88.6	-76.2	5.3	5.8	-29.1	-30.2	-47.4	-35.9	-27.3	-29.1	-36.3	-38.4	-2.1	1.8	2.1	1.8
	LANL2DZ	-36.5	-25.6	-92.6	-80.3	2.2	2.8	-29.6	-33.2	-53.0	-41.4	-27.5	-29.4	-36.5	-38.6	-2.6	1.9	2.6	1.9
	SDDAll	-36.0	-25.2	-92.0	-79.7	4.1	4.6	-28.2	-29.3	-51.3	-39.7	-26.4	-27.9	-35.5	-38.0	-1.8	1.8	1.9	1.7
	Average	-35.3	-24.4	-91.6	-79.3	3.8	4.4	-28.7	-30.4	-51.0	-39.4	-27.3	-28.9	-36.1	-38.4	-2.2		2.2	
	Std Dev	2.9	2.9	2.1	2.1	1.3	1.2	0.8	1.9	2.5	2.4	0.6	0.7	0.4	0.3		1.7		1.7
B3LYP	CEP 31G	-36.0	-25.2	-92.3	-79.8	12.6	13.2	-23.9	-25.2	-48.3	-36.7	-23.4	-25.3	-32.5	-34.6	-2.0	1.9	2.0	1.9
	CEP 121G	-34.6	-23.8	-92.3	-79.8	13.4	14.0	-24.5	-25.9	-48.4	-36.7	-23.3	-25.1	-32.9	-35.0	-2.1	1.8	2.1	1.8
	LANL2DZ	-34.5	-23.8	-91.5	-78.9	11.2	11.6	-26.0	-27.4	-49.1	-37.4	-23.1	-25.0	-33.0	-35.1	-2.5	2.0	2.5	2.0
	SDDAll	-34.5	-23.7	-91.1	-78.5	12.7	13.1	-24.3	-25.7	-47.4	-35.7	-22.1	-24.0	-32.2	-34.3	-1.8	1.9	1.8	1.7
	Average	-34.9	-24.1	-91.8	-79.3	12.5	13.0	-24.7	-26.0	-48.3	-36.6	-23.0	-24.8	-32.6	-34.7	-2.1		2.1	
	Std Dev	0.7	0.7	0.6	0.7	1.0	1.0	0.9	0.9	0.7	0.7	0.6	0.6	0.4	0.4		1.7		1.7
M06	CEP 31G	-39.5	-28.8	-104.0	-91.8	8.5	9.3	-19.4	-20.6	-62.8	-51.2	-31.0	-32.8	-17.6	-19.7	-2.2	2.0	2.2	1.9
	CEP 121G	-38.1	-27.2	-103.2	-90.9	9.0	9.4	-19.2	-20.0	-62.8	-51.2	-30.1	-31.9	-16.5	-18.5	-2.2	1.9	2.2	1.9
	LANL2DZ	-38.6	-27.8	-104.4	-92.1	7.1	7.9	-19.6	-20.5	-64.6	-52.9	-29.8	-31.8	-15.8	-17.9	-2.6	2.1	2.6	2.1
	SDDAll	-38.0	-27.2	-103.2	-90.8	9.1	9.8	-20.5	-20.6	-62.5	-50.8	-29.3	-31.2	-19.3	-21.3	-1.9	2.0	2.2	1.7
	Average	-38.5	-27.8	-103.7	-91.4	8.4	9.1	-19.7	-20.4	-63.2	-51.5	-30.0	-31.9	-17.3	-19.4	-2.2		2.3	
	Std Dev	0.7	0.7	0.6	0.6	0.9	0.8	0.6	0.3	1.0	0.9	0.7	0.7	1.5	1.5		1.8		1.7
BLYP	CEP 31G	-32.5	-21.8	-88.4	-76.1	4.3	4.8	-28.6	-29.6	-47.5	-35.9	-27.4	-29.2	-36.1	-38.2	-1.2	1.7	1.5	1.4
	CEP 121G	-31.1	-20.3	-88.6	-76.2	5.3	5.8	-29.1	-30.2	-47.4	-35.9	-27.3	-29.1	-36.3	-38.4	-1.2	1.7	1.5	1.5
	LANL2DZ	-31.2	-20.4	-88.0	-75.6	3.4	3.9	-30.0	-33.6	-48.3	-36.7	-27.2	-29.0	-36.5	-38.6	-1.7	1.8	1.7	1.8
	SDDAll	-31.1	-20.3	-87.4	-75.0	4.6	5.0	-29.0	-30.1	-46.6	-35.0	-26.2	-28.0	-35.7	-37.8	-0.9	1.7	1.5	1.1
	Average	-31.5	-20.7	-88.1	-75.7	4.4	4.9	-29.2	-30.9	-47.4	-35.9	-27.0	-28.8	-36.1	-38.2	-1.3		1.5	
	Std Dev	0.7	0.7	0.5	0.6	0.8	0.8	0.6	1.8	0.7	0.7	0.5	0.5	0.3	0.3		1.6		1.3
PBEPBE	CEP 31G	-39.3	-28.5	-94.4	-82.3	4.2	5.0	-25.9	-27.0	-53.8	-42.2	-25.9	-27.3	-32.5	-35.0	-2.3	1.8	2.3	1.8
	CEP 121G	-37.9	-27.1	-94.3	-82.1	4.8	5.5	-27.8	-31.6	-53.8	-42.2	-25.8	-27.6	-32.8	-34.9	-2.3	1.8	2.3	1.8
	LANL2DZ	-38.1	-27.4	-93.7	-81.5	2.6	3.2	-27.3	-31.0	-54.5	-42.9	-25.6	-21.3	-33.0	-41.4	-2.7	1.9	2.7	1.9
	SDDAll	-37.6	-26.9	-93.2	-80.9	4.5	5.2	-26.2	-27.3	-52.8	-41.2	-24.6	-26.4	-32.0	-34.0	-2.0	1.8	2.0	1.8
	Average	-38.2	-27.5	-93.9	-81.7	4.1	4.7	-26.8	-29.2	-53.7	-42.1	-25.5	-25.6	-32.6	-36.3	-2.3		2.3	
	Std Dev	0.7	0.7	0.6	0.6	1.0	1.0	0.9	2.4	0.7	0.7	0.6	3.0	0.5	3.4		1.7		1.7
	CEP 31G	-36.1	-25.3	-103.9	-91.2	14.5	14.6	-27.8	-29.0	-72.9	-60.8	-8.7	-11.0	-38.3	-40.4	-2.0	1.6	2.0	1.6

Basis	Pseudo-Potential	Dative Bond		Beaumier Phosphorus Complex						Phosphorus Analog						Beaumier Bond Lengths CCDB			
				σ		π		2nd π		σ		π		2nd π					
		ΔH	ΔG	ΔH	ΔG	ΔH	ΔG	ΔH	ΔG	ΔH	ΔG	ΔH	ΔG	ΔH	ΔG	% Error	Std Dev	% Abs Error	Std Dev
B97D	CEP 121G	-34.8	-24.0	-93.8	-81.2	5.1	5.6	-28.0	-28.9	-52.7	-41.1	-28.6	-30.5	-37.9	-39.9	-2.1	1.6	2.1	1.6
	LANL2DZ	-35.0	-24.2	-93.2	-80.6	2.7	3.1	-29.9	-31.1	-53.7	-42.0	-28.9	-30.8	-39.0	-41.1	-2.5	1.8	2.5	1.8
	SDDAll	-34.7	-23.9	-92.7	-80.1	4.6	5.1	-35.7	-36.1	-51.7	-40.0	-49.8	-51.6	-38.6	-40.7	-1.8	1.6	1.8	1.6
	Average	-35.2	-24.3	-95.9	-83.3	6.7	7.1	-30.3	-31.3	-57.8	-46.0	-29.0	-31.0	-38.4	-40.5	-2.1		2.1	
	Std Dev	0.6	0.6	5.4	5.3	5.3	5.1	3.7	3.4	10.1	9.9	16.8	16.6	0.5	0.5		1.5		1.5
M11L	CEP 31G	-33.5	-23.1	-97.9	-85.7	6.6	8.2	-30.9	-33.0	-57.2	-45.4	-41.1	-43.1	-43.7	-45.8	-2.2	1.5	2.2	1.5
	CEP 121G	-32.4	-21.8	-96.0	-83.7	5.7	6.6	-7.6	-10.8	-56.6	-44.8	-40.3	-42.2	-44.5	-46.6	-2.2	1.5	2.2	1.5
	LANL2DZ	-32.5	-22.0	-96.3	-84.3	4.4	5.8	-31.6	-33.6	-58.5	-46.7	-40.5	-42.6	-42.7	-44.8	-2.7	1.6	2.7	1.6
	SDDAll	-31.7	-21.2	-95.8	-83.5	6.9	6.2	-31.7	-30.8	-56.0	-44.1	-39.9	-41.9	-44.1	-46.2	-2.0	1.5	2.0	1.5
	Average	-32.5	-22.0	-96.5	-84.3	5.9	6.7	-25.4	-27.0	-57.1	-45.3	-40.5	-42.5	-43.8	-45.9	-2.2		2.2	
	Std Dev	0.8	0.8	1.0	1.0	1.1	1.1	11.9	10.9	1.1	1.1	0.5	0.5	0.8	0.8		1.4		1.4
MN12L	CEP 31G	-41.1	-30.3	-102.4	-89.7	2.6	2.9	-25.7	-27.0	-69.0	-57.4	-40.9	-42.7	-41.8	-43.9	-2.0	2.2	2.1	2.0
	CEP 121G	-39.6	-28.8	-101.0	-88.4	2.2	2.6	-26.3	-27.7	-68.6	-57.0	-40.5	-42.3	-42.4	-44.5	-2.0	2.2	2.1	2.0
	LANL2DZ	-40.1	-29.4	-101.4	-88.8	-0.9	-0.5	-28.3	-29.8	-70.4	-58.7	-41.7	-43.6	-41.1	-43.2	-2.3	2.3	2.3	2.3
	SDDAll	-38.9	-28.1	-100.1	-87.3	2.1	2.4	-26.7	-28.2	-68.1	-56.5	-40.0	-41.8	-40.5	-42.6	-1.7	2.1	1.9	1.9
	Average	-39.9	-29.2	-101.2	-88.5	1.5	1.9	-26.8	-28.2	-69.0	-57.4	-40.8	-42.6	-41.5	-43.6	-2.0		2.1	
	Std Dev	0.9	0.9	1.0	1.0	1.6	1.6	1.1	1.2	1.0	0.9	0.7	0.8	0.8	0.8		2.0		1.9
N12	CEP 31G	-38.6	-27.9	-100.6	-88.4	6.3	4.1	-27.5	-28.5	-58.6	-47.2	-28.6	-30.2	-31.5	-33.6	-2.9	1.7	2.9	1.7
	CEP 121G	-37.2	-26.5	-100.8	-88.4	8.2	5.9	-28.3	-29.3	-58.2	-46.5	-28.5	-30.5	-32.0	-34.0	-2.9	1.7	2.9	1.7
	LANL2DZ	-37.4	-26.7	-100.1	-88.0	6.4	3.9	-28.1	-28.9	-60.0	-48.5	-28.4	-30.2	-31.6	-33.7	-3.3	1.8	3.3	1.8
	SDDAll	-37.1	-26.2	-100.1	-87.4	5.5	2.6	-27.9	-28.6	-58.0	-46.5	-27.8	-29.6	-32.0	-34.1	-2.5	1.7	2.5	1.7
	Average	-37.6	-26.8	-100.4	-88.1	6.6	4.2	-27.9	-28.8	-58.7	-47.2	-28.3	-30.1	-31.8	-33.9	-2.9		2.9	
	Std Dev	0.7	0.7	0.4	0.5	1.1	1.4	0.3	0.3	0.9	0.9	0.4	0.4	0.3	0.3		1.6		1.6
SOGGA11	CEP 31G	-35.3	-24.7	-97.0	-85.4	7.1	4.8	-26.8	-27.4	-58.4	-46.7	-27.4	-29.3	-30.5	-32.6	-2.4	1.5	2.4	1.5
	CEP 121G	-34.4	-23.2	-96.5	-84.6	7.7	5.6	-27.3	-28.2	-58.6	-47.1	-27.1	-28.8	-30.6	-32.7	-2.5	1.6	2.5	1.6
	LANL2DZ	-32.8	-22.0	-96.1	-83.4	6.8	3.8	-30.9	-31.9	-56.1	-44.5	-28.3	-30.1	-33.2	-35.3	-2.7	1.7	2.7	1.7
	SDDAll	-32.6	-22.3	-94.9	-83.4	7.2	4.6	-27.7	-27.9	-56.6	-45.0	-26.3	-28.1	-30.8	-32.9	-2.1	1.4	2.1	1.4
	Average	-33.8	-23.0	-96.1	-84.2	7.2	4.7	-28.2	-28.8	-57.4	-45.8	-27.2	-29.1	-31.3	-33.4	-2.4		2.4	
	Std Dev	1.3	1.2	0.9	1.0	0.4	0.7	1.9	2.1	1.3	1.3	0.8	0.8	1.3	1.3		1.4		1.4
B2LYP	CEP 31G	-39.8	-29.1	-119.0	-107.6	25.2	26.4	-24.5	-25.7	-48.1	-36.4	-20.9	-22.4	-30.2	-32.7	-1.3	2.4	2.0	1.6
	CEP 121G	-38.6	-27.9	-119.6	-108.2	25.9	24.7	-25.6	-24.3	-48.5	-36.8	-21.4	-22.9	-31.2	-33.7	-1.4	2.4	2.0	1.7
	LANL2DZ	-37.3	-26.6	-114.4	-102.9	22.5	21.2	-27.2	-26.0	-49.1	-37.4	-20.5	-22.1	-30.6	-33.1	-1.8	2.5	2.1	2.2
	SDDAll	-37.8	-27.1	-118.4	-106.9	25.3	26.5	-25.5	-26.7	-47.3	-35.6	-19.8	-21.3	-30.1	-32.7	0.7	2.4	2.1	1.6
	Average	-38.4	-27.7	-117.9	-106.4	24.7	24.7	-25.7	-25.7	-48.3	-36.5	-20.6	-22.2	-30.5	-33.1	-1.0		2.1	
	Std Dev	1.1	1.1	2.3	2.4	1.5	2.5	1.1	1.0	0.8	0.8	0.7	0.7	0.5	0.5		2.2		1.6

Basis	Pseudo-Potential	Dative Bond		Beaumier Phosphorus Complex						Phosphorus Analog						Beaumier Bond Lengths CCDB			
				σ		π		2nd π		σ		π		2nd π					
		ΔH	ΔG	ΔH	ΔG	ΔH	ΔG	ΔH	ΔG	ΔH	ΔG	ΔH	ΔG	ΔH	ΔG	% Error	Std Dev	% Abs Error	Std Dev
MP2	CEP 31G	-50.5	-39.9	-205.1	-193.5	93.8	92.1	-31.8	-30.3	-47.3	-35.5	-15.2	-16.8	-22.3	-24.8	-1.1	3.4	2.8	1.6
	CEP 121G	-49.7	-39.2	-206.7	-195.3	95.0	93.4	-33.6	-32.0	-48.4	-36.7	-16.9	-18.5	-24.1	-26.6	-1.5	3.4	2.9	1.9
	LANL2DZ	-46.4	-35.8	-194.6	-183.3	87.0	85.5	-35.3	-33.6	-49.2	-37.3	-14.7	-16.3	-22.3	-24.9	-1.8	3.5	3.0	2.2
	SDDAll	-47.8	-37.2	-206.9	-195.4	95.5	94.0	-34.3	-33.1	-46.7	-34.9	-14.3	-15.9	-22.5	-25.0	1.4	3.4	2.9	2.1
	Average	-48.6	-38.0	-203.3	-191.9	92.8	91.3	-33.7	-32.3	-47.9	-36.1	-15.3	-16.9	-22.8	-25.4	-0.7		2.9	
	Std Dev	1.9	1.9	5.9	5.8	3.9	3.9	1.5	1.5	1.1	1.1	1.2	1.1	0.9	0.9		3.1		1.7
Overall Averages	CEP 31G	-38.3	-27.6	-108.2	-96.0	15.8	15.8	-26.7	-27.7	-56.4	-44.7	-26.5	-28.3	-32.7	-35.0	-1.8	1.7	1.8	1.6
	CEP 121G	-36.6	-25.8	-106.8	-94.6	15.6	15.4	-25.5	-26.6	-54.3	-42.7	-28.1	-29.9	-33.1	-35.3	-1.9	1.7	1.9	1.6
	LANL2DZ	-36.7	-26.0	-105.5	-93.3	13.0	12.7	-28.6	-30.0	-55.5	-43.8	-28.0	-29.3	-33.0	-35.6	-2.3	1.8	2.3	1.7
	SDDAll	-36.5	-25.8	-106.3	-94.1	15.2	14.9	-28.1	-28.7	-53.7	-42.1	-28.9	-30.6	-32.8	-35.0	-1.6	1.7	1.6	1.5
	Average	-37.0	-26.3	-106.7	-94.5	14.9	14.7	-27.3	-28.3	-55.0	-43.3	-27.9	-29.5	-32.9	-35.2	-1.9		2.3	
	Std Dev	4.5	4.5	30.4	30.7	24.5	24.1	4.6	4.4	7.1	7.1	8.2	8.3	7.2	7.2		1.7		1.6

B.3.3 Calculated BDEs for WS Bonds, SS Bonds, and Optimized Geometries

Table B.3.3: Calculated bond dissociation enthalpies in kcal/mol for tungsten-sulfur bonds and sulfur-sulfur bonds by functional and valence basis set for the Cotton model with H2S trans to the sulfido moiety.

Basis	Pseudo-Potential	S Cotton Complex - Trans H_2S						Sulfur Homologs			
		Dative Bond		σ		π		HSSH		S_2	
		ΔH	ΔG	ΔH	ΔG	ΔH	ΔG	ΔH	ΔG	ΔH	ΔG
BP 86	CEP 31G	1.3	11.9	-46.4	-46.4	-40.6	-40.6	-60.6	-51.6	-45.0	-47.3
	CEP 121G	1.5	12.1	-46.2	-34.1	-40.5	-41.8	-60.9	-51.9	-44.9	-47.2
	LANL2DZ	-1.3	9.8	-46.7	-34.4	-41.6	-42.7	-60.8	-51.8	-44.7	-47.0
	SDDAll	1.0	11.5	-46.5	-34.3	-41.4	-42.2	-60.2	-51.2	-44.4	-46.7
	Average	0.6	11.3	-46.5	-37.3	-41.0	-41.8	-60.6	-51.6	-44.7	-47.0
	Std Dev	1.3	1.0	0.2	6.1	0.6	0.9	0.3	0.3	0.3	0.3
B3LYP	CEP 31G	-2.1	5.9	-36.2	-24.1	-39.0	-42.2	-54.1	-45.1	-39.9	-42.2
	CEP 121G	-1.8	6.2	-36.0	-23.6	-39.2	-42.9	-54.4	-45.4	-39.8	-42.1
	LANL2DZ	1.6	12.1	-35.3	-22.5	-35.3	-36.9	-54.2	-45.2	-39.7	-42.0
	SDDAll	-1.5	6.0	-36.4	-24.0	-39.5	-43.8	-53.7	-44.7	-39.3	-41.6
	Average	-1.0	7.5	-36.0	-23.6	-38.2	-41.5	-54.1	-45.1	-39.7	-42.0
	Std Dev	1.7	3.1	0.5	0.7	2.0	3.1	0.3	0.3	0.3	0.3
M06	CEP 31G	-2.9	7.4	-50.2	-38.2	-40.1	-41.8	-68.5	-44.7	-45.1	-47.4
	CEP 121G	-2.8	7.7	-50.3	-38.5	-40.0	-41.2	-68.9	-59.9	-44.7	-47.0
	LANL2DZ	-6.1	4.5	-50.7	-39.1	-40.7	-41.7	-69.7	-60.7	-43.4	-45.7
	SDDAll	-3.7	6.4	-50.7	-38.8	-40.2	-41.9	-68.7	-59.7	-44.0	-46.3
	Average	-3.9	6.5	-50.5	-38.7	-40.2	-41.6	-69.0	-56.3	-44.3	-46.6
	Std Dev	1.5	1.4	0.3	0.4	0.3	0.3	0.5	7.7	0.7	0.7
BLYP	CEP 31G	-1.9	6.0	-40.3	-28.3	-46.7	-50.0	-54.9	-46.0	-43.9	-46.2
	CEP 121G	-1.5	6.5	-39.9	-27.6	-46.9	-50.4	-55.2	-46.3	-43.8	-46.1
	LANL2DZ	2.8	13.0	-35.2	-20.5	-46.2	-49.8	-55.1	-46.2	-43.7	-46.0

Basis	Pseudo-Potential	S Cotton Complex - Trans H_2S						Sulfur Homologs			
		Dative Bond		σ		π		HSSH		S_2	
		ΔH	ΔG	ΔH	ΔG	ΔH	ΔG	ΔH	ΔG	ΔH	ΔG
	SDDAll	-1.1	6.5	-45.9	-37.0	-41.4	-41.8	-54.3	-45.4	-43.3	-45.6
	Average	-0.4	8.0	-40.3	-28.3	-45.3	-48.0	-54.9	-45.9	-43.7	-46.0
	Std Dev	2.2	3.4	4.4	6.8	2.6	4.1	0.4	0.4	0.3	0.3
B97D	CEP 31G	-5.8	3.7	-43.7	-31.9	-44.6	-47.2	-59.4	-50.4	-45.0	-47.3
	CEP 121G	-5.4	4.0	-43.5	-31.7	-44.5	-72.5	-59.7	-50.8	-44.7	-47.0
	LANL2DZ	-5.8	4.0	-43.8	-31.9	-44.1	-46.6	-60.1	-51.1	-45.1	-47.4
	SDDAll	-4.9	4.5	-43.8	-32.2	-44.4	-47.0	-58.9	-50.0	-44.3	-46.6
	Average	-5.4	4.0	-43.7	-31.9	-44.4	-53.4	-59.5	-50.6	-44.8	-47.1
	Std Dev	0.4	0.3	0.2	0.2	0.2	12.8	0.5	0.5	0.4	0.4
PBEPBE	CEP 31G	-1.1	9.7	-49.1	-36.9	-39.2	-40.4	-62.3	-53.3	-44.3	-46.6
	CEP 121G	-0.9	9.9	-48.9	-36.7	-39.2	-40.4	-62.7	-53.7	-44.1	-46.5
	LANL2DZ	-3.9	7.3	-49.5	-37.1	-40.4	-41.6	-62.4	-53.4	-43.9	-46.3
	SDDAll	-1.2	9.5	-48.9	-36.7	-40.0	-41.5	-61.8	-52.8	-43.6	-45.9
	Average	-1.8	9.1	-49.1	-36.9	-39.7	-41.0	-62.3	-53.3	-44.0	-46.3
	Std Dev	1.4	1.2	0.3	0.2	0.6	0.6	0.4	0.4	0.3	0.3
M11L	CEP 31G	-5.1	3.1	-45.4	-34.6	-54.4	-56.4	-61.9	-52.8	-69.6	-71.9
	CEP 121G	-4.6	4.5	-45.0	-33.0	-54.1	-56.4	-62.0	-52.9	-69.1	-71.5
	LANL2DZ	-3.9	5.9	-43.4	-32.1	-50.8	-51.8	-61.2	-52.1	-68.9	-71.3
	SDDAll	-5.1	4.0	-45.2	-33.0	-52.9	-55.3	-62.1	-53.0	-68.0	-70.4
	Average	-4.7	4.4	-44.8	-33.2	-53.1	-54.9	-61.8	-52.7	-68.9	-71.3
	Std Dev	0.5	1.2	0.9	1.0	1.6	2.2	0.4	0.4	0.6	0.7
MN12L	CEP 31G	-5.1	5.4	-62.5	-49.2	-51.0	-53.2	-76.7	-67.7	-66.6	-68.9
	CEP 121G	-5.0	5.7	-62.4	-49.5	-50.6	-52.7	-76.9	-68.0	-66.1	-68.4
	LANL2DZ	-7.7	3.3	-62.3	-49.3	-53.5	-54.1	-77.5	-68.5	-68.1	-70.5
	SDDAll	-6.0	4.7	-62.1	-48.9	-50.6	-52.4	-76.6	-67.6	-65.6	-67.9

Basis	Pseudo-Potential	S Cotton Complex - Trans H_2S						Sulfur Homologs			
		Dative Bond		σ		π		HSSH		S_2	
		ΔH	ΔG	ΔH	ΔG	ΔH	ΔG	ΔH	ΔG	ΔH	ΔG
	Average	-5.9	4.8	-62.3	-49.2	-51.4	-53.1	-76.9	-67.9	-66.6	-68.9
	Std Dev	1.3	1.1	0.2	0.2	1.4	0.8	0.4	0.4	1.1	1.1
N12	CEP 31G	-5.1	11.8	-49.8	-37.9	-43.1	-45.1	-66.1	-57.1	-45.2	-47.5
	CEP 121G	1.5	9.9	-49.6	-36.7	-43.1	-40.4	-66.4	-53.7	-45.0	-46.5
	LANL2DZ	-2.0	8.9	-50.5	-38.6	-43.8	-45.4	-66.4	-57.4	-44.2	-46.5
	SDDAll	1.7	12.7	-49.5	-37.4	-44.2	-46.4	-65.3	-56.3	-44.9	-47.2
	Average	-1.0	10.8	-49.9	-37.7	-43.6	-44.3	-66.1	-56.1	-44.8	-46.9
	Std Dev	3.2	1.7	0.5	0.8	0.5	2.7	0.5	1.7	0.4	0.5
SOGGA11	CEP 31G	-2.6	8.5	-55.4	-43.6	-42.1	-43.8	-66.7	-57.7	-44.1	-46.4
	CEP 121G	-2.5	8.6	-55.0	-43.5	-42.0	-43.1	-67.0	-58.0	-43.9	-46.2
	LANL2DZ	0.5	10.9	-50.8	-39.2	-44.8	-45.9	-62.1	-53.2	-46.2	-48.5
	SDDAll	-1.5	9.4	-53.7	-42.1	-43.0	-44.6	-65.5	-56.5	-43.8	-46.1
	Average	-1.5	9.3	-53.7	-42.1	-43.0	-44.3	-65.3	-56.3	-44.5	-46.8
	Std Dev	1.4	1.1	2.1	2.1	1.3	1.2	2.2	2.2	1.1	1.1
B2LYP	CEP 31G	-0.5	9.9	-43.8	-31.8	-37.5	-38.9	-52.9	-43.9	-36.8	-39.1
	CEP 121G	-0.7	9.8	-44.5	-32.4	-37.9	-39.2	-53.8	-44.8	-37.1	-39.4
	LANL2DZ	-2.3	8.6	-42.6	-30.2	-38.7	-39.0	-53.0	-44.0	-36.6	-39.0
	SDDAll	-0.9	9.5	-44.7	-32.5	-39.2	-40.7	-52.9	-43.9	-36.3	-38.7
	Average	-1.1	9.4	-43.9	-31.7	-38.3	-39.4	-53.2	-44.2	-36.7	-39.0
	Std Dev	0.8	0.6	0.9	1.0	0.8	0.9	0.4	0.4	0.3	0.3
MP2	CEP 31G	-7.4	3.3	-63.5	-50.0	-40.9	-43.7	-52.0	-42.9	-30.7	-33.1
	CEP 121G	-8.6	2.0	-42.3	-55.2	-42.3	-41.9	-54.0	-44.9	-31.5	-33.9
	LANL2DZ	-9.5	1.0	-63.0	-49.2	-41.0	-43.8	-52.4	-43.3	-30.8	-33.1
	SDDAll	-8.4	2.4	-65.6	-51.4	-44.3	-47.7	-52.6	-43.5	-30.5	-32.8
	Average	-8.5	2.2	-58.6	-51.4	-42.1	-44.3	-52.7	-43.7	-30.9	-33.2

Basis	Pseudo-Potential	S Cotton Complex - Trans H_2S						Sulfur Homologs			
		Dative Bond		σ		π		HSSH		S_2	
		ΔH	ΔG	ΔH	ΔG	ΔH	ΔG	ΔH	ΔG	ΔH	ΔG
	Std Dev	0.9	0.9	10.9	2.6	1.6	2.4	0.9	0.9	0.5	0.5
Overall Averages	CEP 31G	-3.2	7.2	-48.8	-37.7	-43.3	-45.3	-61.3	-51.1	-46.4	-48.7
	CEP 121G	-2.6	7.2	-47.0	-36.9	-43.4	-46.9	-61.8	-52.5	-46.2	-48.5
	LANL2DZ	-3.1	7.5	-47.8	-35.3	-43.4	-44.9	-61.3	-52.2	-46.3	-48.6
	SDDAll	-2.6	7.3	-49.4	-37.4	-43.4	-45.4	-61.0	-52.0	-45.7	-48.0
	Average	-2.5	7.6	-47.7	-35.9	-44.0	-46.4	-63.0	-53.6	-48.6	-50.9
	Std Dev	0.3	0.1	1.1	1.1	0.1	0.9	0.3	0.6	0.3	0.3

B.4 Component Bond Enthalpies Figures

B.4.1 W-3p Element Bond Component Enthalpies with Respect to the Pseudopotential Used

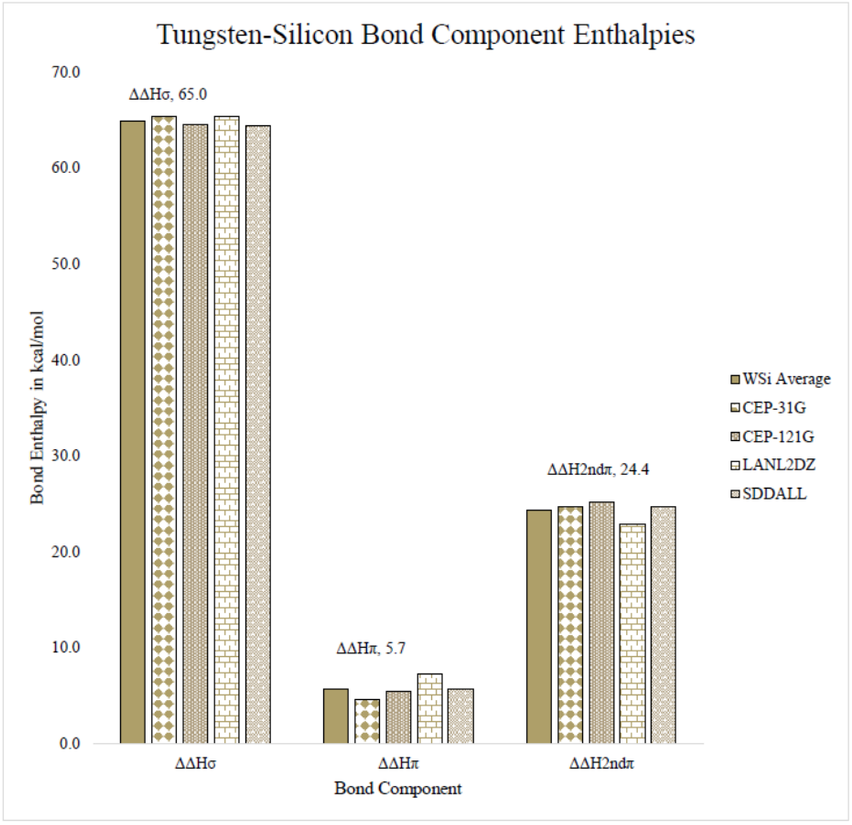

Figure B.4.1-1: Average tungsten-silicon (columns) bond enthalpies by bond type and basis set. Average tungsten-carbon values (left-most solid column) are inset above the columns; the textured columns the average values for each valence basis set.

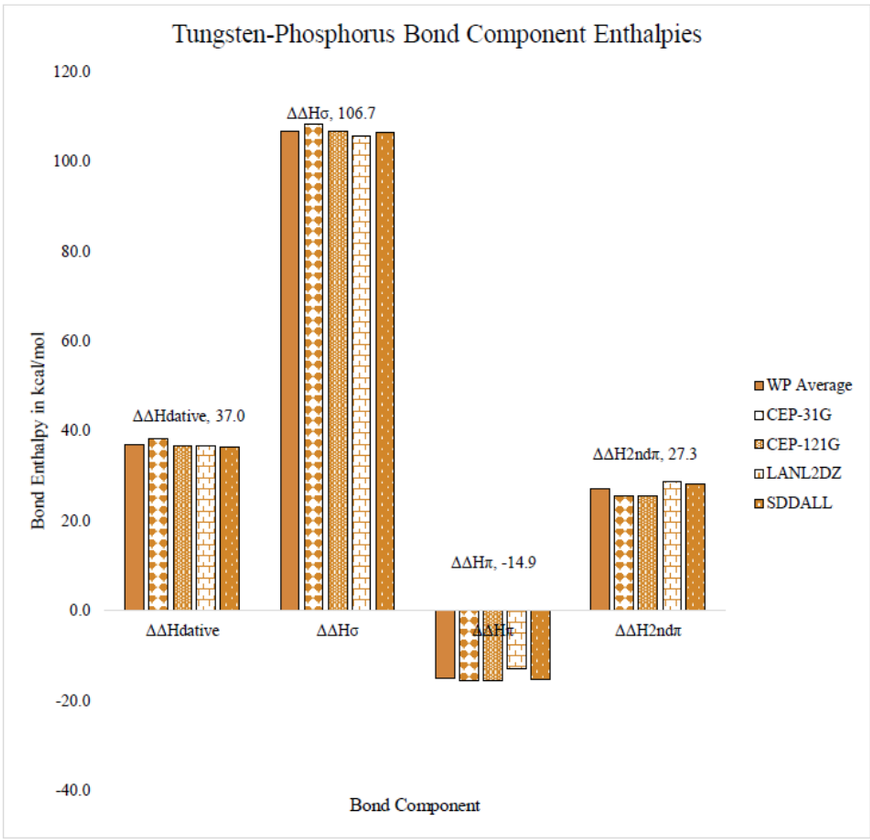

Figure B.4.1-2: Average tungsten-phosphorus (columns) bond enthalpies by bond type and basis set. Average tungsten-carbon values (left-most solid column) are inset above the columns; the textured columns the average values for each valence basis set.

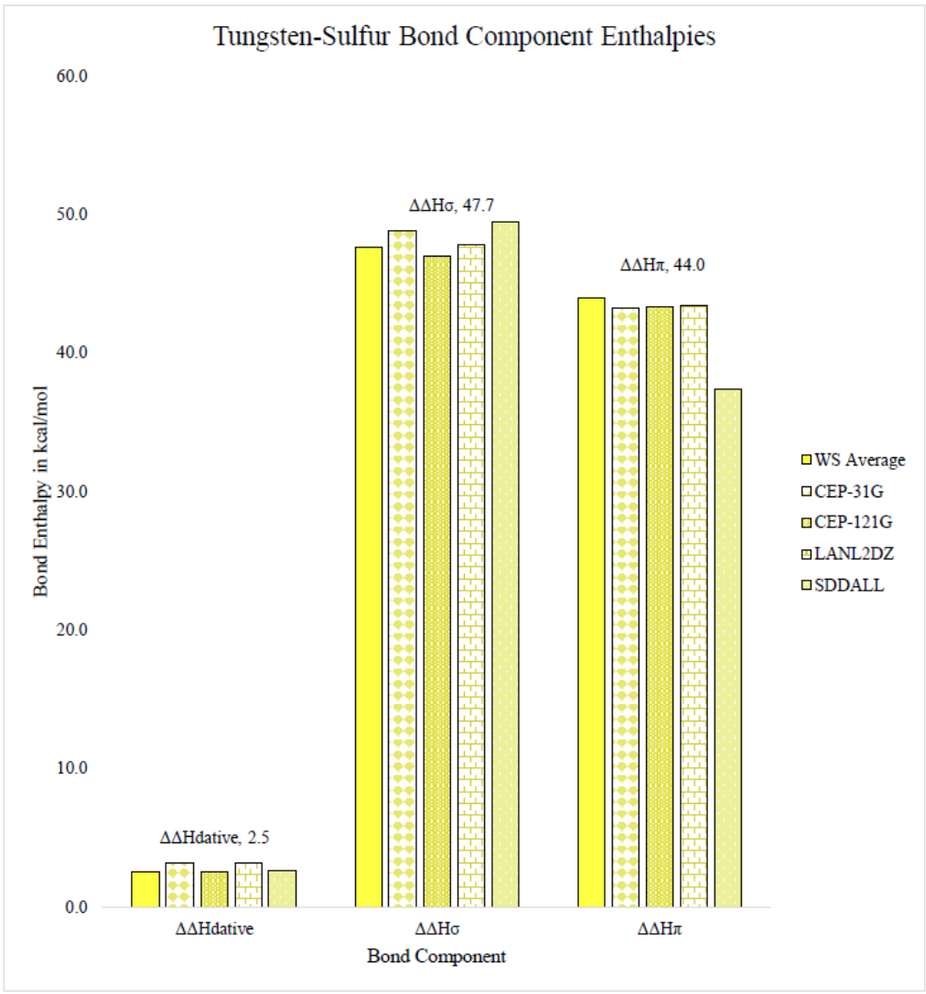

Figure B.4.1-3: Average tungsten-sulfur (columns) bond enthalpies by bond type and basis set. Average tungsten-carbon values (left-most solid column) are inset above the columns; the textured columns the average values for each valence basis set.

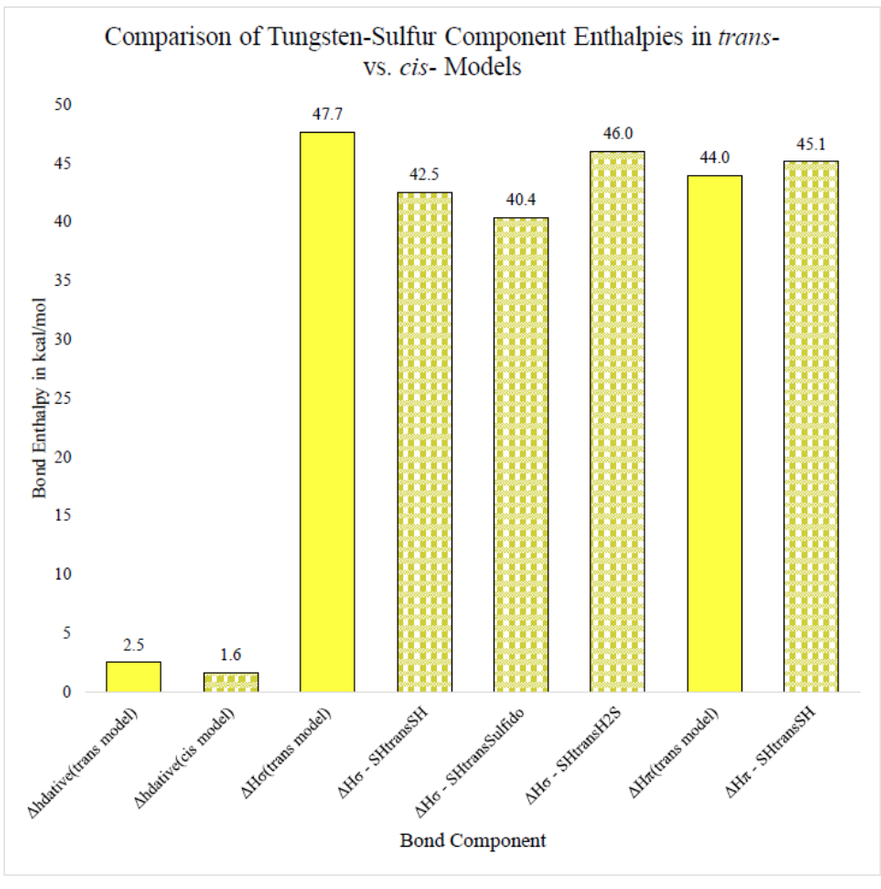

Figure B.4.1-4: Calculated average DFT bond enthalpies for the trans effect in the tungsten-sulfur model, values inset in kcal/mol.

B.4.2 Comparison of Average DFT Calculated BDEs for W-3p Elements to CCSD(T) BDE Calculations

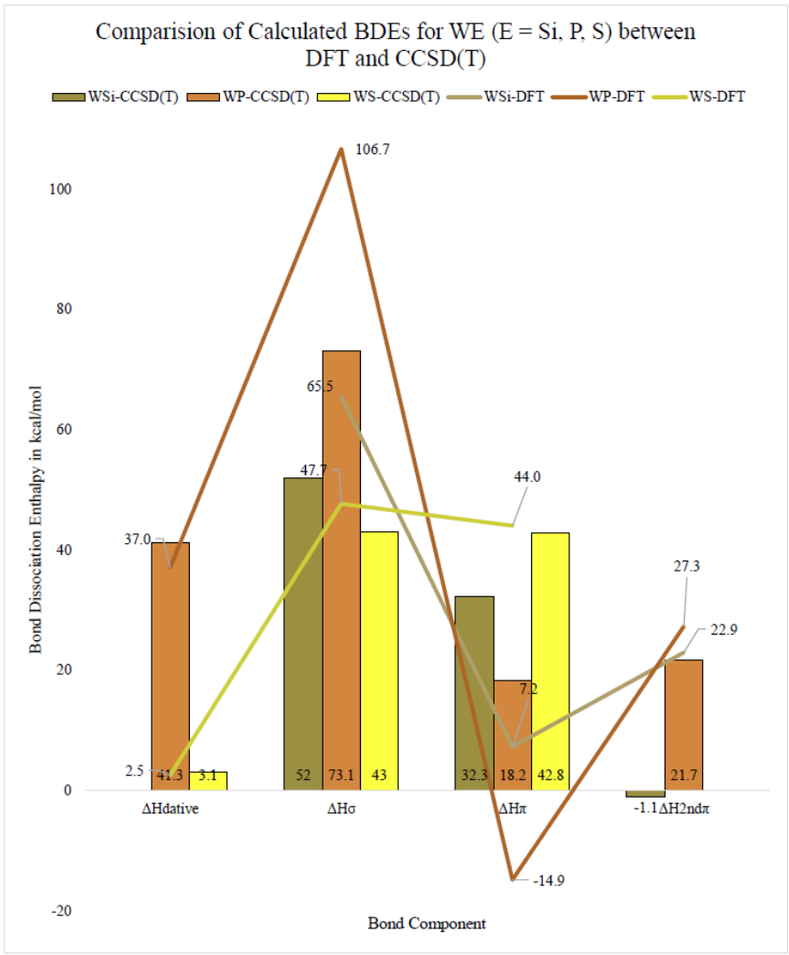

Figure B.4.2: Comparison of average DFT calculated BDEs for W-3p elements to CCSD(T) BDE calculations in kcal/mol with values inset.

B.4.3 Alternate Visualizations of BDEs for Tungsten-Element Bonds and Their Components

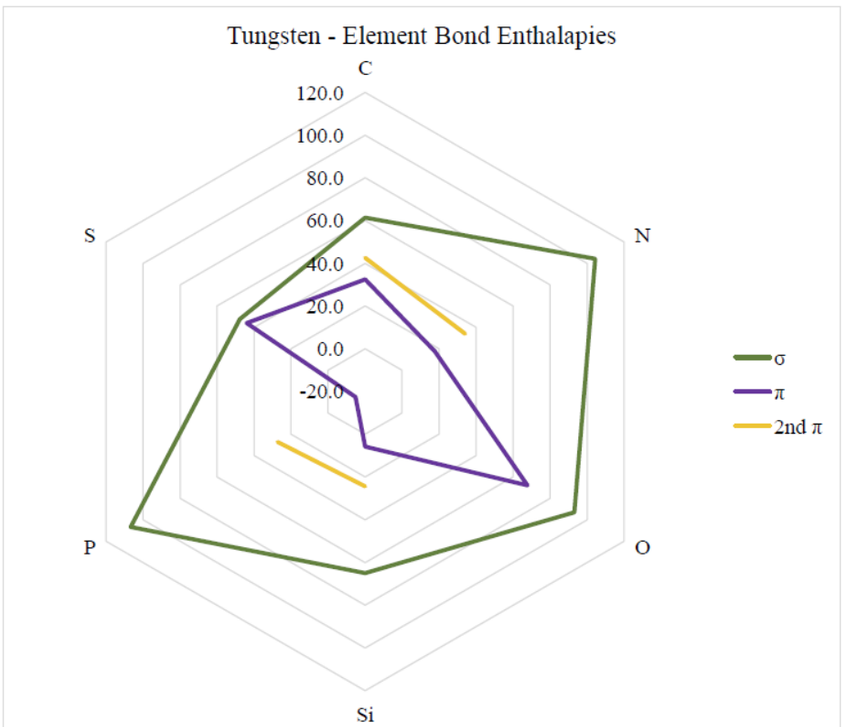

Figure B.4.3-1: Radar chart that illustrates how the 2nd π-bond enthalpies are clearly less than the 1st π-bond enthalpies in all cases modeled and that all π-bonds regardless of bond order have lower BDEs than the σ-bonds.

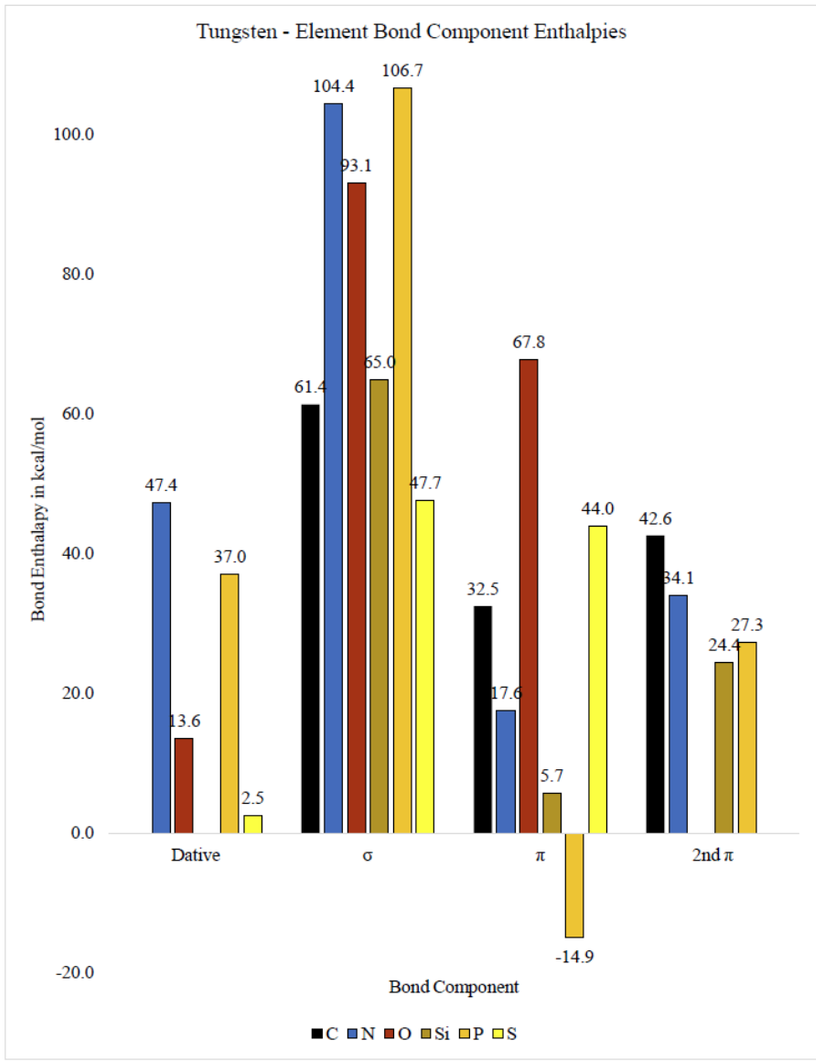

Figure B.4.3-2: Side by side bar chart comparing all tungsten-element bond component enthalpies modeled, all inset values are in kcal/mol for their respective WE bond component.

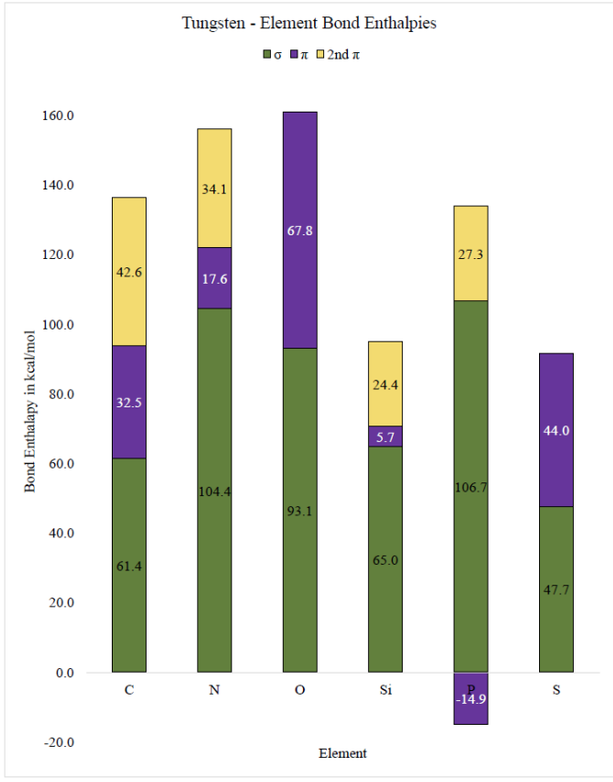

Figure B.4.3-3: Stacked bar chart illustrating how the component bond enthalpies stack together to form the double and triple bond enthalpies calculated. Values inset are the component enthalpies in kcal/mol.

B.5 Perdew's Jacob's Ladder of Chemical Accuracy

Table B.5-1: Comparisons of percent error EE small molecule main group homolog bond dissociation energies with respect to experimental, G4 level of theory for all p-block elements.

Basis	Psuedo-potential	Carbon			Nitrogen			Oxygen		2p Avg	Silicon			Phosphorus			Sulfur		3p Avg	Overall	
		Single	Double	Triple	Single	Double	Triple	Single	Double		Single	Double	Triple	Single	Double	Triple	Single	Double		Avg	Std Dev
BLYP	CEP 31G	16.2	10.5	17.1	15.68	11.70	8.6	3.5	0.8	10.5	7.4	8.3	2.5	8.5	4.7	2.3	10.9	1.5	5.8	8.1	5.3
	CEP 121G	17.2	9.8	13.0	14.35	11.00	6.2	3.5	0.6	9.5	8.8	9.2	3.6	8.7	4.9	2.2	10.3	1.3	6.1	7.8	4.9
	LANL2DZ	11.7	3.8	5.6	3.90	1.43	1.0	11.8	11.5	6.4	3.1	12.6	14.5	7.0	3.9	1.4	10.5	1.6	6.8	6.6	4.7
	Sddall	15.5	7.4	57.1	12.43	7.58	2.0	9.3	3.1	14.3	4.3	2.4	0.9	10.3	11.5	4.5	11.9	2.8	6.1	10.2	13.3
BP86	CEP 31G	10.2	0.9	11.9	15.7	11.7	8.6	4.9	6.9	8.9	2.7	4.4	9.9	0.6	1.8	2.1	1.7	5.1	3.5	6.2	4.6
	CEP 121G	11.1	5.1	7.7	4.8	4.5	2.0	4.9	7.0	5.9	3.5	3.8	8.9	0.5	1.7	2.3	1.1	5.4	3.4	4.6	2.9
	LANL2DZ	6.8	0.4	2.5	3.7	2.8	1.2	19.2	16.2	6.6	1.7	25.5	27.1	2.1	2.6	3.1	1.3	5.1	8.6	7.6	9.0
	Sddall	9.7	2.8	4.5	3.2	1.4	2.0	0.3	4.6	3.6	0.2	8.8	12.4	1.3	1.1	0.3	2.2	4.2	3.8	3.7	3.6
N12	CEP 31G	2.0	0.0	7.6	4.76	0.24	4.7	14.1	7.8	5.2	4.7	11.9	21.6	12.9	11.1	4.6	7.4	10.9	10.6	7.9	5.7
	CEP 121G	3.0	0.9	2.8	6.50	0.65	1.9	14.6	7.6	4.7	3.1	11.2	37.2	12.1	10.4	4.5	7.8	11.0	12.2	8.5	8.8
	LANL2DZ	2.1	15.7	1.6	8.04	5.78	14.7	14.5	2.7	8.1	27.2	11.8	93.3	15.6	12.6	5.7	7.9	10.2	23.0	15.6	21.7
	Sddall	0.7	3.1	0.2	9.53	5.61	2.3	10.1	6.0	4.7	8.0	17.4	27.6	11.8	9.3	3.8	6.0	9.8	11.7	8.2	6.8
PBEPBE	CEP 31G	7.5	3.9	9.9	3.88	3.39	4.0	7.7	8.6	6.1	0.2	10.5	14.1	3.6	1.5	1.2	1.2	6.2	4.8	5.5	4.0
	CEP 121G	8.3	10.5	5.7	3.04	3.22	2.0	7.8	8.8	6.2	1.0	9.8	13.1	3.6	1.3	1.1	1.7	6.4	4.8	5.5	3.9
	LANL2DZ	3.7	1.6	0.3	3.59	5.67	6.8	7.1	6.6	4.4	4.0	31.2	31.0	5.0	2.1	0.3	2.3	4.9	10.1	7.3	9.5
	Sddall	7.1	0.9	2.7	0.83	0.54	1.4	1.7	1.9	2.1	2.7	15.5	16.8	1.7	1.5	3.7	4.3	2.9	6.1	4.1	5.0
SOGGALL	CEP 31G	1.9	1.0	7.6	7.92	3.28	4.3	22.3	16.7	8.1	9.7	10.6	20.2	12.4	9.2	2.4	8.2	10.4	10.4	9.3	6.3
	CEP 121G	0.4	1.9	3.6	9.60	3.94	2.3	21.9	16.9	7.6	8.3	11.0	21.0	12.9	9.1	2.4	8.7	10.5	10.5	9.0	6.6
	LANL2DZ	0.5	4.2	1.5	12.06	0.45	10.4	24.1	15.1	8.5	11.3	24.2	30.6	8.0	7.4	3.5	0.9	8.0	11.7	10.1	9.2
	Sddall	2.9	1.9	1.6	4.57	4.06	1.7	10.1	12.0	4.9	8.2	16.6	25.9	9.1	5.5	0.1	6.3	8.8	10.1	7.5	6.6
M06	CEP 31G	0.1	2.9	9.5	1.48	7.35	19.1	2.7	10.5	6.7	16.8	1.1	11.2	20.9	19.4	1.9	11.3	13.2	12.0	9.3	7.1
	CEP 121G	1.1	2.3	5.4	1.26	9.57	17.2	3.7	11.1	6.5	58.7	3.6	12.7	20.9	18.2	3.7	11.9	13.2	17.9	12.2	13.9
	LANL2DZ	3.3	0.9	3.8	2.62	5.06	9.1	1.1	4.1	3.7	51.2	27.7	28.5	24.4	20.3	2.9	13.2	12.7	22.6	13.2	14.0
	Sddall	2.2	0.3	3.4	0.70	6.35	19.4	16.9	15.4	8.1	55.8	6.7	18.4	20.3	16.8	2.2	11.6	12.3	18.0	13.1	13.4
M11L	CEP 31G	3.2	0.1	14.6	11.48	9.87	10.4	24.9	8.1	10.3	4.2	0.3	22.5	10.2	25.2	25.1	0.5	31.0	14.9	12.6	10.2
	CEP 121G	4.5	0.2	1.3	4.74	8.05	13.5	24.9	4.4	7.7	82.3	1.6	21.9	9.0	23.3	24.5	0.7	30.6	24.2	16.0	20.4
	LANL2DZ	1.1	3.3	7.4	4.45	0.75	1.8	5.0	5.1	3.6	6.9	22.1	39.3	12.7	26.2	24.9	0.6	29.6	20.3	12.0	12.3
	Sddall	2.5	2.4	3.3	11.86	13.27	14.1	34.8	9.6	11.5	6.9	9.0	26.9	7.8	22.1	23.3	0.8	29.6	15.8	13.6	10.6
MN12L	CEP 31G	1.4	4.1	8.9	9.37	7.17	17.7	14.7	1.8	8.1	21.0	10.9	48.2	32.8	40.0	33.6	24.5	42.8	31.7	19.9	15.3
	CEP 121G	0.5	3.4	5.6	9.10	13.73	18.6	14.6	6.3	9.0	20.5	12.8	46.7	32.1	38.9	33.4	25.0	42.5	31.5	20.2	14.6
	LANL2DZ	0.7	0.0	3.1	0.44	4.25	5.6	2.9	11.0	3.5	27.2	11.8	78.6	35.5	42.8	34.9	25.8	45.0	37.7	20.6	22.3
	Sddall	1.4	5.5	1.9	10.52	19.75	22.6	24.4	1.2	10.9	25.5	8.7	60.5	31.2	37.7	30.9	24.3	41.6	32.6	21.7	16.6
	CEP 31G	37.8	23.2	26.1	15.00	15.11	12.4	14.6	8.4	19.1	2.2	5.2	7.7	6.9	8.6	8.2	12.2	6.3	7.2	13.1	9.1

Basis	Psuedo-potential	Carbon			Nitrogen			Oxygen		2p Avg	Silicon			Phosphorus			Sulfur		3p Avg	Overall	
		Single	Double	Triple	Single	Double	Triple	Single	Double		Single	Double	Triple	Single	Double	Triple	Single	Double		Avg	Std Dev
B3LYP	CEP 121G	13.5	10.3	11.3	13.49	14.14	9.7	14.4	8.2	11.9	3.4	5.7	8.7	6.9	8.8	8.0	11.7	6.1	7.4	9.6	3.3
	LANL2DZ	9.3	6.0	5.0	5.13	6.84	6.0	2.9	0.4	5.2	2.1	17.0	9.8	5.5	8.1	7.4	12.0	6.5	8.6	6.9	4.0
	Sddall	12.1	8.0	8.4	12.12	11.27	6.1	19.3	11.0	11.0	0.8	0.4	4.4	8.8	11.5	10.4	12.8	7.4	7.1	9.0	4.7
B97D	CEP 31G	5.2	3.3	10.7	3.17	5.07	6.2	3.1	5.1	5.2	7.9	1.2	10.0	40.4	3.9	5.6	3.6	4.0	9.6	7.4	9.2
	CEP 121G	6.7	2.6	6.6	1.65	4.11	3.7	2.6	4.9	4.1	6.9	0.6	9.0	1.5	3.6	5.0	3.0	4.0	4.2	4.2	2.3
	LANL2DZ	7.8	1.9	5.3	7.11	4.13	1.1	22.0	17.8	8.4	12.6	22.5	27.4	3.4	5.2	7.1	1.4	6.0	10.7	9.5	8.4
	Sddall	5.2	0.1	3.3	0.36	1.46	0.1	1.7	5.3	2.2	10.6	5.9	13.4	0.5	29.2	23.3	0.3	5.0	11.0	6.6	8.6
B2PLYP	CEP 31G	7.9	4.7	12.2	13.09	14.54	12.7	15.0	9.9	11.2	2.8	0.9	2.9	7.3	12.1	12.6	14.0	10.6	7.9	9.6	4.6
	CEP 121G	8.3	3.3	7.1	10.90	12.75	9.4	13.3	8.5	9.2	44.7	47.5	1.8	6.5	11.0	10.9	12.6	9.5	18.1	13.6	13.1
	LANL2DZ	5.6	0.3	2.2	5.17	7.83	7.2	5.8	3.9	4.8	7.7	22.8	15.9	5.4	11.3	11.7	13.9	10.7	12.4	8.6	5.7
	Sddall	7.6	1.2	4.5	10.71	10.90	6.8	17.4	11.0	8.8	5.3	5.1	7.2	9.0	14.6	14.4	14.1	11.1	10.1	9.4	4.4
MP2	CEP 31G	0.4	3.4	3.9				4.9	7.6	4.0	7.7	17.3	1.3	9.0	20.4	25.3	15.6	17.6	14.3	10.3	8.0
	CEP 121G	1.0	6.0	2.8				0.7	4.9	3.1	8.4	21.2	48.8	6.8	16.8	21.3	12.4	14.8	18.8	12.8	12.9
	LANL2DZ	0.9	7.0	5.4				0.2	4.8	3.7	14.0	40.9	22.9	5.3	18.7	24.1	14.9	17.1	19.7	13.6	11.5
	Sddall	0.5	7.5	5.0				4.3	6.5	4.8	9.2	23.1	7.3	10.0	22.3	26.5	14.6	17.3	16.3	11.9	8.2

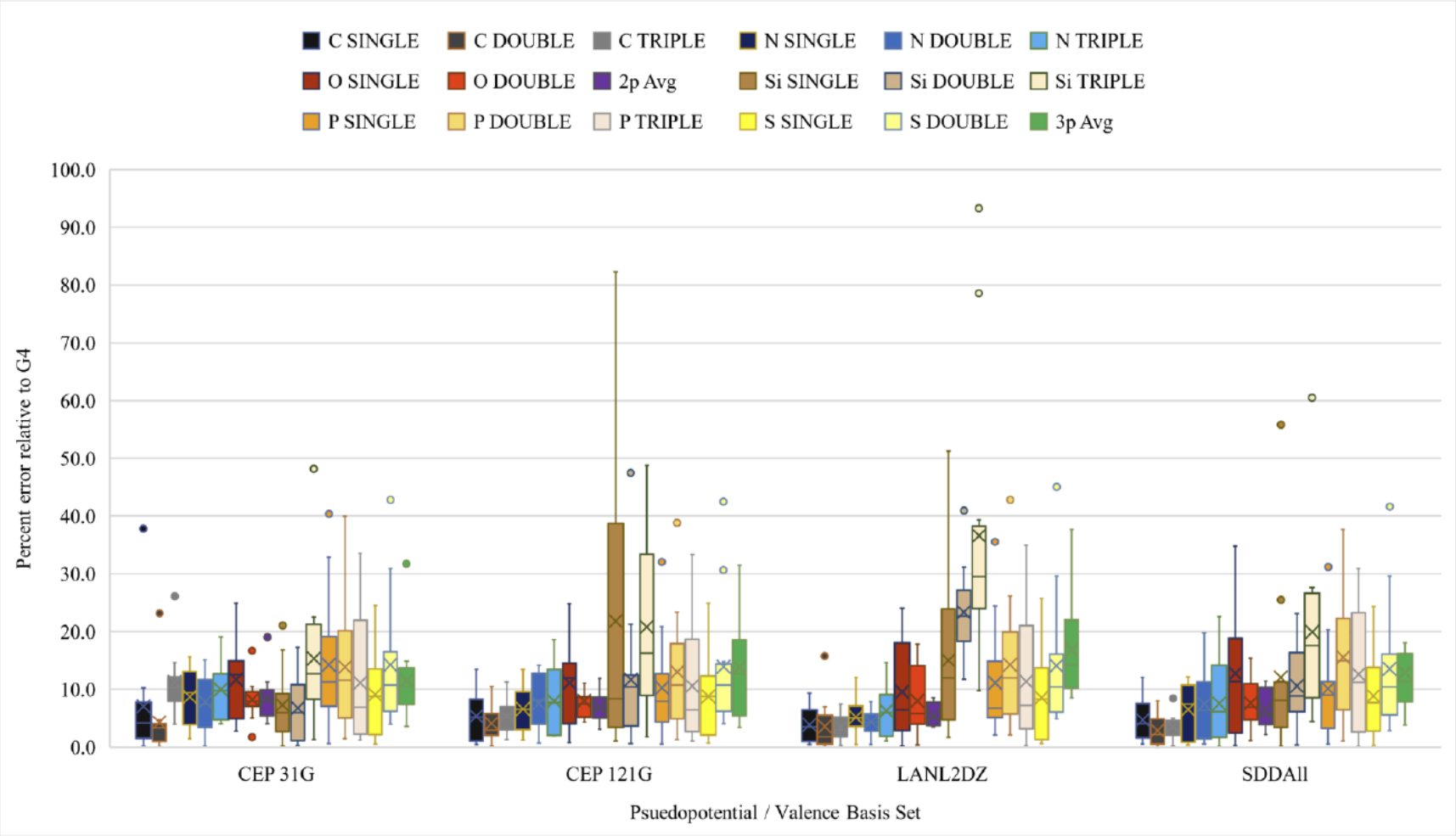

Figure B.5-1: Box and whisker plot showing percent absolute error (y-axis) in DFT-predicted BDEs as a function of bond type for main group molecules with respect to G4 calculated BDEs. The arithmetic mean is indicated with an X, the median depicted with a horizontal line, and the outliers are left as dots.

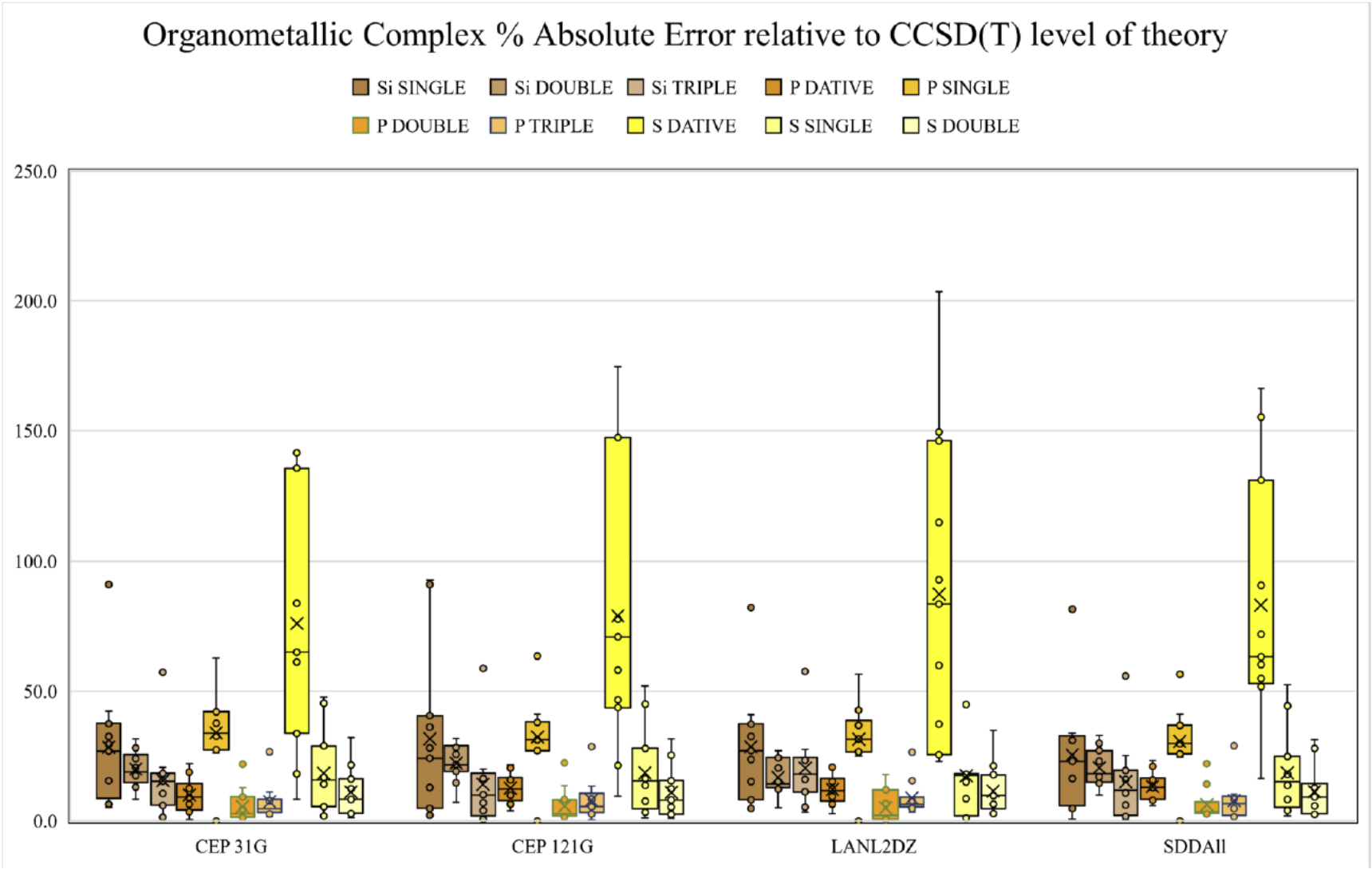

Figure B.5-2: Box and whisker plot showing percent absolute error (y-axis) in DFT-predicted BDEs as a function of bond type for main organometallic molecules with respect to DLPNO-CCSD(T) calculated BDEs. The arithmetic mean is indicated with an X, the median depicted with a horizontal line, and the outliers are left as dots.

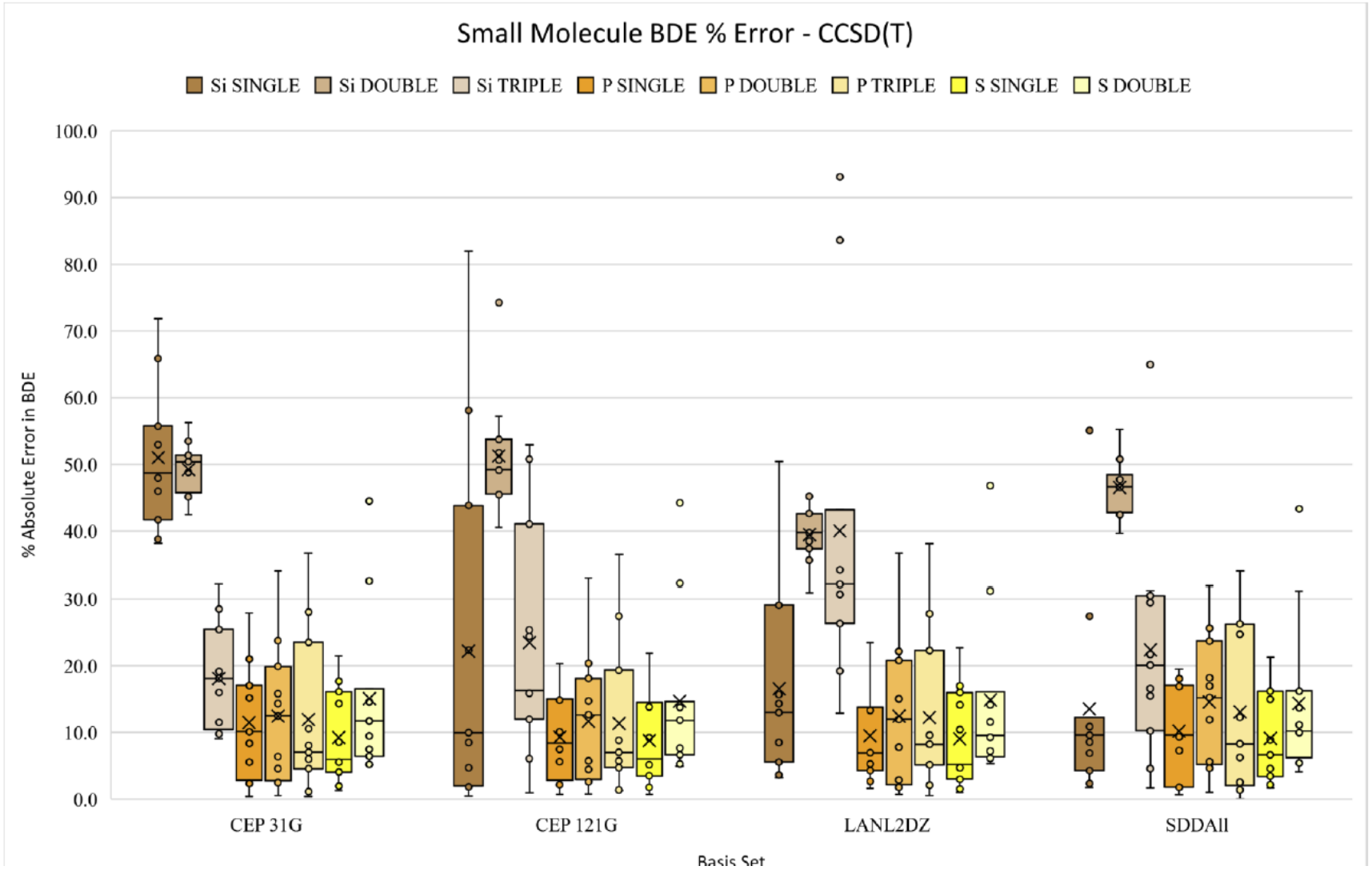

Figure B.5-3: Box and whisker plot showing percent absolute error (y-axis) in DFT-predicted BDEs as a function of bond type for main group molecules with respect to DLPNO-CCSD(T) calculated BDEs. The arithmetic mean is indicated with an X, the median depicted with a horizontal line, and the outliers are left as dots.

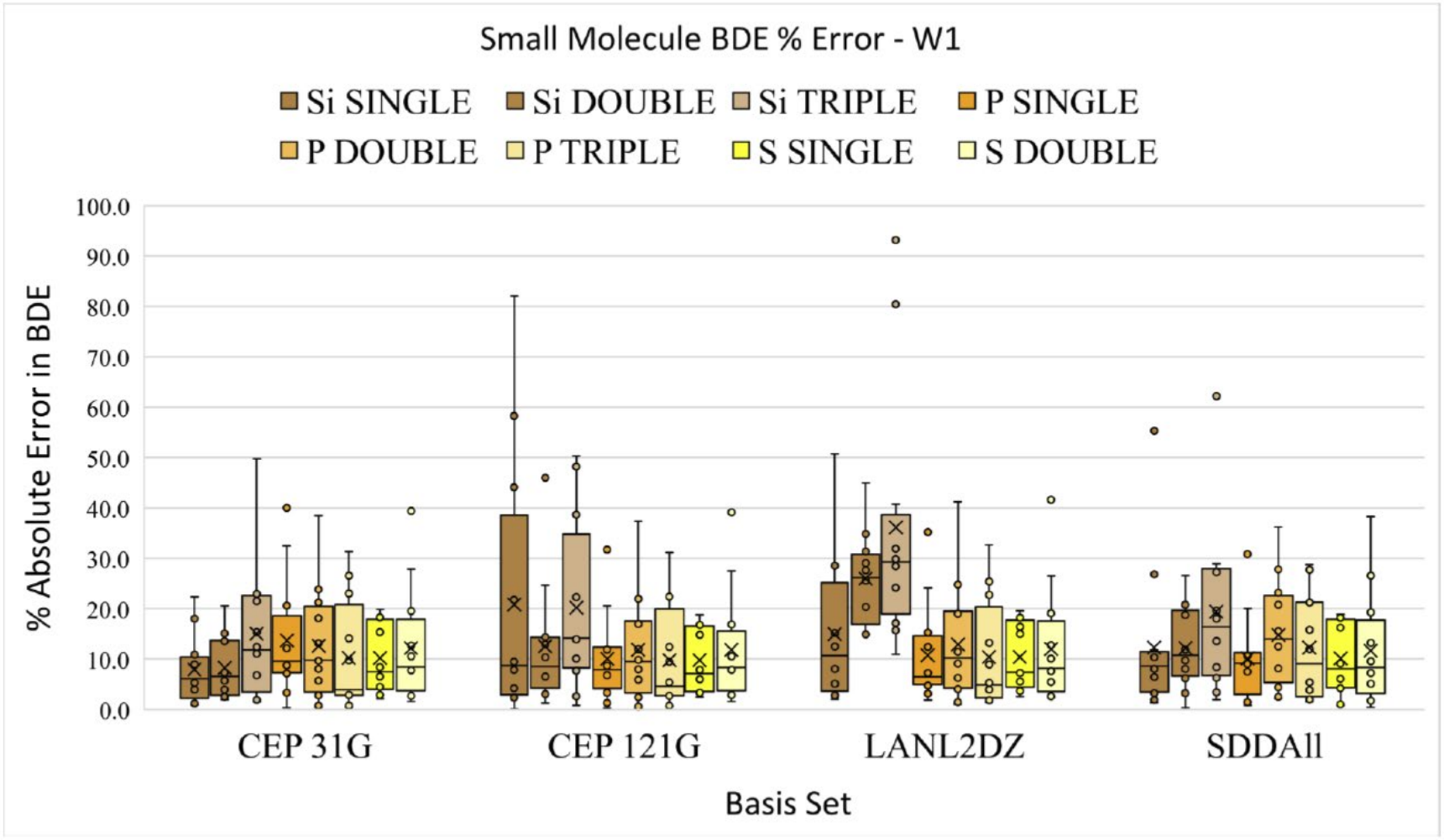

Figure B.5-4: Box and whisker plot showing percent absolute error (y-axis) in DFT-predicted BDEs as a function of bond type for main group molecules with respect to W1 calculated BDEs. The arithmetic mean is indicated with an X, the median depicted with a horizontal line, and the outliers are left as dots.

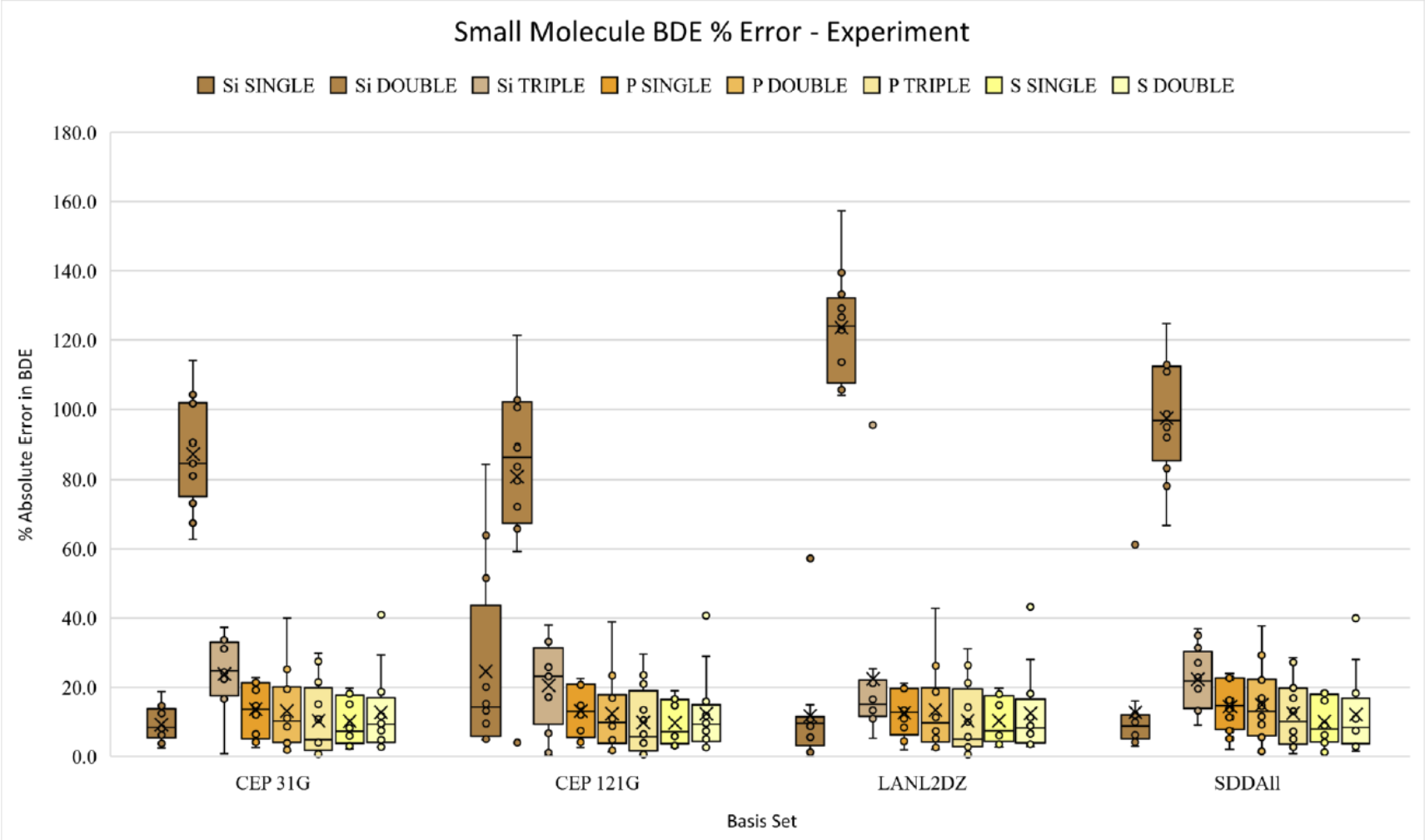

Figure B.5-5: Box and whisker plot showing percent absolute error (y-axis) in DFT-predicted BDEs as a function of bond type for main group molecules with respect to experimental data BDEs. The arithmetic mean is indicated with an X, the median depicted with a horizontal line, and the outliers are left as dots.

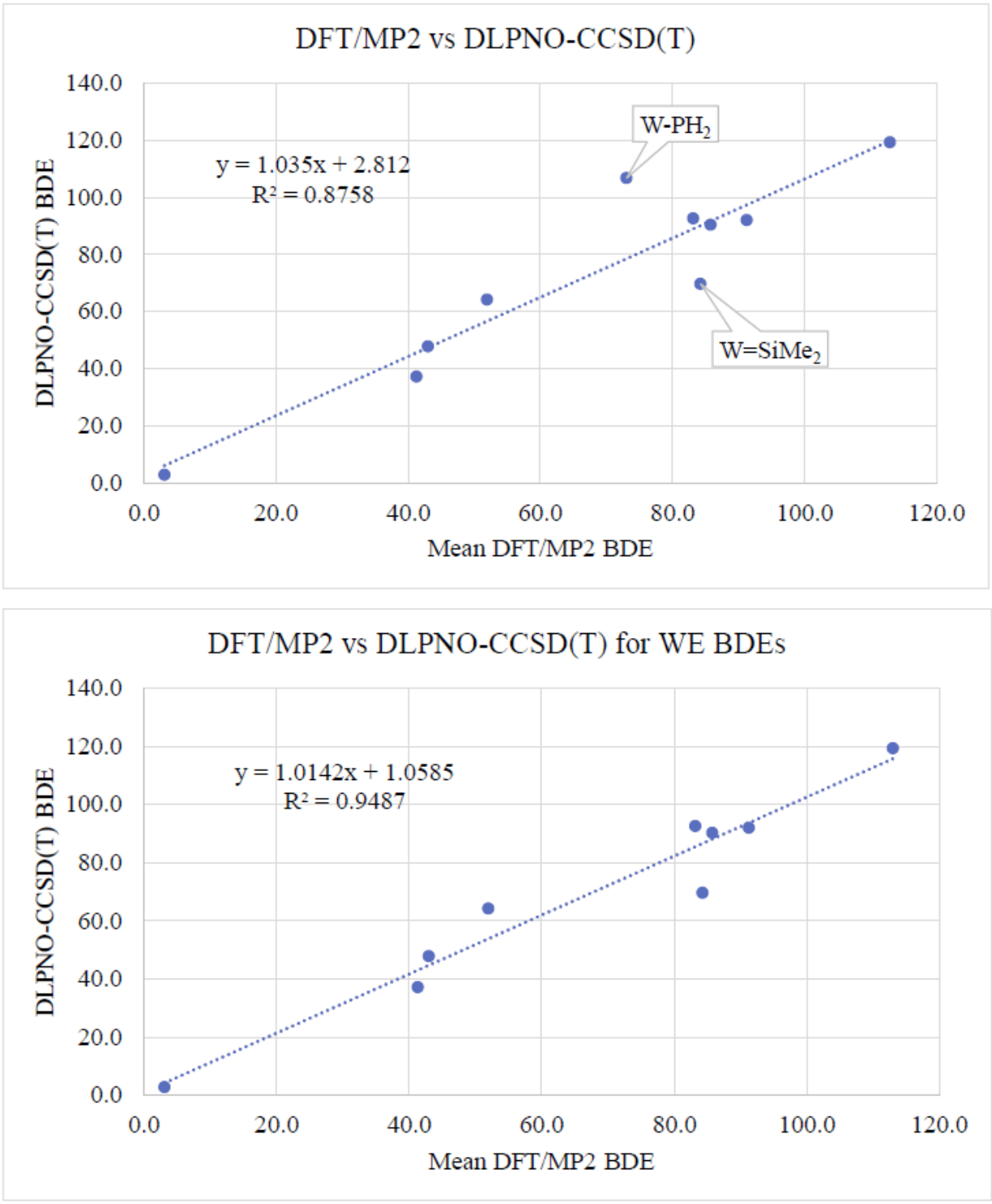

Figure B.5-6: Side by side comparison of DFT/MP2 vs. DLPNO-CCSD(T) WE BDE correlations with and without the most significant outliers.

Table B.5-2: The precent absolute errors found as each of the DFT functionals is compared to the BDEs calculated G4 for the 3p small molecule homologs, then the 2p and 3p small molecule homologs, then a comparison of the small molecule homolog BDEs to the CCSD(T) BDEs under the SM column, and finally the organometallic complex BDEs compared to the CCSD(T) BDEs presented as a Jacob's Ladder, a specific note is made of whether or not the dative moiety is coordinated to the organometallic model or not at the top.

	Basis	G4			CCSD(T)		
		2p	3p	overall 2/3p	SM	OM-3p	OM-3p w/o dat
Double hybrid - GGA	B2PLYP	8.5	12.1	10.3	20.0	20.1	16.1
w/dispersion	B97D	8.5	12.1	10.3	16.3	18.1	13.2
hybrid-GGA	B3LYP	11.8	7.5	9.7	16.2	19.5	13.7
meta-GGA	M06	6.3	17.6	11.9	21.8	17.5	17.1
	M11L	8.3	18.8	13.5	24.1	16.9	12.3
	MN12L	7.9	33.4	20.6	37.7	30.4	26.4
GGA	BLYP	10.1	6.2	8.2	14.5	19.0	9.9
	BP86	6.2	4.8	5.5	12.8	23.5	12.9
	N12	5.7	14.4	10.0	18.1	26.1	16.5
	PBEPBE	4.7	6.4	5.6	12.2	16.5	11.1
	SOGGALL	7.3	10.7	9.0	14.4	20.2	16.5
Post-HF	MP2	3.9	17.3	12.1	22.9	53.3	41.7

B.6 Further Explanation

B.6.1 MP2 Homolytic Bond Dissociation Enthalpies (BDEs)

B.6.1.1 Silicon

There is a modest difference when the MP2 results are not included in the averages for the BDE values. The W≡Si, W=Si, W–Si bonds have calculated BDEs of 91.8 ± 5.9, 67.5 ± 5.7, and 62.0 ± 7.3 kcal/mol, respectively, for just the DFT functionals. This difference in the averages yields WSi component bond enthalpies: 24.3 ± 6.3, 5.5 ± 3.4, and 62.0 ± 7.3 kcal/mol, respectively, for the 2nd π bond, 1st π bond, and σ-bonds. The small main group homologs: MeSi≡SiMe, Me_2Si=$SiMe_2$, and Me_3Si–$SiMe_3$, have a similar modest difference when only averaging DFT functionals: 58.4 ± 15.0, 52.4 ± 15.9, and 68.7 ± 15.9 kcal/mol, respectively.

B.6.1.2 Phosphorous

There is another issue with regard to the average values: the MP2 computed values for the σ-bond BDE ~100 kcal/mol higher than those from the DFT functionals. This result implies that the assumption of a dominant, single-determinant reference state for some of the W fragments is likely not met. When the mean BDEs are computed with the MP2 functional data the 2nd π, 1st π, and σ-bond component enthalpies computed are 27.3 ± 4.6, -14.9 ± 24.5, 106.7 ± 30.4 kcal/mol, respectively. This also means the triple, double and single bond enthalpies with the MP2 computations are 119.1 ± 22.6, 91.8 ± 27.5 106.7 ± 30.4, and 37.1 ± 4.5 kcal/mol greatly increasing the standard deviations.

The small molecule homologs have bond component enthalpies of 32.9 ± 7.2, 27.9 ± 8.2, 55.0 ± 7.1 kcal/mol respectively for the 2nd π, 1st π, and σ-bonds. Once more, the 1st π-bond is considerably weaker than the 2nd π-bond, thus continuing the pattern observed with the silicon model and the work on the 2p element ligands for the model complex. There is also a similar

difference in the average BDEs when the MP2 values are removed from the dataset. The triple, double and single bond enthalpies for the small molecule main homologs without the MP2 computations are 118.5 ± 7.1, 84.6 ± 7.3, 55.6 ± 7.1 kcal/mol. The standard deviations do not change as significantly for these congeners for the inorganic bonds in the tungsten model implying the error is more in the modeling of the tungsten fragment.

B.6.1.3 Sulfur

In comparison to the tungsten-sulfur models, the small molecule homologs triplet-S_2 and HS=SH have BDEs of 107.5 ± 0.3 and 61.4 ± 0.3 kcal/mol, respectively for the sulfur-sulfur bonds. The bond component enthalpies are 46.1 ± 0.3 and 61.4 ± 0.3 for the π and σ-bonds in the main group sulfur compounds. Unlike the phosphorus and silicon cases, there is greater similarity in s and p BDEs for the sulfur models.

As the octahedral geometry allowed for the opportunity to assess the impact of the trans effect of the sulfido moiety, a second coordination isomer of the W(≡S)(–SH)$_4$(←SH_2) model was modeled in which the sulfido bond is cis to the dihydrogensulfide. A small, but significant, difference in the homolytic BDE for the bond immediately trans to the sulfido bond (≡S) of ~7.0 kcal/mol, with all other bonds less effected, was calculated.

As with the previous models, the MP2 level of theory does bias the averages. Without the MP2 values, the BDEs calculated for W(≡S)(–SH)$_4$(←SH_2) are 90.8 ± 0.5, 47.3 ± 0.6, 2.4 ± 0.4 kcal/mol, by decreasing bond order with the dative bond last. In comparison the small molecule homologs triplet-S_2 and HS=SH have BDEs of 109.7 ± 0.3 and 62.1 ± 0.3 kcal/mol, respectively for the sulfur-sulfur bonds. The bond component enthalpies are thus 43.5 ± 0.1, 47.3 ± 0.6, and 2.4 ± 0.4, respectively for the π-, σ- and dative bonds in the tungsten complex and 47.5 ± 0.3 and 62.1

± 0.3 for the π and σ-bonds in the main group sulfur compounds. However, in this case the differences are minor compared to those observed with the other models.

B.6.2 Comparison among Computational Methods

B.6.2.1 Calculated Bond Lengths vs. Crystal Structure Data

The WSi model complex has mean bond lengths of 2.57 ± 0.05 Å for the tungsten-silyl bond, 2.39 ± 0.01 Å for the tungsten-silylene bond, and 2.23 ± 0.02 Å for the tungsten-silyne bond. The average from the Cambridge database for these bond types are 2.55 ± 0.08 Å, 2.50 ± 0.09 Å, and 2.37 Å for the tungsten-silyl, -silylene, and -silyne bonds, respectively. The overall mean absolute error for tungsten-silicon bonds is 1.7 ± 1.1%. The paucity of structures with these bond types is such that there are only sixty-eight tungsten-silyl structures, eleven tungsten-silylene structures, and only a single unambiguous tungsten-silyne bond published by Fukuda *et al.*[1] The discrepancy between the model and the crystal structure averages may be a small sample set effect due to the scarcity of crystal structures with unambiguous W=Si double bonding, or differences arising from the formal oxidation state of the metal.

The mean DFT calculated bond lengths are 2.14 ± 0.02 Å, 2.27 ± 0.01 Å, 2.38 ± 0.02 Å, 2.48 ± 0.03 Å for the tungsten-phosphido (≡P), -hydrophosphinidene (=PH), dihydrophosphide (–PH_2), and -phosphine (←PH_3) respectively. There are four explicitly defined W≡P bonds[1-4] with an average length of 2.15 ± 0.02 Å and four W=P bonds with 2.34 ± 0.13 Å in the CCDC. For the W–P and the W←P bond motifs, there is a problem of definitions. There are 188 W–P single bonds where the phosphorus is clearly three-coordinate, but there are an additional 229 complexes where tungsten is ligated to a 3-coordinate phosphorus; there is no functional difference in the average bond length of these subsets: 2.49 ± 0.08 Å and 2.48 ± 0.09 Å, respectively. Tungsten-phosphine moieties are quite plentiful with 3335 entries that average 2.50 ± 0.06 Å. The mean absolute error

of 2.3 ± 1.6% in the calculated bond lengths from these structural data is respectable, but may be artificially inflated due to the small experimental sample sizes for multiply bonded moieties. However, there is reasonable agreement between theory and experiment for the measurements that do exist.

The WS model complex has a mean absolute difference for the metal-sulfur bond lengths of 1.5 ± 0.8% relative to experimental structural data, excluding the dative moiety (5.1 ± 9.5% with). In the CCDB, terminal W=S bonds average 2.16 ± 0.03 Å for 351 entries whereas tungsten-sulfur single bonds average 2.38 ± 0.11 Å for 1500 entries. The bond lengths for tungsten-thiol (W←SR_2) moieties average 2.42 ± 0.11 Å across 1012 entries. The sheer number of entries with W=S/W≡S motifs speaks to their inherent stability vis-à-vis the WP and WSi congeners, and is reflected by the computed p-bond strength. The computed DFT average bond lengths found are 2.15 ± 0.02 Å, 2.42 ± 0.02 Å, and 3.48 ± 1.06 Å for W=S/W≡S, W–S, and W←S respectively.

B.6.2.2 Oddities in the Computational Data

In the WSi model calculations, the degree of variability is a concern. Certain basis set and functional combinations yield numbers that are well out of line with the rest of the data. These are often extreme outliers. For the tungsten-silylene π-bond BDE, the LANL2DZ basis set does not yield numbers in line with the other three basis sets in nine out of the twelve functional combinations, the exceptions being SOGGALL, B2PLYP, and MP2. For example, the N12/LANL2DZ(d), tungsten-silylene π-bond BDE is 0.9 kcal/mol whereas the PBEPBE/LANL2DZ(d) tungsten-silylene π-bond BDE is 11.6 kcal/mol both beyond the standard deviation of 3.3 kcal/mol for the mean value of 5.7 kcal/mol. Furthermore, for the organometallic fragments less the single bond, viz W(=SiMe2)(≡SiMe)(dmpe), the MN12L functional optimized to a lower minima for the quartet rather than the doublet spin state for each ECP modeled, with

the exception of SDDALL; this was also the case with the N12/LANL2DZ(d) combination. The B2PLYP /SDDALL(d), M11L/CEP-121G(d), and M11L/CEP-31G(d) levels of theory found the triplet spin state to be the more stable minima for Si_2Me_2.

In the WP model, as noted above, the MP2 wavefunction – with any of the valence basis set/pseudopotential combinations – yields predicted BDEs so far out of line with the DFT data that it was removed from the averages as an outlier. To wit, the σ bond enthalpies found with the MP2 method are 203.3 ± 5.9 kcal/mol for the different valence basis set/pseudopotential combinations. This value is more than 100 kcal/mol higher than those predicted via the DFT functionals, and 96 kcal/mol adrift of the DLPNO-CCSD(T)/def2-QZVPP value. The underlying assumptions required for the perturbation theory to be effective are obviously invalid for the fragments derived from W–P homolysis, possibly due to weaker metal-3p ligand bonding and the potential for low energy states in these fragments. It is worth noting that analysis of the DLPNO-CCSD(T) amplitudes did not indicate any higher than 0.08. The large discrepancies seen in MP2 predictions are consistent with the observations of Pople and coworkers in terms of small molecule thermochemistry, which motivated their initial research efforts into composite Gaussian-n methods.[1]

In the WS model complexes, the homolytic cleavage of the W–S single bond from the tungsten frequently resulted in the H_2S ligand dissociating from the organometallic fragment as well. Likewise, for the W←S bond about three quarters of the models coordinate a dative bond and the other quarter do not. For such simulations, the bond between the tungsten and the dihydrogensulfide was manually enforced through the ModRedundant command in Gaussian. In view of the small calculated W←SH_2 BDE of 2.7 ± 3.0 kcal/mol (DLPNO-CCSD(T)/def2-QZVPP, 3.1 kcal/mol), this is not expected to have a major impact on the other tungsten-sulfur BDEs. Also,

there is a small valence basis set dependence for the WS BDEs where SDDALL gives lower values for the tungsten-sulfide (~7 kcal/mol) and higher values for tungsten-thiolate bonds (~2 kcal/mol).

B.6.2.3 Accuracy vs. Higher-level Theory and Experiment for BDEs of Main Group Homologs

With respect to the G4 level of theory for the main group 3p homologs, the best performing valence basis set/functional combination is BP86/CEP-121G(d) whereas for the overall set of 2p and 3p homologs it is BP86/SDDALL(d). This is different from the PBEPBE/SDDALL(d) as the best performer for the 2p homologs. The Minnesota functionals and the MP2 methods perform particularly poorly and caution is advised for their use in BDE calculations.

It is reasonable to conclude that the increased error in the 3p BDE models convolutes with the error in modeling the 5d metal-3p element BDEs thereby increasing the total error of tungsten-3p element models. Data also imply that the overall variance in the DFT-predicted bond enthalpies are more due to limitations in modeling of tungsten-containing rather than the 3p-containing fragment. A full reporting of the values calculated for E–E, E=E, and E≡E bond with the reported error with respect to experiment and *ab initio* calculations is given in the Supporting Information spreadsheets.

B.6.3 Comparison of W-3p Ligands with W-2p Ligands

Overall, the computed bond enthalpies for WE-3p bonds show an expected decrease in strength relative to their WE-2p congeners. The net sum of all bond components in the WSi is ~41 kcal/mol less than these components in the corresponding WC model; the WP model is ~37 kcal lower than the net sum of all bonds for the WN model. Interestingly, the chalcogen models have computed BDE sums that are roughly equivalent: WS model ~ 92 kcal double bond to the single bonds in the WO model (~91 for WO), which is consistent with tungsten's oxophilicity.[2] With the

exception of the WC vs. WSi σ-bonds and WN vs. WP σ-bonds, each of the bond components is observed to be weaker in the W-3p congener.

B.6.4 References for this Section

1. Fukuda,T.; Yoshimoto, T.; Hashimoto, H.; Tobita, H.; synthesis of a tungsten–silylyne complex via stepwise proton and hydride abstraction from a hydrido hydrosilylene complex. *Organometallics* **2016** *35*, 921-924

2. Balázs, G.; Green, J. C.; Scheer, M. Terminally coordinated AsS and PS ligands. *Chem. - A Eur. J.* **2006***, 12*, 8603–8608.

3. Scheer, M.; Kramkowski, P.; Schuster, K. An approach to novel complexes with a tungsten-phosphorus triple bond. *Organometallics* **1999***, 18*, 2874–2883.

4. Cowley, A. H.; Pellerin, B.; Atwood, J. L.; Bott, S. G. Cleavage of a phosphorus-carbon double bond and formation of a linear terminal phosphinidene complex. *J. Am. Chem. Soc.* **1990***, 112*, 6734–6735.

5. Zanetti, N. C.; Schrock, R. R.; Davis, W. M. Monomeric molybdenum and tungsten complexes that contain a metal–phosphorus triple bond. *Angew. Chemie Int. Ed. English* **1995***, 34*, 2044–2046.

6. Sterenberg, B. T.; Udachin, K. A.; Carty, A. J. Electrophilic “fischer type” phosphinidene complexes of molybdenum, tungsten, and ruthenium. *Organometallics* **2001***, 20*, 2657–2659.

APPENDIX C

SUPPLEMENTAL INFORMATION FOR CHAPTER 4 ON π-LOADING

C.1 Commentary on d^1 and d^2 Models

This trend continues with the d^1 models with a caveat. Each of the triply bonded moieties have decreased bond enthalpies by between 26.3 and 78.8 kcal/mol. Experimental d^1 tungsten complexes are uncommon. It is more probable that a tungsten complex would involve a redox non-innocent ligand to donate an electron to a d^0 metal center to generate a temporary d^1 state. This unusual d^1 tungsten case is where the classical π-loading is seen. When both the CH_2^{2-}, NH^{2-}, or O^{2-} moieties are bonded to the d^1 tungsten in any combination only the bond enthalpy consistently decreases as seen in Figure C.1-1.

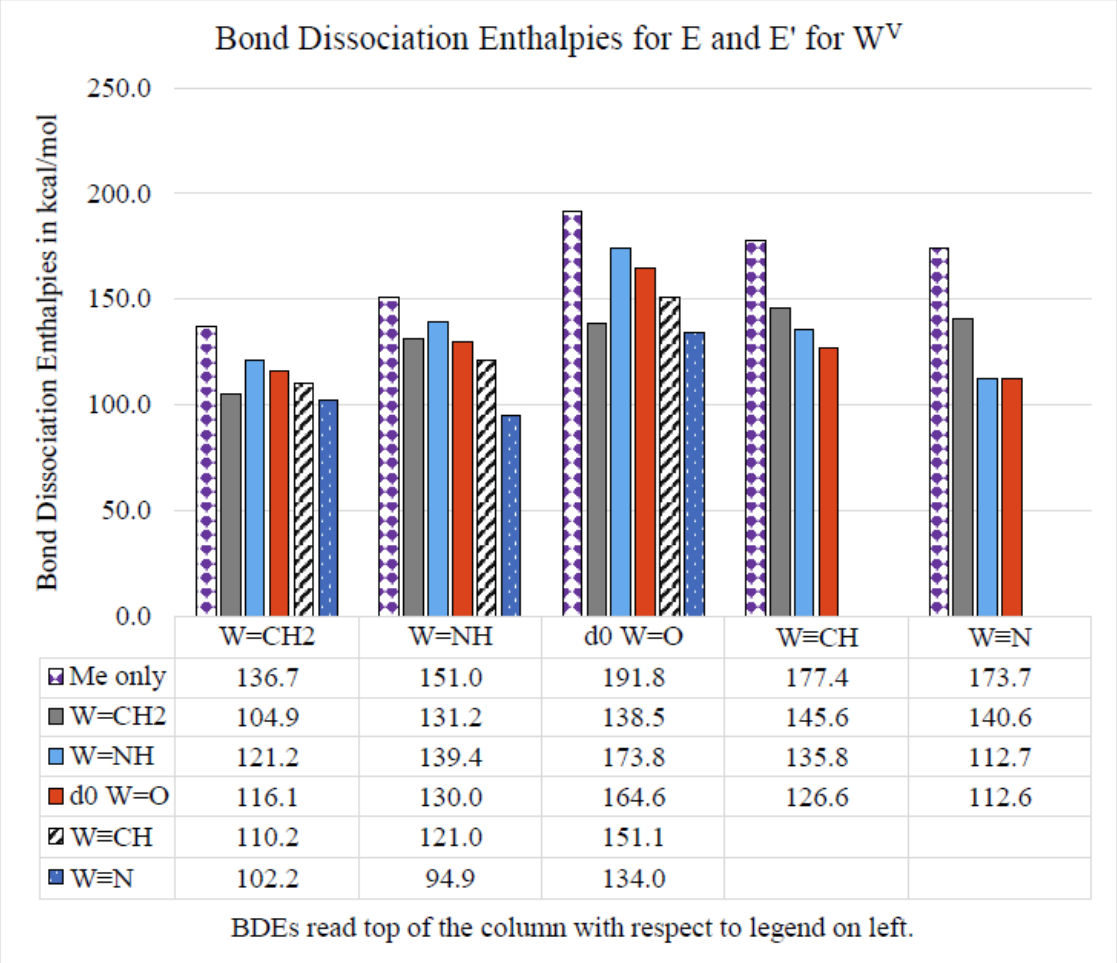

	W=CH2	W=NH	d0 W=O	W≡CH	W≡N
Me only	136.7	151.0	191.8	177.4	173.7
W=CH2	104.9	131.2	138.5	145.6	140.6
W=NH	121.2	139.4	173.8	135.8	112.7
d0 W=O	116.1	130.0	164.6	126.6	112.6
W≡CH	110.2	121.0	151.1		
W≡N	102.2	94.9	134.0		

BDEs read top of the column with respect to legend on left.

Figure C.1-1: Calculated bond dissociation enthalpies in kcal/mol for d^1 tungsten (V) complexes. Columns are clustered enthalpies for one moiety, the rows are which moiety the enthalpy listed in the column is in respect to. Note, the 'Me Only' in the purple checkerboard is the BDE of the mono-ligated species for that moiety.

The d^2 models show the continued trend (Fig. C.1-2). It seems that the additional electron density afforded by the higher d-count for the metal is key to lowering the bond dissociation enthalpy of the π-bonds. This is unlikely to exist in an experimental set up under common conditions and is only mentioned for completeness of the analysis and as a potential lead for future work.

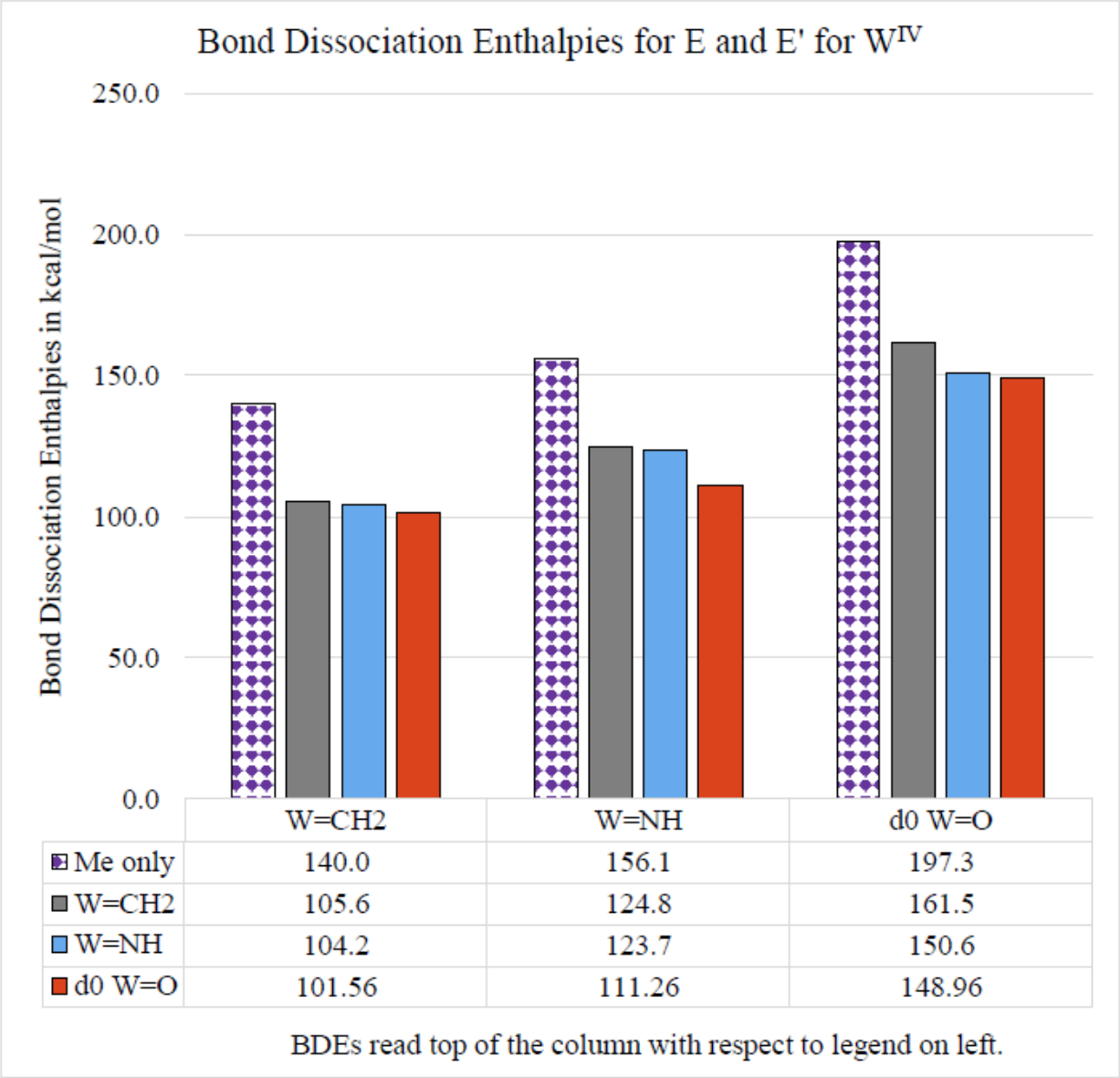

	W=CH2	W=NH	d0 W=O
Me only	140.0	156.1	197.3
W=CH2	105.6	124.8	161.5
W=NH	104.2	123.7	150.6
d0 W=O	101.56	111.26	148.96

BDEs read top of the column with respect to legend on left.

Figure C.1-2: Calculated bond dissociation enthalpies in kcal/mol for d^2 tungsten (IV) complexes. Columns are clustered enthalpies for one moiety, the rows are which moiety the enthalpy listed in the column is in respect to. Note, the 'Me Only' in the purple checkerboard is the BDE of the mono-ligated species for that moiety.

C.2 Commentary on the Distortion Energy

Next, there is the concept of distortion energy, also called snap or strain energy.[3,4] Snap energy is the energy difference between the single point instantaneous of bond cleavage and the relaxation of the two fragments into their optimized geometries which provides some insight into the molecular orbital strain found with multiple bonds.[5] The energy input needed to 'strain' the bond at the start of the reaction decreases the overall energy needed to reach the transition state ($\Delta E_{int} = \Delta E^{\ddagger} - \Sigma\Delta E_{strain}$). There is potential for this deformation energy to be the cause of the π-loading observations. These calculations are modeled at the DLPNO-CCSD(T)/def2-QZVPP//PBEPBE/SDDALL(d) level of theory.

This deformation energy consists of two parts for a single bond, the σ-bond enthalpy and the enthalpic difference from the changes in the geometry of the fragments. The higher bond orders are not quite so tidy. There is not necessarily as marked a change in the geometry between the single points at the instant of cleavage and the optimization relaxed fragments for the double and triple bonds. The difference between the relaxed and snap π-bond enthalpies are equal to the sum of individual differences between the relaxed and snapped single and double bonds in this model, by definition. This provides a means of attributing the energy in excess of what is needed to form a single bond to the π-bond enthalpies that is logically consistent.

There are significant differences in the deformation enthalpies for the tungsten-element models and the element-element models. Consider the tungsten-carbon and carbon-carbon models (Fig. C.2-1): the methyl groups have an sp^3 tetrahedral geometry prior to the cleavage, but after the geometry shifts to an sp^2 trigonal planar position. This large change explains why the difference in the deformation enthalpy would be larger for the carbon-carbon model than for the tungsten-

carbon model. The tungsten-carbon fragment in the model does not relax as dramatically as the methyl group does.

The formation of the first π-bond sees a significant jump in the deformation enthalpy for all WE models (Figs. C.2-1, C.2-2, & C.2-3). The deformation enthalpy for the first π-bonds are 20.6 and 18.0 kcal/mol for W=C and W=N, respectively. This is greater than the 15.0 and 1.5 kcal/mol deformation enthalpies for the respective W—C and W—N σ-bonds.

Once the first π-bond is in place the second π-bond only takes slightly more snap energy to form. For the WC model, the deformation enthalpy needed for from the second π-bond is only 2.1 kcal/mol higher. The WN model has second π-bond forming with only 3.7 kcal/mol greater deformation enthalpy. This is consistent with the changes in the geometry of the fragments being proportionally smaller than the difference between the σ-bond and the first π-bond.

This is further supported by the element-element congeners for the organometallic bonds. The snap enthalpy for the main group homologs decreases with the increase in hybridization. There are simply too few degrees of freedom from too few atoms in the higher bond order small molecule fragments to significantly affect the snap enthalpies.

The deformation enthalpies in the WO model (Fig. C.2-3) are almost entirely from the tungsten containing fragments. In this WO model, considerable reorganization occurs when the fragments of tungsten complex relax into their optimal geometry which results in considerably higher snap enthalpies. The deformation enthalpy for the formation of a W—O σ-bond is 16.7 kcal/mol. The tungsten oxo bond was previously found to be a triple bond, not a double bond. This means that the individual π-bond enthalpies regardless of whether deformed or relaxed are not accessible in this model. The combined first and second π-bond deformation enthalpies for the formation of the oxo moiety are 15.8 kcal/mol.

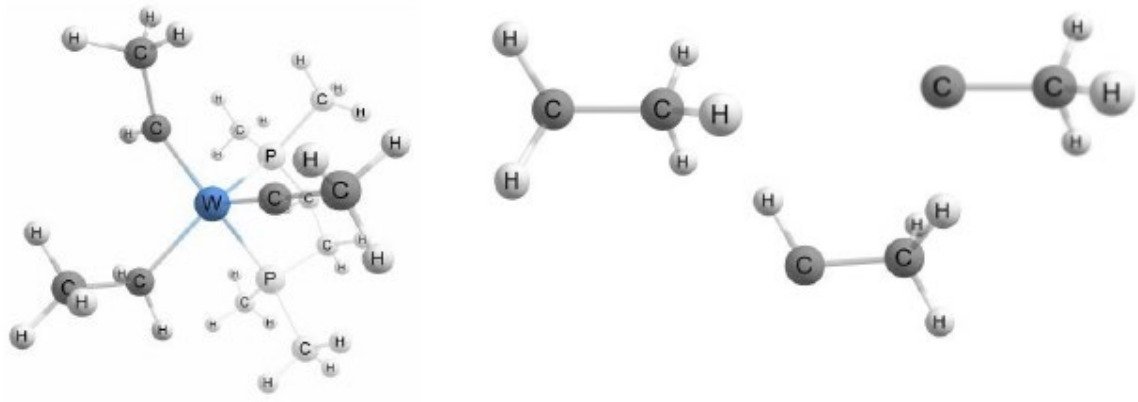

Tungsten - Element Snap Energy Calculations					Element - Element Snap Energy Calculations			
	Relaxed	Snapped	difference			Relaxed	Snapped	difference
W-C	67.2	82.2	15.0	Single	Butane	93.2	114.3	21.1
W=C	98.1	133.7	35.5	Double	Butene	174.6	187.5	12.9
W≡C	144.5	182.2	37.7	Triple	Butyne	208.8	211.3	2.5

Figure C.2-1: Deformation energies for the homolytic cleavage of the bonds for both WC (left) and CC (right) models. The table inset gives homolytic bond cleavage enthalpies in kcal/mol. The 'Snapped' enthalpies are calculated from the single points with the geometries frozen prior to the bond cleavage. The 'Relaxed' enthalpies are calculated from the optimized geometries that the fragments relax into after the homolytic cleavage is complete, (C-fragments on right). The 'difference' column gives how much higher the snap enthalpies are than the relaxed enthalpies.

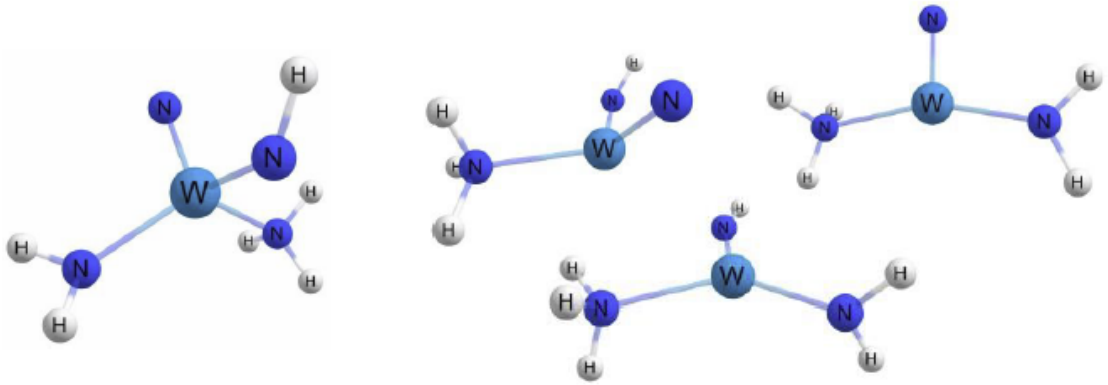

Tungsten - Element Snap Energy Calculations					Element - Element Snap Energy Calculations			
	Relaxed	Snapped	difference			Relaxed	Snapped	difference
W-N	107.0	108.5	1.5	Single	H_2N-NH_2	70.2	71.0	0.8
W=N	125.3	144.9	19.6	Double	HNNH	123.3	123.2	-0.1
W≡N	149.3	172.6	23.3	Triple	N_2	216.4	216.4	0.0
W←N	50.6	52.2	1.5	Dative				

Figure C.2-2: Deformation energies for the homolytic cleavage of the bonds for both WN (left) and NN (not shown) models. The table inset gives homolytic bond cleavage enthalpies in kcal/mol. The 'Snapped' enthalpies are calculated from the single points with the geometries frozen prior to the bond cleavage (WN fragments on right). The 'Relaxed' enthalpies are calculated from the optimized geometries that the fragments relax into after the homolytic cleavage is complete. The 'difference' column gives how much higher the snap enthalpies are than the relaxed enthalpies.

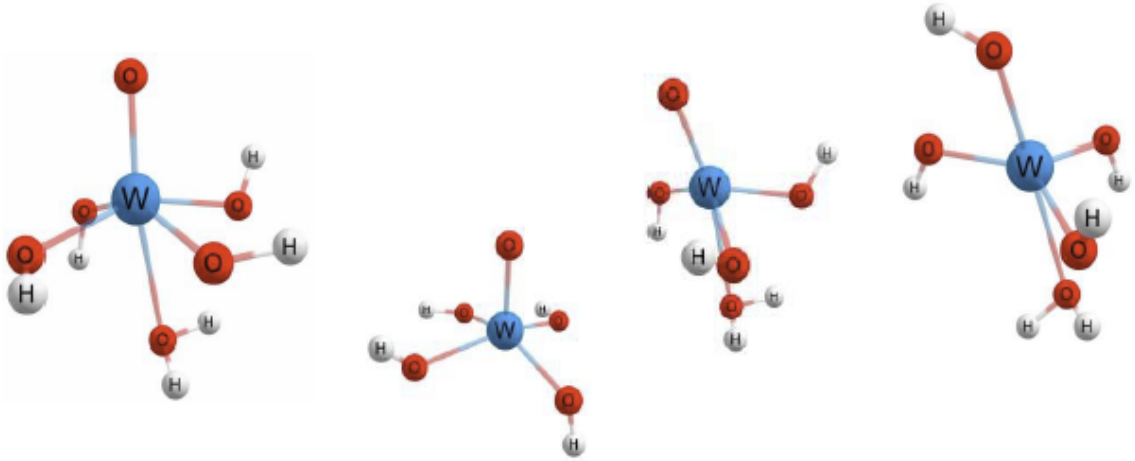

Tungsten - Element Snap Energy Calculations					Element - Element Snap Energy Calculations			
	Relaxed	Snapped	difference			Relaxed	Snapped	difference
W-OH	100.3	117.0	16.7	Single	HOOH	50.8	50.4	-0.4
W≡O	164.2	196.7	32.4	Double/trip	O_2	112.5	112.5	0.0
W←OH_2	15.1	19.6	4.6	Dative				

Figure C.2-3: Deformation energies for the homolytic cleavage of the bonds for both WO (left) and OO models (not shown). The table inset gives homolytic bond cleavage enthalpies in kcal/mol. The 'Snapped' enthalpies are calculated from the single points with the geometries frozen prior to the bond cleavage (WO fragments on right). The 'Relaxed' enthalpies are calculated from the optimized geometries that the fragments relax into after the homolytic cleavage is complete. The 'difference' column gives how much higher the snap enthalpies are than the relaxed enthalpies.

APPENDIX D

”MOMMALIES” AND OTHER QUOTES FROM THE OFFICE DOOR

1. The world is beautiful and all the more fascinating for its study.
2. Science is the iterative study of being less wrong.
3. Math is the arbiter of whether or not something is logically sound, not of whether or not it is actually true.
4. Science is about learning is beautiful and terrible truths.
5. One must love the truth to be a scientist.
6. The truth will set one free, but that does not mean it will not hurt.
7. Science: do not take someone's word that something is true, test it and know.
8. A scientist is a grown child who never left the why phase and better for it.
9. "If an elderly but distinguished scientist says that something is possible, he is almost certainly right; but if he says that it is impossible, he is very probably wrong." —Arthur C. Clarke
10. "Science never solves a problem without creating ten more." —George Bernard Shaw
11. "The saddest aspect of life right now is that science gathers knowledge faster than society gathers wisdom." —Isaac Asimov
12. "There is a single light of science, and to brighten it anywhere is to brighten it everywhere." —Isaac Asimov
13. "Science does not know its debt to imagination." —Ralph Waldo Emerson
14. "Touch a scientist and you touch a child." —Ray Bradbury
15. "No amount of experimentation can ever prove me right; a single experiment can prove me wrong." —Albert Einstein
16. "Science without religion is lame, religion without science is blind." —Albert Einstein
17. "Somewhere, something incredible is waiting to be known." —Carl Sagan
18. "Science is a way of thinking much more than it is a body of knowledge." —Carl Sagan
19. "By denying scientific principles, one may maintain any paradox." —Galileo Galilei
20. "Geologists have a saying—rocks remember." —Neil Armstrong
21. "Nothing in life is to be feared, it is only to be understood. Now is the time to understand more, so that we may fear less." —Marie Curie

22. “A new scientific truth does not triumph by convincing its opponents and making them see the light, but rather because its opponents eventually die and a new generation grows up that is familiar with it.” —Max Planck

23. “Anybody who has been seriously engaged in scientific work of any kind realizes that over the entrance to the gates of the temple of science are written the words: ‘Ye must have faith’” —Max Planck

24. “Scientists have become the bearers of the torch of discovery in our quest for knowledge.” — Stephen Hawking

25. “The reward of the young scientist is the emotional thrill of being the first person in the history of the world to see something or to understand something. Nothing can compare with that experience.” – Cecilia Payne-Gaposchkin

26. “Everything is theoretically impossible, until it is done.” – Robert A. Heinlein.

27. "If I have seen further it is by standing on the shoulders of Giants." – Issac Newton

28. “What you learn from a life in science is the vastness of our ignorance.” – David Eagleman

29. “Impossible only means that you haven’t found the solution yet.” – Anonymous

30. “Every brilliant experiment, like every great work of art, starts with an act of imagination.” – Jonah Lehrer

31. “The good thing about science is that it's true whether or not you believe in it.” – Neil deGrasse Tyson

32. “Science and everyday life cannot and should not be separated.” – Rosalind Franklin

33. “Above all, don't fear difficult moments. The best comes from them.” – Rita Levi-Montalcini

34. “Research is to see what everybody else has seen, and to think what nobody else has thought.” – Albert Szent-Györgyi

35. “If you want to have good ideas, you must have many ideas.” – Linus Pauling

36. “Science knows no country, because knowledge belongs to humanity, and is the torch which illuminates the world.” – Louis Pasteur

37. “Science means constantly walking a tightrope between blind faith and curiosity; between expertise and creativity; between bias and openness; between experience and epiphany; between ambition and passion; and between arrogance and conviction – in short, between and old today and a new tomorrow.” — Henrich Rohrer

38. “I am among those who think that science has great beauty.” – Marie Curie

39. “Research is what I'm doing when I don't know what I'm doing.” – Wernher von Braun

40. “Equipped with his five senses, man explores the universe around him and calls the adventure Science.” – Edwin Powell Hubble

41. “What is research but a blind date with knowledge?” – Will Harvey

42. “Science, my lad, is made up of mistakes, but they are mistakes which it is useful to make, because they lead little by little to the truth.” – Jules Verne

43. “Science is wonderfully equipped to answer the question 'How?' but it gets terribly confused when you ask the question 'Why?'” —Erwin Chargaff

44. “We don't regard any scientific theory as the absolute truth.” —Kenneth R. Miller

45. “The most exciting phrase to hear in science, the one that heralds new discoveries, is not 'Eureka!' but 'That's funny...'” — Isaac Asimov

46. “Science is simply common sense at its best, that is, rigidly accurate in observation, and merciless to fallacy in logic.” — Thomas Huxley

47. “Nothing has such power to broaden the mind as the ability to investigate systematically and truly all that comes under thy observation in life.” — Marcus Aurelius

48. “Men love to wonder, and that is the seed of science.” — Ralph Waldo Emerson

49. “Your theory is crazy, but it's not crazy enough to be true.” — Niels Bohr

50. “Each problem that I solved became a rule, which served afterwards to solve other problems.” — Rene Descartes

51. “Facts are not science - as the dictionary is not literature.” — Martin H. Fischer

52. “Science is a beautiful gift to humanity; we should not distort it.” — A. P. J. Abdul Kalam

53. “Good, better, best. Never let it rest. 'Til your good is better and your better is best.” — St. Jerome

54. “Only I can change my life. No one can do it for me.” — Carol Burnett

55. “If you fell down yesterday, stand up today.” — H. G. Wells

56. “Ever tried. Ever failed. No matter. Try Again. Fail again. Fail better.” — Samuel Beckett

57. “You simply have to put one foot in front of the other and keep going. Put blinders on and plow right ahead.” — George Lucas

58. “Small deeds done are better than great deeds planned.” — Peter Marshall

59. “I am not afraid... I was born to do this.” — Joan of Arc

60. “Act as if what you do makes a difference. It does.” — William James

61. “Step by step and the thing is done.” — Charles Atlas

62. “Your talent is God's gift to you. What you do with it is your gift back to God.” — Leo Buscaglia

63. “If you're going through hell, keep going.” — Winston Churchill

64. “Be kind whenever possible. It is always possible.” — Dalai Lama

65. “It always seems impossible until it's done.” — Nelson Mandela

COMPREHENSIVE REFERENCE LIST

Abdel-Karim, R., Electrochemical Synthesis of Nanocomposites. In *Electrodeposition of Composite Materials*, **2016**.

Adamo, C.; Barone, V. Inexpensive and Accurate Predictions of Optical Excitations in Transition-Metal Complexes: the TDDFT/PBE0 Route. *Theor. Chem. Acc.* **2000***, 105*, 169–172.

Adamo, C.; Scuseria, G. E.; Barone, V. Accurate Excitation Energies from Time-Dependent Density Functional Theory: Assessing the PBE0 Model. *J. Chem. Phys.* **1999***, 111*, 2889–2899.

Aktas, H.; Slootweg, J. C.; Lammertsma, K., Nucleophilic phosphinidene complexes: access and applicability. *Angew Chem Int Ed Engl* **2010***, 49* (12), 2102-13.

Aldrich, K. E.; Fales, B. S.; Singh, A. K.; Staples, R. J.; Levine, B. G.; McCracken, J.; Smith, M. R., 3rd; Odom, A. L., Electronic and Structural Comparisons between Iron(II/III) and Ruthenium(II/III) Imide Analogs. *Inorg Chem* **2019***, 58* (17), 11699-11715.

Alonso-de Castro, S.; Cortajarena, A. L.; Lopez-Gallego, F.; Salassa, L., Bioorthogonal Catalytic Activation of Platinum and Ruthenium Anticancer Complexes by FAD and Flavoproteins. *Angew Chem Int Ed Engl* **2018***, 57* (12), 3143-3147.

Alvarado, E.; Liu, Z.; Servis, M. J.; Krishnamoorthy, B.; Clark, A. E., A Geometric Measure Theory Approach to Identify Complex Structural Features on Soft Matter Surfaces. *J Chem Theory Comput* **2020***, 16* (7), 4579-4587.

Anderson, J. S. M.; Heidar-Zadeh, F.; Ayers, P. W., Breaking the curse of dimension for the electronic Schrödinger equation with functional analysis. *Computational and Theoretical Chemistry* **2018***, 1142*, 66-77.

Anderson, M. E.; Braida, B.; Hiberty, P. C.; Cundari, T. R., Revealing a Decisive Role for Secondary Coordination Sphere Nucleophiles on Methane Activation. *J Am Chem Soc* **2020***, 142* (6), 3125-3131.

Anderson, R.; Biong, A.; Gomez-Gualdron, D. A., Adsorption Isotherm Predictions for Multiple Molecules in MOFs Using the Same Deep Learning Model. *J Chem Theory Comput* **2020**.

Andrada, D. M.; Foroutan-Nejad, C., Energy components in energy decomposition analysis (EDA) are path functions; why does it matter? *Phys Chem Chem Phys* **2020***, 22* (39), 22459-22464.

Andrew, R. E.; Gonzalez-Sebastian, L.; Chaplin, A. B., NHC-based pincer ligands: carbenes with a bite. *Dalton Trans* **2016***, 45* (4), 1299-305.

Aquino, F. W.; Shinde, R.; Wong, B. M., Fractional occupation numbers and self-interaction correction-scaling methods with the Fermi-Lowdin orbital self-interaction correction approach. *J Comput Chem* **2020***, 41* (12), 1200-1208.

Arashiba, K.; Tanaka, H.; Yoshizawa, K.; Nishibayashi, Y., Cycling between Molybdenum-Dinitrogen and -Nitride Complexes to Support the Reaction Pathway for Catalytic Formation of Ammonia from Dinitrogen. *Chemistry* **2020***, 26* (59), 13383-13389.

Ashida, Y.; Arashiba, K.; Tanaka, H.; Egi, A.; Nakajima, K.; Yoshizawa, K.; Nishibayashi, Y., Molybdenum-Catalyzed Ammonia Formation Using Simple Monodentate and Bidentate Phosphines as Auxiliary Ligands. *Inorg Chem* **2019***, 58*, 8927-8932.

Atkins, P.; dePaula, J. *Atkins' Physical Chemistry*, 9th ed.; Oxford University Press, Oxford, UK, **2010**.

Baek, Y.; Das, A.; Zheng, S. L.; Reibenspies, J. H.; Powers, D. C.; Betley, T. A., C-H Amination Mediated by Cobalt Organoazide Adducts and the Corresponding Cobalt Nitrenoid Intermediates. *J Am Chem Soc* **2020***, 142* (25), 11232-11243.

Bagus, P. S.; Ilton, E. S.; Nelin, C. J., The interpretation of XPS spectra: Insights into materials properties. *Surface Science Reports* **2013***, 68* (2), 273-304.

Bagus, P. S.; Nelin, C. J., Covalent interactions in oxides. *Journal of Electron Spectroscopy and Related Phenomena* **2014***, 194*, 37-44.

Bagus, P. S.; Nelin, C. J.; Hrovat, D. A.; Ilton, E. S., Covalent bonding in heavy metal oxides. *J Chem Phys* **2017***, 146* (13), 134706.

Bairagya, M. D.; Bujol, R. J.; Elgrishi, N., Fighting Deactivation: Classical and Emerging Strategies for Efficient Stabilization of Molecular Electrocatalysts. *Chemistry* **2019**.

Baird, L.; Yamamoto, M., The Molecular Mechanisms Regulating the KEAP1-NRF2 Pathway. *Mol Cell Biol* **2020***, 40* (13).

Balazs, G.; Green, J. C.; Scheer, M., Terminally coordinated AsS and PS ligands. *Chemistry* **2006***, 12* (33), 8603-8.

Ball, M. R.; Rivera-Dones, K. R.; Gilcher, E. B.; Ausman, S. F.; Hullfish, C. W.; Lebrón, E. A.; Dumesic, J. A., AgPd and CuPd Catalysts for Selective Hydrogenation of Acetylene. ACS Catalysis 2020, 10 (15), 8567-8581.Ballhausen, C. J.; Gray, H. B. The Electronic Structure of the Vanadyl Ion. *Inorg. Chem.* **1962***, 1*, 111–122.

Barber, T.; Argent, S. P.; Ball, L. T., Expanding Ligand Space: Preparation, Characterization, and Synthetic Applications of Air-Stable, Odorless Di-tert-alkylphosphine Surrogates. *ACS Catalysis* **2020***, 10* (10), 5454-5461.

Barnes, E. C.; Petersson, G. A.; Montgomery, J. A.; Frisch, M. J.; Martin, J. M. L. Unrestricted Coupled Cluster and Brueckner Doubles Variations of W1 Theory. *J. Chem. Theory Comput.* **2009***, 5*, 2687–2693.

Bartlett, R. J. Perspective On "On the Correlation Problem in Atomic and Molecular Systems. Calculation of Wavefunction Components in Ursell-Type Expansion Using Quantum-Field Theoretical Methods." *Theor. Chem. Acc.* **2000***, 103*, 273–275.

Bartlett, R. J., Adventures in DFT by a wavefunction theorist. *J Chem Phys* **2019***, 151* (16), 160901.

Bartok, A. P.; Yates, J. R., Response to "Comment on 'Regularized SCAN functional'" *J Chem Phys* **2019***, 151* (20), 207102.

Bauer, C. A.; Hansen, A.; Grimme, S., The Fractional Occupation Number Weighted Density as a Versatile Analysis Tool for Molecules with a Complicated Electronic Structure. *Chemistry* **2017***, 23* (25), 6150-6164.

Beaumier, E. P.; Billow, B. S.; Singh, A. K.; Biros, S. M.; Odom, A. L., A Complex with Nitrogen Single, Double, and Triple Bonds to the Same Chromium Atom: Synthesis, Structure, and Reactivity. *Chem Sci* **2016***, 7*, 2532-2536.

Beaumier, E. P.; Gordon, C. P.; Harkins, R. P.; McGreal, M. E.; Wen, X.; Coperet, C.; Goodpaster, J. D.; Tonks, I. A., Cp2Ti(kappa(2)-(t)BuNCN(t)Bu): A Complex with an Unusual kappa(2) Coordination Mode of a Heterocumulene Featuring a Free Carbene. *J Am Chem Soc* **2020***, 142*, 8006-8018.

Becke, A. D. Density-Functional Exchange-Energy Approximation with Correct Asymptotic Behavior. *Phys. Rev. A* **1988***, 38*, 3098–3100.

Becke, A. D., Density Functional Thermochemistry. III. The Role of Exact Exchange. *J. Chem. Phys.* **1993***, 98*, 5648-5652.

Behler, J., Atom-centered symmetry functions for constructing high-dimensional neural network potentials. *J Chem Phys* **2011***, 134* (7), 074106.

Behler, J., Perspective: Machine learning potentials for atomistic simulations. *J Chem Phys* **2016***, 145* (17), 170901.

Bencini, A. Some Considerations on the Proper Use of Computational Tools in Transition Metal Chemistry. *Inorganica Chim. Acta* **2008***, 361*, 3820–3831.

Benson, M. T. B., J. C.; Burrell, A. K.; Cundari, T. R. , Bonding and structure of Heavily π-Loaded Complexes. *Inorg. Chem.* **1995***, 34*, 2348-2355.

Bentley, J. N.; Elgadi, S. A.; Gaffen, J. R.; Demay-Drouhard, P.; Baumgartner, T.; Caputo, C. B., Fluorescent Lewis Adducts: A Practical Guide to Relative Lewis Acidity. *Organometallics* **2020***, 39* (20), 3645-3655.

Berry, J. F. Terminal Nitrido and Imido Complexes of The Late Transition Metals. Comments *Inorg. Chem.* **2009***, 30*, 28−66.

Berry, J. F., The role of three-center/four-electron bonds in superelectrophilic dirhodium carbene and nitrene catalytic intermediates. *Dalton Trans* **2012***, 41* (3), 700-13.

Bettens, T.; Alonso, M.; De Proft, F.; Hamlin, T. A.; Bickelhaupt, F. M., Ambident Nucleophilic Substitution: Understanding Non-HSAB Behavior through Activation Strain and Conceptual DFT Analyses. *Chemistry* **2020***, 26* (17), 3884-3893.

Bezdek, M. J.; Chirik, P. J. Expanding Boundaries: N2 Cleavage and Functionalization beyond Early Transition Metals. *Angew. Chem., Int. Ed.* **2016***, 55*, 7892−7896.

Bezdek, M. J.; Pelczer, I.; Chirik, P. J., Coordination-Induced N–H Bond Weakening in a Molybdenum Pyrrolidine Complex: Isotopic Labeling Provides Insight into the Pathway for H2 Evolution. *Organometallics* **2020***, 39* (16), 3050-3059.

Bianchi, S.; Bortoluzzi, M.; Castelvetro, V.; Marchetti, F.; Pampaloni, G.; Pinzino, C.; Zacchini, S. The Reactivity of Tungsten Hexachloride with Tetrahydrofuran and 2-Methoxyethanol. *Polyhedron* **2016***, 117*, 769–776.

Billow, B. S.; McDaniel, T. J.; Odom, A. L., Quantifying Ligand Effects in High-Oxidation-State Metal Catalysis. *Nat Chem* **2017***, 9*, 837-842.

Bimetallic Migratory Insertion, H-Elimination and Other Reactions. *Chemical Communications* **2018***, 54* (66), 9186-9189.

Bismuto, A.; Delcaillau, T.; Müller, P.; Morandi, B., Nickel-Catalyzed Amination of Aryl Thioethers: A Combined Synthetic and Mechanistic Study. *ACS Catalysis* **2020***, 10* (8), 4630-4639.

Bismuto, A.; Duarte, F.; Nichol, G. S.; Cowley, M. J.; Thomas, S., Characterization of the zwitterionic intermediate in 1,1-carboboration of alkynes. *Angew Chem Int Ed Engl* **2020**.

Black, C. C.; Gorden, A. E. V., Oxidative Mannich Reactions of Tertiary Amines Using a Cu(II) 2-Quinoxalinol Salen Catalyst. *J Org Chem* **2019***, 84*, 9806-9810.

Boatz, J. A. G., Mark S.*Sita, Lawrence R., Theoretical Studies of Metallacyclopropenes c-[MX2C2H2] (M = C, Si, Ge, Sn, X = H, F). *J. Phys. Chem.* **1990***, 94* (14), 5488-5493.

Boehme, C.; Frenking, G. Electronic Structure of Stable Carbenes, Silylenes, and Germylenes. *J. Am. Chem. Soc.* **1996***, 118*, 2039-2046.

Bolton, P. D.; Mountford, P., Transition Metal Imido Compounds as Ziegler-Natta Olefin Polymerisation Catalysts. *Advanced Synthesis & Catalysis* **2005***, 347* (2-3), 355-366.

Bonanno, J. B.; Wolczanski, P. T.; Lobkovsky, E. B.; Arsinidene, Phosphinidene, and Imide Formation via L,2-H2-Elimination from (Silox)3htaehph (E = N, P, As): Structures Of (Silox)3Ta=EPh (E = As). *J. Am. Chem. Soc.* **1994**, *116*, 11159-11160.

Brandenburg, J. G.; Bannwarth, C.; Hansen, A.; Grimme, S., B97-3c: A revised low-cost variant of the B97-D density functional method. *J Chem Phys* **2018**, *148* (6), 064104.

Brandi M. Cossairt, N. A. P., and Christopher C. Cummins, Early-Transition-Metal-Mediated Activation and Transformation of White Phosphorus. *Chem. Rev.* **2010**, *110*, 4164–4177.

Bretz, S. L., Evidence for the Importance of Laboratory Courses. *Journal of Chemical Education* **2019**, *96* (2), 193-195.

Buchmeiser, M. R.; Sen, S.; Lienert, C.; Widmann, L.; Schowner, R.; Herz, K.; Hauser, P.; Frey, W.; Wang, D., Molybdenum Imido Alkylidene N-Heterocyclic Carbene Complexes: Structure-Productivity Correlations and Mechanistic Insights. *ChemCatChem* **2016**, *8*, 2710-2723.

Bucur, C. B.; Gregory, T.; Oliver, A. G.; Muldoon, J., Confession of a Magnesium Battery. *J Phys Chem Lett* **2015**, *6* (18), 3578-91.

Cameron, M. I.; Morisco, D.; Hofstetter, D.; Uman, E.; Wilkinson, J.; Kennedy, Z. C.; Fontenot, S. A.; Lee, W. T.; Hendon, C. H.; Foster, J. M., Systematically Improving Espresso: Insights from Mathematical Modeling and Experiment. *Matter* **2020**.

Camp, C.; Grant, L. N.; Bergman, R. G.; Arnold, J., Photo-activation of d(0) niobium imido azides: en route to nitrido complexes. *Chem Commun (Camb)* **2016**, *52* (32), 5538-41.

Campos, C. T.; Ceolin, G. A.; Canal Neto, A.; Jorge, F. E.; Pansini, F. N. N., Gaussian basis set of sextuple zeta quality for hydrogen through argon. *Chemical Physics Letters* **2011**, *516* (4-6), 125-130.

Canning, P.; Cooper, C. D. O.; Krojer, T.; Murray, J. W.; Pike, A. C. W.; Chaikuad, A.; Keates, T.; Thangaratnarajah, C.; Hojzan, V.; Marsden, B. D.; Gileadi, O.; Knapp, S.; von Delft, F.; Bullock, A. N., Structural basis for Cul3 protein assembly with the BTB-Kelch family of E3 ubiquitin ligases. *J Biol Chem* **2013**, *288* (11), 7803-7814.

Carlson, A. W.; Primka, D. A.; Douma, E. D.; Bowring, M. A., Evaluation of air-free glassware using the ketyl test. *Dalton Trans* **2020**.

Carreras, V.; Besnard, C.; Gandon, V.; Ollevier, T., Asymmetric Cu(I)-Catalyzed Insertion Reaction of 1-Aryl-2,2,2-trifluoro-1-diazoethanes into Si-H Bonds. *Org Lett* **2019**, *21* (22), 9094-9098.

Carter, C. C.; Allen, B. R.; Bui, D. V.; Daley, D. A.; Goncalves, J. M.; Holinej, C. M.; Lira, S.; Muniz, D. E.; Santiago, A. I.; Sukran, N.; Cundari, T. R.; Yousufuddin, M., Synthesis, crystal structures, and DFT calculations of tungsten (IV) and tungsten (VI) phosphino polyhydrides. *Inorganica Chimica Acta* **2020**, *508*.

Ceylan, Y. S.; Cundari, T. R. Computational Analysis of Transition Metal-Terminal Boride Complexes. *J. Phys. Chem. A.* **2017***, 121*, 9358–9368.

Chan, B.; Gill, P. M. W.; Kimura, M., Assessment of DFT Methods for Transition Metals with the TMC151 Compilation of Data Sets and Comparison with Accuracies for Main-Group Chemistry. *J Chem Theory Comput* **2019***, 15* (6), 3610-3622.

Chao, Y. W.; Rodgers, P. M.; Wigley, D. E.; Alexander, S. J.; Rheingold, A. L. Tris(phenylimido) Complexes of Tungsten: Preparation and Properties of the d0 W(:NR)3 Functional Group. *J. Am. Chem. Soc.* **1991***, 113*, 6326-6328.

Chapman, A. M.; Haddow, M. F.; Wass, D. F., Frustrated Lewis pairs beyond the main group: cationic zirconocene-phosphinoaryloxide complexes and their application in catalytic dehydrogenation of amine boranes. *J Am Chem Soc* **2011***, 133* (23), 8826-9.

Chapman, K., The transuranic elements and the island of stability. *Philos Trans A Math Phys Eng Sci* **2020***, 378* (2180), 20190535.

Chapovetsky, A.; Langeslay, R. R.; Celik, G.; Perras, F. A.; Pruski, M.; Ferrandon, M. S.; Wegener, E. C.; Kim, H.; Dogan, F.; Wen, J.; Khetrapal, N.; Sharma, P.; White, J.; Kropf, A. J.; Sattelberger, A. P.; Kaphan, D. M.; Delferro, M., Activation of Low-Valent, Multiply M–M Bonded Group VI Dimers toward Catalytic Olefin Metathesis via Surface Organometallic Chemistry. *Organometallics* **2020**.

Charette, B. J.; Ziller, J. W.; Heyduk, A. F., Metal-Ion Influence on Ligand-Centered Hydrogen-Atom Transfer. *Inorg Chem* **2021***, 60* (3), 1579-1589.

Chatterjee, S.; Huang, K. W., Unrealistic energy and materials requirement for direct air capture in deep mitigation pathways. *Nat Commun* **2020***, 11* (1), 3287.

Chattopadhyay, S.; Mahapatra, U. S.; Chaudhuri, R. K., State specific multireference Møller–Plesset perturbation theory: A few applications to ground, excited and ionized states. *Chemical Physics* **2012***, 401*, 15-26.

Chen, H.; Wang, Y. X.; Luan, Y. X.; Ye, M., Enantioselective Twofold C-H Annulation of Formamides and Alkynes without Built-in Chelating Groups. *Angew Chem Int Ed Engl* **2020**.

Chen, X.; Qiao, W.; Miao, W.; Zhang, Y.; Mu, X.; Wang, J., The Dependence of Implicit Solvent Model Parameters and Electronic Absorption Spectra and Photoinduced Charge Transfer. *Sci Rep* **2020***, 10* (1), 3713.

Chen, Z.; Wannere, C. S.; Corminboeuf, C.; Puchta, R.; Schleyer, P., Nucleus-independent chemical shifts (NICS) as an aromaticity criterion. *Chem Rev* **2005***, 105* (10), 3842-88.

Chiu, H. C.; Tonks, I. A., Trimethylsilyl-Protected Alkynes as Selective Cross-Coupling Partners in Titanium-Catalyzed [2+2+1] Pyrrole Synthesis. *Angew Chem Int Ed Engl* **2018***, 57* (21), 6090-6094.

Choe, R. C.; Scuric, Z.; Eshkol, E.; Cruser, S.; Arndt, A.; Cox, R.; Toma, S. P.; Shapiro, C.; Levis-Fitzgerald, M.; Barnes, G.; Crosbie, R. H., Student Satisfaction and Learning Outcomes in Asynchronous Online Lecture Videos. *CBE Life Sci Educ* **2019***, 18* (4), ar55.

Churchill, M. R. Y., W. J., Crystal Structure and Molecular Geometry of W(≡CCMe3)(:CHCMe3)(CH2CMe3)(Dmpe), a Mononuclear Tungsten(VI) Complex with Metal-Alkylidyne, Metal-Alkylidene, and Metal-Alkyl Linkages. *Inorg. Chem.* **1979***, 18,* 2454-2458.

Clark, A. E.; Sonnenberg, J. L.; Hay, P. J.; Martin, R. L., Density and wave function analysis of actinide complexes: what can fuzzy atom, atoms-in-molecules, Mulliken, Lowdin, and natural population analysis tell us? *J Chem Phys* **2004***, 121* (6), 2563-70.

Clarkson, J. M.; Schafer, L. L., Bis(tert-butylimido)bis(N,O-chelate)tungsten(VI) Complexes: Probing Amidate and Pyridonate Hemilability. *Inorg Chem* **2017***, 56* (10), 5553-5566.

Clough, B. A.; Mellino, S.; Protchenko, A. V.; Slusarczyk, M.; Stevenson, L. C.; Blake, M. P.; Xie, B.; Clot, E.; Mountford, P., New Titanium Borylimido Compounds: Synthesis, Structure, and Bonding. *Inorg Chem* **2017***, 56*, 10794-10814.

Cooke, K. O., Parametric Analysis of Electrodeposited Nano-composite Coatings for Abrasive Wear Resistance. In *Electrodeposition of Composite Materials,* **2016**.

Cooper, A.; Leonard, D.; Bajo, S.; Burton, P. M.; Nelson, D. J., Aldehydes and Ketones Influence Reactivity and Selectivity in Nickel-Catalysed Suzuki-Miyaura Reactions Chemical *Science* **2020**.

Cordas, C. M.; Moura, J. J. G., Molybdenum and tungsten enzymes redox properties – A brief overview. *Coordination Chemistry Reviews* **2019***, 394*, 53-64.

Corradini, P.; Guerra, G.; Cavallo, L., Do New Century Catalysts Unravel the Mechanism of Stereocontrol of Old Ziegler-Natta Catalysts? *Acc. Chem. Res.* **2004***, 37*, 231-241.

Cotton, F. A.; Schwotzer, W.; Shamshoum, E. S. Further Studies of the Reactions of Ditungsten Hexa-T- Butoxide with Acetylenes. Isolation and Characterization of WO(OCMe3)4(THF), [W3(OCMe3)5(μ-O)(μ-CC3H7)O]2 and W(CPh)(OCMe3)3. J. *Organomet. Chem.* **1985***, 296*, 55–68.

Cowley, A. H.; Pellerin, B.; Atwood, J. L.; Bott, S. G. Cleavage of a Phosphorus-Carbon Double Bond and Formation of a Linear Terminal Phosphinidene Complex. *J. Am. Chem. Soc.* **1990***, 112*, 6734–6735.

Crabtree, R. H. *The Organometallic Chemistry of the Transition Metals*, 5th ed.; Wiley: Hoboken, NJ, **2009**.

Crabtree, R. H., Fifty years of coordination chemistry reviews. *Coordination Chemistry Reviews* **2017***, 344*.

Cramer, C. J. *Essentials of Computational Chemistry; Theories and Models*, 2nd ed.; Wiley: Hoboken, NJ, **2004**.

Cullinan, S. B.; Gordan, J. D.; Jin, J.; Harper, J. W.; Diehl, J. A., The Keap1-BTB protein is an adaptor that bridges Nrf2 to a Cul3-based E3 ligase: oxidative stress sensing by a Cul3-Keap1 ligase. *Mol Cell Biol* **2004***, 24* (19), 8477-86.

Cundari, T. R. Computational Studies of Transition Metal-Main Group Multiple Bonding. *Chem. Rev.* **2000***, 100*, 807–818.

Cundari, T. R. Methane Activation by Group V Bis(Imido) Complexes. *Organometallics* **1994***, 13*, 2987–2994.

Cundari, T. R., Computational Studies of Transition Metal-Main Group Multiple Bonding. *Chem. Rev.* **2000***, 100*, 807-818.

Cundari, T. R.; Stevens, W. J. Effective Core Potential Methods for the Lanthanides. *J. Chem. Phys.* **1993***, 98*, 5555–5565.

Curtiss, L. A.; Raghavachari, K.; Deutsch, P. W.; Pople, J. A. Theoretical Study of Si2Hn (N=0-6) and Si 2Hn+ (N=0-7): Appearance Potentials, Ionization Potentials, and Enthalpies of Formation. *J. Chem. Phys.* **1991***, 95*, 2433–2444.

Curtiss, L. A.; Raghavachari, K.; Redfern, P. C.; Stefanov, B. B., Assessment of complete basis set methods for calculation of enthalpies of formation. *The Journal of Chemical Physics* **1998***, 108* (2), 692-697.

Curtiss, L. A.; Redfern, P. C.; Raghavachari, K. Gaussian-4 Theory. *J. Chem. Phys.* **2007***, 126*, 084108.

Curtiss, L. A.; Redfern, P. C.; Raghavachari, K. Gn Theory. *Wiley Interdisciplinary Reviews: Computational Molecular Science*. John Wiley & Sons, Ltd September 1, **2011**, pp 810–825.

Davies, D. L.; Macgregor, S. A.; McMullin, C. L., Computational Studies of Carboxylate-Assisted C-H Activation and Functionalization at Group 8-10 Transition Metal Centers. *Chem Rev* **2017***, 117*, 8649-8709.

Davies, H. M. L.; Morton, D. Recent Advances in C-H Functionalization. *J. Org. Chem.* **2016***, 81*, 343-350.

Davis-Gilbert, Z. W.; Tonks, I. A., Titanium redox catalysis: insights and applications of an earth-abundant base metal. *Dalton Transactions* **2017***, 46* (35), 11522-11528.

Davis-Gilbert, Z. W.; Wen, X.; Goodpaster, J. D.; Tonks, I. A., Mechanism of Ti-Catalyzed Oxidative Nitrene Transfer in [2 + 2 + 1] Pyrrole Synthesis from Alkynes and Azobenzene. *J. Am. Chem. Soc.* **2018***, 140*, 7267-7281.

Davis-Gilbert, Z. W.; Yao, L. J.; Tonks, I. A., Ti-Catalyzed Multicomponent Oxidative Carboamination of Alkynes with Alkenes and Diazenes. *J. Am. Chem. Soc.* **2016***, 138*, 14570-14573.

Deblonde, G. J.; Mattocks, J. A.; Park, D. M.; Reed, D. W.; Cotruvo, J. A., Jr.; Jiao, Y., Selective and Efficient Biomacromolecular Extraction of Rare-Earth Elements using Lanmodulin. *Inorg Chem* **2020***, 59* (17), 11855-11867.

Delcaillau, T.; Bismuto, A.; Lian, Z.; Morandi, B., Nickel-Catalyzed Inter- and Intramolecular Aryl Thioether Metathesis by Reversible Arylation. *Angew Chem Int Ed Engl* **2020***, 59* (5), 2110-2114.

Desnoyer, A. N.; See, X. Y.; Tonks, I. A., Diverse Reactivity of Diazatitanacyclohexenes: Coupling Reactions of 2H-Azirines Mediated by Titanium(II). *Organometallics* **2018***, 37* (23), 4327-4331.

DeYonker, N. J.; Williams, T. G.; Imel, A. E.; Cundari, T. R.; Wilson, A. K. Accurate Thermochemistry for Transition Metal Complexes from First-Principles Calculations. *J. Chem. Phys.* **2009***, 131*, 24106.

DeYonker, N. J.; Wilson, B. R.; Pierpont, A. W.; Cundari, T. R.; Wilson, A. K. Towards the Intrinsic Error of the Correlation Consistent Composite Approach (CcCA). *Mol. Phys.* **2009***, 107*, 1107–1121.

Dohm, S.; Hansen, A.; Steinmetz, M.; Grimme, S.; Checinski, M. P., Comprehensive Thermochemical Benchmark Set of Realistic Closed-Shell Metal Organic Reactions. *J Chem Theory Comput* **2018***, 14* (5), 2596-2608.

Domski, G. J.; Eagan, J. M.; De Rosa, C.; Di Girolamo, R.; LaPointe, A. M.; Lobkovsky, E. B.; Talarico, G.; Coates, G. W., Combined Experimental and Theoretical Approach for Living and Isoselective Propylene Polymerization. *ACS Catalysis* **2017***, 7* (10), 6930-6937.

Dong, Y.; Lund, C. J.; Porter, G. J.; Clarke, R. M.; Zheng, S. L.; Cundari, T. R.; Betley, T. A., Enantioselective C-H Amination Catalyzed by Nickel Iminyl Complexes Supported by Anionic Bisoxazoline (BOX) Ligands. *J Am Chem Soc* **2021***, 143* (2), 817-829.

Dral, P. O., Quantum Chemistry in the Age of Machine Learning. *J Phys Chem Lett* **2020***, 11* (6), 2336-2347.

Dunning, T. H.; Peterson, K. A.; Wilson, A. K., Gaussian basis sets for use in correlated molecular calculations. X. The atoms aluminum through argon revisited. *The Journal of Chemical Physics* **2001***, 114* (21), 9244-9253.

Durand, D.; Fey, N. Computational Ligand Descriptors for Catalyst Design; *Chem. Rev.* **2019***, 119*, 6561-6594.

Edens, L. E.; Pednekar, S.; Morris, J. F.; Schenter, G. K.; Clark, A. E.; Chun, J., Global topology of contact force networks: Insight into shear thickening suspensions. *Phys Rev E* **2019***, 99* (1-1), 012607.

Ehm, C.; Budzelaar, P. H. M.; Busico, V., Calculating accurate barriers for olefin insertion and related reactions. *Journal of Organometallic Chemistry* **2015***, 775*, 39-49.

Ehrhorn, H.; Bockfeld, D.; Freytag, M.; Bannenberg, T.; Kefalidis, C. E.; Maron, L.; Tamm, M., Studies on Molybdena- and Tungstenacyclobutadiene Complexes Supported by Fluoroalkoxy Ligands as Intermediates of Alkyne Metathesis. *Organometallics* **2019***, 38* (7), 1627-1639.

Eikey, R. A.; Abu-Omar, M. M. Nitrido and Imido Transition Metal Complexes of Groups 6−8. Coord. *Chem. Rev.* **2003***, 243*, 83−124.

Eisch, J. J., Fifty Years of Ziegler–Natta Polymerization: From Serendipity to Science. A Personal Account. *Organometallics* **2012***, 31*, 4917-4932.

Eisenberger, P.; Bestvater, B. P.; Keske, E. C.; Crudden, C. M., Hydrogenations at room temperature and atmospheric pressure with mesoionic carbene-stabilized borenium catalysts. *Angew Chem Int Ed Engl* **2015***, 54* (8), 2467-71.

Elsen, H.; Langer, J.; Wiesinger, M.; Harder, S., Alkaline Earth Metal Aluminates as Catalysts for Imine Hydrogenation. *Organometallics* **2020**.

Evangelista, F. A., Perspective: Multireference coupled cluster theories of dynamical electron correlation. *J Chem Phys* **2018***, 149* (3), 030901.

Eymann, L. Y. M.; Varava, P.; Shved, A. M.; Curchod, B. F. E.; Liu, Y.; Planes, O. M.; Sienkiewicz, A.; Scopelliti, R.; Fadaei Tirani, F.; Severin, K., Synthesis of Organic Super-Electron-Donors by Reaction of Nitrous Oxide with N-Heterocyclic Olefins. *J Am Chem Soc* **2019***, 141* (43), 17112-17116.

Eymann, L. Y.; Tskhovrebov, A. G.; Sienkiewicz, A.; Bila, J. L.; Zivkovic, I.; Ronnow, H. M.; Wodrich, M. D.; Vannay, L.; Corminboeuf, C.; Pattison, P.; Solari, E.; Scopelliti, R.; Severin, K., Neutral Aminyl Radicals Derived from Azoimidazolium Dyes. *J Am Chem Soc* **2016***, 138* (46), 15126-15129.

Fajardo, J., Jr.; Peters, J. C., Tripodal P3(X)Fe-N2 Complexes (X = B, Al, Ga): Effect of the Apical Atom on Bonding, Electronic Structure, and Catalytic N2-to-NH3 Conversion. *Inorg Chem* **2021***, 60* (2), 1220-1227.

Falguni Basuli; Brad C. Bailey; Douglas Brown; John Tomaszewski; John C. Huffman; Mu-Hyun Baik; Mindiola, D. J., Terminal Vanadium-Neopentylidyne Complexes and Intramolecular Cross-Metathesis Reactions to Generate Azametalacyclohexatrienes. *J. Am. Chem. Soc.* **2004***, 126* (34), 10506-10507.

Falivene, L.; Cao, Z.; Petta, A.; Serra, L.; Poater, A.; Oliva, R.; Scarano, V.; Cavallo, L., Towards the online computer-aided design of catalytic pockets. *Nat Chem* **2019***, 11* (10), 872-879.

Fang, T.; Lakey, P. S. J.; Rivera-Rios, J. C.; Keutsch, F. N.; Shiraiwa, M., Aqueous-Phase Decomposition of Isoprene Hydroxy Hydroperoxide and Hydroxyl Radical Formation by Fenton-like Reactions with Iron Ions. *J Phys Chem A* **2020***, 124* (25), 5230-5236.

Feller, D., Benchmarks of Improved Complete Basis Set Extrapolation Schemes Designed for Standard CCSD(T) Atomization Energies. *J Chem Phys* **2013***, 138*, 074103.

Feller, D.; Peterson, K. A.; de Jong, W. A.; Dixon, D. A., Performance of coupled cluster theory in thermochemical calculations of small halogenated compounds. *The Journal of Chemical Physics* **2003***, 118* (8), 3510-3522.

Feller, D.; Peterson, K. A.; Hill, J. G., On the Effectiveness of CCSD(T) Complete Basis Set Extrapolations for Atomization Energies. *J Chem Phys* **2011***, 135*, 044102.

Ferrando-Soria, J.; Vallejo, J.; Castellano, M.; Martínez-Lillo, J.; Pardo, E.; Cano, J.; Castro, I.; Lloret, F.; Ruiz-García, R.; Julve, M., Molecular magnetism, quo vadis? A historical perspective from a coordination chemist viewpoint☆. *Coordination Chemistry Reviews* **2017***, 339*, 17-103.

Flaxman, S.; Mishra, S.; Gandy, A.; Unwin, H. J. T.; Mellan, T. A.; Coupland, H.; Whittaker, C.; Zhu, H.; Berah, T.; Eaton, J. W.; Monod, M.; Imperial College, C.-R. T.; Ghani, A. C.; Donnelly, C. A.; Riley, S.; Vollmer, M. A. C.; Ferguson, N. M.; Okell, L. C.; Bhatt, S., Estimating the effects of non-pharmaceutical interventions on COVID-19 in Europe. *Nature* **2020***, 584* (7820), 257-261.

Foroutan-Nejad, C.; Ghosh, A., Magnetic Diversity in Heteroisocorroles: Aromatic Pathways in 10-Heteroatom-Substituted Isocorroles. *ACS* **Omega** *2018, 3* (11), 15865-15869.

Forster, C.; Heinze, K., Photophysics and photochemistry with Earth-abundant metals - fundamentals and concepts. *Chem Soc Rev* **2020***, 49* (4), 1057-1070.

Fraleigh, J. B., A first course in abstract algebra. Addison-Wesley

Frenking, G., Dative bonds in main-group compounds: a case for more arrows! *Angew Chem Int Ed Engl* **2014***, 53* (24), 6040-6.

Frenking, G.; Fröhlich, N. The Nature of the Bonding in Transition-Metal Compounds. *Chem. Rev.* **2000***, 100*, 717-774.

Frenking, G.; Krapp, A. Unicorns in the World of Chemical Bonding. *J. Comput. Chem.* **2007***, 28*, 15-24.

Fukuda, T.; Yoshimoto, T.; Hashimoto, H.; Tobita, H., Synthesis of a Tungsten–Silylyne Complex via Stepwise Proton and Hydride Abstraction from a Hydrido Hydrosilylene Complex. *Organometallics* **2016***, 35* (7), 921-924.

Fulmer, G. R.; Miller, A. J. M.; Sherden, N. H.; Gottlieb, H. E.; Nudelman, A.; Stoltz, B. M.; Bercaw, J. E.; Goldberg, K. I., NMR Chemical Shifts of Trace Impurities: Common Laboratory Solvents, Organics, and Gases in Deuterated Solvents Relevant to the Organometallic Chemist. *Organometallics* **2010***, 29* (9), 2176-2179.

Furukawa, M.; Xiong, Y., BTB protein Keap1 targets antioxidant transcription factor Nrf2 for ubiquitination by the Cullin 3-Roc1 ligase. *Mol Cell Biol* **2005***, 25* (1), 162-71.

Galloway, K. R.; Bretz, S. L., Development of an Assessment Tool To Measure Students' Meaningful Learning in the Undergraduate Chemistry Laboratory. *Journal of Chemical Education* **2015***, 92* (7), 1149-1158.

Garbe, M.; Budweg, S.; Papa, V.; Wei, Z.; Hornke, H.; Bachmann, S.; Scalone, M.; Spannenberg, A.; Jiao, H.; Junge, K.; Beller, M., Chemoselective semihydrogenation of alkynes catalyzed by manganese(i)-PNP pincer complexes. *Catalysis Science & Technology* **2020***, 10* (12), 3994-4001.

Garhwal, S.; Fridman, N.; de Ruiter, G., Z-Selective Alkyne Functionalization Catalyzed by a trans-Dihydride N-Heterocyclic Carbene (NHC) Iron Complex. *Inorg Chem* **2020***, 59* (19), 13817-13821.

Gaussian 09, Revision E.03, Frisch, M. J.; Trucks, G. W.; Schlegel, H. B.; Scuseria, G. E.; Robb, M. A.; Cheeseman, J. R.; Scalmani, G.; Barone, V.; Mennucci, B.; Petersson, G. A.; et al. Gaussian, Inc., Wallingford CT, 2009.

Gaussian 16, Revision A.03. Frisch, M. J.; Trucks, G. W.; Schlegel, H. B.; Scuseria, G. E.; Robb, M. A.; Cheeseman, J. R.; Scalmani, G.; Barone, V.; Petersson, G. A.; Nakatsuji, H.; et al. Gaussian, Inc., Wallingford CT, 2016.

Geeson, M. B.; Cummins, C. C., Let's Make White Phosphorus Obsolete. *ACS Central Science* **2020**.

George J. P. Britovsek; Vernon C. Gibson; Wass, D. F., The Search for New-Generation Olefin Polymerization Catalysts: Life beyond Metallocenes. *Angew. Chem. Int. Ed.* **1999***, 38*, 428 - 447.

George, G. M.; Wolczanski, P. T.; MacMillan, S. N.; Cundari, T. R., Unrealized concepts of masked alkylidenes in (PNP)FeXY systems and alternative approaches to LnXmFe(IV)=CHR. *Polyhedron* **2020***, 181*.

Georgios C. Vougioukalakis; Grubbs, R. H., Ruthenium-Based Heterocyclic Carbene-Coordinated Olefin Metathesis Catalysts. *Chem. Rev.* **2010***, 110*, 1746–1787.

Ghadar, Y.; Christensen, S. L.; Clark, A. E., Influence of aqueous ionic strength upon liquid:liquid interfacial structure and microsolvation. *Fluid Phase Equilibria* **2016***, 407*, 126-134.

Ghosh, S.; Verma, P.; Cramer, C. J.; Gagliardi, L.; Truhlar, D. G. Combining Wave Function Methods with Density Functional Theory for Excited States. *Chem. Rev.* **2018***, 118*, 7249–7292.

Gianetti, T. L.; La Pierre, H. S.; Arnold, J., Group 5 Imides and Bis(imide)s as Selective Hydrogenation Catalysts. *European Journal of Inorganic Chemistry,* **2013**, 3771-3783.

Giese, T. J.; York, D. M., Complete basis set extrapolated potential energy, dipole, and polarizability surfaces of alkali halide ion-neutral weakly avoided crossings with and without applied electric fields. *J Chem Phys* **2004***, 120* (17), 7939-48.

Glick, Z. L.; Metcalf, D. P.; Koutsoukas, A.; Spronk, S. A.; Cheney, D. L.; Sherrill, C. D., AP-Net: An atomic-pairwise neural network for smooth and transferable interaction potentials. *J Chem Phys* **2020***, 153* (4), 044112.

Goerigk, L.; Casanova-Paéz, M., The Trip to the Density Functional Theory Zoo Continues: Making a Case for Time-Dependent Double Hybrids for Excited-State Problems*. *Australian Journal of Chemistry* **2020**.

Goerigk, L.; Hansen, A.; Bauer, C.; Ehrlich, S.; Najibi, A.; Grimme, S., A look at the density functional theory zoo with the advanced GMTKN55 database for general main group thermochemistry, kinetics and noncovalent interactions. *Phys Chem Chem Phys* **2017***, 19* (48), 32184-32215.

Goerigk, L.; Kruse, H.; Grimme, S., Benchmarking density functional methods against the S66 and S66x8 datasets for non-covalent interactions. *Chemphyschem* **2011***, 12* (17), 3421-33.

Gray, H. B.; Winkler, J. R. Living with Oxygen. *Acc. Chem. Res.* **2018***, 51*, 1850–1857.

Grev, R. S.; Schaefer, H. F. The Remarkable Monobridged Structure of Si_2H_2. *J. Chem. Phys.* **1992***, 97*, 7990–7998.

Grimme, S.; Antony, J.; Ehrlich, S.; Krieg, H., A consistent and accurate ab initio parametrization of density functional dispersion correction (DFT-D) for the 94 elements H-Pu. *J Chem Phys* **2010***, 132* (15), 154104.

Grimme, S.; Hansen, A., A practicable real-space measure and visualization of static electron-correlation effects. *Angew Chem Int Ed Engl* **2015***, 54* (42), 12308-13.

Groom, C. R.; Bruno, I. J.; Lightfoot, M. P.; Ward, S. C.; *Acta Cryst.* **2016***, B72*, 171-179.

Grubba, R.; Ordyszewska, A.; Ponikiewski, L.; Gudat, D.; Pikies, J., An Investigation on the Chemistry of the R2P = P Ligand: Reactions of a Phosphanylphosphinidene Complex of Tungsten(VI) with Electrophilic Reagents. *Dalton Trans.* **2016***, 45*, 2172-9.

Grumbles, W. M.; Cundari, T. R., Computational Determination of pKa(C–H) in 3d Transition Metal-Methyl Complexes. *Organometallics* **2020**, *39* (15), 2803-2812.

Güler, E. S., Effects of Electroplating Characteristics on the Coating Properties. In *Electrodeposition of Composite Materials*, **2016**.

Gunsalus, N. J.; Koppaka, A.; Park, S. H.; Bischof, S. M.; Hashiguchi, B. G.; Periana, R. A., Homogeneous Functionalization of Methane. *Chem Rev* **2017**, *117* (13), 8521-8573.

Guo, J.; Deng, X.; Song, C.; Lu, Y.; Qu, S.; Dang, Y.; Wang, Z. X., Differences between the elimination of early and late transition metals: DFT mechanistic insights into the titanium-catalyzed synthesis of pyrroles from alkynes and diazenes. *Chem Sci* **2017**, *8* (3), 2413-2425.

Guo, Y.; Riplinger, C.; Becker, U.; Liakos, D. G.; Minenkov, Y.; Cavallo, L.; Neese, F. Communication: An Improved Linear Scaling Perturbative Triples Correction for the Domain Based Local Pair-Natural Orbital Based Singles and Doubles Coupled Cluster Method [DLPNO-CCSD(T)]. *J. Chem. Phys.* **2018**, *148*, 11101.

Hahn, F. E. Introduction: Carbene Chemistry. *Chem. Rev.* **2018**, *118*, 9455-9456.

Hansch, C. L., A.; Taft, R. W., A Survey of Hammett Substituent Constants and Resonance and Field Parameters. *Chem. Rev.* **1991**, *91* (2), 165-195.

Harding, M. E.; Vázquez, J.; Ruscic, B.; Wilson, A. K.; Gauss, J.; Stanton, J. F. High-Accuracy Extrapolated Ab Initio Thermochemistry. III. Additional Improvements and Overview. *J. Chem. Phys.* **2008**, *128*, 114111.

Harrold, N. D.; Rory Waterman; Gregory L. Hillhouse; Cundari, T. R., Group-Transfer Reactions of Nickel-Carbene and -Nitrene Complexes with Organoazides and Nitrous Oxide that Form New CdN, CdO, and NdN Bonds. *J. Am. Chem. Soc.* **2009**, *131* (36), 12872–12873.

Hartwig, J. F. *Organotransition Metal Chemistry: from Bonding to Catalysis*; University Science Books: Mill Valley, CA, **2010**.

Hasegawa, M.; Haga, S.; Nishinaga, T.; Mazaki, Y., Selenacalix[4]selenophene: Synthesis, Structure, and Gel Formation of Cyclic Selenoether of Selenophene. *Org Lett* **2020**.

Haxel, G. B.; Hedrick, J. B.; Orris, G. J. Rare Earth Elements — Critical Resources for High Technology. *United States Geol. Surv. Fact Sheet* **2002**, 87, 4 ff. https://pubs.usgs.gov/fs/2002/fs087-02/fs087-02.pdf, (Accessed April 4, 2019).

Hay, P. J. Ab Initio Theoretical Studies of Dihydrogen Coordination vs. Oxidative Addition of H2 to Five-Coordinate Tungsten Complexes. *J. Am. Chem. Soc.* **1987**, *109*, 705–710.

Hay, P. J.; Wadt, W. R. Ab Initio Effective Core Potentials for Molecular Calculations. Potentials for the Transition Metal Atoms Sc to Hg. J. *Chem. Phys.* **1985**, *82*, 270–283.

Hayes, P. G.; Xu, Z.; Beddie, C.; Keith, J. M.; Hall, M. B.; Tilley, T. D., The osmium-silicon triple bond: synthesis, characterization, and reactivity of an osmium silylyne complex. *J Am Chem Soc* **2013***, 135* (32), 11780-3.

Haynes, W. M. *CRC Handbook of Chemistry and Physics 2016-2017*, 96th ed.; CRC Press: Boca Raton, FL, **2016**.

He, B.; Zhou, H.; Yang, F.; Li, W.-K., A Method for Calculating the Heats of Formation of Medium-Sized and Large-Sized Molecules. *Open Journal of Physical Chemistry* **2015***, 05* (03), 71-86.

Heemstra, J. M., A Scientist's Guide to Social Media. ACS Central Science 2020.

Helgert, T. R.; Zhang, X.; Box, H. K.; Denny, J. A.; Valle, H. U.; Oliver, A. G.; Akurathi, G.; Webster, C. E.; Hollis, T. K., Extreme π-Loading as a Design Element for Accessing Imido Ligand Reactivity. A CCC-NHC Pincer Tantalum Bis(imido) Complex: Synthesis, Characterization, and Catalytic Oxidative Amination of Alkenes. *Organometallics* **2016***, 35*, 3452-3460.

Hendon, C. H.; Walsh, A.; Akiyama, N.; Konno, Y.; Kajiwara, T.; Ito, T.; Kitagawa, H.; Sakai, K., One-dimensional Magnus-type platinum double salts. *Nature Communications* **2016***, 7*, 11950.

Hice, S. A.; Varona, M.; Brost, A.; Dai, F.; Anderson, J. L.; Brehm-Stecher, B. F., Magnetic ionic liquids: interactions with bacterial cells, behavior in aqueous suspension, and broader applications. *Anal Bioanal Chem* **2020***, 412* (8), 1741-1755.

Hidalgo, N.; Moreno, J. J.; Pérez-Jiménez, M.; Maya, C.; López-Serrano, J.; Campos, J., Tuning Activity and Selectivity during Alkyne Activation by Gold(I)/Platinum(0) Frustrated Lewis Pairs. *Organometallics* **2020***, 39* (13), 2534-2544.

High-energy emission from a magnetar giant flare in the Sculptor galaxy. Nature Astronomy **2021**.

Hille, R.; Hall, J.; Basu, P., The mononuclear molybdenum enzymes. *Chem Rev* **2014***, 114* (7), 3963-4038.

Hillhouse, G. L. W., R.;, Group Transfer from Nickel Imido, Phosphinidene, and Carbene Complexes to Ethylene with Formation of Aziridine, Phosphirane, and Cyclopropane Products. *J. Am. Chem. Soc.* **2003***, 1254*, 13350-13351.

Hirsekorn, K. F.; Hulley, E. B.; Wolczanski, P. T.; Cundari, T. R. Olefin Substitution in (Silox)3M(Olefin) (Silox = tBu3SiO; M = Nb, Ta): The Role of Density of States in Second vs Third Row Transition Metal Reactivity. *J. Am. Chem. Soc.* **2008***, 130*, 1183–1196.

Hix, M. A.; Cisneros, G. A., Computational Investigation of APOBEC3H Substrate Orientation and Selectivity. *J Phys Chem B* **2020**.

Hobson, K.; Carmalt, C. J.; Bakewell, C., Recent advances in low oxidation state aluminium chemistry. *Chemical Science* **2020***, 11* (27), 6942-6956.

Hohenberger, J.; Ray, K.; Meyer, K., The biology and chemistry of high-valent iron-oxo and iron-nitrido complexes. *Nat Commun* **2012***, 3*, 720.

Holmes, S. M., D. F. S. I., Peter T. Wolczanski,* and Emil B. Lobkovsky, Synthesis of (tBu3SiNH)2ClWtWCl(NHSitBu3)2 and Its Degradation via NH Bond Activation. *J. Am. Chem. Soc.* **2001***, 123*, 10571-10583.

Hossain, M. K.; Köhntopp, A.; Haukka, M.; Richmond, M. G.; Lehtonen, A.; Nordlander, E., Cis- and trans molybdenum oxo complexes of a prochiral tetradentate aminophenolate ligand: Synthesis, characterization and oxotransfer activity. *Polyhedron* **2020***, 178*.

Hulley, E. B.; Bonanno, J. B.; Wolczanski, P. T.; Cundari, T. R.; Lobkovsky, E. B., Pnictogen-hydride activation by (silox)3Ta (silox = (t)Bu3SiO); attempts to circumvent the constraints of orbital symmetry in N2 activation. *Inorg Chem* **2010***, 49* (18), 8524-44.

Ibanez, S.; Poyatos, M.; Peris, E., N-Heterocyclic Carbenes: A Door Open to Supramolecular Organometallic Chemistry. *Acc Chem Res* **2020***, 53* (7), 1401-1413.

Isaev, A. N., Ammonia and phosphine complexes with proton donors. Hydrogen bonding from the backside of the N(P) lone pair. *Computational and Theoretical Chemistry* **2018***, 1142*, 28-38.

Jakhar, V.; Pal, D.; Ghiviriga, I.; Abboud, K. A.; Lester, D. W.; Sumerlin, B. S.; Veige, A. S., Tethered Tungsten-Alkylidenes for the Synthesis of Cyclic Polynorbornene via Ring Expansion Metathesis: Unprecedented Stereoselectivity and Trapping of Key Catalytic Intermediates. *J Am Chem Soc* **2021***, 143*, 1235-1246.

James, C. D.; Wiley, S.; Ragsdale, S. W.; Hoffman, B. M., (13)C Electron Nuclear Double Resonance Spectroscopy Shows Acetyl-CoA Synthase Binds Two Substrate CO in Multiple Binding Modes and Reveals the Importance of a CO-Binding "Alcove". *J Am Chem Soc* **2020***, 142* (36), 15362-15370.

Jazzar, R.; Soleilhavoup, M.; Bertrand, G., Cyclic (Alkyl)- and (Aryl)-(amino)carbene Coinage Metal Complexes and Their Applications. *Chem Rev* **2020**.

Jensen, F. *Introduction to Computational Chemistry*, 3rd ed.; Wiley: Hoboken, NJ, **2017**.

Jensen, F., How Large is the Elephant in the Density Functional Theory Room? *J Phys Chem A* **2017***, 121* (32), 6104-6107.

Jiang, N.; Ramanathan, A.; Bacsa, J.; La Pierre, H. S., Synthesis of a d(1)-titanium fluoride kagome lattice antiferromagnet. *Nat Chem* **2020***, 12* (8), 691-696.

Jiang, Q.; Cundari, T. R., DFT Calculations Investigate Competing Pathways to Form Dimeric Neopentylpalladium(II) Amido Complexes: The Critical Importance of Dispersion. *J Phys Chem A* **2020***, 124* (42), 8798-8805.

Joannou, M. V.; Hoyt, J. M.; Chirik, P. J., Investigations into the Mechanism of Inter- and Intramolecular Iron-Catalyzed [2 + 2] Cycloaddition of Alkenes. *J Am Chem Soc* **2020***, 142* (11), 5314-5330.

Kaim, W.; Paretzki, A., Interacting metal and ligand based open shell systems: Challenges for experiment and theory. *Coordination Chemistry Reviews* **2017***, 344*, 345-354.

Karimi, M.; Borthakur, R.; Dorsey, C. L.; Chen, C. H.; Lajeune, S.; Gabbai, F. P., Bifunctional Carbenium Dications as Metal-Free Catalysts for the Reduction of Oxygen. *J Am Chem Soc* **2020***, 142* (32), 13651-13656.

Katayama, A.; Ohta, T.; Wasada-Tsutsui, Y.; Inomata, T.; Ozawa, T.; Ogura, T.; Masuda, H., Dinitrogen-Molybdenum Complex Induces Dinitrogen Cleavage by One-Electron Oxidation. *Angew Chem Int Ed Engl* **2019***, 58* (33), 11279-11284.

Kaufhold, O.; Hahn, F. E., Carbodicarbenes: divalent carbon(0) compounds. *Angew Chem Int Ed Engl* **2008***, 47* (22), 4057-61.

Kawakita, K.; Beaumier, E. P.; Kakiuchi, Y.; Tsurugi, H.; Tonks, I. A.; Mashima, K., Bis(imido)vanadium(V)-Catalyzed [2+2+1] Coupling of Alkynes and Azobenzenes Giving Multisubstituted Pyrroles. *J Am Chem Soc* **2019***, 141* (10), 4194-4198.

Kawakita, K.; Kakiuchi, Y.; Tsurugi, H.; Mashima, K.; Parker, B. F.; Arnold, J.; Tonks, I. A., Reactivity of terminal imido complexes of group 4-6 metals: stoichiometric and catalytic reactions involving cycloaddition with unsaturated organic molecules. *Coord Chem Rev* **2020***, 407*.

Kellett, C. W.; Kennepohl, P.; Berlinguette, C. P., pi covalency in the halogen bond. *Nat Commun* **2020***, 11* (1), 3310.

Kelley, M. P.; Su, J.; Urban, M.; Luckey, M.; Batista, E. R.; Yang, P.; Shafer, J. C., On the Origin of Covalent Bonding in Heavy Actinides. *J Am Chem Soc* **2017***, 139* (29), 9901-9908.

Kendall, R. A.; Dunning, T. H.; Harrison, R. J., Electron affinities of the first-row atoms revisited. Systematic basis sets and wave functions. *Journal of Chemical Physics* **1992***, 96* (9), 6796-6806.

Kerridge, A., Quantification of f-element covalency through analysis of the electron density: insights from simulation. *Chem Commun (Camb)* **2017***, 53* (50), 6685-6695.

King, A. E.; Nippe, M.; Atanasov, M.; Chantarojsiri, T.; Wray, C. A.; Bill, E.; Neese, F.; Long, J. R.; Chang, C. J., A well-defined terminal vanadium(III) oxo complex. *Inorg Chem* **2014***, 53* (21), 11388-95.

Kinzhalov, M. A.; Luzyanin, K. V., Reactivity of acyclic diaminocarbene ligands. *Coordination Chemistry Reviews* **2019***, 399*.

Kissin, Y. V.; Liu, X.; Pollick, D. J.; Brungard, N. L.; Chang, M. Ziegler-Natta Catalysts for Propylene Polymerization: Chemistry of Reactions Leading to the Formation of Active Centers. *J. Mol. Catal. A Chem.* **2008***, 287*, 45–52.

Kitagawa, Y.; Matsui, T.; Yasuda, N.; Hatake, H.; Kawakami, T.; Yamanaka, S.; Nihei, M.; Okumura, M.; Oshio, H.; Yamaguchi, K., DFT calculations of effective exchange integrals at the complete basis set limit on oxo-vanadium ring complex. *Polyhedron* **2013***, 66*, 97-101.

Klapotke, T. M.; Piercey, D. G., 1,1'-azobis(tetrazole): a highly energetic nitrogen-rich compound with a N10 chain. *Inorg Chem* **2011***, 50* (7), 2732-4.

Kobayashi, K.; Nagase, S. Silicon-Silicon Triple Bonds: Do Substituents Make Disilynes Synthetically Accessible? *Organometallics* **1997***, 16*, 2489–2491.

Kornecki, K. P.; Berry, J. F., Evidence for a one-electron mechanistic regime in dirhodium-catalyzed intermolecular C-H amination. *Chemistry* **2011***, 17* (21), 5827-32.

Korth, M.; Grimme, S. "Mindless" DFT Benchmarking *J. Chem. Theory Comput.* **2009***, 5*, 993-1003.

Kozlowski, P. M.; Kumar, M.; Piecuch, P.; Li, W.; Bauman, N. P.; Hansen, J. A.; Lodowski, P.; Jaworska, M., The Cobalt-Methyl Bond Dissociation in Methylcobalamin: New Benchmark Analysis Based on Density Functional Theory and Completely Renormalized Coupled-Cluster Calculations. *J Chem Theory Comput* **2012***, 8* (6), 1870-94.

Kramkowski, Peter; Gerhard Baum, M. K., Udo Radius, Manfred Scheer, Novel Complexes with a Short Tungsten - Phosphorus Triple Bond. *Chem. Eur. J.* **1999***, 5*, 2890-2898.

Kraus, P.; Frank, I., Density Functional Theory for Microwave Spectroscopy of Noncovalent Complexes: A Benchmark Study. *J Phys Chem A* **2018***, 122* (21), 4894-4901.

Kriegel, B. M.; Bergman, R. G.; Arnold, J. Nitrene Metathesis and Catalytic Nitrene Transfer Promoted by Niobium Bis(imido) Complexes. *J. Am. Chem. Soc.* **2016***, 138*, 52-55.

Kroll, A.; Steinert, H.; Scharf, L. T.; Scherpf, T.; Mallick, B.; Gessner, V. H., A diamino-substituted carbodiphosphorane as strong C-donor and weak N-donor: isolation of monomeric trigonal-planar L.ZnCl2. *Chem Commun (Camb)* **2020***, 56* (58), 8051-8054.

Krylov, A.; Windus, T. L.; Barnes, T.; Marin-Rimoldi, E.; Nash, J. A.; Pritchard, B.; Smith, D. G. A.; Altarawy, D.; Saxe, P.; Clementi, C.; Crawford, T. D.; Harrison, R. J.; Jha, S.; Pande, V. S.; Head-Gordon, T., Perspective: Computational chemistry software and its advancement as illustrated through three grand challenge cases for molecular science. *J Chem Phys* **2018***, 149* (18), 180901.

Kubas, G. J., Dihydrogen complexes as prototypes for the coordination chemistry of saturated molecules. *PNAS* **2007***, 104* (17), 6901–6907.

Kubas, J. G. Molecular Hydrogen Complexes: Coordination of a σ Bond to Transition Metals. *Acc. Chem. Res.* **1988***, 21*, 120-128.

Kurogi, T.; Manor, B. C.; Carroll, P. J.; Mindiola, D. J., Trimethylsilyl imide complexes of tantalum: Can the silyl group be eliminated? *Polyhedron* **2017***, 125*, 80-85.

Kurtz, D. A.; Rossman, G. R.; Hunter, B. M., The Nature of the Mn(III) Color Centers in Elbaite Tourmalines. *Inorg Chem* **2020***, 59* (14), 9618-9626.

Kwon, D.-H.; Fuller, J. T.; Kilgore, U. J.; Sydora, O. L.; Bischof, S. M.; Ess, D. H., Computational Transition-State Design Provides Experimentally Verified Cr(P,N) Catalysts for Control of Ethylene Trimerization and Tetramerization. *ACS Catalysis* **2018***, 8* (2), 1138-1142.

Labinger, J. A., Does cyclopentadienyl iron dicarbonyl dimer have a metal–metal bond? Who's asking? *Inorganica Chimica Acta* **2015***, 424*, 14-19.

Laskowski, C. A.; Miller, A. J.; Hillhouse, G. L.; Cundari, T. R., A two-coordinate nickel imido complex that effects C-H amination. *J Am Chem Soc* **2011***, 133* (4), 771-3.

Laurent, A.; Jacquemin, D. TD-DFT Benchmarks; A Review. *Int. J. Quantum Chem.* **2013***, 113*, 2019-2039.

Laury, M. L.; Deyonker, N. J.; Jiang, W.; Wilson, A. K. A Pseudopotential-Based Composite Method: The Relativistic Pseudopotential Correlation Consistent Composite Approach for Molecules Containing 4d Transition Metals (Y-Cd). *J. Chem. Phys.* **2011***, 135*, 214103.

Laury, M. L.; Wilson, A. K. Performance of Density Functional Theory for Second Row (4d) Transition Metal Thermochemistry. J. Chem. Theory Comput. 2013, 9, 3939–3946.

Lee, T. S.; Allen, B. K.; Giese, T. J.; Guo, Z.; Li, P.; Lin, C.; McGee, T. D., Jr.; Pearlman, D. A.; Radak, B. K.; Tao, Y.; Tsai, H. C.; Xu, H.; Sherman, W.; York, D. M., Alchemical Binding Free Energy Calculations in AMBER20: Advances and Best Practices for Drug Discovery. *J Chem Inf Model* **2020**.

Lemonick, S. As DFT Matures, Will It Become a Push-Button Technology? *C&EN Glob. Enterp.* **2019***, 97*, 16–18.

Levine, I. N. *Quantum Chemistry,* 7th ed. Pearson: New York, NY, **2014**.

Li, Y.; Go, Y. K.; Ooka, H.; He, D.; Jin, F.; Kim, S. H.; Nakamura, R., Enzyme Mimetic Active Intermediates for Nitrate Reduction in Neutral Aqueous Media. *Angew Chem Int Ed Engl* **2020**.

Liakos, D. G.; Sparta, M.; Kesharwani, M. K.; Martin, J. M.; Neese, F., Exploring the Accuracy Limits of Local Pair Natural Orbital Coupled-Cluster Theory. *J Chem Theory Comput* **2015***, 11*, 1525-39.

Liang, G. *Computational studies of catalysis: bioinorganic, inorganic, and organometallic chemistry*. Mississippi State University, Proquest, **2018**.

Liang, G.; Hollis, T. K.; Webster, C. E., Computational Analysis of the Intramolecular Oxidative Amination of an Alkene Catalyzed by the Extreme π-Loading N-Heterocyclic Carbene Pincer Tantalum(V) Bis(imido) Complex. *Organometallics* **2018***, 37*, 1671-1681.

Lin, Y. S.; Li, G. D.; Mao, S. P.; Chai, J. D., Long-Range Corrected Hybrid Density Functionals with Improved Dispersion Corrections. *J Chem Theory Comput* **2013***, 9* (1), 263-72.

Ling, C.; Zhang, R.; Jia, H., Quantum Chemical Design of Doped Ca2MnAlO(5+delta) as Oxygen Storage Media. *ACS Appl Mater Interfaces* **2015***, 7* (26), 14518-27.

Lischka, H.; Nachtigallová, D.; Aquino, A. J. A.; Szalay, P. G.; Plasser, F.; MacHado, F. B. C.; Barbatti, M. Multireference Approaches for Excited States of Molecules. *Chem. Rev.* **2018***, 118*, 7293–7361.

Liu, Y.; Frankcombe, T. J.; Schmidt, T. W., Chemical bonding motifs from a tiling of the many-electron wavefunction. *Phys Chem Chem Phys* **2016***, 18* (19), 13385-94.

Liu, Y.; Varava, P.; Fabrizio, A.; Eymann, L. Y. M.; Tskhovrebov, A. G.; Planes, O. M.; Solari, E.; Fadaei-Tirani, F.; Scopelliti, R.; Sienkiewicz, A.; Corminboeuf, C.; Severin, K., Synthesis of aminyl biradicals by base-induced Csp(3)-Csp(3) coupling of cationic azo dyes. *Chem Sci* **2019***, 10* (22), 5719-5724.

Lo, Y. H.; Gabbaï, F. P., An Antimony(V) Dication as a Z-Type Ligand: Turning on Styrene Activation at Gold. *Angewandte Chemie* **2019***, 131* (30), 10300-10303.

Long, Z.; Atsango, A. O.; Napoli, J. A.; Markland, T. E.; Tuckerman, M. E., Elucidating the Proton Transport Pathways in Liquid Imidazole with First-Principles Molecular Dynamics. *J Phys Chem Lett* **2020***, 11* (15), 6156-6163.

Lorber, C., Titanium and vanadium imido-bridged complexes. *Coordination Chemistry Reviews* **2016***, 308*, 76-96.

Lowe, P.; Feldt, M.; Wunsche, M. A.; Wilm, L. F. B.; Dielmann, F., Oxophosphonium-Alkyne Cycloaddition Reactions: Reversible Formation of 1,2-Oxaphosphetes and Six-membered Phosphorus Heterocycles. *J Am Chem Soc* **2020**.

Lu, H.; Zhang, X. P., Catalytic C-H functionalization by metalloporphyrins: recent developments and future directions. *Chem Soc Rev* **2011***, 40* (4), 1899-909.

Lugosan, A.; Cundari, T.; Fleming, K.; Dickie, D.A.; Zeller, M.; Ghannam, J.; Lee, W. Synthesis, characterization, DFT calculations, and reactivity study of a nitrido-bridged dimeric vanadium(iv) complex. *Dalton Trans.,* **2020***, 49*, 1200-1206.

Luo, Y.-R. *Handbook of Bond Dissociation Energies in Organic Compounds*; CRC Press: Boca Raton, FL, **2003**.

Lupp, D.; Christensen, N. J.; Fristrup, P., Synergy between Experimental and Theoretical Methods in the Exploration of Homogeneous Transition Metal Catalysis. *Dalton Trans.,* **2014***, 43*, 11093-105.

Ma, F.; Xie, H. Bin; Chen, J. Benchmarking of DFT Functionals for the Kinetics and Mechanisms of Atmospheric Addition Reactions of OH Radicals with Phenyl and Substituted Phenyl-Based Organic Pollutants. *Int. J. Quantum Chem.* **2018***, 118*, e25533.

Ma, P.; Chen, H., Ligand-Dependent Multi-State Reactivity in Cobalt(III)-Catalyzed C–H Activations. *ACS Catalysis* **2019***, 9* (3), 1962-1972.

Ma, Q.; Wang, Y.; Tsui, G. C., Stereoselective Palladium-Catalyzed C-F Bond Alkynylation of Tetrasubstituted gem-Difluoroalkenes. *Angew Chem Int Ed Engl* **2020**.

Ma, X.; Hu, J.; Zheng, M.; Li, D.; Lv, H.; He, H.; Huang, C., N2 reduction using single transition-metal atom supported on defective WS2 monolayer as promising catalysts: A DFT study. *Applied Surface Science* **2019***, 489*, 684-692.

Macetti, G.; Wieduwilt, E. K.; Assfeld, X.; Genoni, A., Localized Molecular Orbital-Based Embedding Scheme for Correlated Methods. *J Chem Theory Comput* **2020**.

Malatji, N.; Popoola, P. A. I., Tribological and Corrosion Performance of Electrodeposited Nickel Composite Coatings. In *Electrodeposition of Composite Materials*, **2016**.

Mardirossian, N.; Head-Gordon, M., Thirty Years of Density Functional Theory in Computational Chemistry: An Overview and Extensive Assessment of 200 Density Functionals. *Molecular Physics* **2017***, 115*, 2315-2372.

Mardirossian, N.; Head-Gordon, M., Thirty years of density functional theory in computational chemistry: an overview and extensive assessment of 200 density functionals. *Molecular Physics* **2017***, 115* (19), 2315-2372.

Margulieux, G. W.; Bezdek, M. J.; Turner, Z. R.; Chirik, P. J., Ammonia Activation, H2 Evolution and Nitride Formation from a Molybdenum Complex with a Chemically and Redox Noninnocent Ligand. *J Am Chem Soc* **2017***, 139*, 6110-6113.

Mark S. Gordon, K. A. N., and Donald G. Truhlar*, Parameters for Scaling the Correlation Energy of the Bonds Si-H, P-H, S-H, and CI-H and Application to the Reaction of Silyl Radical with Silane. *J. Phys. Chem.* **1989***, 93* (21), 7356-7358.

Marko, J. A.; Durgham, A.; Bretz, S. L.; Liu, W., Electrochemical benzylic oxidation of C-H bonds. *Chem Commun (Camb)* **2019**, *55* (7), 937-940.

Martin, J. M. L.; De Oliveira, G. Towards Standard Methods for Benchmark Quality ab initio Thermochemistry - W1 and W2 Theory. *J. Chem. Phys.* **1999**, *111*, 1843–1856.

Martínez-Hernández, A.; Manríquez-Guerrero, F.; Torres, J.; Ortega, R.; Pérez-Bueno, J. d. J.; Meas, Y.; Trejo, G.; Méndez-Albores, A., Electrodeposition of Ni-P/SiC Composite Films with High Hardness. In *Electrodeposition of Composite Materials*, **2016**.

Martin-Louis Y. Riu, R. L. J., Wesley J. Transue, Peter Müller, Christopher C. Cummins, Isolation of an elusive phosphatetrahedrane. *Sci. Adv.* **2020**, *6*, 8.

Mashima, K., Redox-Active α-Diimine Complexes of Early Transition Metals: From Bonding to Catalysis. *Bulletin of the Chemical Society of Japan* **2020**, *93* (6), 799-820.

Máté J. Bezdek, S. G., Paul J. Chirik, Coordination-induced weakening of ammonia,water, and hydrazine X–H bonds in a molybdenum complex. *Science* **2016**, *354* (6313), 730-733.

Matsunaga, N. K., Shiro Gordon, Mark S. , Relativistic potential energy surfaces of XH_2 (X_5C, Si, Ge, Sn, and Pb) molecules: Coupling of 1A1 and 3B1 states. *J. Chem. Phys.* **1996**, *104*, 7988-7996.

Matxain, J. M.; Piris, M.; Lopez, X.; Ugalde, J. M., Complete Basis Set Limit Extrapolation Calculations with $PNOF_3$. *Chemical Physics Letters* **2010**, *499*, 164-167.

Maurya, M. R.; Rana, L.; Avecilla, F. Oxidoperoxidotungsten(VI) and Dioxidotungsten(VI) Complexes Catalyzed Oxidative Bromination of Thymol in Presence of H_2O_2-KBr-$HClO_4$. *Inorg. Chim. Acta* **2016**, *440*, 172–180.

Mayernick, A. D.; Janik, M. J. Methane Activation and Oxygen Vacancy Formation over CeO2 and Zr, Pd Substituted CeO 2 Surfaces. *J. Phys. Chem. C* **2008**, *112*, 14955–14964.

McGill, T. L.; Williams, L. C.; Mulford, D. R.; Blakey, S. B.; Harris, R. J.; Kindt, J. T.; Lynn, D. G.; Marsteller, P. A.; McDonald, F. E.; Powell, N. L., Chemistry Unbound: Designing a New Four-Year Undergraduate Curriculum. *Journal of Chemical Education* **2018**, *96* (1), 35-46.

McMahon, M.; Lamont, D. J.; Beattie, K. A.; Hayes, J. D., Keap1 perceives stress via three sensors for the endogenous signaling molecules nitric oxide, zinc, and alkenals. *Proc Natl Acad Sci U S A* **2010**, *107* (44), 18838-43.

Meek, S. J.; Pitman, C. L.; Miller, A. J. M., Deducing Reaction Mechanism: A Guide for Students, Researchers, and Instructors. *Journal of Chemical Education* **2016**, *93* (2), 275-286.

Mehta, N.; Casanova-Paez, M.; Goerigk, L., Semi-empirical or non-empirical double-hybrid density functionals: which are more robust? *Phys Chem Chem Phys* **2018***, 20* (36), 23175-23194.

Messinis, A. M.; Batsanov, A. S.; Wright, W. R. H.; Howard, J. A. K.; Hanton, M. J.; Dyer, P. W., Bis(Imido) Tungsten Complexes: Efficient Precatalysts for the Homogeneous Dimerization of Ethylene. *ACS Catalysis* **2018***, 8*, 11249-11263.

Metz, M. P.; Szalewicz, K., Automatic Generation of Flexible-Monomer Intermolecular Potential Energy Surfaces. *J Chem Theory Comput* **2020***, 16* (4), 2317-2339.

Miessler, G. L.; Fischer, P.J.; Tarr, D. A.; *Inorganic Chemistry* 5th ed.; Pearson: New York, NY, **2014**.

Miliordos, E.; Xantheas, S. S., An accurate and efficient computational protocol for obtaining the complete basis set limits of the binding energies of water clusters at the MP2 and CCSD(T) levels of theory: Application to $(H_2O)m$, m = 2-6, 8, 11, 16, and 17. *J Chem Phys* **2015***, 142* (23), 234303.

Minasian, S. G.; Batista, E. R.; Booth, C. H.; Clark, D. L.; Keith, J. M.; Kozimor, S. A.; Lukens, W. W.; Martin, R. L.; Shuh, D. K.; Stieber, S. C. E.; Tylisczcak, T.; Wen, X. D., Quantitative Evidence for Lanthanide-Oxygen Orbital Mixing in CeO_2, PrO_2, and TbO_2. *J Am Chem Soc* **2017***, 139* (49), 18052-18064.

Mindiola, D. J.; Hillhouse, G. L., Terminal Amido and Imido Complexes of Three-Coordinate Nickel. *J. Am. Chem. Soc.* **2001***, 123*, 4623-4624.

Moerdyk, J. P.; Bielawski, C. W. Stable Carbenes. *Contemp. Carbene Chem.* **2013***,* 40–74.

Møller, C.; Plesset, M. S. Note on an Approximation Treatment for Many-Electron Systems. *Phys. Rev.* **1934***, 46*, 618–622.

Montgomery, C. Fischer and Schrock Carbene Complexes: A Molecular Modeling Exercise. *J. Chem. Educ.* **2015***, 92*, 1653-1660.

Montoya, E.; Cundari, T. R., Computational study of the impact of ancillary ligands upon a tungsten (IV) imide complex for catalytic methane functionalization. *Computational and Theoretical Chemistry* **2018***, 1142*, 9-14.

Morrow, R.; Sturza, M. I.; Ray, R.; Himcinschi, C.; Kern, J.; Schlender, P.; Richter, M.; Wurmehl, S.; Büchner, B., *Discovery, Crystal Growth, and Characterization of Garnet* Eu_2.

Moulder, C. A.; Cundari, T. R., 5d Metal(IV) Imide Complexes. The Impact (or Lack Thereof) of d-Orbital Occupation on Methane Activation and Functionalization. *Inorg Chem* **2017***, 56*, 1823-1829.

Moulder, C. A.; Cundari, T. R., A DFT Survey of the Effects of d-Electron Count and Metal Identity on the Activation and Functionalization of C−H Bonds for Mid to Late Transition Metals. *Isr. J. Chem.* **2017***, 57*, 1023-1031.

Moulder, C. A.; Kafle, K.; Zhou, C. X.; Cundari, T. R., Thermochemistry of Tungsten-3p Elements for Density Functional Theory, Caveat Lector! *J Phys Chem A* **2021***, 125*, 681-690.

Moulder, C.; A.; Kafle, K.; R. Cundari, T.; Cundari, T. R. Tungsten–Ligand Bond Strengths for 2p Elements Including σ- and π-Bond Strength Components, a Density Functional Theory and ab initio Study. *J. Phys. Chem. A* **2019***, 123*, 7940–7949.

Moysiadou, A.; Lee, S.; Hsu, C. S.; Chen, H. M.; Hu, X., Mechanism of Oxygen Evolution Catalyzed by Cobalt Oxyhydroxide: Cobalt Superoxide Species as a Key Intermediate and Dioxygen Release as a Rate-Determining Step. *J Am Chem Soc* **2020***, 142* (27), 11901-11914.

Muldoon, J.; Bucur, C. B.; Gregory, T., Fervent Hype behind Magnesium Batteries: An Open Call to Synthetic Chemists-Electrolytes and Cathodes Needed. *Angew Chem Int Ed Engl* **2017***, 56* (40), 12064-12084.

Murray, R., Skillful writing of an awful research paper. *Anal Chem* **2011***, 83* (3), 633.

Najafian, A.; Cundari, T. R., Computational Mechanistic Study of Electro-Oxidation of Ammonia to N2 by Homogenous Ruthenium and Iron Complexes. *J Phys Chem A* **2019***, 123*, 7973-7982.

Nakai, H.; Miyata, S.; Kajiwara, Y.; Ozawa, Y.; Abe, M., A non-linear phenomenon observed in the photochromic crystals of a rhodium dithionite complex with n-propyl moieties. *Dalton Trans* **2020***, 49* (6), 1721-1725.

Nandi, A.; Kozuch, S., History and Future of Dative Bonds. *Chemistry* **2020***, 26* (4), 759-772.

Nazemi, A.; Cundari, T. R., Computational Analysis of Proton-Coupled Electron Transfer in Hydrotris(triazolyl)borate Mid–Late 3d and 4d Transition Metal Complexes. *Organometallics* **2019***, 38* (19), 3521-3531.

Neese, F. Software Update: The ORCA Program System, Version 4.0. Wiley Interdiscip. *Rev. Comput. Mol. Sci.* **2018***, 8*.

Neese, F. The ORCA Program System. Wiley Interdiscip. *Rev. Comput. Mol. Sci.* **2012***, 2*, 73–78.

Niklas, J. E.; Hardy, E. E.; Gorden, A. E. V., Solid-state structural elucidation and electrochemical analysis of uranyl naphthylsalophen. *Chem Commun (Camb)* **2018***, 54* (83), 11693-11696.

Nilova, A.; Campeau, L. C.; Sherer, E. C.; Stuart, D. R., Analysis of Benzenoid Substitution Patterns in Small Molecule Active Pharmaceutical Ingredients. *J Med Chem* **2020**.

Niwa, T.; Hosoya, T., Molecular Renovation Strategy for Expeditious Synthesis of Molecular Probes. *Bulletin of the Chemical Society of Japan* **2020***, 93* (2), 230-248.

Nurdin, L.; Piers, W. E.; Lin, J.-B.; Gelfand, B. S., Synthesis, Characterization, and Reactivity of Neutral Octahedral Alkyl-Cobalt(III) Complexes Bearing a Dianionic Pentadentate Ligand. *Organometallics* **2020***, 39* (12), 2269-2277.

O'Connor, K. S.; Lamb, J. R.; Vaidya, T.; Keresztes, I.; Klimovica, K.; LaPointe, A. M.; Daugulis, O.; Coates, G. W., Understanding the Insertion Pathways and Chain Walking Mechanisms of α-Diimine Nickel Catalysts for α-Olefin Polymerization: A 13C NMR Spectroscopic Investigation. *Macromolecules* **2017***, 50*, 7010-7027.

O'Connor, K. S.; Watts, A.; Vaidya, T.; LaPointe, A. M.; Hillmyer, M. A.; Coates, G. W., Controlled Chain Walking for the Synthesis of Thermoplastic Polyolefin Elastomers: Synthesis, Structure, and Properties. *Macromolecules* **2016***, 49* (18), 6743-6751.

Odetola, P.; Popoola, P.; Popoola, O.; Delport, D., Electrodeposition of Functional Coatings on Bipolar Plates for Fuel Cell Applications – A Review. In *Electrodeposition of Composite Materials*, **2016**.

Odetola, P.; Popoola, P.; Popoola, O.; Delport, D., Parametric Variables in Electro-deposition of Composite Coatings. In *Electrodeposition of Composite Materials*, **2016**.

Odugbesi, G. A.; Nan, H.; Soltani, M.; Davis, J. H., Jr.; Anderson, J. L., Ultra-high thermal stability perarylated ionic liquids as gas chromatographic stationary phases for the selective separation of polyaromatic hydrocarbons and polychlorinated biphenyls. *J Chromatogr A* **2019***, 1604*, 460466.

Oeschger, R.; BoSu; Isaac Yu; Christian Ehinger; Erik Romero; Sam He; Hartwig, J., Diverse functionalization of strong alkyl C–H bonds by undirected borylation. *Science* **2020***, 368*, 736–741.

Ogura, T.; Tong, K. I.; Mio, K.; Maruyama, Y.; Kurokawa, H.; Sato, C.; Yamamoto, M., Keap1 is a forked-stem dimer structure with two large spheres enclosing the intervening, double glycine repeat, and C-terminal domains. *Proc Natl Acad Sci U S A* **2010***, 107* (7), 2842-7.

Olivos Suarez, A. I.; Lyaskovskyy, V.; Reek, J. N.; van der Vlugt, J. I.; de Bruin, B., Complexes with nitrogen-centered radical ligands: classification, spectroscopic features, reactivity, and catalytic applications. *Angew Chem Int Ed Engl* **2013***, 52* (48), 12510-29.

Omiya, T.; Natta, S.; Wised, K.; Tsutsumi, K.; Nomura, K., Synthesis and structural analysis of niobium(V) complexes containing amine triphenolate ligands of the type, [NbCl(X)(O-2,4-R2C6H2-6-CH2)3N] (R = Me, Bu; X = Cl, CF3SO3), and their use in catalysis for ethylene polymerization. *Polyhedron* **2017***, 125*, 9-17.

O'Reilly, M. E.; Kim, R. S.; Oh, S.; Surendranath, Y., Catalytic Methane Monofunctionalization by an Electrogenerated High-Valent Pd Intermediate. *ACS Cent Sci* **2017***, 3* (11), 1174-1179.

Ozkanlar, A.; Zhou, T.; Clark, A. E., Towards a unified description of the hydrogen bond network of liquid water: a dynamics based approach. *J Chem Phys* **2014***, 141* (21), 214107.

Padilla-Velez, O.; O'Connor, K. S.; LaPointe, A. M.; MacMillan, S. N.; Coates, G. W., Switchable living nickel(ii) alpha-diimine catalyst for ethylene polymerisation. *Chem Commun (Camb)* **2019***, 55* (53), 7607-7610.

Pansini, F. N. N.; Neto, A. C.; Varandas, A. J. C., On the performance of various hierarchized bases in extrapolating the correlation energy to the complete basis set limit. *Chemical Physics Letters* **2015***, 641*, 90-96.

Pappas, I.; Chirik, P. J. Catalytic Proton Coupled Electron Transfer from Metal Hydrides to Titanocene Amides, Hydrazides and Imides: Determination of Thermodynamic Parameters Relevant to Nitrogen Fixation. *J. Am. Chem. Soc.* **2016***, 138*, 13379−13389.

Park, J. W.; Al-Saadon, R.; MacLeod, M. K.; Shiozaki, T.; Vlaisavljevich, B., Multireference Electron Correlation Methods: Journeys along Potential Energy Surfaces. *Chem Rev* **2020**.

Parveen, R.; Cundari, T. R.; Younker, J. M.; Rodriguez, G., Computational Assessment of Counterion Effect of Borate Anions on Ethylene Polymerization by Zirconocene and Hafnocene Catalysts. *Organometallics* **2020**.

Parveen, R.; Cundari, T. R.; Younker, J. M.; Rodriguez, G.; McCullough, L., DFT And QSAR Studies of Ethylene Polymerization by Zirconocene Catalysts. *ACS Catalysis* **2019***,* 9339-9349.

Patel, P.; Wang, J.; Wilson, A. K., Prediction of pKa s of Late Transition-Metal Hydrides via a QM/QM Approach. *J Comput Chem* **2020***, 41* (3), 171-183.

Paul, S. S.; Selim, M.; Saha, A.; Mukherjea, K. K. Synthesis and Structural Characterization of Dioxomolybdenum and Dioxotungsten Hydroxamato Complexes and Their Function in the Protection of Radiation Induced DNA Damage. *Dalton Trans.* **2014***, 43*, 2835–2848.

Peltzer, R. M.; Gauss, J.; Eisenstein, O.; Cascella, M., The Grignard Reaction - Unraveling a Chemical Puzzle. *J Am Chem Soc* **2020***, 142* (6), 2984-2994.

Penchoff, D. A.; Peterson, C. C.; Quint, M. S.; Auxier, J. D., 2nd; Schweitzer, G. K.; Jenkins, D. M.; Harrison, R. J.; Hall, H. L., Structural Characteristics, Population Analysis, and Binding Energies of [An(NO3)](2+) (with An = Ac to Lr). *ACS Omega* **2018***, 3* (10), 14127-14143.

Perdew, J. P.; Ruzsinszky, A.; Tao, J.; Staroverov, V. N.; Scuseria, G. E.; Csonka, G. I., Prescription for the Design and Selection of Density Functional Approximations: More Constraint Satisfaction with Fewer Fits. *J Chem Phys* **2005***, 123*, 62201.

Pérez-Jiméneza, Marina; Camposa, Jesús; López-Serranoa, Joaquín; Carmona, E., *Reactivity of a trans-[H-Mo≡Mo-H] Unit Towards Alkenes and Alkynes*.

Peterson, A. A., Acceleration of saddle-point searches with machine learning. *J Chem Phys* **2016***, 145* (7), 074106.

Peterson, D. A. M., Dear Reviewer 2: Go F' Yourself. *Social Science Quarterly* **2020***, 101* (4), 1648-1652.

Pignedoli, C. A.; Curioni, A.; Andreoni, W., Disproving A Silicon Analog of an Alkyne with the Aid of Topological Analyses of the Electronic Structure and ab initio Molecular Dynamics Calculations. *Chemphyschem* **2005***, 6*, 1795-9.

Piro, N. A.; Lichterman, M. F.; Harman, W. H.; Chang, C. J., A structurally characterized nitrous oxide complex of vanadium. *J Am Chem Soc* **2011***, 133* (7), 2108-11.

Pitzer, K. S., Repulsive Forces in Relation to Bond Energies, Distances and Other Properties. *J. Am. Chem. Soc.* **1948***, 70*, 2140-2145.

Planas, O.; Peciukenas, V.; Cornella, J., Bismuth-Catalyzed Oxidative Coupling of Arylboronic Acids with Triflate and Nonaflate Salts. *J Am Chem Soc* **2020***, 142* (26), 11382-11387.

Plessow, P. N.; Studt, F., How Accurately Do Approximate Density Functionals Predict Trends in Acidic Zeolite Catalysis? *J Phys Chem Lett* **2020**, 4305-4310.

Pluth, M. D.; Tonzetich, Z. J., Hydrosulfide Complexes of the Transition Elements: Diverse Roles in Bioinorganic, Cluster, Coordination, and Organometallic Chemistry. *Chem Soc Rev* **2020**.

Pople, J. A.; Head-Gordon, M.; Fox, D. J.; Raghavachari, K.; Curtiss, L. A. Gaussian-1 Theory: a General Procedure for Prediction of Molecular Energies. *J. Chem. Phys.* **1989***, 90*, 5622–5629.

Poskrebyshev, G. A., The values of ΔfG°T(Aln) (n = 3–10 atoms, T ≤ 3000 K), determined using the ROCBS-QB3 values of S°T(Aln) and of the corrected values of ΔfH°T(Aln). *Computational and Theoretical Chemistry* **2018***, 1143*, 52-63.

Potential scarcity relative to world demand. Courtesy of the Center for Sustainable Materials Chemistry Oregon State University and the University of Oregon

Prascher, B. P.; Lai, J. D.; Wilson, A. K., The resolution of the identity approximation applied to the correlation consistent composite approach. *J Chem Phys* **2009***, 131* (4), 044130.

Prascher, B. P.; Lucente-Schultz, R. M.; Wilson, A. K., A CCSD(T) and ccCA study of mixed silicon hydrides and halides: Structures and thermochemistry. *Chemical Physics* **2009***, 359* (1-3), 1-13.

Prascher, B. P.; Wilson, A. K., A computational study of dihalogen-μ-dichalcogenides: XAAX (X=F, Cl, Br; A=S, Se). *Journal of Molecular Structure: THEOCHEM* **2007***, 814* (1-3), 1-10.

Prascher, B. P.; Wilson, B. R.; Wilson, A. K., Behavior of density functionals with respect to basis set. VI. Truncation of the correlation consistent basis sets. *J Chem Phys* **2007***, 127* (12), 124110.

Prascher, B. P.; Woon, D. E.; Peterson, K. A.; Dunning, T. H.; Wilson, A. K., Gaussian basis sets for use in correlated molecular calculations. VII. Valence, core-valence, and scalar relativistic basis sets for Li, Be, Na, and Mg. *Theoretical Chemistry Accounts* **2010***, 128* (1), 69-82.

Price, J. S.; Emslie, D. J. H., Interconversion and Reactivity of Manganese Silyl, Silylene, and Silene Complexes. *Chem. Sci.* **2019***, 10*, 10853-10869.

Radius, U.; Nitsch, J.; Krahfuss, M. J.; Bickelhaupt, F. M.; Marder, T. B., N-Heterocyclic Silylenes as Ligands in Transition Metal Carbonyl Chemistry: Nature of their Bonding and Supposed Innocence. *Chemistry* **2020**.

Reiher, M., A Theoretical Challenge: Transition-Metal Compounds. *CHIMIA International Journal for Chemistry* **2009***, 63* (3), 140-145.

Rettew, D. C.; McGinnis, E. W.; Copeland, W.; Nardone, H. Y.; Bai, Y.; Rettew, J.; Devadenam, V.; Hudziak, J. J., Personality trait predictors of adjustment during the COVID pandemic among college students. *PLoS One* **2021***, 16* (3), e0248895.

Rezac, J.; Simova, L.; Hobza, P., CCSD[T] Describes Noncovalent Interactions Better than the CCSD(T), CCSD(TQ), and CCSDT Methods. *J Chem Theory Comput* **2013***, 9*, 364-9.

Rezende, T. G. L.; Cesar, D. V.; do Lago, D. C. B.; Senna, L. F., A review of Corrosion Resistance Nanocomposite Coatings. In *Electrodeposition of Composite Materials*, **2016**.

Rickhaus, M.; Jirasek, M.; Tejerina, L.; Gotfredsen, H.; Peeks, M. D.; Haver, R.; Jiang, H. W.; Claridge, T. D. W.; Anderson, H. L., Global aromaticity at the nanoscale. *Nat Chem* **2020**.

Rintelman, J. M.; Gordon, M. S., Structure and energetics of the silicon carbide clusters SiC3 and Si_2C_2. *Journal of Chemical Physics* **2001***, 115* (4), 1795-1803.

Riplinger, C.; Sandhoefer, B.; Hansen, A.; Neese, F., Natural Triple Excitations in Local Coupled Cluster Calculations with Pair Natural Orbitals. *J Chem Phys* **2013***, 139*, 134101.

Roche Allred, Z. D.; Bretz, S. L., Development of the Quantization and Probability Representations Inventory as a Measure of Students' Understandings of Particulate and Symbolic Representations of Electron Structure. *Journal of Chemical Education* **2019***, 96* (8), 1558-1570.

Roque, J. B.; Kuroda, Y.; Jurczyk, J.; Xu, L.-P.; Ham, J. S.; Göttemann, L. T.; Roberts, C. A.; Adpressa, D.; Saurí, J.; Joyce, L. A.; Musaev, D. G.; Yeung, C. S.; Sarpong, R., C–C Cleavage Approach to C–H Functionalization of Saturated Aza-Cycles. *ACS Catalysis* **2020***, 10* (5), 2929-2941.

Rosen, A. S.; Mian, M. R.; Islamoglu, T.; Chen, H.; Farha, O. K.; Notestein, J. M.; Snurr, R. Q., Tuning the Redox Activity of Metal-Organic Frameworks for Enhanced, Selective O2 Binding: Design Rules and Ambient Temperature O2 Chemisorption in a Cobalt-Triazolate Framework. *J Am Chem Soc* **2020***, 142* (9), 4317-4328.

Roy, S.; Mondal, K. C.; Roesky, H. W., Cyclic Alkyl(amino) Carbene Stabilized Complexes with Low Coordinate Metals of Enduring Nature. *Acc Chem Res* **2016***, 49* (3), 357-69.

Ruan, W.; Yang, T.; Shi, C.; Bai, W.; Sung, H. H. Y.; Williams, I. D.; Lin, Z.; Jia, G., Substituent Effect on the Reactions of OsCl2(PPh3)3 with o-Ethynylphenyl Carbonyl Compounds. *Organometallics* **2020***, 39* (4), 574-584.

Ruscic, B.; Berkowitz, J. Photoionization Mass Spectrometric Studies of the Transient Species Si 2Hn (N=2-5). *J. Chem. Phys.* **1991***, 95*, 2416–2432.

Ryu, H.; Park, J.; Kim, H. K.; Park, J. Y.; Kim, S.-T.; Baik, M.-H., Pitfalls in Computational Modeling of Chemical Reactions and How to Avoid Them. *Organometallics* **2018***, 37*, 3228-3239.

Sadow, A. D.; Tilley, T. D. Activation of Arene C-H Bonds by a Cationic Hafnium Silyl Complex Possessing an α-Agostic Si-H Interaction. *J. Am. Chem. Soc.* **2002***, 124*, 6814–6815.

Safaei, Z.; Shayesteh, A., Ab Initio Calculations on Sequential Reactions of Nitric Oxide with Titanium Ions in the Gas Phase. *J Phys Chem A* **2020***, 124* (25), 5194-5203.

Saito, M.; Hamada, J.; Furukawa, S.; Hada, M.; Dostál, L.; Růžička, A., Transition-Metal Capping to Suppress Back-Donation to Enhance Donor Ability. *Organometallics* **2020**.

Sancakoglu, O., A New Approach — In-Situ Codeposition of Composite Coatings. In *Electrodeposition of Composite Materials*, **2016**.

Sánchez-Márquez, J.; García, V.; Zorrilla, D.; Fernández, M., On Electronegativity, Hardness, and Reactivity Descriptors: A New Property-Oriented Basis Set. *Journal of Physical Chemistry A* **2020**.

Saouma, C. T.; Peters, J. C., M identical withE and M=E Complexes of Iron and Cobalt that Emphasize Three-fold Symmetry (E = O, N, NR). *Coord Chem Rev* **2011***, 255* (7-8), 920-937.

Schafer, D. F.; Wolczanski, P. T.; Lobkovsky, E. B., Alkane Binding Implicated in Reactions of (tBu3SiN═)3WHK and Alkyl Halides. *Organometallics* **2011***, 30*, 6518-6538.

Schafer, D. F.; Wolczanski, P. T.; Lobkovsky, E. B., Reactivity Studies of (tBu3SiNH)(tBu3SiN═)2WH Including Anionic Derivatives Featuring the Tris-tri-tert-butylsilylimide Tungsten Core. *Organometallics* **2011***, 30*, 6539-6561.

Scheer, M.; Kramkowski, P.; Schuster, K. An Approach to Novel Complexes with a Tungsten-Phosphorus Triple Bond. *Organometallics* **1999***, 18*, 2874–2883.

Scheibel, M. G.; Abbenseth, J.; Kinauer, M.; Heinemann, F. W.; Würtele, C.; de Bruin, B.; Schneider, S. Homolytic N−H Activation of Ammonia: Hydrogen Transfer of Parent Iridium Ammine, Amide, Imide, and Nitride Species. *Inorg. Chem.* **2015***, 54*, 9290−9302.

Scheiner, S.; Wysokinski, R.; Michalczyk, M.; Zierkiewicz, W., Pnicogen Bonds Pairing Anionic Lewis Acid with Neutral and Anionic Bases. *J Phys Chem A* **2020***, 124* (24), 4998-5006.

Schipper, D. E.; Young, B. E.; Whitmire, K. H., Transformations in Transition-Metal Carbonyls Containing Arsenic: Exploring the Chemistry of [Et4N]2[HAs{Fe(CO)4}3] in the Search for Single-Source Precursors for Advanced Metal Pnictide Materials. *Organometallics* **2016***, 35* (4), 471-483.

Schrock, R. R. Catalytic Reduction of Dinitrogen to Ammonia by Molybdenum: Theory versus Experiment. *Angew. Chem., Int. Ed.* **2008***, 47*, 5512−5522.

Schrock, R. R., High Oxidation State Multiple Metal−Carbon Bonds. *Chem. Rev.* **2002***, 102*, 145−179.

Schrock, R. R., Meakin, P. Pentamethyl Complexes of Niobium and Tantalum. *Journal of the American Chemical Society* **1974***, 96*, 5288-5290.

Schwarz, A. D.; Nova, A.; Clot, E.; Mountford, P., Titanium tert-butoxyimido compounds. *Inorg Chem* **2011***, 50* (23), 12155-71.

Schwendt, P.; Tatiersky, J.; Krivosudský, L.; Šimuneková, M., Peroxido complexes of vanadium. *Coordination Chemistry Reviews* **2016***, 318*, 135-157.

Seery, M. K.; Flaherty, A. A., Ten Tips for Running an Online Conference. *Journal of Chemical Education* **2020***, 97* (9), 2779-2782.

Shan, X.; Guo, F.; Charles, D. S.; Lebens-Higgins, Z.; Abdel Razek, S.; Wu, J.; Xu, W.; Yang, W.; Page, K. L.; Neuefeind, J. C.; Feygenson, M.; Piper, L. F. J.; Teng, X., Structural

water and disordered structure promote aqueous sodium-ion energy storage in sodium-birnessite. *Nat Commun* **2019***, 10* (1), 4975.

Sharma, A.; Das, S.; Das, K., Pulse Electrodeposition of Lead-Free Tin-Based Composites for Microelectronic Packaging. In *Electrodeposition of Composite Materials*, **2016**.

Shea, J. A. R.; Neuscamman, E., Communication: A mean field platform for excited state quantum chemistry. *J Chem Phys* **2018***, 149* (8), 081101.

Shennan, B. D. A.; Smith, P. W.; Ogura, Y.; Dixon, D. J., A modular and divergent approach to spirocyclic pyrrolidines. *Chemical Science* **2020**.

Shoaf, A. L.; Bayse, C. A., The Effect of Nitro Groups on N2 Extrusion from Aromatic Azide-based Energetic Materials. *New J. Chem.* **2019***, 43*, 15326-15334.

Shoaf, A. L.; Bayse, C. A., Trigger Bond Analysis of Nitroaromatic Energetic Materials Using Wiberg Bond Indices. *J Comput Chem* **2018***, 39*, 1236-1248.

Shoemaker, J.; Burggraf, L. W.; Gordon, M. S., An ab initio cluster study of the structure of the Si(001) surface. *Journal of Chemical Physics* **2000***, 112* (6), 2994-3005.

Shoji, S.; Peng, X.; Yamaguchi, A.; Watanabe, R.; Fukuhara, C.; Cho, Y.; Yamamoto, T.; Matsumura, S.; Yu, M.-W.; Ishii, S.; Fujita, T.; Abe, H.; Miyauchi, M., Photocatalytic uphill conversion of natural gas beyond the limitation of thermal reaction systems. *Nature Catalysis* **2020***, 3* (2), 148-153.

Sicilia, E.; Mazzone, G.; Pérez-González, A.; Pirillo, J.; Galano, A.; Heine, T.; Russo, N. Direct and Cluster-Assisted Dehydrogenation of Methane by Nb+and Ta+: A Theoretical Investigation. *Phys. Chem. Chem. Phys.* **2017***, 19*, 16178–16188.

Simões, J. A. M.; Beauchamp, J. L. Transition Metal–Hydrogen and Metal–Carbon Bond Strengths: The Keys to Catalysis. *Chem. Rev.* **1990***, 90*, 629–688.

Simonneau, A.; Turrel, R.; Vendier, L.; Etienne, M., Group 6 Transition-Metal/Boron Frustrated Lewis Pair Templates Activate N2 and Allow its Facile Borylation and Silylation. *Angew Chem Int Ed Engl* **2017***, 56* (40), 12268-12272.

Singh, S. K.; Eng, J.; Atanasov, M.; Neese, F., Covalency and chemical bonding in transition metal complexes: An ab initio based ligand field perspective. *Coordination Chemistry Reviews* **2017***, 344*, 2-25.

Sinha, V.; Laan, J. J.; Pidko, E. A., Accurate and rapid prediction of pKa of transition metal complexes: semiempirical quantum chemistry with a data-augmented approach. *Phys Chem Chem Phys* **2021***, 23* (4), 2557-2567.

Slanina, T.; Ayub, R.; Toldo, J.; Sundell, J.; Rabten, W.; Nicaso, M.; Alabugin, I.; Fdez Galvan, I.; Gupta, A. K.; Lindh, R.; Orthaber, A.; Lewis, R. J.; Gronberg, G.; Bergman, J.; Ottosson, H., Impact of Excited-State Antiaromaticity Relief in a Fundamental Benzene

Photoreaction Leading to Substituted Bicyclo[3.1.0]hexenes. *J Am Chem Soc* **2020***, 142* (25), 10942-10954.

Smith, J. M. Smith; Lachicotte, R. J.; Pittard, K. A.; Cundari, T. R.; Lukat-Rodgers, G; Rodgers, K. R.; Holland, P. L., Stepwise Reduction of Dinitrogen Bond Order by a Low-Coordinate Iron Complex. *J. Am. Chem. Soc.* **2001***, 123*, 9222-9223.

Smith, J. M.; Azwana R. Sadique; Thomas R. Cundari; Kenton R. Rodgers; Gudrun Lukat-Rodgers; Rene J. Lachicotte; Christine J. Flaschenriem; Javier Vela; Holland, P. L., Studies of Low-Coordinate Iron Dinitrogen Complexes. *J. Am. Chem. Soc.* **2006***, 128* (3), 756-769.

Smith, J. M.; Rene J. Lachicotte; Karl A. Pittard; Thomas R. Cundari; Gudrun Lukat-Rodgers; Kenton R. Rodgers; Holland, P. L., Stepwise Reduction of Dinitrogen Bond Order by a Low-Coordinate Iron Complex. *J. Am. Chem. Soc.* **2001***, 123*, 9222-9223.

Solowey, D. P.; Mane, M. V.; Kurogi, T.; Carroll, P. J.; Manor, B. C.; Baik, M. H.; Mindiola, D. J., A new and selective cycle for dehydrogenation of linear and cyclic alkanes under mild conditions using a base metal. *Nat Chem* **2017***, 9* (11), 1126-1132.

Spielvogel, K. D.; Luna, J. A.; Loria, S. M.; Weisburn, L. P.; Stumme, N. C.; Ringenberg, M. R.; Durgaprasad, G.; Keith, J. M.; Shaw, S. K.; Daly, S. R., Influence of Multisite Metal-Ligand Cooperativity on the Redox Activity of Noninnocent N2S2 Ligands. *Inorg Chem* **2020***, 59* (15), 10845-10853.

Sterenberg, B. T.; Senturk, O. S.; Udachin, K. A.; Carty, A. J., Reactivity of Terminal, Electrophilic Phosphinidene Complexes of Molybdenum and Tungsten. Nucleophilic Addition at Phosphorus and P-P Bond Forming Reactions with Phosphines and Diphosphines. *Organometallics* **2007***, 26*, 925-937.

Sterenberg, B. T.; Udachin, K. A.; Carty, A. J., Electrophilic "Fischer Type" Phosphinidene Complexes of Molybdenum, Tungsten, and Ruthenium. *Organometallics* **2001***, 20*, 2657-2659.

Stuyver, T.; De Proft, F.; Geerlings, P.; Shaik, S., How Do Local Reactivity Descriptors Shape the Potential Energy Surface Associated with Chemical Reactions? The Valence Bond Delocalization Perspective. *J Am Chem Soc* **2020**.

Su, J.; Batista, E. R.; Boland, K. S.; Bone, S. E.; Bradley, J. A.; Cary, S. K.; Clark, D. L.; Conradson, S. D.; Ditter, A. S.; Kaltsoyannis, N.; Keith, J. M.; Kerridge, A.; Kozimor, S. A.; Loble, M. W.; Martin, R. L.; Minasian, S. G.; Mocko, V.; La Pierre, H. S.; Seidler, G. T.; Shuh, D. K.; Wilkerson, M. P.; Wolfsberg, L. E.; Yang, P., Energy-Degeneracy-Driven Covalency in Actinide Bonding. *J Am Chem Soc* **2018***, 140* (51), 17977-17984.

Sugahara, T.; Guo, J. D.; Hashizume, D.; Sasamori, T.; Nagase, S.; Tokitoh, N., The selective formation of a 1,2-disilabenzene from the reaction of a disilyne with phenylacetylene. *Dalton Trans* **2018***, 47* (38), 13318-13322.

Suh, S. E.; Chen, S. J.; Mandal, M.; Guzei, I. A.; Cramer, C. J.; Stahl, S. S., Site-Selective Copper-Catalyzed Azidation of Benzylic C-H Bonds. *J Am Chem Soc* **2020***, 142* (26), 11388-11393.

Sun, Z.; Hull, O. A.; Cundari, T. R., Computational Study of Methane C-H Activation by Diiminopyridine Nitride/Nitridyl Complexes of 3d Transition Metals and Main-Group Elements. *Inorg Chem* **2018***, 57*, 6807-6815.

Szecsenyi, A.; Li, G.; Gascon, J.; Pidko, E. A., Unraveling reaction networks behind the catalytic oxidation of methane with H2O2 over a mixed-metal MIL-53(Al,Fe) MOF catalyst. *Chem Sci* **2018***, 9* (33), 6765-6773.

Takahiro Sasamori, K. H., † Yusuke Sugiyama,† Nozomi Takagi,‡ Shigeru Nagase,‡ Yoshinobu Hosoi,§ Yukio Furukawa,§ and Norihiro Tokitoh*, Synthesis and Reactions of a Stable 1,2-Diaryl-1,2-dibromodisilene: A Precursor for Substituted Disilenes and a 1,2-Diaryldisilyne. *J. Am. Chem. Soc.* **2008***, 130* (42), 13856-138-57.

Takusagawa, F. K., T. F.; Sharp, P. R.; Schrock, R. R, A Neutron Diffraction Study of Bis(cyclopentadienyl)(methyl)(methylene)tantalum(V) at 15K. *Acta Cryst.* **1988***, 44*, 439-443.

Tanaka, H.; Nishibayashi, Y.; Yoshizawa, K. Interplay between Theory and Experiment for Ammonia Synthesis Catalyzed by Transition Metal Complexes. *Acc. Chem. Res.* **2016***, 49*, 987−995.

Taylor, D. E.; Angyan, J. G.; Galli, G.; Zhang, C.; Gygi, F.; Hirao, K.; Song, J. W.; Rahul, K.; Anatole von Lilienfeld, O.; Podeszwa, R.; Bulik, I. W.; Henderson, T. M.; Scuseria, G. E.; Toulouse, J.; Peverati, R.; Truhlar, D. G.; Szalewicz, K., Blind test of density-functional-based methods on intermolecular interaction energies. *J Chem Phys* **2016***, 145* (12), 124105.

Tenne, R., Genut L. M. & G. Hodes, Polyhedral and cylindrical structures of tungsten disulphide. *Nature* **1992***, 360*, 444-446.

Thomas, G. T.; Donnecke, S.; Paci, I.; McIndoe, J. S., Trichloro(Dinitrogen)Platinate(II). *Chemistry* **2020***, 26* (54), 12359-12362.

Thorpe, J. H.; Lopez, C. A.; Nguyen, T. L.; Baraban, J. H.; Bross, D. H.; Ruscic, B.; Stanton, J. F., High-accuracy extrapolated ab initio thermochemistry. IV. A modified recipe for computational efficiency. *J Chem Phys 2019,* **150** (22), 224102.

Thurber, C. R.; Mohamed, A. M. A.; Golden, T. D., Electrodeposition of Cu–Ni Composite Coatings. In *Electrodeposition of Composite Materials*, **2016**.

Tientong, J.; Ahmad, Y. H.; Nar, M.; D'Souza, N.; Mohamed, A. M. A.; Golden, T. D., Improved mechanical and corrosion properties of nickel composite coatings by incorporation of layered silicates. *Materials Chemistry and Physics* **2014***, 145* (1-2), 44-50.

Tiong, P. J.; Nova, A.; Groom, L. R.; Schwarz, A. D.; Selby, J. D.; Schofield, A. D.; Clot, E.; Mountford, P., Reactions of Cyclopentadienyl−Amidinate Titanium Hydrazides with CO2, CS2, and Isocyanates: Ti═NαCycloaddition, Cycloaddition−Insertion, and Cycloaddition−NNR2Group Transfer Reactions. *Organometallics* **2011***, 30* (5), 1182-1201.

Tomson, N. C.; Arnold, J.; Bergman, R. G. Halo, Alkyl, Aryl, and Bis(Imido) Complexes of Niobium Supported by the β-Diketiminato Ligand. *Organometallics* **2010***, 29*, 2926–2942.

Tskhovrebov, A. G.; Solari, E.; Wodrich, M. D.; Scopelliti, R.; Severin, K., Sequential N-O and N-N bond cleavage of N-heterocyclic carbene-activated nitrous oxide with a vanadium complex. *J Am Chem Soc* **2012***, 134* (3), 1471-3.

Ung, G.; Bertrand, G., Stability and electronic properties of imidazole-based mesoionic carbenes. *Chemistry* **2011***, 17* (30), 8269-72.

Uyeda, Y.-Y. Z. a. C., Catalytic reductive [4 + 1]-cycloadditions of vinylidenes and dienes. *Science* **2019***, 363*, 857–862.

Vaidya, T.; Klimovica, K.; LaPointe, A. M.; Keresztes, I.; Lobkovsky, E. B.; Daugulis, O.; Coates, G. W., Secondary alkene insertion and precision chain-walking: a new route to semicrystalline "polyethylene" from alpha-olefins by combining two rare catalytic events. *J Am Chem Soc* **2014***, 136* (20), 7213-6.

van Zeist, W. J.; Bickelhaupt, F. M. The Activation Strain Model of Chemical Reactivity. *Org. Biomol. Chem.* **2010***, 8*, 3118−3127.

van Zeist, W.; Visser, R.; Bickelhaupt, F. M. The Steric Nature of the Bite Angle. *Chem. - Eur. J.* **2009***, 15*, 6112−6115.

Varona, M.; Eitzmann, D. R.; Pagariya, D.; Anand, R. K.; Anderson, J. L., Solid-Phase Microextraction Enables Isolation of BRAF V600E Circulating Tumor DNA from Human Plasma for Detection with a Molecular Beacon Loop-Mediated Isothermal Amplification Assay. *Anal Chem* **2020***, 92* (4), 3346-3353.

Vasilyev, V., Online complete basis set limit extrapolation calculator. *Computational and Theoretical Chemistry* **2017***, 1115*, 1-3.

Verhoeven, D. G. A.; Orsino, A. F.; Bienenmann, R. L. M.; Lutz, M.; Moret, M.-E., Cooperative Si–H Addition to Side-On Ni(0)-Imine Complexes Forms Reactive Hydrosilazane Complexes. *Organometallics* **2020***, 39* (4), 623-629.

Vermeeren, P.; van der Lubbe, S. C. C.; Fonseca Guerra, C.; Bickelhaupt, F. M.; Hamlin, T. A., Understanding Chemical Reactivity Using the Activation Strain Model. *Nat Protoc* **2020***, 15*, 649-667.

Vesborg, P. C. K.; Jaramillo, T. F., Addressing the terawatt challenge: scalability in the supply of chemical elements for renewable energy. *RSC Advances* **2012***, 2* (21).

Vogiatzis, K. D.; Polynski, M. V.; Kirkland, J. K.; Townsend, J.; Hashemi, A.; Liu, C.; Pidko, E. A., Computational Approach to Molecular Catalysis by 3d Transition Metals: Challenges and Opportunities. *Chem Rev* **2019***, 119* (4), 2453-2523.

Vougioukalakis, G. C.; Grubbs, R. H. Ruthenium-Based Heterocyclic Carbene-Coordinated Olefin Metathesis Catalysts. *Chem. Rev.* **2010***, 110*, 1746–1787.

Wagner, E.; Pina, E. C. M., Dogs at the Workplace: A Multiple Case Study. *Animals (Basel)* **2021***, 11* (1).

Wang, C. H.; Gao, W. Y.; Powers, D. C., Measuring and Modulating Substrate Confinement during Nitrogen-Atom Transfer in a Ru2-Based Metal-Organic Framework. *J Am Chem Soc* **2019***, 141* (49), 19203-19207.

Wang, D.; Astruc, D., The recent development of efficient Earth-abundant transition-metal nanocatalysts. *Chem Soc Rev* **2017***, 46* (3), 816-854.

Wang, D.; Loose, F.; Chirik, P. J.; Knowles, R. R., N-H Bond Formation in a Manganese(V) Nitride Yields Ammonia by Light-Driven Proton-Coupled Electron Transfer. *J. Am. Chem. Soc.* **2019***, 141*, 4795-4799.

Wang, D. D.; Ou-Yang, L.; Xie, H.; Zhu, M.; Yan, H., Predicting the impacts of mutations on protein-ligand binding affinity based on molecular dynamics simulations and machine learning methods. *Comput Struct Biotechnol J* **2020***, 18*, 439-454.

Wang, L.; Sofer, Z.; Pumera, M., Will Any Crap We Put into Graphene Increase Its Electrocatalytic Effect? *ACS Nano* **2020**.

Wang, R.; Carnevale, V.; Klein, M. L.; Borguet, E., First-Principles Calculation of Water pKa Using the Newly Developed SCAN Functional. *J Phys Chem Lett* **2020***, 11* (1), 54-59.

Wang, Y.; Gao, W., Nanocomposite Coatings Deposited by Sol-Enhanced Electrochemical Methods. In *Electrodeposition of Composite Materials*, **2016**.

Waterman, R.; Hayes, P. G.; Tilley, T. D.; Synthetic Development and Chemical Reactivity of Transition-Metal Silylene Complexes. *Acc. Chem. Res.* **2007***, 40*, 712–719.

Waterman, R.; Hillhouse, G. L., Group Transfer from Nickel Imido, Phosphinidene, and Carbene Complexes to Ethylene with Formation of Aziridine, Phosphirane, and Cyclopropane Products. *J. Am. Chem. Soc.* **2003***, 125*, 13350-13351.

Webb, J. R.; Burgess, S. A.; Cundari, T. R.; Gunnoe, T. B.; Activation of Carbon–Hydrogen Bonds and Dihydrogen by 1,2-CH-Addition Across Metal–Heteroatom Bonds. *Dalton Trans.* **2013***, 42*, 16646-16665.

Weeden, K. A.; Cornwell, B., *The Small World Network of College Classes: Implications for Epidemic Spread on a University Campus*. **2020**.

Wehlin, S. A. M.; Troian-Gautier, L.; Maurer, A. B.; Brennaman, M. K.; Meyer, G. J., Photophysical characterization of new osmium (II) photocatalysts for hydrohalic acid splitting. *J Chem Phys* **2020***, 153* (5), 054307.

Weinhold, F.; Klein, R. A., What is a hydrogen bond? Mutually consistent theoretical and experimental criteria for characterizing H-bonding interactions. *Molecular Physics* **2012***, 110* (9-10), 565-579.

Wengrovius, J. H.; Schrock R. R.; Churchill, M. R.; Missert, J. R.; Youngs, W. J., Tungsten-Oxo Alkylidene Complexes as Olefin Metathesis Catalysts and the Crystal Structure of W(O)(CHCMe3)(PEt3)Cl2. *J. Am. Chem. Soc.***1980***, 102*, 4515-4516.

Whittaker, J. J.; Harding, P.; Clegg, J. K.; Harding, D. J., Structural Origin of Magnetic Hysteresis in an Iron(III) Spin-Crossover Material. *Crystal Growth & Design* **2020***, 20* (10), 7006-7011.

Wiese, S.; Badiei, Y. M.; Gephart, R. T.; Mossin, S.; Varonka, M. S.; Melzer, M. M.; Meyer, K.; Cundari, T. R.; Warren, T. H., Catalytic C-H amination with unactivated amines through copper(II) amides. *Angew Chem Int Ed Engl* **2010***, 49* (47), 8850-5.

Williams, T. G.; DeYonker, N. J.; Ho, B. S.; Wilson, A. K., The correlation Consistent composite Approach: The spin contamination effect on an MP2-based composite methodology. *Chemical Physics Letters* **2011***, 504* (1-3), 88-94.

Winkler, J. R.; Gray, H. B., Electronic Structures of Oxo-Metal Ions. In *Molecular Electronic Structures of Transition Metal Complexes I*, **2011**; pp 17-28.

Winter. M. *WebElements Periodic Table* https://www.webelements.com/tungsten/ (accessed Nov 13, 2018).

Wolczanski, P. T., Activation of Carbon–Hydrogen Bonds via 1,2-RH-Addition/-Elimination to Early Transition Metal Imides. *Organometallics* **2018***, 37* (4), 505-516.

Wu, P.; Yap, G. P. A.; Theopold, K. H., Structure nd Reactivity of Chromium(VI) Alkylidenes. *J. Am. Chem. Soc.* **2018***, 140*, 7088-7091.

Wu, S.; Wang, Z.; Bao, Y.; Chen, C.; Liu, K.; Zhu, B., A novel approach for rhodium(iii)-catalyzed C-H functionalization of 2,2'-bipyridine derivatives with alkynes: a significant substituent effect. *Chem Commun (Camb)* **2020***, 56* (32), 4408-4411.

Wyss, K. M.; Hardy, E. E.; Gorden, A. E. V., An example of enhanced emission of a pyridine containing schiff base zinc2+ complex. *Inorganica Chimica Acta* **2019***, 492*, 156-160.

Xiaoqiang Shan, D. S. C., Wenqian Xu, Mikhail Feygenson, Dong Su, and Xiaowei Teng, Bi-phase Cobalt-Manganese Oxide with High Capacity and Rate Performance for Aqueous Sodium-ion Electrochemical Energy Storage. *Advanced Functional Materials* **2018**.

Xu, J.; Eagan, J. M.; Kim, S.-S.; Pan, S.; Lee, B.; Klimovica, K.; Jin, K.; Lin, T.-W.; Howard, M. J.; Ellison, C. J.; LaPointe, A. M.; Coates, G. W.; Bates, F. S., Compatibilization of Isotactic Polypropylene (iPP) and High-Density Polyethylene (HDPE) with iPP–PE Multiblock Copolymers. *Macromolecules* **2018***, 51*, 8585-8596.

Yamamoto, K.; Nagae, H.; Tsurugi, H.; Mashima, K., Mechanistic understanding of alkyne cyclotrimerization on mononuclear and dinuclear scaffolds: [4 + 2] cycloaddition of the third alkyne onto metallacyclopentadienes and dimetallacyclopentadienes. *Dalton Trans* **2016***, 45* (43), 17072-17081.

Yang, G.; Farsi, L.; Mei, Y.; Xu, X.; Li, A.; Deskins, N. A.; Teng, X., Conversion of Ethanol via C-C Splitting on Noble Metal Surfaces in Room-Temperature Liquid-Phase. *J Am Chem Soc* **2019***, 141* (24), 9444-9447.

Yaoming Xie; R. S. Grev; Jiande Gu; Henry F. Schaefer III; Paul v. R. Schleyer; Jianrui Su; Xiao-Wang Li; Robinson, G. H., The Nature of the Gallium-Gallium Triple Bond. *J. Am. Chem. Soc.* **1998***, 120* (15), 3773-3780.

Yoshimoto, T.; Hashimoto, H.; Hayakawa, N.; Matsuo, T.; Tobita, H., A Silylyne Tungsten Complex Having an Eind Group on Silicon: Its Dimer–Monomer Equilibrium and Cycloaddition Reactions with Carbodiimide and Diaryl Ketones. *Organometallics* **2016***, 35* (20), 3444-3447.

Yoshimoto, T.; Hashimoto, H.; Ray, M.; Hayakawa, N.; Matsuo, T.; Chakrabarti, J.; Tobita, H., Products of [2+2] Cycloaddition between a W≡Si Triple-Bonded Complex and Alkynes: Isolation, Structure, and Non-Classical Bonding Interaction. *Chemistry Letters* **2020**.

Yoshimoto, T.; Hashimoto, H.; Takagi, N.; Sakaki, S.; Hayakawa, N.; Matsuo, T.; Tobita, H., Reactions of a Silylyne Complex with Aldehydes: Formation of W-Si-O-C Four-Membered Metallacycles and Their Metathesis-Like Fragmentation. *Chemistry* **2019***, 25* (15), 3795-3798.

You, D.; Smith, J. E.; Sen, S.; Gabbaï, F. P., A Stiboranyl Platinum Triflate Complex as an Electrophilic Catalyst. *Organometallics* **2020**.

Yuvaraj, K.; Douair, I.; Maron, L.; Jones, C., Activation of Ethylene by N-Heterocyclic Carbene Coordinated Magnesium(I) Compounds. *Chemistry* **2020***, 26* (64), 14665-14670.

Zamora, M. T.; Ferguson, M. J.; McDonald, R.; Cowie, M., Unsymmetrical Dicarbenes Based on N-Heterocyclic/Mesoionic Carbene Frameworks: A Stepwise Metalation Strategy for the Generation of a Dicarbene-Bridged Mixed-Metal Pd/Rh Complex. *Organometallics* **2012***, 31* (15), 5463-5477.

Zanetti, N. C.; Schrock, R. R.; Davis, W. M. Monomeric Molybdenum and Tungsten Complexes that Contain a Metal–Phosphorus Triple Bond. *Angew. Chemie Int. Ed. English* **1995***, 34*, 2044–2046.

Zhang, D. D.; Lo, S. C.; Cross, J. V.; Templeton, D. J.; Hannink, M., Keap1 is a redox-regulated substrate adaptor protein for a Cul3-dependent ubiquitin ligase complex. *Mol Cell Biol* **2004***, 24* (24), 10941-53.

Zhang, G.; Li, Y.; Wang, Y.; Zhang, Q.; Xiong, T.; Zhang, Q., Asymmetric Synthesis of Silicon-Stereogenic Silanes by Copper-Catalyzed Desymmetrizing Protoboration of Vinylsilanes. *Angew Chem Int Ed Engl* **2020***, 59* (29), 11927-11931.

Zhang, R.; Tutusaus, O.; Mohtadi, R.; Ling, C., Magnesium-Sodium Hybrid Battery With High Voltage, Capacity and Cyclability. *Front Chem* **2018***, 6*, 611.

Zhang, S.; Bedi, D.; Cheng, L.; Unruh, D. K.; Li, G.; Findlater, M., Cobalt(II)-Catalyzed Stereoselective Olefin Isomerization: Facile Access to Acyclic Trisubstituted Alkenes. *J Am Chem Soc* **2020**.

Zhang, Y.; Zhang, M.; Han, Z.; Huang, S.; Yuan, D.; Su, W., Atmosphere-Pressure Methane Oxidation to Methyl Trifluoroacetate Enabled by a Porous Organic Polymer-Supported Single-Site Palladium Catalyst. *ACS Catalysis* **2021***, 11* (3), 1008-1013.

Zhang, Z.; Li, D.; Jiang, W.; Wang, Z., The electron density delocalization of hydrogen bond systems. *Advances in Physics: X* **2018**, 3 (1).

Zhao, L.; Pan, S.; Holzmann, N.; Schwerdtfeger, P.; Frenking, G., Chemical Bonding and Bonding Models of Main-Group Compounds. *Chem Rev* **2019***, 119* (14), 8781-8845.

Zheng, W.; Ying, L.-a.; Ding, P., Numerical solutions of the Schrödinger equation for the ground lithium by the finite element method. *Applied Mathematics and Computation* **2004***, 153* (3), 685-695.

Zhizhko, P. A.; Pichugov, A. V.; Bushkov, N. S.; Rumyantsev, A. V.; Utegenov, K. I.; Talanova, V. N.; Strelkova, T. V.; Lebedev, D.; Mance, D.; Zarubin, D. N., Catalytic Imido-Transfer Reactions of Well-Defined Silica-Supported Titanium Imido Complexes Prepared via Surface Organometallic Chemistry. *Organometallics* **2020***, 39* (7), 1014-1023.

Zhong, S.; Barnes, E. C.; Petersson, G. A., Uniformly convergent n-tuple-zeta augmented polarized (nZaP) basis sets for complete basis set extrapolations. I. Self-consistent field energies. *J Chem Phys* **2008***, 129* (18), 184116.

Zhou, C. X.; Cundari, T. R., Computational Study of 3d Metals and Their Influence on the Acidity of Methane C-H Bonds. *ACS Omega* **2019***, 4* (23), 20159-20163.

Zhou, T.; Martinez-Baez, E.; Schenter, G.; Clark, A. E., PageRank as a collective variable to study complex chemical transformations and their energy landscapes. *J Chem Phys* **2019**, *150* (13), 134102.

Zhuang, Z.; Yu, J. Q., Pd(II)-Catalyzed Enantioselective gamma-C(sp(3))-H Functionalizations of Free Cyclopropylmethylamines. *J Am Chem Soc* **2020**, *142* (28), 12015-12019.

Ziegler, J. A.; Buckley, H. L.; Arnold, J., Synthesis and reactivity of tantalum corrole complexes. *Dalton Trans* **2017**, *46* (3), 780-785.

Ziegler, K. Serial No. 232,476 Claims Priority, Application Germany, 1951.

Ziegler, K.; Gellert, H.-G. *Polymerization of Ethylene*. Jan. 11, 1955, 1955.

Ziegler, T.; Tschinke, V.; Becke, A. A Theoretical Study on the Relative Strengths of the Metal—Hydrogen and Metal—Methyl Bonds in Complexes of Middle to Late Transition Metals. *J. Am. Chem. Soc.* **1987**, *109*, 1351–1358.